Exploring the potential of modifying leaf colour to increase rice productivity via

improving photosynthesis and source–sink relationships

Zhenxiang Zhou

Propositions

1. Modifying the leaf-colour trait alone does not improve rice photosynthesis and yield.
   (this thesis)
2. Nitrogen metabolism is the linking pin between source-sink relationships at leaf level and at crop level.
   (this thesis)
3. Science progresses faster when crossing borders and frontiers.
4. The ultimate goal of theoretical research lies in its practical application.
5. All reviewers are by definition biased.
6. ChatGPT is only a language polishing tool.
7. Social media platforms are responsible for enforcing strict content rules to prevent misinformation.

Propositions belong to the thesis, entitled

Exploring the potential of modifying leaf colour to increase rice productivity via improving photosynthesis and source-sink relationships

Zhenxiang Zhou

Wageningen, 27 November, 2023

Exploring the potential of modifying leaf colour to increase rice productivity via improving photosynthesis and source-sink relationships

Zhenxiang Zhou

Thesis committee

Promotor
Prof. Dr P.C. Struik
Professor of Crop Physiology
Wageningen University & Research

Co-promotors
Dr X. Yin
Senior scientist, Centre for Crop Systems Analysis
Wageningen University & Research

Prof. Dr J. Yang
Professor of Crop Physiology
Agricultural College of Yangzhou University, Jiangsu Province, China

Other members
Prof. Dr. M.J. Kropff, Wageningen University & Research
Prof. Dr. D.M. Kramer, Michigan State University, USA
Dr. J. Kromdijk, University of Cambridge, UK
Dr. W. van Ieperen, Wageningen University & Research

This research was conducted under the auspices of the C.T. de Wit Graduate School for Production Ecology and Resource Conservation

Exploring the potential of modifying leaf colour to increase rice productivity via improving photosynthesis and source-sink relationships

Zhenxiang Zhou

Thesis

submitted in fulfilment of the requirements for the degree of doctor
at Wageningen University
by the authority of the Rector Magnificus,
Prof. Dr A.P.J. Mol,
in the presence of the
Thesis Committee appointed by the Academic Board to be defended in public
on Monday 27 November 2023
at 1:30 p.m. in the Omnia Auditorium.

Zhenxiang Zhou

Exploring the potential of modifying leaf colour to increase rice productivity via improving photosynthesis and source-sink relationships, 208 pages.

PhD thesis, Wageningen University, Wageningen, NL (2023)
With references, with summary in English

ISBN: 978-94-6447-911-9
DOI: https://doi.org/10.18174/639486

Abstract

Zhenxiang Zhou, 2023, *Exploring the potential of modifying leaf colour to increase rice productivity via improving photosynthesis and source-sink relationships*. PhD thesis, Wageningen University & Research, Wageningen, The Netherlands. 208 pp.

Rice (*Oryza sativa* L.) stands as a cornerstone of global food security, providing sustenance to over half of the world's population. As the world faces mounting challenges, such as population growth and climate change, the importance of maximising rice productivity has become increasingly evident. In the past, ways to improve rice yields mainly relied on improving the harvest index or increasing nitrogen (N) fertiliser application. With the recognition that the harvest index has more or less reached a plateau and input levels should not be increased further for reasons of sustainability, the next advance in crop productivity will most likely come from improvements in photosynthesis. One of the options of increasing photosynthetic competence is to modify leaf colour so as to raise canopy carbon gain by an optimised vertical light environment. However, manipulation of leaf colour means an alternation of N investment in chlorophyll, which will lead to a series of subsequent uncertainties across leaf, canopy, and crop scales. This dissertation aims to understand how this altered N allocation affects the crop's photosynthesis and associated source-sink relationships, as well as on the dynamic feedforward or feedback between these processes across different scales.

Effects of leaf-colour modification on rice photosynthesis at both leaf and canopy scales were investigated using nine rice genotypes comprising different genetic backgrounds and their leaf-colour variants grown in a greenhouse experiment and a field experiment. Stay-green (G) and yellow-leaf (Y) are two common traits derived from leaf-colour modification. Earlier and larger effects were normally observed for Y variants than for G variants. Among the Y variants from two genetic backgrounds, only the one from the ZF (cv. Zhefu 802) background showed advantages in photosynthesis compared with its control genotype. At leaf level, its improved photosynthetic capacity parameters and photosynthetic N-use efficiency under saturated light intensity were associated with an efficient reallocation of saved N from leaf chlorophyll to more rate-limiting proteins, e.g., Cytochrome b_6/f and Rubisco. At canopy level, its improved canopy photosynthesis was attributed to the adaptive adjustment of N distribution to the light profile across the canopy, evidenced by a steeper N gradient with a higher allocation of N to the upper leaf layer of the canopy.

Effects of leaf-colour modification on rice whole-plant source-sink relationships during grain filling were examined, using a model-fitting method. Leaf-colour modification affected biomass source-sink relationships, predominantly through the adjustment of post-flowering source capacity, but the approach to attaining this differed among genetic backgrounds. Among all variants, only ZF-Y showed a simultaneous increase in source capacity and sink growth when compared to its control genotype. This increase was associated with its prolonged leaf-N duration, resulting from more post-flowering N uptake and less N remobilisation from leaves to grains.

Effects of leaf-colour modification on rice source-sink relationships were further analysed at the sub-foliar scale, to assess any possible interconnection between the sub-foliar and the whole-plant scales and to identify any association with whole-plant N budgets. The sub-foliar source-sink (im)balance was addressed by parameters related to triose phosphate utilisation (TPU). Model analyses of leaf gas-exchange data showed that TPU parameter values were positively correlated with leaf N content, while higher leaf N (observed at early growth stages or at high N inputs) caused TPU limitation to occur at lower intercellular CO_2 concentrations. Panicle pruning had no apparent impact on the rate of TPU, presumably suggesting that the feedback inhibition of whole-plant sink limitation was offset by the positive effect of increased leaf N resulting from no need to remobilise N from leaves to support grain growth. These results revealed that sub-foliar sink limitations on leaf photosynthesis can be modulated by whole-plant source-sink relations and N budgets.

Above findings suggest versatile roles of N as a link across leaf, canopy, and crop scales within the context of leaf-colour modification. Thus, modifying leaf colour as a promising strategy to improve rice photosynthesis and yield has to take nitrogen into account at each level of biological organisation.

Keywords: Stay-green and yellow-leaf traits, leaf/canopy photosynthesis, source-sink relationship, triose phosphate utilisation, nitrogen, *Oryza sativa*, leaf-colour modification.

Table of contents

Chapter 1	General introduction	1
Chapter 2	Enhancing leaf photosynthesis from altered chlorophyll content requires optimal partitioning of nitrogen	19
Chapter 3	Leaf-colour modification affects canopy photosynthesis, dry-matter accumulation and yield traits in rice	59
Chapter 4	Quantifying source-sink relationships in leaf-colour modified rice genotypes during grain filling phase	95
Chapter 5	Triose phosphate utilisation in leaves is modulated by whole-plant sink-source ratios and nitrogen budgets in rice	135
Chapter 6	General discussion	175
	Summary	195
	Acknowledgements	199
	List of publications	203
	PE&RC Training and Education Statement	204
	Curriculum Vitae	207
	Funding	208

Chapter 1

General introduction

1.1 General background

The current level of productivity of the major crops falls significantly short of meeting society's diverse needs. This is primarily due to the mounting pressures exerted on the agricultural industry by increasing human population, rising affluence leading to higher meat and dairy consumption, and the escalating demand for biofuels (Grassini et al., 2013; Ray et al., 2013). With a predicted doubling demand for global food from 2010 to 2050 and a changing climate and growing competition for resources, these challenges will increase (Chen et al., 2014; Ray et al., 2013; Samal and Babu, 2018). These challenges are particularly apparent in terms of the required increase in grain production. Rice (*Oryza sativa* L.), as one of the most important cereal crops, provides a food source for more than half of the world's population, making it indispensable for global food security (Xu et al., 2016; Senthilkumar et al., 2020). With about 154 million hectares annually or a share of 11% in global cultivated area, China is the world's largest rice producer, making up 28% of global rice production (Khush, 2005; Qiu, 2008). Although China has basically achieved self-sufficiency in rice under the premise that the current rice production level and arable land area remain unchanged, yield growth rates have slowed down, and even reached a plateau (Deng et al., 2019; Yuan et al., 2021). Given the increasing need for land for other purposes and the large impact of current rice production on the natural resources and the environment, it is imperative to explore innovative approaches that can revitalize and enhance rice production, especially in China.

1.1.1 Enhancing photosynthesis: A key to advancing rice yields

In the past decades, the improvement of rice yields largely depended on the increase in fertiliser input (especially heavy nitrogen application; Sheehy et al., 1998) and selection of cultivars with high harvest index (achieved from introducing semi-dwarf genes in major crops; Hedden, 2003; Khush, 1995). However, nitrogen (N) fertiliser input comes at the cost of high energy use and serious environmental pollution while the harvest index of rice is now approaching a plateau, and it is unlikely that it can be increased beyond this level much further (Wissuwa et al., 2016; Éva et al., 2019). Photosynthesis, a complicated biosynthetic process, is the primary determinant of crop biomass production. It has therefore been suggested to be the next target for yield improvement (Zhu et al., 2010).

From a physiological perspective, the photosynthetic process consists of two steps, referred to as the light and dark reactions, respectively. The light reaction concerns the capture of light

energy by chlorophyll and electron transport on the chloroplast membrane, reducing $NADP^+$ into NADPH and providing the proton gradient that powers the phosphorylation of ADP, thereby producing ATP. The resulting NAPDH and ATP provide the chemical energy to run the dark reaction, the Calvin–Benson-Bassham (CBB) cycle. This CBB cycle assimilates CO_2 and reduces it to carbohydrate (Blankenship et al., 2011). Considering each step involved from leaf light absorption up to CH_2O synthesis, it has been estimated that the theoretical maximum solar energy conversion efficiency of leaf photosynthesis on the basis of incoming global solar radiation is 12.3%; however, the typical solar energy conversion efficiency for C_3 crops like rice and wheat is merely around 1.9% throughout the growing season under relatively favourable field conditions (Yin and Struik, 2015). This low efficiency results from a series of energy losses along the chain of leaf, canopy, and crop scales, and a decrease of any loss along this chain could have a significant impact on crop productivity. So, decreasing the efficiency losses along these levels would allow farmers to significantly increase yields of these crops on the same acreage of land, not necessarily using more water, fertiliser and other inputs. Great efforts have been devoted to exploring various options of improving the potential efficiency of photosynthesis so as to shift the yield potential of rice (Ali et al., 2018; Gao et al., 2020; Wei et al., 2022).

1.1.2 Leaf-colour modification as a potential means to improve photosynthesis

Leaf-colour modification, referring to the "stay-green" and "yellow-leaf" traits, has emerged as a promising avenue for potentially enhancing photosynthesis and thus crop yields by optimising the interception of photosynthetic photon flux density (PPFD) or/and the conversion of intercepted PPFD into biomass production. This modification primarily involves altering the chlorophyll content within the leaf, directly impacting its light-absorbing capacity. Retarding chlorophyll degradation, as observed in the "stay-green" trait, allows plants to prolong the duration of green canopy cover during a late grain-filling phase for continued light interception (Gregersen et al., 2013). This advantageous trait, characterized by delayed whole-plant senescence, enables crop plants to maintain green leaves with active photosynthetic function, ensuring a continued assimilation process. The delay of leaf senescence has been recognized as a significant trait that has undergone intensive selection for genetic improvement in a range of agricultural species (particularly maize) to promote stress tolerance and yield gain (Duvick et al., 2010). Borrell et al. (2014) reported that near-isogenic sorghum lines with stay-green traits exhibited increased accumulation of photosynthetic assimilates after flowering, particularly

under drought conditions, although subsequent research indicated that an adequate N supply was also necessary to achieve this increase (Hou et al., 2021).

A more recent approach to leaf-colour modification, proposed by Ort et al. (2011), focuses on reducing leaf greenness to enhance canopy photosynthesis. The idea behind this approach is to achieve an optimised distribution of incoming light throughout the depth of the canopy. It is theorised that, by decreasing chlorophyll content (especially of leaves at the top of the canopy), the overall efficiency of canopy photosynthesis can be improved, leading to increased crop productivity. This innovative strategy challenges the traditional belief from empirical cultivation that the greener the rice leaves are, the higher the photosynthesis and yield will be, a belief which was based on the correlation between leaf greenness and N content, or even crop yield (Harris and Griffin, 1961; Wood et al., 1993). However, after breeding for greenness and increasing N fertiliser application, the chlorophyll content in rice leaves has reached a point of redundancy, potentially resulting in the suboptimal conversion efficiency from PPFD to biomass production at canopy level. This is particularly problematic when the leaf area index (LAI) of the canopy is high, or when the upper leaves are droopy, which creates an unfavourable light profile along the canopy height, resulting in most of the middle and lower leaves in the canopy to not receive sufficient light. Furthermore, photosynthetic rates of dark green upper leaves, when receiving high PPFD, become easily (over-)saturated. To overcome these problems, adopting a light-green canopy by modifying leaf colour may serve as a robust strategy to improve photosynthetic efficiency and maximise carbon gain in the crop canopy. Selecting genotypes with pale-green or even yellow leaves can effectively minimise the sunlight absorption by individual chloroplasts and thus alleviate saturation of the upper leaves, while it can increase light penetration to lower layers in a canopy (Ort et al., 2011; Slattery and Ort, 2021). Implementation and validation of this method have been investigated in rice (Gu et al., 2017a; Li et al., 2013) and soybean (Walker et al., 2018). Modelling simulations have suggested that reducing chlorophyll content accompanied with strategic reinvestment of conserved N can further amplify the gain in photosynthesis (Song et al., 2017).

1.2 Effects of leaf-colour modification on photosynthesis at different scales

Leaf-colour modification is not merely a visual transformation associated with chlorophyll catabolism but a manifestation of the underlying N dynamics in the plant's metabolic processes. Manipulation of leaf colour means an alteration of the N investment in chlorophyll, leading to a series of subsequent uncertainties across leaf, canopy, and whole-crop scales or levels. These

uncertainties can be confounded when working with diverse genetic backgrounds. Hence, in the next part of this general introduction, I will give background information on the potential effects of modifying leaf chlorophyll content on the photosynthesis and associated relationships at different scales based on current knowledge.

1.2.1 Reducing non-photochemical quenching and altering the nitrogen partitioning within the leaf

Light is the driving force of plant growth, providing the energy required for the dark reaction of photosynthesis. However, at the leaf level, an important drawback to achieving efficient photosynthesis lies in the fact that chlorophyll antennae capture a larger amount of light energy than the photosynthetic system can effectively utilise for driving electron transport. This results in great energy losses along the pathway. Especially under non-limiting-light conditions, high-light intensities give rise to excess excitation beyond the maximal capacity for photochemical and biochemical reactions in C_3 leaves, causing the production of reactive oxygen species and deleterious singlet O_2 ($^1O_2$) (Vass and Cser, 2009), which reduce the quantum yield of Photosystem II as well as Photosystem I (Krieger-Liszkay et al., 2008; Takagi et al., 2016). To protect the photosystems from the photodamage by excess radiation, as much as 80% of absorbed photons are dissipated as heat via non-photochemical quenching (NPQ) under full sunlight (Dall'Osto et al., 2017), which accounts for a significant loss of light energy (Gu et al., 2017b; Meacham et al., 2017). In this circumstance, appropriate adjustment of leaf light-absorption capacity by modifying chlorophyll content may be an effective way to reduce this energy loss and to prevent light-induced damage. By reducing the chlorophyll content and consequently the size of the chlorophyll antennae in the photosynthetic apparatus, there is a decreased demand for engaging in photoprotective mechanisms such as NPQ (Melis, 2009; Ort et al., 2011; de Mooij et al., 2015). Gu et al. (2017a) indeed observed that the mutant with pale-green leaves exhibited lower energy dissipation as heat than the wild type. However, whether truncated antenna size of the photosystems would mitigate efficiency losses and whether this process is always associated with NPQ remains unclear. Also, it is necessary to examine to what extent the relationships between NPQ and modified chlorophyll content vary genotypically, given the reports about the effect of genetic variations in rice varieties on the total light absorption by leaves (Horton, 2000; Tsai et al., 2019).

In addition to the energy saved through NPQ, modifying leaf colour offers an opportunity to optimise the leaf N partitioning pattern by saving N from investment in chlorophyll to other,

more rate-limiting, photosynthetic proteins. Leaf net CO_2 assimilation rate (A) is closely related to the leaf photosynthetic N content per unit area (N_{photo}, the physiologically effective total N content partitioned to photosynthetic protein complexes) (Makino et al., 1984, 1985; Sinclair and Horie, 1989; Yao et al., 2015). N_{photo} and its partitioning over the different photosynthetic components, such as the light-harvesting complex, components of the electron transport system, Rubisco and other soluble proteins, are variable during the whole-leaf life cycle (Mu et al., 2018) and acclimate to growth environment (Yin et al., 2018). This means that macromolecules (e.g., chlorophyll or Rubisco) may continuously degrade or recycle into amino acids as a source of protein for new assimilation (Chiba et al., 2003; Chen et al., 2014). In a natural environment, plants often tend to over-invest in chlorophyll synthesis to capture more light than they need for the sake of competitive advantages (Melis, 2009; Ort et al., 2011). But for improving productivity, lowering leaf-N investment in chlorophyll might be advantageous. This method could allow for a redistribution of leaf N saved from chlorophyll to other photosynthetic components if the N_{photo} is constant. However, until now, limited information is available on the impact of modifying leaf colour on leaf-N partitioning pattern and its associations with the whole-leaf photosynthetic competence.

1.2.2 Matching the light absorption profile with the vertical distribution of leaf nitrogen

Carbon assimilation at the leaf level is closely linked to incident light density and leaf-N content, while upscaling to the canopy level involves considering factors such as the acclimation of photosynthetic N resources to varying light conditions within the canopy (Yin and Struik, 2015). As stated above, photosynthesis saturates at around 25% of full sunlight for most of the modern conventional rice varieties. The vertical distributions of sunlight in a canopy of rice are generally following an exponential decline over canopy depth according to the Beer-Lambert law (Hirose and Werger, 1987; Monsi et al., 2005). Dark-green top leaves should result in the least efficiency in the upper parts of the canopy (because of high light energy absorbed), whereas the photosynthetic performance of lower layers of the canopy is light-limited (Walker et al., 2018). It is reported that shaded leaves within the canopy make up over 70% of the total leaf area, absorbing ~30% of the total solar energy and contributing ~47% to the overall canopy photosynthesis (Song et al., 2013). In theory, the adoption of pale-leaf rice varieties with reduced canopy chlorophyll content can potentially alleviate this situation by providing an

improved vertical light environment throughout the canopy, thereby possibly maximising canopy photosynthetic efficiency (Ort et al., 2011).

Besides the light absorption profile, nitrogen vertical distribution also determines the carbon gain of the canopy by influencing photosynthesis of each individual layer (Hikosaka, 2014). According to the "optimisation" theory, it is recognised that the canopy photosynthesis is maximal if the light-saturated maximum leaf-photosynthesis (A_{max}) profile follows the light profile in the canopy (Anten et al., 1995; Goudriaan, 1995; Hikosaka, 2016), i.e., light extinction coefficient (K_L) = active N_{photo} extinction coefficient (K_N). Indeed, it is witnessed that the K_N was closely associated with the K_L, indicating the vertical canopy N profile can be driven to some extent by the light. However, the K_N in an actual canopy is generally significantly smaller than the K_L (Archontoulis et al., 2011). The expected decrease in K_L in genotypes with yellower-leaf canopy may make it possible to close the gap between light and N profile distribution, putting the K_L closer to the K_N. Nevertheless, leaf-colour traits with altered leaf chlorophyll content may indirectly change the partitioning of N_{photo} among various photosynthetic proteins; so, the profile of A_{max} in leaf layers of canopy may not necessarily follow more closely the light profile. Further research is needed to examine the ratios of K_N to K_L in genotypes with varying canopy greenness, as well as to explore how leaf-colour traits could potentially enhance canopy photosynthesis and thus rice yield.

1.2.3 Complexity of yield formation: needs to maintain the balance between source and sink

Improving photosynthesis ultimately aims to improve crop yield; but from a crop physiological viewpoint, grain yield depends on relationships between source (the ability of leaves to supply assimilates) and sink (the ability of grains to utilise assimilates), especially during grain filling. The source-sink coordination theory is frequently used to elucidate constraints to dry matter accumulation and yield formation, in order to explore the efficient approaches to achieving high-yield crops (Rossi et al., 2015). This has been applied in rice (Shi et al., 2013; Yang, 2015), wheat (Uddling et al., 2008; Zhang et al., 2010), maize (Ning et al., 2018; Hisse et al., 2019), and other common crop types (Sugiura et al., 2017; Chen et al., 2018; Pincovici et al., 2018).

Stay green, i.e., delaying onset of leaf senescence, has often been used to extend the photosynthesis period during the grain-filling phase and, thereby, to achieve a larger dry matter accumulation and yield potential (Kumar et al., 2019). This visible trait, caused by retaining

high chlorophyll content in leaves, postpones or slows the N transition from vegetative organs to storing organs in order to maintain the structure and function of chloroplast and its photosynthetic capacity, when plants go through the initial process of senescence (Yamamoto et al., 2017). This has been an effective strategy to achieve high yields in genotypes having a high number of grains. As the presently advocated light-coloured leaf traits with less chlorophyll are fundamentally different from the classical "stay-green" traits, further research is needed on whether this will have an impact on source-sink relationships after flowering.

It is well-known that N plays a critical role in regulating biomass production and yield formation, as it is quantitatively associated with both vegetative and reproductive growth, reallocation between source and sink organs (Lawlor et al., 2001; Sinclair et al., 2019). After flowering, adequate N uptake by roots can lead to high photosynthetic capacity of the source organs (leaves), and delayed whole-plant senescence (Evans, 1989; Yang and Zhang, 2006). Besides, post-flowering N reallocation is an important component of grain N accumulation (Gaju et al., 2014). Wei et al. (2018) reported that grain N concentrations have a consequence for post-flowering stay-green traits and sink-source balance. A high demand for N remobilisation from leaves to grains will hasten senescence of vegetative tissues, and shorten the period of grain filling, reduce the supply of assimilates, and finally limit grain production. The relationship between carbon capture and N remobilisation during grain filling is tight (Thomas and Ougham, 2014). Stay-green characteristics, which impede or delay the breakdown of chlorophyll into amino acids that can be exported as a source of N to sink organs, can significantly impact the duration and rate of grain filling. Similarly, lower chlorophyll content in pale- or yellower-leaf variants might affect the source of the N supply to grains. However, there is little information available concerning the effects of yellower-leaf traits on source and sink relationships and the interplay between carbon and N. Quantifying the source-sink relationships could provide valuable insights about the traits favourable for high yields.

1.2.4 Relationship between leaf-level sink limitation and whole-plant sink limitation

Source-sink relationships are associated not only with yield formation at the whole-plant or crop scales, but also with the biochemical processes at the (sub)foliar scale. Specifically, the interaction between photosynthesis and sink limitation has been widely observed, with the impact of sink limitation on photosynthesis being evident at multiple scales (Arp, 1991; Paul et al., 1992; Sharkey, 1985; Tanaka and Fujita, 1974). At (sub)foliar scale, the limitation to

photosynthesis is imposed by the capacity for triose phosphate, the primary product from the CBB cycle, to be utilised for carbohydrate synthesis. Thus, triose phosphate utilisation (TPU) reflects the short-term source-sink (im)balance between carbon fixation by and carbon export from the CBB cycle. The TPU limitation, as one of the three canonical biochemical limitations of photosynthesis (A_c, the Rubisco-limited rate; A_j, the electron transport limited rate; A_p, the TPU-limited rate) in gas exchange analysis, is normally hard to detect at ambient conditions unless there is a high photosynthetic rate under elevated [CO_2] and saturated light intensity (Yang et al., 2016). In comparison, the long-term sink limitation at whole-plant scale involving feedback inhibition on photosynthetic activity (source) is easy to detect by various experimental manipulations or the selection of plants with contrasting sink-source ratios (Crafts-Brandner & Egli, 1987; Li et al., 2015; Aslani et al., 2020). Recently, the physiological experiments from Fabre et al. (2019) attempted to link these sink limitations at the two scales. They found that the decreased rate of TPU, thus reduced A_{max} (light-saturated maximum leaf photosynthesis), after midday was caused by sucrose accumulation in the flag leaf. This sucrose build-up was a result of the sink limitation induced by panicle pruning and elevated [CO_2]. Their follow-up study suggested that the local sink-source ratio could be a reliable proxy trait used for selecting genotypes with adaptation to elevated [CO_2] conditions (Fabre et al., 2020). All these findings suggest that TPU limitation at sub-foliar scale may be regulated by a sink feedback effect at whole-plant scale. As mentioned above, modifying leaf colouration has the potential to impact both photosynthesis and sink-source relationships, making leaf-colour traits important candidates to be explored for establishing connections across different scales. Leaf-colour variant genotypes may differ from their default counterparts in photosynthetic capacity and, thus, in the extent of TPU limitation. Moreover, it is crucial to investigate how leaf-colour traits alter the local source-sink ratio, as this will provide valuable insights into the feedback inhibition by whole-plant source-sink ratios of leaf-scale TPU limitation.

As for the whole-plant scale, in addition to carbon assimilation, N may play roles in coordinating sink limitation within a leaf. The occurrence of TPU limitation is often dependent on a high photosynthetic rate, which, in turn, is associated with abundant leaf-N content (Sage et al., 1990; Yang et al., 2016). Rice leaves lacking sufficient N content are unable to achieve a high photosynthetic capacity, possibly also resulting in an inability to reach TPU limitation. The whole-plant growing sink (e.g., grains) demands not only carbon but also N. As much of grain N comes from N remobilisation from leaves, this may yield a feedback effect on photosynthesis by alleviating or removing TPU limitation via reduced leaf source activity.

Besides, photorespiration may play a role in N assimilation (Bloom, 2015), via which N may participate in regulating local sink-source mechanisms of TPU limitation. When a leaf experiences the TPU limitation, the photorespiratory pathway can stimulate its photosynthetic rate, as a fraction of photorespiratory carbon can be diverted in the form of exporting N-rich amino-acids for being used for metabolism elsewhere (Harley and Sharkey, 1991; Busch et al., 2018). This photorespiration-associated N assimilation may also be associated with leaf N content. Overall, understanding the role of N budgets is crucial for building the link between leaf-level TPU limitation and whole-plant sink limitation.

1.3 Research objectives

The overall objective of this thesis is to examine the potential of using leaf-colour modification (greener or yellower) to improve photosynthesis and yield of rice genotypes. To that end, experiments are defined to explore the effects of leaf-colour modification on photosynthesis at both leaf and canopy levels, as well as investigate the relationships between source and sink dynamics at the crop level. Based on these, I also aim to establish the intrinsic link between leaf-level TPU limitation and whole-plant sink limitation. The specific objectives outlined for the research chapters are as follows:

1) To explore the possibilities of decreasing the energy losses via NPQ, and investigate the effect of leaf-colour modification on leaf photosynthetic capacity parameters and its associated N partitioning patterns in rice genotypes of different genetic backgrounds;
2) To examine the ability of canopy N profile acclimation to canopy light profile in rice genotypes with contrasting chlorophyll content;
3) To compare crop sink-source differences in leaf-colour modified rice genotypes by quantifying the carbon and N partitioning among source and sink organs;
4) To obtain information on how leaf-scale sink limitation as manifested by TPU is modulated by whole-plant sink-source ratios and N budgets in leaf-colour modified rice genotypes.

1.4 Outline of the thesis

This thesis consists of six chapters, including this general introduction as Chapter 1, which provides a brief overview of the current situation of rice yield, and introduces the potential possibilities to apply greener or yellower traits created by leaf-colour modification to improve

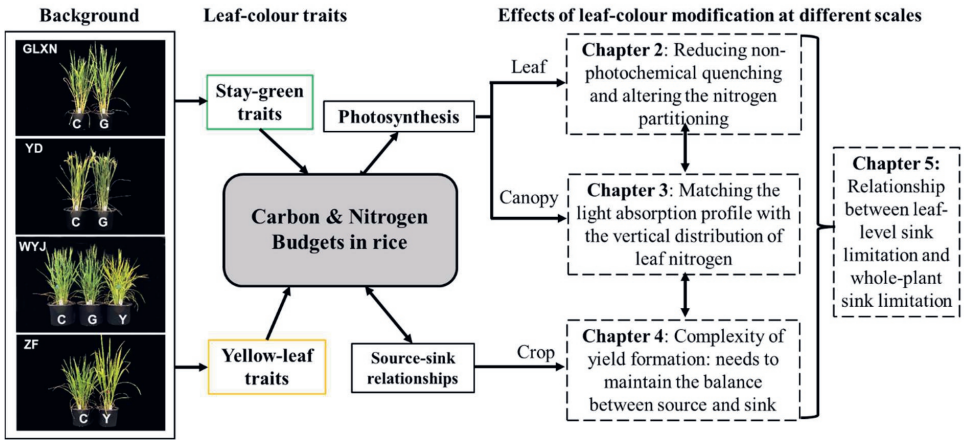

Fig. 1.1 Outline of the dissertation. Rice pictures taken in greenhouse experiment, representing four rice control (C) genotypes and their greener-leaf variant (G) and/or their yellower-leaf variant (Y) genotypes. Genotype-background abbreviations: GLXN, cv. Guanglingxiangnuo; YD, cv. Yandao 8; WYJ, cv. Wuyunjing 3; ZF, cv. Zhefu 802.

rice photosynthesis, source-sink relations, and thus grain yields. Following this chapter, there are four research chapters (Chapter 2 to Chapter 5) and a general discussion (Chapter 6). The schematic structure of this thesis and the interrelations between the different chapters are illustrated in Fig. 1.1.

In **Chapter 2**, the impact of leaf-colour modification on rice leaf photosynthesis is examined (Fig. 1.1). A greenhouse experiment is conducted in Wageningen (Netherlands) to measure leaf gas exchange and chlorophyll fluorescence at stem elongation stage, anthesis, and 20 d after anthesis. Based on these measurements, I first quantify the relative energy loss primarily via NPQ among leaf-colour modified variants. For that an alternative way to estimate the loss via NPQ is proposed. Then, the relationship between NPQ and modified chlorophyll content is investigated. Thirdly, the distribution of leaf nitrogen among photosynthetic proteins is assessed by combining proteomic analysis with estimated photosynthetic parameters. Finally, the relationships between genetic background and the investment of leaf photosynthetic nitrogen are further discussed.

In **Chapter 3**, the impact of leaf-colour modification on rice canopy photosynthesis and yield is examined (Fig. 1.1). A field experiment is conducted in Yangzhou University (China) to quantify the light and N profiles among a complete canopy of rice. The vertical distribution of photosynthetic photon flux density (PPFD) is measured to calculate its attenuation coefficient

(K_L) with the canopy depth according to the Beer-Lambert law (Monsi et al., 2005). Similarly, the coefficient for gradient of N in the canopy (K_N) is also estimated as an exponential function. Besides the light and N profile, some agronomic and physiological characteristics of the rice canopy resulting from leaf-colour modification are investigated to understand their role in enhancing rice biomass and yields.

In **Chapter 4**, the impact of leaf-colour modification on rice source-sink relationships during grain filling is examined by using a model-fitting method (Fig. 1.1). This method, derived from the determinate sigmoid growth function (Yin et al., 2003), enables the analysis of experimental data obtained through periodical sampling measurements of aboveground and panicle biomass and N accumulation. By estimating the parameters of this model, I quantify the relative importance of source and sink among diverse genetic backgrounds, and understand the role of N budgets in regulating the source capacity and sink growth after flowering. Besides, an additional field density experiment is analysed to test whether current crop cultivation practices, especially in terms of planting density, remain applicable for these leaf-colour modified genotypes.

The source-sink relations are further analysed in **Chapter 5,** specifically to study how parameters of leaf-level sink-limited photosynthesis are related to whole-plant source-sink ratios and N budget. The source-sink ratio is manipulated by three means (genotypic leaf-colour variants, panicle pruning, and adaxial vs abaxial illumination while measuring gas exchange). Altered N status is obtained by two means (N treatments and plant developmental stages) to quantify how sink-limited leaf photosynthetic carbon uptake is affected by N assimilation, possibly via the photorespiration pathway.

Chapter 6 summarises the main findings of this thesis, and provides the insights on the effects of leaf-colour modification on photosynthesis and source-sink relationships from a broad perspective. The relationships between photosynthesis and source-sink relations within the leaf and at whole-plant scale are further discussed. In the final section, implications of leaf-colour traits for crop breeding and cultivation in improving rice biomass accumulation and grain yields are also discussed.

References

Ali J, Jewel ZA, Mahender A, Anandan A, Hernandez J, Li Z. 2018. Molecular genetics and breeding for nutrient use efficiency in rice. *International Journal of Molecular Sciences* 19, 1762.

Anten NPR, Schieving F, Werger MJA. 1995. Patterns of light and nitrogen distribution in relation to whole canopy carbon gain in C_3 and C_4 mono- and dicotyledonous species. *Oecologia* 101, 504–513.

Archontoulis S V., Vos J, Yin X, Bastiaans L, Danalatos NG, Struik PC. 2011. Temporal dynamics of light and nitrogen vertical distributions in canopies of sunflower, kenaf and cynara. *Field Crops Research* 122, 186–198.

ARP WJ. 1991. Effects of source-sink relations on photosynthetic acclimation to elevated CO_2. *Plant, Cell & Environment* 14, 869–875.

Aslani L, Gholami M, Mobli M, Sabzalian MR. 2020. The influence of altered sink-source balance on the plant growth and yield of greenhouse tomato. *Physiology and Molecular Biology of Plants* 26, 2109–2123.

Blankenship RE, Tiede DM, Barber J, Sayre RT. 2011. Comparing photosynthetic and photovoltaic efficiencies and recognizing the potential for improvement. *Science* 332, 805–809.

Bloom AJ. 2015. Photorespiration and nitrate assimilation: A major intersection between plant carbon and nitrogen. *Photosynthesis Research* 123, 117–128.

Borrell AK, van Oosterom EJ, Mullet JE, George-Jaeggli B, Jordan DR, Klein PE, Hammer GL. 2014. Stay-green alleles individually enhance grain yield in sorghum under drought by modifying canopy development and water uptake patterns. *New Phytologist* 203, 817–830.

Busch FA, Sage RF, Farquhar GD. 2018. Plants increase CO_2 uptake by assimilating nitrogen via the photorespiratory pathway. *Nature Plants* 4, 46–54.

Chen X, Cui Z, Fan M, *et al.* 2014. Producingmore grain with lower environmental costs. *Nature* 514, 486–489.

Chen Y, Kong X, Dong H. 2018. Removal of early fruiting branches impacts leaf senescence and yield by altering the sink/source ratio of field-grown cotton. *Field Crops Research* 216, 10–21.

Chen Y, Xiao C, Chen X, Li Q, Zhang J, Chen F, Yuan L, Mi G. 2014. Characterization of the plant traits contributed to high grain yield and high grain nitrogen concentration in maize. *Field Crops Research* 159, 1–9.

Chiba A, Ishida H, Nishizawa NK, Makino A, Mae T. 2003. Exclusion of Ribulose-1,5-bisphosphate Carboxylase/oxygenase from Chloroplasts by Specific Bodies in Naturally Senescing Leaves of Wheat. *Plant and Cell Physiology* 44, 914–921.

Crafts-Brandner SJ, Egli DB. 1987. Sink Removal and Leaf Senescence in Soybean: Cultivar Effects. *Plant Physiology* 85, 662–666.

Dall'Osto L, Cazzaniga S, Bressan M, Paleeèk D, Židek K, Niyogi KK, Fleming GR, Zigmantas D, Bassi R. 2017. Two mechanisms for dissipation of excess light in

monomeric and trimeric light-harvesting complexes. *Nature Plants* 3, 1–9.

Deng N, Grassini P, Yang H, Huang J, Cassman KG, Peng S. 2019. Closing yield gaps for rice self-sufficiency in China. *Nature Communications* 10, 1725

Duvick DN, Smith JSC, Cooper M. 2010. Long-term selection in a commercial hybrid maize breeding program. *Plant Breeding Reviews* 24, 109–152.

Éva C, Oszvald M, Tamás L. 2019. Current and possible approaches for improving photosynthetic efficiency. *Plant Science* 280, 433–440.

Evans JR. 1989. Photosynthesis and nitrogen relationships in leaves of C_3 plants. *Oecologia* 78, 9–19.

Fabre D, Dingkuhn M, Yin X, Clément-Vidal A, Roques S, Soutiras A, Luquet D. 2020. Genotypic variation in source and sink traits affects the response of photosynthesis and growth to elevated atmospheric CO_2. *Plant, Cell & Environment* 43, 579–593.

Fabre D, Yin X, Dingkuhn M, Clément-Vidal A, Roques S, Rouan L, Soutiras A, Luquet D. 2019. Is triose phosphate utilization involved in the feedback inhibition of photosynthesis in rice under conditions of sink limitation. *Journal of Experimental Botany* 70, 5773–5785.

Gaju O, Allard V, Martre P, Le Gouis J, Moreau D, Bogard M, Hubbart S, Foulkes MJ. 2014. Nitrogen partitioning and remobilization in relation to leaf senescence, grain yield and grain nitrogen concentration in wheat cultivars. *Field Crops Research* 155, 213–223.

Gao Y, Xu Z, Zhang L, *et al.* 2020. MYB61 is regulated by GRF4 and promotes nitrogen utilization and biomass production in rice. *Nature Communications* 11, 5219.

Goudriaan J. 1995. Optimization of nitrogen distribution and of leaf area index for maximum canopy photosynthesis rate. *In: Thiyagarajan, T.M., ten Berge, H.F.M., Wopereis, M.C.S. (Eds.), Nitrogen Management Studies in Irrigated Rice. AB-DLO and TPE-WAU, SARP Research Proceedings*. pp. 85–97.

Grassini P, Eskridge KM, Cassman KG. 2013. Distinguishing between yield advances and yield plateaus in historical crop production trends. *Nature Communications* 4, 2918.

Gregersen PL, Culetic A, Boschian L, Krupinska K. 2013. Plant senescence and crop productivity. *Plant Molecular Biology* 82, 603–622.

Gu J, Zhou Z, Li Z, Chen Y, Wang Z, Zhang H. 2017a. Rice (*Oryza sativa* L.) with reduced chlorophyll content exhibit higher photosynthetic rate and efficiency, improved canopy light distribution, and greater yields than normally pigmented plants. *Field Crops Research* 200, 58–70.

Gu J, Zhou Z, Li Z, Chen Y, Wang Z, Zhang H, Yang J. 2017b. Photosynthetic properties and potentials for improvement of photosynthesis in pale green leaf rice under high light conditions. *Frontiers in Plant Science* 8, 1–14.

Harley PC, Sharkey TD. 1991. An improved model of C_3 photosynthesis at high CO_2: Reversed O_2 sensitivity explained by lack of glycerate reentry into the chloroplast. *Photosynthesis Research* 27, 169–178.

Harris GP, Griffin JE. 1961. Flower initiation in the carnation in response to photoperiod. *Nature* 191, 614–614.

Hedden P. 2003. The genes of the Green Revolution. *Trends in Genetics* 19, 5–9.

Hikosaka K. 2014. Optimal nitrogen distribution within a leaf canopy under direct and diffuse

light. *Plant, Cell & Environment* 37, 2077–2085.

Hikosaka K. 2016. Optimality of nitrogen distribution among leaves in plant canopies. *Journal of Plant Research* 129, 299–311.

Hirose T, Werger MJA. 1987. Maximizing daily canopy photosynthesis with respect to the leaf nitrogen allocation pattern in the canopy. *Oecologia* 72, 520–526.

Hisse IR, D'Andrea KE, Otegui ME. 2019. Source-sink relations and kernel weight in maize inbred lines and hybrids: Responses to contrasting nitrogen supply levels. *Field Crops Research* 230, 151–159.

Horton P. 2000. Prospects for crop improvement through the genetic manipulation of photosynthesis: Morphological and biochemical aspects of light capture. *Journal of Experimental Botany* 51, 475–485.

Hou X, Xue Q, Jessup KE, Zhang Y, Blaser B, Stewart BA, Baltensperger DD. 2021. Effect of nitrogen supply on stay-green sorghum in differing post-flowering water regimes. *Planta* 254, 1–11.

Khush GS. 1995. Breaking the yield frontier of rice. *GeoJournal* 35, 329–332.

Khush GS. 2005. What it will take to Feed 5.0 Billion Rice consumers in 2030. *Plant Molecular Biology* 59, 1–6.

Krieger-Liszkay A, Fufezan C, Trebst A. 2008. Singlet oxygen production in photosystem II and related protection mechanism. *Photosynthesis Research* 98, 551–564.

Kumar R, Bishop E, Bridges WC, Tharayil N, Sekhon RS. 2019. Sugar partitioning and source–sink interaction are key determinants of leaf senescence in maize. *Plant, Cell & Environment* 42, 2597–2611.

Lawlor DW, Lemaire G, Gastal F. 2001. Nitrogen, plant growth and crop yield. *Plant Nitrogen*. pp. 343–367.

Li T, Heuvelink E, Marcelis LFM. 2015. Quantifying the source-sink balance and carbohydrate content in three tomato cultivars. *Frontiers in Plant Science* 6, 416.

Li Y, Ren B, Gao L, Ding L, Jiang D, Xu X, Shen Q, Guo S. 2013. Less chlorophyll does not necessarily restrain light capture ability and photosynthesis in a chlorophyll-deficient rice mutant. *Journal of Agronomy and Crop Science* 199, 49–56.

Makino A, Mae T, Ohira K. 1984. Changes in photosynthetic capacity in rice leaves from emergence through senescence. Analysis from ribulose-1,5-bisphosphate carobxylase and leaf conductance. *Plant and Cell Physiology* 25, 511–521.

Makino A, Mae T, Ohira K. 1985. Photosynthesis and ribulose-1,5-bisphosphate carboxylase/oxygenase in rice leaves from emergence through senescence. Quantitative analysis by carboxylation/oxygenation and regeneration of ribulose 1,5-bisphosphate. *Planta* 166, 414–420.

Meacham K, Sirault X, Quick WP, von Caemmerer S, Furbank R. 2017. Diurnal Solar Energy Conversion and Photoprotection in Rice Canopies. *Plant Physiology* 173, 495–508.

Melis A. 2009. Solar energy conversion efficiencies in photosynthesis: Minimizing the chlorophyll antennae to maximize efficiency. *Plant Science* 177, 272–280.

Monsi M, Saeki T, Schortemeyer M. 2005. On the factor light in plant communities and its importance for matter production. *Annals of Botany* 95, 549–567.

de Mooij T, Janssen M, Cerezo-Chinarro O, Mussgnug JH, Kruse O, Ballottari M, Bassi R, Bujaldon S, Wollman FA, Wijffels RH. 2015. Antenna size reduction as a strategy to increase biomass productivity: A great potential not yet realized. *Journal of Applied Phycology* 27, 1063–1077.

Mu X, Chen Q, Chen F, Yuan L, Mi G. 2018. Dynamic remobilization of leaf nitrogen components in relation to photosynthetic rate during grain filling in maize. *Plant Physiology and Biochemistry* 129, 27–34.

Ning P, Yang L, Li C, Fritschi FB. 2018. Post-silking carbon partitioning under nitrogen deficiency revealed sink limitation of grain yield in maize. *Journal of Experimental Botany* 69, 1707–1719.

Ort DR, Zhu X, Melis A. 2011. Optimizing antenna size to maximize photosynthetic efficiency. *Plant Physiology* 155, 79–85.

Paul MJ, Driscoll SP, Lawlor DW. 1992. Sink-regulation of photosynthesis in relation to temperature in sunflower and rape. *Journal of Experimental Botany* 43, 147–153.

Pincovici S, Cochavi A, Karnieli A, Ephrath J, Rachmilevitch S. 2018. Source-sink relations of sunflower plants as affected by a parasite modifies carbon allocations and leaf traits. *Plant Science* 271, 100–107.

Qiu J. 2008. Is China ready for GM rice? In an effort to avoid a food crisis as the population grows, China is putting its weight behind genetically modified strains of the country's staple food crop. Jane Qiu explores the reasons for the unprecedented push. *Nature* 455, 850–853.

Ray DK, Mueller ND, West PC, Foley JA. 2013. Yield trends are insufficient to double global crop production by 2050. *PloS One* 8, e66428.

Rossi M, Bermudez L, Carrari F. 2015. Crop yield: Challenges from a metabolic perspective. *Current Opinion in Plant Biology* 25, 79–89.

Sage R, Sharkey T, Pearcy R. 1990. The Effect of Leaf Nitrogen and Temperature on the CO_2 Response of Photosynthesis in the C_3 Dicot MChenopodium album L. *Functional Plant Biology* 17, 135–148.

Senthilkumar K, Rodenburg J, Dieng I, *et al.* 2020. Quantifying rice yield gaps and their causes in Eastern and Southern Africa. *Journal of Agronomy and Crop Science* 206, 478–490.

Sharkey TD. 1985. Photosynthesis in intact leaves of C_3 plants: Physics, physiology and rate limitations. *The Botanical Review* 51, 53–105.

Sheehy JE, Dionora MJA, Mitchell PL, Peng S, Cassman KG, Lemaire G, Williams RL. 1998. Critical nitrogen concentrations: Implications for high-yielding rice (*Oryza sativa* L.) cultivars in the tropics. *Field Crops Research* 59, 31–41.

Shi W, Muthurajan R, Rahman H, Selvam J, Peng S, Zou Y, Jagadish KS V. 2013. Source-sink dynamics and proteomic reprogramming under elevated night temperature and their impact on rice yield and grain quality. *New Phytologist* 197, 825–837.

Sinclair TR, Horie T. 1989. Leaf Nitrogen, Photosynthesis, and Crop Radiation Use Efficiency: A Review. *Crop Science* 29, 90–98.

Sinclair TR, Rufty TW, Lewis RS. 2019. Increasing photosynthesis: Unlikely solution for world food problem. *Trends in Plant Science* 24, 1032–1039.

Slattery RA, Ort DR. 2021. Perspectives on improving light distribution and light use efficiency in crop canopies. *Plant Physiology* 185, 34–48.

Song Q, Wang Y, Qu M, Ort DR, Zhu XG. 2017. The impact of modifying photosystem antenna size on canopy photosynthetic efficiency—Development of a new canopy photosynthesis model scaling from metabolism to canopy level processes. *Plant, Cell & Environment* 40, 2946–2957.

Song Q, Zhang G, Zhu XG. 2013. Optimal crop canopy architecture to maximise canopy photosynthetic CO_2 uptake under elevated CO_2-A theoretical study using a mechanistic model of canopy photosynthesis. *Functional Plant Biology* 40, 108–124.

Sugiura D, Watanabe CKA, Betsuyaku E, Terashima I. 2017. Sink–source balance and down-regulation of photosynthesis in Raphanus sativus: Effects of grafting, N and CO_2. *Plant and Cell Physiology* 58, 2043–2056.

Takagi D, Takumi S, Hashiguchi M, Sejima T, Miyake C. 2016. Superoxide and singlet oxygen produced within the thylakoid membranes both cause photosystem I photoinhibition. *Plant Physiology* 171, 1626–1634.

Tanaka A, Fujita K. 1974. Nutrio-physiological studies on the tomato plant IV. Source-sink relationship and structure of the source-sink unit. *Soil Science and Plant Nutrition* 20, 305–315.

Thomas H, Ougham H. 2014. The stay-green trait. *Journal of Experimental Botany* 65, 3889–3900.

Tsai YC, Chen KC, Cheng TS, Lee C, Lin SH, Tung CW. 2019. Chlorophyll fluorescence analysis in diverse rice varieties reveals the positive correlation between the seedlings salt tolerance and photosynthetic efficiency. *BMC Plant Biology* 19, 1–17.

Uddling J, Gelang-Alfredsson J, Karlsson PE, Selldén G, Pleijel H. 2008. Source-sink balance of wheat determines responsiveness of grain production to increased [CO_2] and water supply. *Agriculture, Ecosystems & Environment* 127, 215–222.

Vass I, Cser K. 2009. Janus-faced charge recombinations in photosystem II photoinhibition. *Trends in Plant Science* 14, 200–205.

Walker BJ, Drewry DT, Slattery RA, VanLoocke A, Cho YB, Ort DR. 2018. Chlorophyll can be reduced in crop canopies with little penalty to photosynthesis. *Plant Physiology* 176, 1215–1232.

Wei S, Li X, Lu Z, *et al.* 2022. A transcriptional regulator that boosts grain yields and shortens the growth duration of rice. *Science* 377, eabi8455.

Wei H, Meng T, Li X, Dai Q, Zhang H, Yin X. 2018. Sink-source relationship during rice grain filling is associated with grain nitrogen concentration. *Field Crops Research* 215, 23–38.

Wissuwa M, Kretzschmar T, Rose TJ. 2016. From promise to application: root traits for enhanced nutrient capture in rice breeding. *Journal of Experimental Botany* 67, 3605–3615.

Wood CW, Reeves DW, Himelrick DG. 1993. Relationships between chlorophyll meter readings and leaf chlorophyll concentration, N status, and crop yield: A review. *In Proceedings of the Agronomy Society of New Zealand*. 23. pp. 1–9.

Xu S, Xu Y, Gong L, Zhang Q. 2016. Metabolomic prediction of yield in hybrid rice. *The Plant*

Journal 88, 219–227.

Yamamoto T, Suzuki T, Suzuki K, Adachi S, Sun J, Yano M, Ookawa T, Hirasawa T. 2017. Characterization of a genomic region that maintains chlorophyll and nitrogen contents during ripening in a high-yielding stay-green rice cultivar. *Field Crops Research* 206, 54–64.

Yang J. 2015. Approaches to achieve high grain yield and high resource use efficiency in rice. *Frontiers of Agricultural Science and Engineering* 2, 115–123.

Yang JT, Preiser AL, Li Z, Weise SE, Sharkey TD. 2016. Triose phosphate use limitation of photosynthesis: short-term and long-term effects. *Planta* 243, 687–698.

Yang J, Zhang J. 2006. Grain filling of cereals under soil drying. *New Phytologist* 169, 223–236.

Yao H, Zhang Y, Yi X, Hu Y, Luo H, Gou L, Zhang W. 2015. Plant density alters nitrogen partitioning among photosynthetic components, leaf photosynthetic capacity and photosynthetic nitrogen use efficiency in field-grown cotton. *Field Crops Research* 184, 39–49.

Yin X, Goudriaan J, Lantinga EA, Vos J, Spiertz HJ. 2003. A flexible sigmoid function of determinate growth. *Annals of Botany* 91, 361–371.

Yin X, Schapendonk AHCM, Struik PC. 2018. Exploring the optimum nitrogen partitioning to predict the acclimation of C_3 leaf photosynthesis to varying growth conditions. *Journal of Experimental Botany* 70, 2435–2447.

Yin X, Struik PC. 2015. Constraints to the potential efficiency of converting solar radiation into phytoenergy in annual crops: From leaf biochemistry to canopy physiology and crop ecology. *Journal of Experimental Botany* 66, 6535–6549.

Yuan S, Linquist BA, Wilson LT, Cassman KG, Stuart AM, Pede V, Grassini P. 2021. Sustainable intensification for a larger global rice bowl. *Nature Communications* 12, 7163.

Zhang H, Turner NC, Poole ML. 2010. Source-sink balance and manipulating sink-source relations of wheat indicate that the yield potential of wheat is sink-limited in high-rainfall zones. *Crop and Pasture Science* 61, 852–861.

Zhu X-G, Long SP, Ort DR. 2010. Improving photosynthetic efficiency for greater yield. *Annual Review of Plant Biology* 61, 235–261.

Chapter 2

Enhancing leaf photosynthesis from altered chlorophyll content requires optimal partitioning of nitrogen

Zhenxiang Zhou[1], Paul C. Struik[1], Junfei Gu[2], Peter E.L. van der Putten[1], Zhiqin Wang[2], Xinyou Yin[1] and Jianchang Yang[2]

[1] Centre for Crop Systems Analysis, Department of Plant Sciences, Wageningen University & Research, 6700 AK Wageningen, The Netherlands

[2] College of Agriculture, Yangzhou University, 48 Wenhui East Road, Yangzhou, Jiangsu 225009, China

This chapter has been published in *Crop and Environment* (2023), 2, 24−36.

Abstract

While optimising leaf chlorophyll content ([CHL]) has been proposed as a relevant means to manipulate canopy light penetration and canopy photosynthesis, effects of modifying [CHL] on leaf photosynthesis are yet to be investigated thoroughly. A greenhouse experiment and a field experiment were conducted involving rice genotypes of different genetic backgrounds and their leaf-colour variants. Leaf photosynthesis was more influenced by alteration to yellow-leaf than to stay-green cases. Higher specific leaf area and stomatal conductance were observed in two yellow-leaf variants, while only one yellow-leaf variant showed significantly increased Rubisco carboxylation capacity (V_{cmax}), maximum electron transport rate (J_{max}), and photosynthetic nitrogen-use efficiency (PNUE). Model analysis indicated that reducing leaf [CHL] decreased the energy loss via non-photochemical quenching, but improving V_{cmax}, J_{max}, and PNUE would require an improved nitrogen distribution pattern within the leaf. Label-free quantitative proteomics confirmed that an increased investment of nitrogen in Cyt b_6/f and Rubisco was observed in the yellow-leaf variant of the genetic background with improved V_{cmax}, J_{max}, and PNUE, but not in the other background. Our results suggest that reducing [CHL] can improve leaf photosynthesis only if the saved nitrogen is optimally distributed to proteins that are more rate-limiting to photosynthesis.

Keywords: Chlorophyll content, Light energy utilisation efficiency, Nitrogen partitioning, Non-photochemical quenching, *Oryza sativa*, Photosynthetic capacity

2.1 Introduction

Research on exploring ways to improve photosynthesis has never been to a standstill. Since the 1960s, stay-green, known as increased duration of greenness, has been well-established as a superior trait in extending photosynthesis (especially during grain filling) and thus improves crop yield (see review by Thomas and Ougham, 2014; also see Gregersen et al., 2013; Borrell et al., 2014). Soon afterwards, a deceptively linear relationship between nitrogen (N) content, leaf greenness and crop yield from empirical cultivation made farmers to continuously increase the input of N resources, which forced the leaf greenness into a saturated level (Wood et al., 1993; Swain and Sandip, 2010). In fact, for a long time breeders also tended to select greener leaves with the hope to improve photosynthesis (Hossain and Fischer, 1995; Khush, 1995).

Leaf greenness is determined by the concentration of chlorophyll molecules ([CHL]). Genotypes with greener leaves would mean that most of the incoming irradiance (ca. 70%) is intercepted by upper leaves in a canopy (Song et al., 2013), while lower leaves are being shaded and probably contribute less to canopy productivity. Therefore, more recently, optimising [CHL] to increase light penetration to lower layers in a canopy was proposed to improve canopy photosynthesis (Ort et al., 2011). A number of studies (Song et al., 2017; Walker et al., 2018) have explored the potential of using light-green or yellow variant genotypes in improving canopy photosynthesis. However, canopy photosynthesis is the sum of photosynthetic rates of individual leaves in the stand. While exploring the potential to improve canopy photosynthesis, one cannot bypass the impact of modifying [CHL] on leaf photosynthesis *per se*.

Theoretically, when other components are kept constant, the impact of modifying [CHL] on leaf photosynthesis can be reflected at least in two ways: (i) altered non-photochemical quenching (NPQ) due to changes in absorbed energy, and (ii) altered leaf N distribution pattern. The NPQ serving not only as one of the leaf photo-protective mechanisms but also as one of the energy decay paths, competes with photochemical processes for the light energy absorbed by leaves (Ruban, 2016). This decay path is often present when the absorbed light intensity of (greener) leaves is higher than the capacity of energy utilisation by the photosynthetic metabolisms. For C_3 plants, solar conversion efficiency is negatively correlated with irradiance, and photosynthesis may become saturated at a quarter of maximum full sunlight (Melis, 2009). Excess light will give rise to undue excitation beyond the maximal capacity for photochemical reactions in leaves, which may result in damage to Photosystem II (PSII) (Krieger-Liszkay et al., 2008; Takagi et al., 2016). Under these circumstances, it would be unwise to continue

breeding green-leaf crops for higher photosynthetic potential. Instead, making leaf colour lighter may result in lower requirement to engage NPQ for dissipating excessive energy (Melis, 2009; Kirst et al., 2017) and higher 'work efficiency' of individual chlorophyll molecules (Gilmore and Ball, 2000; Kirst et al., 2018). However, whether lighter-coloured leaves would always be associated with the alteration of NPQ, and whether the capacity of photochemical energy utilisation could be improved if less light energy is dissipated via NPQ in light-green leaves remain to be quantified.

More importantly, modifying leaf greenness provides the chance to save N from excessive [CHL] to be invested in other, more rate-limiting photosynthetic proteins. Many studies have shown that partitioning of leaf photosynthetic N (N_{photo}) among the elements of the photosynthetic apparatus is suboptimal, and the N investment in chlorophyll molecules is superfluous and can be saved for other purposes (Polle et al., 2002; Slattery et al., 2017; Walker et al., 2018). In a typical plant photosystem, only ca. 25% of the chlorophyll molecules are needed to maintain the stable operation of photosynthetic electron transport (Glick and Melis, 1988). Under high-light conditions, the energy harvested by the chlorophyll-protein complex is far more than the capacity of energy that can be utilised by the photosynthetic metabolisms. So, a lower leaf [CHL] in top leaves to lower light absorptance and NPQ may serve the purpose of optimising leaf N allocation. It is expected that a decreased leaf [CHL] might improve parameters (such as V_{cmax} - the maximum carboxylation capacity of Rubisco, and J_{max} - the maximum electron transport rate under saturated light), which often limit the top-leaf photosynthetic capacity. As a result, leaf photosynthetic nitrogen-use efficiency (PNUE) can also be expected to increase. However, so far, there is no evidence that saved N from reduced [CHL] will result in an improved photosynthetic N allocation.

Given that the concept of a reduced leaf [CHL] fundamentally differs from the traditional recommendation by crop physiologists for stay-green traits (i.e. sustaining the green colour and photosynthetic competence during later grain filling), comparing the effects of these contrasting leaf-colour traits could therefore help better explore the opportunities of further improving photosynthesis by modifying leaf [CHL]. In this study, we used four rice cultivars, in which each cultivar had been modified [CHL] to have leaves that were either yellower or greener than the control type. We intended to examine (i) the relationship between NPQ and modified [CHL]; (ii) whether modifying leaf [CHL] might improve the N partitioning and thus leaf photosynthesis; and (iii) if so, whether these effects depend on cultivar backgrounds.

2.2 Materials and Methods

2.2.1 Plant material

Our rice (*Oryza sativa* L.) materials were derived from four background groups, and each group was modified for either greener or yellower or both leaf colours, resulting in a total of nine genotypes (Table 2.1). Two groups (cv. Guanglingxiangnuo, abbreviated as "GLXN", and cv. Yandao 8, abbreviated as "YD") belonged to mid-season *japonica* rice material, of which GLXN was modified via tissue culture (a T-DNA insertion variant carrying the *Wx* gene relating to amylose content, see Liu et al., 2014) and YD was modified via radiation mutagenesis (with ^{60}Co γ-rays), to have stay-green leaves. The other two groups of rice materials were also obtained by radiation mutagenesis (with ^{60}Co γ-rays): one group of rice material (cv. Wuyunjing 3, abbreviated as "WYJ") belonged to a *japonica* type and was modified to have either greener or yellower leaves; the other group was early *indica* rice material (cv. Zhefu 802, abbreviated as "ZF") and was modified to have the yellower leaves. Resulting stay-green and yellower genotypes are marked as G and Y, respectively, while the nonmodified or default genotypes are labelled as control (C) (Table 2.1). Seeds of GLXN, YD, WYJ and their variant genotypes were from Yangzhou University, and seeds of ZF and its variant genotype were from Zhejiang

Table 2.1 Rice genotypes of four genetic backgrounds used in this study, as a result of modifying leaf chlorophyll content of the default control (C) genotype into either greener-leaf (G) or yellower-leaf (Y) variants.

Background	Genotype	Abbreviation	Characteristics
Guanglingxiangnuo	Default control	GLXN-C	a mid-season *japonica* rice cultivar with high grain quality
	Stay-green variant	GLXN-G	a form of GLXN from tissue culture with stay-green trait
Yandao 8	Default control	YD-C	a mid-season *japonica* rice cultivar
	Stay-green variant	YD-G	a radiation mutagenesis form of YD with stay-green trait
Wuyunjing 3	Default control	WYJ-C	a *japonica* rice cultivar
	Stay-green variant	WYJ-G	a radiation mutagenesis form of WYJ with stay-green trait
	Yellow-leaf variant	WYJ-Y	a radiation mutagenesis form of WYJ with yellow leaves
Zhefu 802	Default control	ZF-C	an early *indica* rice cultivar
	Yellow-leaf variant	ZF-Y	a radiation mutagenesis form of ZF with light-green leaves

University, China. Our pre-experiments, in which these genotypes were grown for several generations, have shown the stability of the G and Y variant lines.

2.2.2 Greenhouse experiment and measurements

A greenhouse compartment was conducted at Wageningen University & Research, Wageningen, the Netherlands (51°58′N, 05°40′E). Temperature was set at 26 °C (12 h day) and 23 °C (12 h night). The CO_2 level was about 400 μmol mol^{-1} and the relative humidity was set at 65%. Extra SON-T lights were switched on when incoming solar radiation intensity outside the greenhouse became less than 400 W m^{-2} and then switched off once it exceeded 500 W m^{-2}. Pre-germinated seeds of the nine genotypes were sown in porous plastic trays (filled with nutrition-rich substrate) twice, on April 10 and 17, 2019, to spread out time windows for measurement (see later). Seedlings were then transplanted to pots (24 cm in diameter and 20 cm in height, and 7 litres in volume) at the three-leaf stage with two seedlings per pot. Each pot contained 6.5 kg of sandy loam soil with 84.5 mg alkali-hydrolysable N, 6.5 mg Olsen-P, and 229.7 mg exchangeable K. All pots were placed on movable lorries according to a randomised complete block design, with three replications per genotype. One day before transplanting, 1.5 g KH_2PO_4 and 0.5 g urea per pot as basal fertiliser were pre-mixed through the soil. Extra nitrogen fertilisers were split-applied at early tillering stage (0.2 g urea per pot) and at panicle initiation stage (0.3 g urea per pot).

Photosynthesis measurements were conducted at stem-elongating (2^{nd} leaf from the top), flowering (flag leaf) and grain-filling (ca 20 days after flowering, flag leaf) stages, respectively. Pre-labelled and fully expanded leaves on the main stems of four representative plants of each genotype were chosen for measurements. An open-path gas exchange system integrated with a fluorescence chamber head (Li-Cor 6800; Li-Cor Inc., Lincoln, NE, USA) was used to simultaneously measure gas exchange and chlorophyll fluorescence parameters. All measurements were carried out at a leaf temperature of 25 °C and a leaf-to-air vapour pressure deficit between 1.0 and 1.6 kPa.

Light and CO_2 response curves were measured at the same position of the leaves. Prior to measurements of light response curves, leaves were acclimated to initial incident irradiance (I_{inc}) setting of 2,000 μmol m^{-2} s^{-1} (for ca. 30 min) until the net CO_2 assimilation rate (A) was stable. Then the automatic programming was operated with I_{inc} in the leaf cuvette in a decreasing series: 2000, 1500, 1000, 500, 280, 150, 100, 80, and 50 μmol m^{-2} s^{-1} (6~8 min per step), while keeping

ambient CO_2 level (C_a) at 400 μmol mol^{-1}. The CO_2 response curves were measured at I_{inc} of 1000 μmol m^{-2} s^{-1}, with the C_a steps: 400, 250, 150, 80, 50, 400, 400, 400, 650, 1000, and 1500 μmol mol^{-1} (3~5 min per step; but note that using the three repeated 400 μmol mol^{-1} was merely to re-adapt leaves and the data from these three points were excluded in analysis). The above two curves were measured at ambient O_2 (21%) level. To convert fluorescence-based Photosystem II (PSII) photochemical efficiency into electron transport flux, we also conducted the measurements under non-photorespiratory conditions (2% O_2 combined with C_a at 1000 μmol mol^{-1}) to establish a calibration curve (see later). The low O_2 level was realised by using a cylinder containing a gas mixture of 2% O_2 and 98% N_2. Under this circumstance, only half of the light response curve was measured with I_{inc} being 280, 150, 100, 80, and 50 μmol m^{-2} s^{-1}, to ensure that data used for calibration were within the electron transport-limited range. All gas exchange data were corrected for basal leakage of CO_2 into and out of the leaf cuvette, based on measurements on boiled leaves across the same range of CO_2 levels, and intercellular CO_2 levels (C_i) were then re-calculated. The flow rate for all measurements was 400 μmol s^{-1}.

The dark-adapted maximum fluorescence yields (F_m) were measured after the plants had been placed in the darkness for the whole night. For measurements at each irradiance or CO_2 step of the response curves, F_s (the steady-state fluorescence) was recorded after A reached the steady state. At the same time, the maximum fluorescence under light-adapted condition (F'_m) was determined using a multiphase flash method (Loriaux et al., 2013): each of the three phases went through a duration of 300 ms, and flash intensity of 6500 μmol m^{-2} s^{-1} in the second phase was attenuated by 40%. The apparent operating photochemical efficiency of PSII was derived as: $\Phi_2 = 1 - F_s/F'_m$ (Genty et al., 1989). The non-photochemical quenching (NPQ) was calculated as: $NPQ = F_m/F'_m - 1$ (Bilger and Björkman, 1990; Ruban, 2016).

All leaf segments used for photosynthesis measurements were cut out and used immediately to measure the leaf area with a Li-3100 area meter (Li-Cor, Lincoln, NE, USA), the values for SPAD using a chlorophyll meter (SPAD-502, Minolta Camera Co., Japan) and light absorptance (β) using a spectrometer (STS-VIS miniature spectrometer, Ocean Optics, USA), respectively. All leaf materials were then oven-dried at 70 °C for 48 h to constant weight. Specific leaf area (SLA) was calculated as the leaf area to leaf mass ratio. Each leaf segment was ground into powder in a 2-ml centrifuge tube, which was used to measure the N content by an element analyser based on the micro-Dumas combustion method. Specific leaf nitrogen (SLN, in g N m^{-2}) was then calculated.

2.2.3 Field experiment and measurements

A field experiment was conducted at Yangzhou University, Jiangsu Province, China (32°30′N, 119°25′E), during the rice growing season from May to November 2020. The soil used in the experiment was a sandy loam (Typic Fluvaquent, Etisols [U.S. taxonomy]) with 25.5 g kg^{-1} organic matter, 103 mg kg^{-1} alkali-hydrolysable N, 33.4 mg kg^{-1} Olsen-P, and 70.5 mg kg^{-1} exchangeable K. The seeds were first sown in the paddy seedbed field plots on May 27, 2020. The seedlings were then transplanted to the experimental field on June 23, 2020 with a hill spacing of 0.25 m × 0.16 m and two seedlings per hill. A split-plot design was used with main plots for the genetic backgrounds and split plots for genotypes in a randomised block arrangement with three replicates. The main plots were separated by ridges at a 1-m width covered by plastic film inserted in the soil at a depth of 0.5 m. Every split-plot area was 20 m^2, and, thus, the size of each main plot for the WYJ background (having three genotypes, Table 2.1) was 60 m^2 while it was 40 m^2 for each of the other three backgrounds (i.e. GLXN, YD, and ZF). For fertiliser management, N (120 kg N ha^{-1} as urea), phosphorus (30 kg ha^{-1} as single superphosphate) and potassium (40 kg ha^{-1} as KCl) as basal fertiliser were applied just before transplanting. A total of additional 120 kg N ha^{-1}, again in the form of urea, was applied at the stages of early tillering and panicle initiation (4:6). The proportions of urea application across stages were the same as in the greenhouse study.

The SPAD values and SLN data were measured as described for the greenhouse experiment. The leaf [CHL] was measured only in the field experiment, according to the method of Arnon (1949). The newly expanded leaves were ground to extract chlorophyll with 95% ethanol at 60-65 °C, and then the chlorophyll content was determined using an ultraviolet spectrophotometer (Lambda 650, PerkinElmer, USA). Maximum net photosynthesis rate at the ambient CO_2 level (A_{max}) was measured under saturated light (2,000 μmol photon m^{-2} s^{-1}) using an open-path gas exchange system (Li-Cor 6400XT; Li-Cor Inc., Lincoln, NE, USA) at flowering stage. Other environmental conditions were set as for the measurements in the greenhouse experiment.

Part of leaf materials sampled after photosynthesis measurements were stored in liquid nitrogen for proteomic measurements. A quantitative proteomic analysis was conducted, following the same procedure as described by Cui et al. (2021) and Zhou et al. (2021). This included the steps of sample preparation, protein extraction, protein extraction quality control, protein enzymatic hydrolysis, high pH reversed-phase peptide separation, DDA (data dependent acquisition) and DIA (data independent acquisition) analysis by nano-LC-MS/MS, and bioinformatics analysis.

All sample data were generated from a high-resolution mass spectrometer (Thermo Fisher Scientific, CA, USA), and protein identification was performed using a database consisting of the rice proteome, downloaded from UniProt (https://www.uniprot.org/). DDA data was identified by the Andromeda search engine within MaxQuant (V. 1.5.3.30) (Cox and Mann, 2008), and identification results were used for spectral library construction with the false discovery rate (FDR) being set at 1% for protein and peptides. For large-scale DIA data, the mProphet algorithm in Spectronaut (12.0.20491.14.21367) software was used to complete analytical quality control, thus obtaining a large number of reliable quantitative results. Statistical evaluation of significant differences in proteins or peptides was carried out using the "MSstats" package in R with its core algorithm being a linear mixed effect model. Then the significance test was performed according to the predefined comparison group. Differential protein screening was performed based on the Log_2(Foldchange) > 1 and *P*-value < 0.05 as the criterion for the significant difference. At the same time, an enrichment analysis was performed on the differential proteins.

2.2.4 Estimating photosynthesis parameters

We used the model of Farquhar, von Caemmerer and Berry (1980) ('FvCB model'; see Supplementary Appendix A) to analyse the data for net photosynthetic rate (A; see Table 2.2 for the explanation of all model symbols). Model parameters were estimated according to the step-wise procedures described by Yin et al. (2009). First, the apparent quantum efficiency of PSII electron transport under strictly limiting light (Φ_{2LL}) was estimated by extrapolating data for the light response of Φ_2 to the zero light, using the method of Yin et al. (2009). Next, a linear regression plot of electron transport-limited photosynthetic rate, A_j, against ($I_{inc}\Phi_2/4$) was made using data from limiting light under non-photorespiratory condition (NPR):

$$A_j = s\,(I_{inc}\Phi_2/4) - R_d \tag{2.1}$$

where the intercept of this linear regression provides an estimate of day respiration (R_d) (also see Yin et al. 2011) while the slope s can be used to calculate the conversion efficiency of I_{inc} into electron transport under limiting-light conditions, κ_{2LL} (see Eqn A2.3b from Supplementary Appendix A):

$$\kappa_{2LL} = s\Phi_{2LL} \tag{2.2}$$

The slope factor s of Eqn (2.1) is also as a calibration factor, with which fluorescence-based Φ_2

Table 2.2 List of model symbols and their units.

Symbol	Definition	Unit
A	Net photosynthesis rate	μmol CO_2 m^{-2} s^{-1}
A_c	Rubisco activity limited net photosynthesis rate	μmol CO_2 m^{-2} s^{-1}
A_j	Electron transport limited net photosynthesis rate	μmol CO_2 m^{-2} s^{-1}
A_p	Triose phosphate utilization limited net photosynthesis rate	μmol CO_2 m^{-2} s^{-1}
A_{max}	Maximum net photosynthesis rate under saturated light situation at ambient CO_2 level	μmol CO_2 m^{-2} s^{-1}
C_a	Ambient air CO_2 concentration	μmol mol^{-1}
C_c	Chloroplast CO_2 partial pressure	μbar
C_i	Intercellular CO_2 partial pressure	μbar
CE	Carboxylation efficiency of Rubisco, described by the initial slope of the A-C_i curve	mol m^{-2} s^{-1} bar^{-1}
F_{npq}	Fraction of the energy flow that is lost via NPQ	–
g_s	Stomatal conductance for CO_2	mol m^{-2} s^{-1}
g_m	Mesophyll diffusion conductance	mol m^{-2} s^{-1} bar^{-1}
g_{mo}	Residual mesophyll diffusion conductance in the g_m model	mol m^{-2} s^{-1} bar^{-1}
I_{inc}	Photon flux density incident to leaves	μmol photons m^{-2} s^{-1}
I_{abs}	Photon flux density absorbed by leaf photosynthetic pigments	μmol photons m^{-2} s^{-1}
I_{50}	Photon flux density incident to leaves when $J_{NPQ} = J_2$	μmol photons m^{-2} s^{-1}
J	Linear electron transport rate through PSII	μmol e^- m^{-2} s^{-1}
J_2	Rate of all (i.e. linear plus pseudocyclic) electron transport through PSII	μmol e^- m^{-2} s^{-1}
J_{NPQ}	Rate of an electron-equivalent flux through PSII used for NPQ	μmol e^- m^{-2} s^{-1}
J_{50}	Value of J when $J_{NPQ} = J_2$	μmol e^- m^{-2} s^{-1}
J_{max}	Maximum value of J under saturated light	μmol e^- m^{-2} s^{-1}
K_{mC}	Michaelis–Menten constant of Rubisco for CO_2	μbar
K_{mO}	Michaelis–Menten constant of Rubisco for O_2	mbar
O	Oxygen partial pressure	mbar
R_d	Day respiration (i.e. respiratory CO_2 release other than by photorespiration)	μmol CO_2 m^{-2} s^{-1}
s	Slope factor for linear regression of A versus $I_{inc}\Phi_2/4$ under non-photorespiratory conditions	–
s'	Slope factor for linear regression of A versus $I_{inc}\Phi_2/4$ under photorespiratory conditions	–
$S_{c/o}$	Relative CO_2/O_2 specificity factor for Rubisco	mbar μbar^{-1}
T_p	Rate of triose phosphate (TP) utilisation	μmol TP m^{-2} s^{-1}
V_{cmax}	Maximum rate of carboxylation by Rubisco	μmol CO_2 m^{-2} s^{-1}
α_2	Quantum efficiency of PSII e^- transport on the leaf pigment-absorbed light (i.e. I_{abs}) basis	mol e^- (mol photons)$^{-1}$
α_{2LL}	Value of a_2 at strictly limiting light	mol e^- (mol photons)$^{-1}$
β	Absorptance by leaf photosynthetic pigments	–
Γ_*	C_c-based CO_2 compensation point in the absence of R_d (= $0.5O/S_{c/o}$)	μbar
δ	A parameter in the g_m model	–
θ	Convexity factor for response of J to I_{inc}	–
κ_2	Conversion efficiency of incident light (i.e. I_{inc}) into J	mol e^- (mol photons)$^{-1}$
κ_{2LL}	Value of κ_2 at strictly limiting light	mol e^- (mol photons)$^{-1}$
ρ_2	Proportion of I_{abs} partitioned to PSII	–
Φ_2	Quantum efficiency of PSII e^- flow on PSII-absorbed light basis	mol e^- (mol photons)$^{-1}$
Φ_{2LL}	Value of Φ_2 at the strictly limiting light level	mol e^- (mol photons)$^{-1}$
$\Phi_{CO2LL(inc)}$	Quantum yield of CO_2 assimilation on the basis of I_{inc}	mol CO_2 (mol photons)$^{-1}$
$\Phi_{CO2LL(abs)}$	Quantum yield of CO_2 assimilation on the basis of I_{abs}	mol CO_2 (mol photons)$^{-1}$

can be converted into the potential linear electron transport rate used for CO_2 fixation and photorespiration (J) under all conditions (Yin et al. 2009):

$$J = sI_{\mathrm{inc}}\Phi_2 \tag{2.3}$$

The calculated J values along the light response curves were fitted to Eqn (A2.3b) of Supplementary Appendix A to estimate fluorescence-based J_{max} (the maximum value of J under saturated light) and the curve factor θ. When fitting Eqn (A2.3b), we found that the curvature factor θ did not vary much, and we therefore estimated a common θ (0.76) for all nine genotypes and three measurement stages. This also allowed a better comparison of parameter J_{max} among the genotypes and stages.

In order to examine whether mesophyll conductance for CO_2 diffusion (g_m) varied with I_{inc} and C_i level, a variable J method from Harley et al. (1992) was first applied to calculate g_m. This analysis showed that g_m is variable and declines with increasing C_i and decreasing I_{inc} (results not shown). Therefore, we used an equation of Yin et al. (2009) to model variable g_m: $g_m = g_{mo} + \delta\,(A + R_d)/(C_c - \Gamma_*)$, where g_{mo} represents the minimum mesophyll conductance as I_{inc} is close to zero (set to zero here according to the result of the variable J method), parameter δ is the dimensionless coefficient that can accommodate a variable-g_m mode and its value actually represents the carboxylation resistance to mesophyll resistance ratio (Yin et al., 2020), C_c is the chloroplast partial pressure of CO_2, and Γ_* is the C_c-based CO_2 compensation point in the absence of R_d. Then, this equation was combined with Eqns (A2.2) and (A2.3a), and C_c was replaced by (C_i–A/g_m) to solve for A_c (Rubisco-limited rate of net photosynthetic rate) and A_j, respectively (Yin et al., 2009):

$$A_c \text{ or } A_j = \left(-b - \sqrt{b^2 - 4ac}\right)/(2a) \tag{2.4}$$

where $a = x_2 + \Gamma_* + \delta(C_i + x_2)$

$$b = -\{(x_2 + \Gamma_*)(x_1 - R_d) + (C_i + x_2)[g_{mo}(x_2 + \Gamma_*) + \delta(x_1 - R_d)]$$

$$+\delta[x_1(C_i - \Gamma_*) - R_d(C_i + x_2)]\}$$

$$c = [g_{mo}(x_2 + \Gamma_*) + \delta(x_1 - R_d)][x_1(C_i - \Gamma_*) - R_d(C_i + x_2)]$$

with $x_1 = \begin{cases} V_{cmax} & \text{for } A_c \\ J/4 & \text{for } A_j \end{cases}$

$$x_2 = \begin{cases} K_{\mathrm{mC}}(1 + O/K_{\mathrm{mO}}) & \text{for } A_{\mathrm{c}} \\ 2\Gamma_* & \text{for } A_{\mathrm{j}} \end{cases}$$

To avoid overfitting, δ was calculated beforehand using data from the A_j-limited range (i.e. both low I_{inc} range of light response curves and high C_i range of CO_2-response curves), by combining Eqn (2.4) with Eqn (2.3). Then, J_{max}, V_{cmax}, and T_p (the rate of triose phosphate utilisation) can be estimated simultaneously by fitting combined Eqn (A2.1), Eqn (A2.3b), Eqn (A2.4), and Eqn (2.4) to all CO_2 exchange data. For all these analyses, we used the values of Rubisco parameters measured at 25 °C by Cousins et al. (2010): i.e. 3.022 mbar μbar^{-1} for $S_{c/o}$ (the relative CO_2/O_2 specificity factor for Rubisco), 291 µbar for K_{mC} (Michaelis-Menten constant of Rubisco for CO_2) and 194 mbar for K_{mO} (Michaelis-Menten constant of Rubisco for O_2), given that values of these Rubisco parameters are believed to be conserved among C_3 species (von Caemmerer, 2000).

2.2.5 Quantifying energy levels for non-photochemical quenching

The commonly used fluorescence parameter NPQ [$= F_m/F'_m - 1$] can indicate a magnitude of thermal dissipation; however, this parameter can go up to high values of > 1.0, which is not conducive to quantifying the relative share of energy by NPQ vs photochemistry (Hendrickson et al., 2004). Here, to better quantify the relative energy loss primarily via NPQ, we propose an alternative way as described below, using the measured Φ_2. If there were no thermal dissipation, one would expect that the total PSII electron flux (J_2) increases linearly with increasing absorbed irradiance (I_{abs}) and then J_2 would be expressed as $\rho_2 I_{abs} \Phi_{2LL}$, where ρ_2 is the partitioning factor of I_{abs} to PSII, and combined $\rho_2 \Phi_{2LL}$ may also be denoted as the PSII electron transport efficiency based on light absorbed by both photosystems (α_{2LL}). As Φ_2 decreases with increasing I_{abs}, the difference between $\rho_2 I_{abs} \Phi_{2LL}$ and $\rho_2 I_{abs} \Phi_2$ must be the electron-equivalent flux of energy dissipated as NPQ (J_{NPQ}) (See Fig. S2.1a). Then the fraction of the energy that is lost via NPQ (F_{npq}) can be expressed relative to $\rho_2 I_{abs} \Phi_{2LL}$, which can be simplified to:

$$F_{\mathrm{npq}} = \frac{J_{\mathrm{NPQ}}}{\rho_2 I_{\mathrm{abs}} \Phi_{2\mathrm{LL}}} = \frac{\rho_2 I_{\mathrm{abs}} \Phi_{2\mathrm{LL}} - \rho_2 I_{\mathrm{abs}} \Phi_2}{\rho_2 I_{\mathrm{abs}} \Phi_{2\mathrm{LL}}} = 1 - \frac{\Phi_2}{\Phi_{2\mathrm{LL}}} \quad (2.5)$$

Unlike the fluorescence parameter NPQ, values of F_{npq} are within the range between 0 and 1. Similar to the method of Hendrickson et al. (2004), Eqn (2.5) quantifies the relative partitioning of excitation energy between photochemistry and thermal dissipation. The third (but small) share of energy lost by fluorescence, which is shown to be quite constant (ca 0.25) across light

levels (Hendrickson et al., 2004), is only implicitly accounted for via parameter Φ_{2LL} in Eqn (2.5), whose value was ca 0.70-0.75 for our genotypes (Table 2.3). Because Eqn (2.5) uses the strictly limiting light level as a departure point (Fig. S2.1a), it does not require F_m (the dark-adapted maximum fluorescence yield) to calculate F_{npq}; but, as shown later, the obtained F_{npq} gives similar patterns of response to the light level as NPQ.

It is useful to calculate the incident-irradiance level at which the energy flux lost via NPQ (J_{NPQ}) is equal to total PSII electron flux (J_2), i.e. the point where 50% of the absorbed light energy is consumed by PSII electron transport and NPQ each (Fig. S2.1b). We denote this point of incident-irradiance as I_{50} and the corresponding J_2 as J_{50}. Values of I_{50} and J_{50} are commonly solved from fitting additional empirical quadratic equations for both J_{NPQ} and PSII electron flux (Meacham et al., 2017). We found introducing additional empirical equations unnecessary, and I_{50} and J_{50} can be calculated from earlier estimated parameter values of Eqn (A2.3b) of the 'FvCB model':

$$\begin{cases} I_{50} = \frac{2J_{\max}}{(2-\theta)\kappa_{2LL}} \\ J_{50} = \frac{J_{\max}}{2-\theta} \end{cases} \quad (2.6)$$

The derivation of Eqn (2.6) is given in Supplementary Appendix B.

2.2.6 Estimation of quantum yield of leaf photosynthesis

The quantum yield for leaf CO_2 assimilation under limiting light conditions (Φ_{CO2LL}) was calculated on the basis of either incident or absorbed irradiance, according to the method described by Yin et al. (2014):

$$\begin{cases} \Phi_{CO2LL(inc)} = s'\Phi_{2LL}/4 \\ \Phi_{CO2LL(abs)} = s'\Phi_{2LL}/(4\beta) \end{cases} \quad (2.7)$$

where Φ_{2LL} is Φ_2 at the irradiances approaching to zero, which can be estimated as earlier described, and s' is the linear slope factor of regressing A against ($\Phi_2 I_{inc}/4$). Mathematically s' is equal to $s[(C_c - \Gamma_*)/(C_c + 2\Gamma_*)]$ (Yin et al., 2014). For non-photorespiratory conditions, parameter s' is equal to the above-mentioned calibration factor s. This method overcomes the error of the conventional quantum yield estimating method that assumes a constant Φ_2 over the irradiance range used to estimate Φ_{CO2LL}.

2.2.7 Statistical analyses and curve fitting

Simple linear regressions were conducted using Microsoft Excel. Non-linear regressions were performed using the Gauss method in PROC NLIN of SAS (SAS Institute Inc., Cary, NC, USA). Significance of differences was assessed based on one-way analysis of variance (ANOVA) and least significant difference (LSD) test. The photosynthesis parameters were estimated by using pooled data of three or four replicates from gas exchange and chlorophyll fluorescence, which in fact are close to the mean of replicated estimates but have better statistical predictions of all data points than the mean. Therefore, no significant-difference tests were applied in these estimated photosynthesis parameters (Table 2.3).

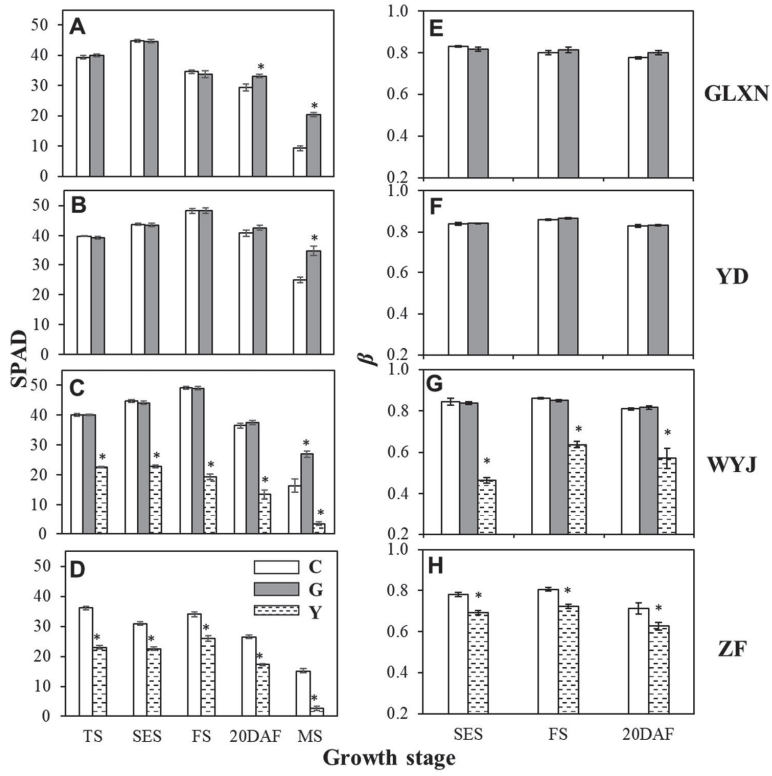

Fig. 2.1 Changes of leaf SPAD (A-D) and leaf light absorptance (β, E-H) for four rice control (C) genotypes and their greener-leaf variants (G) or yellower-leaf variants (Y) at different stages: tillering stage (TS), stem-elongating stage (SES), flowering stage (FS), 20 d after flowering (20DAF), and maturity stage (MS). Vertical bars ± standard errors represent the means of four replicates. The asterisks (*) indicate statistical significance at the $P < 0.05$ level between variant genotype and its control genotype within a given stage. Genotype-background abbreviations - GLXN: cv. Guanglingxiangnuo; YD: cv. Yandao 8; WYJ: cv. Wuyunjing 3; and ZF: cv. Zhefu 802.

2.3 Results

2.3.1 Altered leaf chlorophyll content of variant genotypes

In the field experiment, we measured both [CHL] and SPAD for all genotypes, which were positively correlated ($R^2 = 0.99$) (Fig. S2.2a). Data obtained from the greenhouse experiment showed that leaf absorptance (β) was hyperbolically related to SPAD (Fig. S2.2b), in a shape similar to the function that Evans (1996) described for the correlation between β and [CHL]. These observations together suggest that SPAD values of leaves can reflect the trend of [CHL]. Moreover, the similar trends of SPAD (Fig. S2.2c) and of A_{max} (Fig. S2.3) in the greenhouse experiment and the field experiment indicated that the character of altered [CHL] had been well maintained across the environments. Visual images of leaf colour differences among genotypes from the greenhouse experiment can be found in Fig. S2.4.

For the greenhouse experiment, there were no significant differences between stay-green genotype variants (G) and their control genotypes (C) in terms of SPAD value and β, except for the former at post-flowering stages when the stay-green genotypes began to exhibit the delayed senescence of leaves (Fig. 2.1A-D). For yellow-leaf genotype variants (Y), however, a significant drop in SPAD was observed with, on average, 57.4% and 28.5% decrease for WYJ and ZF background, respectively, across stages. Similar patterns were shown in β between Y variants and their C genotypes (Fig. 2.1E-H); β declined much more in WYJ-Y than in ZF-Y across the stages.

2.3.2 Proportions of energy for non-photochemical quenching

The two G genotypes showed higher NPQ than their C genotypes, particularly in GLXN based on either I_{inc} or I_{abs} (Fig. 2.2A-H). Fig. 2.2I-P show values of F_{npq} calculated using Eqn (2.5). The response curve of F_{npq} for each G genotype almost coincided with its C counterpart (Fig. 2.2I-K). Like their NPQ values, values of F_{npq} were lower in Y genotypes than in other genotypes, when plotted against I_{inc}. When plotted against I_{abs}, curves of F_{npq} for three genotypes from the WYJ background almost overlapped, but the Y genotype from the ZF background still had lower F_{npq} than its C counterpart (Fig. 2.2O-P).

Fig. 2.2I-L also describes an equilibrium state of dissipation and photochemical energy utilisation at the flowering stage, calculated by Eqn (2.6). There were variations in I_{50} or J_{50}, beyond which J_{NPQ} started to exceed J_2 and to become dominant. Compared with the slight differences between G and C, there were more significant differences between Y and C genotypes. The I_{50} values increased significantly in both Y materials, compared with their C. For J_{50}, the Y genotypes of two backgrounds showed different trends relative to their C counterparts. There was a slight decrease (4%) in J_{50} of WYJ-Y whereas ZF-Y showed a large increase (80%) in J_{50}.

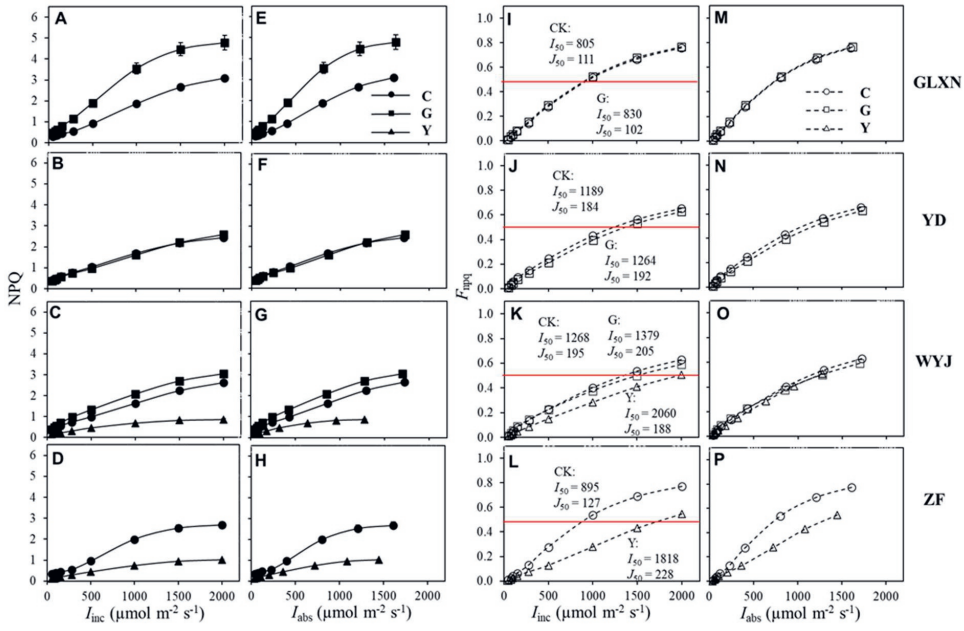

Fig. 2.2 The response curves of NPQ (A-H) and F_{npq} (I-P) for four rice control (C, circle) genotypes and their greener-leaf variants (G, square) or yellower-leaf variants (Y, triangle) at flowering stage based on incident light (I_{inc}) or absorbed light (I_{abs}). Each data point from the NPQ response curve (represented by filled symbols with continuous curves) is the mean value of three or four replicates (± standard errors). The curves of F_{npq} (represented by open symbols with dotted curves) were drawn using Eqn (2.5). The red horizontal line in panels I-L is the line that F_{npq} = 0.5, whose intersection points with the curves correspond to the incident light level (I_{50}), at which the absorbed light energy is equally used between NPQ and driving electron transport, i.e. $J_2 = J_{NPQ}$ (see Fig. S2.1b). Values of I_{50} (μmol m^{-2} s^{-1}) and its corresponding potential e^- transport rate J_{50} (μmol m^{-2} s^{-1}), calculated by Eqn (2.6), are given. Genotype-background abbreviations - GLXN: cv. Guanglingxiangnuo; YD: cv. Yandao 8; WYJ: cv. Wuyunjing 3; and ZF: cv. Zhefu 802.

2.3.3 Photosynthetic characteristics derived from response curves

Light response curves of *A* measured in the greenhouse experiment for different stages are given in Fig. 2.3. Since the stay-green variants did not yet begin to manifest themselves, there were slight differences in *A* between G and C genotypes. Under saturated light intensity, GLXN showed a slightly lower *A* in G than in C while YD had slightly increased *A* in G over C genotypes. By comparison, a completely different effect of Y variants was noted between WYJ and ZF backgrounds. *A* in WYJ-Y was much lower than that in WYJ-C under high I_{inc}, whereas the difference was opposite between ZF-Y and ZF-C. If *A* is plotted against I_{abs}, the curves for

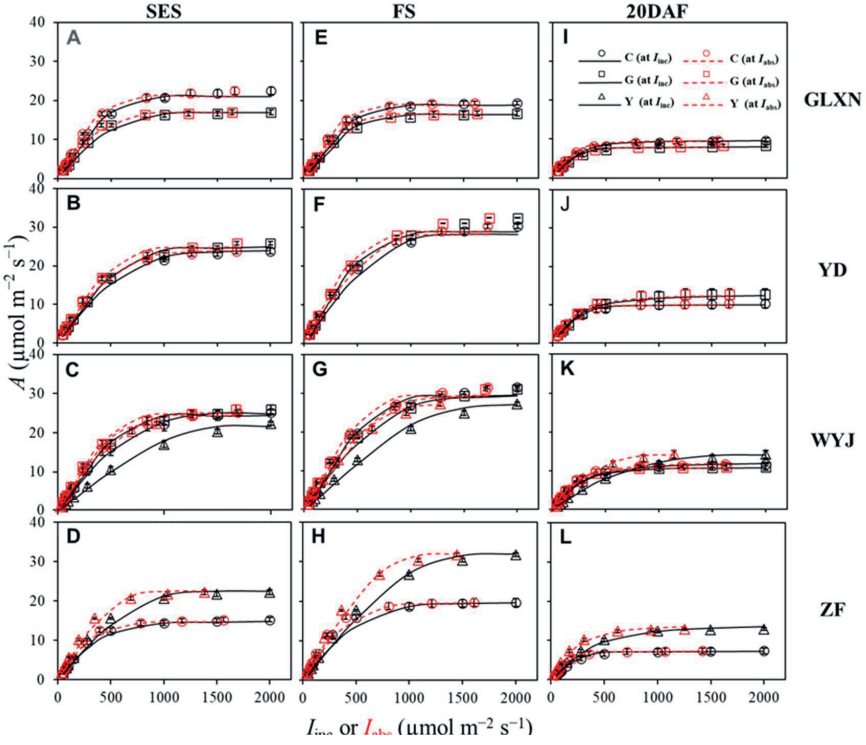

Fig. 2.3 The response curves of photosynthesis (*A*) for four rice control (C, circle) genotypes and their greener-leaf variants (G, square) or yellower-leaf variants (Y, triangle) (GLXN: A, E, I; YD: B, F, J; WYJ: C, G, K; ZF: D, H, L) at stem-elongating stage (SES, A-D), flowering stage (FS, E-H), and 20 d after flowering (20DAF, I-L), based on I_{inc} (black symbols and continuous curves) or I_{abs} (red symbols and dotted curves) under CO_2 concentration of 400 μmol mol^{-1}. Data (represented by different symbols) are shown as means of three or four replicates (± standard errors) for each genotype. The curves were drawn from using fitted parameter values of Eqn (2.4). Genotype-background abbreviations - GLXN: cv. Guanglingxiangnuo; YD: cv. Yandao 8; WYJ: cv. Wuyunjing 3; and ZF: cv. Zhefu 802.

WYJ-Y and WYJ-C almost overlapped while the advantage of ZF-Y under high light levels was maintained. This indicated that the difference between WYJ-Y and WYJ-C can predominantly be attributed to the difference in β, whereas for the ZF background, the effect of the Y variant involved additional mechanisms. A similar difference between variant genotype and its control genotype was observed from their CO_2 response curves (Fig. 2.4).

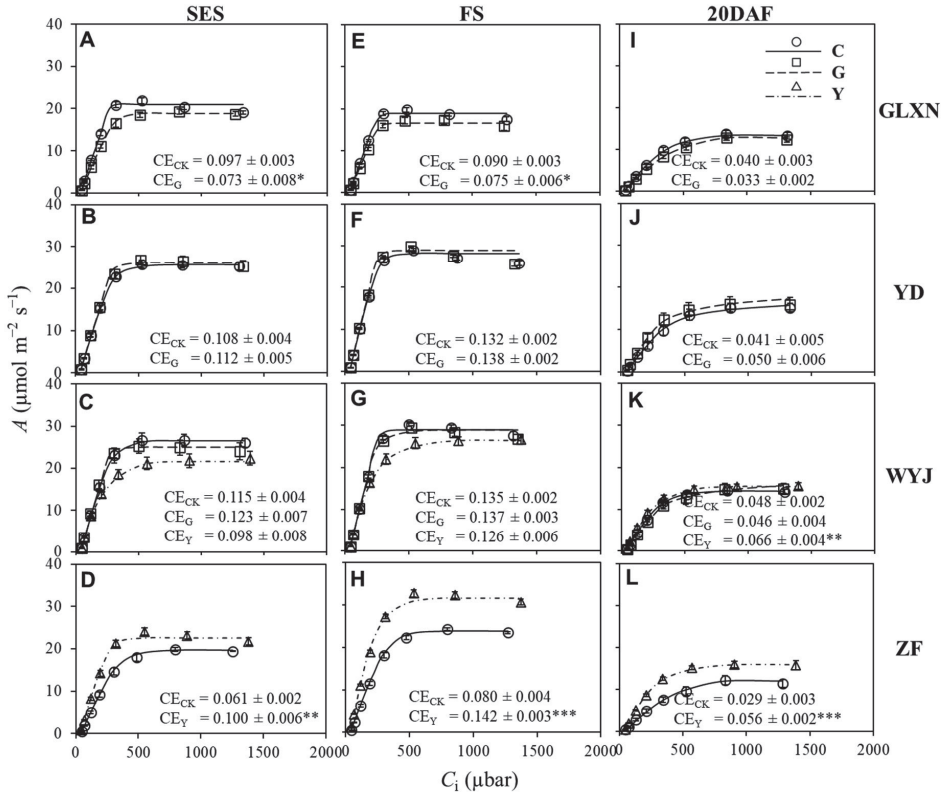

Fig. 2.4 The CO_2 response curves for four rice control (C, circle) genotypes and their greener-leaf variants (G, square) or yellower-leaf variants (Y, triangle) (GLXN: A, E, I; YD: B, F, J; WYJ: C, G, K; ZF: D, H, L) at stem-elongating stage (SES, A-D), flowering stage (FS, E-H), and 20 d after flowering (20DAF, I-L) under light intensity of 1000 μmol m^{-2} s^{-1}. Apparent carboxylation efficiency (CE, mol m^{-2} s^{-1} bar^{-1}) was calculated as the initial slope of the CO_2 response curve as listed in each panel. The word "apparent" is used here because the initial slope also includes a component of mesophyll conductance (see Fig. 2.6). A significant difference between variant genotype and its control genotype in CE is shown by asterisks: * $P < 0.05$, ** $P < 0.01$, *** $P < 0.001$. Data (represented by different symbols) are shown as means of three or four replicates (± standard errors) for each genotype. The curves were drawn from using fitted parameter values of Eqn (2.4). Genotype-background abbreviations - GLXN: cv. Guanglingxiangnuo; YD: cv. Yandao 8; WYJ: cv. Wuyunjing 3; and ZF: cv. Zhefu 802.

The estimated photosynthetic parameters for these genotypes at three stages are shown in Table 2.3. There were no significant differences between variants and their control genotypes at any stage for parameter R_d ($P > 0.05$). There were negligible differences in the efficiency of converting irradiance into electron transport (κ_{2LL}) and photosynthetic capacity parameters (i.e. J_{max}, V_{cmax}, and T_p) for G genotypes, but larger differences were found between Y and C genotypes. Compared with the C genotypes, parameters Φ_{2LL} and s were lower in Y materials, and as a result, κ_{2LL} derived from Eqn (2.2) decreased by ca. 40% and 10% in WYJ-Y and ZF-Y, respectively. The WYJ-Y demonstrated no apparent change in J_{max} and V_{cmax} but a decline occurred in T_p at stem-elongating and flowering stages. However, for the ZF-Y genotype, simultaneous improvements in J_{max}, V_{cmax} and T_p were observed with an average increase by 61%, 69%, and 26%, respectively, across the three stages. In addition, the apparent carboxylation efficiency (CE) of ZF-Y also increased significantly (Fig. 2.4), suggesting a possibly improved Rubisco activity.

Stomatal conductance (g_s) was little affected in G variants except for some variations in GLXN at stem-elongating stage, while a greater impact was observed in Y variants due to significantly increased g_s relative to the C (Table 2.4). Both GLXN-G and WYJ-Y had a significantly lower mesophyll conductance (g_m) at stem-elongating and flowering stages, but a higher g_m was observed in YD-G. Notably, ZF-Y maintained the higher g_m at all stages.

2.3.4 Photosynthetic nitrogen distribution pattern

Since SPAD increased proportionally with the increase of [CHL] (Fig. S2.2a), we calculated the ratio of each of the earlier estimated photosynthesis parameters to the SPAD value as indicators of these parameters per unit [CHL] (Table S2.1). A large increase in the ratios were found in both Y genotypes at all stages, suggesting a change in the relative N investment between light-harvesting complex and other photosynthetic proteins.

Uniprot ID	GLXN	YD	WYJ		ZF		
	G-vs-C	G-vs-C	G-vs-C	Y-vs-C	Y-vs-C		
P12331	-0.2420	0.5768	0.2456	-2.0001	-1.0766	Lhcb1	Photosystem II
Q10HD0	-0.7174	0.3301	0.1291	-2.8031	-0.4196	Lhcb2	
A3BL59	-0.8704	0.5867	-0.0657	-3.1804	-0.7351	Lhcb3	
Q0D5I4	-0.1174	0.6355	0.0446	-2.7484	-1.0470	Lhcb4	
A3CA44	-0.6874	0.4175	0.1217	-1.6199	-0.3082	Lhcb5	
Q0JCQ4	-0.8256	0.3863	-0.1261	-2.3349	-0.2060	Lhcb6	
P0C434	-0.0990	0.6497	-0.2602	-0.9274	-0.5135	PsbA	
P0C437	-0.8898	1.0468	-0.2160	-0.2333	0.2750	PsbD	
P0C364	-0.0270	0.5830	-0.0766	-0.6974	-0.4527	PsbB	
A0A0P0WWB9	-2.1490	0.3844	-1.9131	-2.8264	-0.4724	Lhca1	Photosystem I
A0A0P0X812	-1.0799	0.1334	-1.7069	-3.7381	-0.6059	Lhca2	
A3A460	-2.2421	0.3073	-1.6763	-3.3090	-0.6427	Lhca3	
A3BTG2	NA	0.0849	-2.8658	-4.1452	-0.4813	Lhca4	
P0C355	0.2214	0.7943	0.0285	-1.7501	-1.5910	PsaA	
P0C358	-1.8618	1.2141	-0.2188	-1.4393	-0.2533	PsaB	
P0C389	-0.0149	0.2230	-0.0905	-0.6174	0.2763	PetA	Cytochrome b6/f complex
P12123	-1.0687	0.3261	-0.0517	-0.5080	0.6134	PetB	
Q69S39	-1.5072	-0.2666	-0.5107	-0.2797	1.5697	PetC	
P12124	-1.5589	0.5868	-0.2746	-0.2008	0.4788	PQ	Photosynthetic electron transport
Q0DFC9	0.0297	0.1545	-0.6023	-1.1007	0.0060	PC	
A0A5S6R7Q0	0.4484	-0.6733	0.6449	0.0046	-0.7291	Fd	
P41344	0.2106	0.1300	0.0504	-0.2456	-0.1499	FNR1	
Q6ZFJ3	0.1311	-0.2645	0.0091	-0.5180	-0.2987	FNR2	
P12085	0.0960	-0.0231	-0.1747	-0.5486	-0.3247	beta	F-type ATPase
P0C2Z6	0.0995	0.5413	-0.0233	-0.4137	-0.6764	alpha	
Q0D641	0.0430	0.6261	0.0337	-0.3134	-0.8762	gamma	
Q6Z8K7	-0.7172	-0.5954	-0.8154	0.0702	0.7837	delta	
P0C2Z3	-0.1321	0.1435	-0.2142	-0.3450	0.1460	epsilon	
P0C2Z0	-0.8140	1.0271	-0.5358	-0.8163	0.2693	b	
P0C512	0.1499	0.2331	0.0127	-0.3252	-0.0940	rbcL	Rubisco related proteins
Q0DB64	2.9939	2.3313	0.2112	-0.5387	3.2524	rbcL	
Q0IPF7	-0.1394	-0.2988	-0.4041	0.0232	0.0000	rbcL	
Q339G9	0.2065	0.6013	0.8805	-0.0370	0.1494	rbcL	
P18566	-0.8209	0.7299	-0.2722	0.0114	1.1706	rbcS	
Q2QTK0	-1.4176	0.5931	-0.8418	-0.5177	1.7170	rbcS	
P93431	-0.2906	-0.3306	-0.1482	-0.4034	0.2521	RCA	
H2KVX3	-0.4159	-0.0271	-0.4086	-0.4122	0.5939	RCA	
A2ZVV8	-0.1979	0.5308	-0.2663	0.4069	0.6330	CA	

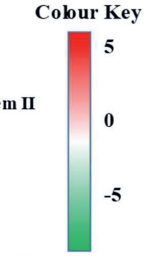

Fig. 2.5 Heat map of proteins of photosynthesis in four rice control (C) genotypes and their greener-leaf variants (G) or yellower-leaf variants (Y) at flowering stage. Each column represents a comparison group (i.e. variant genotype vs control genotype), and each row represents a protein with its uniprot ID listed on the left. The Log_2(Foldchange) value of the protein was shown in a heat map in different colours, with red representing up-regulation and green representing down-regulation. Significant difference existed when log_2(Foldchange) > 1. NA means the protein of sample was not detected. Protein abbreviations on the right: Lhcb1-6, chlorophyll a-b binding proteins in the light-harvesting complex of Photosystem II (LHCII); PsbA, D1 protein of Photosystem II; PsbD, D2 protein of Photosystem II; PsbB, cp47 reaction centre protein of Photosystem II; Lhca1-4, chlorophyll a-b binding proteins in the light-harvesting complex of Photosystem I (LHCI); PsaA, P700 chlorophyll a apoprotein A1 of Photosystem I; PsaB, P700 chlorophyll a apoprotein A2 of Photosystem I; PetA-C, components of the cytochrome b_6/f complex (cyt b_6/f); PQ, NAD(P)H-quinone oxidoreductase subunit; PC, Plastocyanin; Fd, Ferredoxin; FNR1-2, Ferredoxin-NADP reductase; beta, alpha, gamma, delta, epsilon, and b are ATP synthase subunits; rbcL, Ribulose bisphosphate carboxylase large chain; rbcS, Ribulose bisphosphate carboxylase small chain; RCA, Rubisco activase; CA, carbonic anhydrase. Genotype-background abbreviations - GLXN: cv. Guanglingxiangnuo; YD: cv. Yandao 8; WYJ: cv. Wuyunjing 3; and ZF: cv. Zhefu 802.

The leaf N partitioning to photosynthetic proteins was further assessed with the relative abundance of photosynthetic proteins as shown in a heatmap via a proteomic enrichment analysis (Fig. 2.5). For the stay-green case, the relative expression of most photosynthetic proteins in the YD background was slightly increased while an opposite trend was observed in GLXN background. There was almost no difference of these photosynthetic proteins in WYJ-G compared with its C, except for a downregulation in Lhca1-4 involved in Photosystem I (PSI). For the yellow-leaf case, both Y genotypes showed a lower relative abundance of light-harvesting proteins (Lhcb1-6 and Lhca1-4 from PSII and PSI, respectively), with a much more significant decline in WYJ than in ZF. In addition, other photosynthetic proteins did not change much in WYJ-Y. However, ZF-Y notably increased the relative abundance of Cytochrome b_6/f complex (Cyt b_6/f) and Rubisco related proteins.

Following the proteomic data format, we calculated the relative changes of Rubisco carboxylation activity from the CE derived from A-C_i curves. There was a positive correlation between relative Rubisco content from proteomic data and relative Rubisco carboxylation activity from gas exchange data (Fig. 2.6).

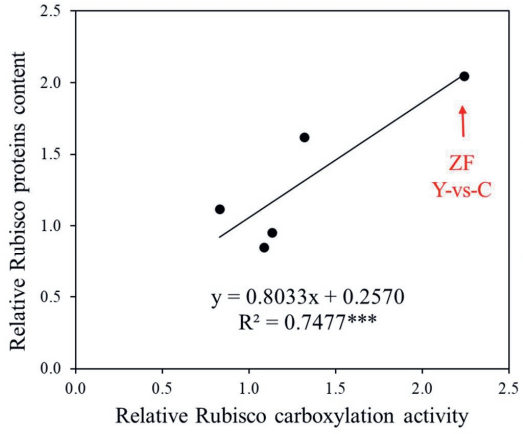

Fig. 2.6 Relationship between relative Rubisco proteins content and relative Rubisco carboxylation activity. Linear regression was fitted for overall data with its significance of correlation shown by asterisks: *** $P < 0.001$.

Note: The relative Rubisco protein content was obtained by averaging the back-calculated relative contents (from proteomics data in Fig. 2.5 for $\log_2$(Foldchange)) of all the subunits of Rubisco protein from each comparison group (i.e. variant genotype vs control genotype). The relative Rubisco carboxylation activity was calculated from the residual Rubisco carboxylation resistance, which is ($1/CE - 1/g_m$) according to the method described in Yin et al. (2009), where CE is carboxylation efficiency (mol m^{-2} s^{-1} bar^{-1}) calculated as the initial slope of the photosynthetic CO_2 response curve (see Fig. 2.4), and g_m is mesophyll diffusion conductance (mol m^{-2} s^{-1} bar^{-1}) calculated based on Eqn (2.4) at C_i*, the C_i-based CO_2 compensation point in the absence of R_d. Then the relative Rubisco carboxylation activity shown in the X-axis can be calculated as the ratio of [$1/(1/CE - 1/g_m)$] of the variant genotype to that of its control genotype.

Table 2.3 Values (standard errors of estimate in brackets if applicable) of photosynthetic parameters for four rice control (C) genotypes and their greener-leaf variants (G) or yellower-leaf variants (Y) at three stages. Genotypes codes are explained in Table 2.1. Parameter definitions and units are given in Table 2.2 or in the text. δ was estimated from the data of the A_j-limited part of both A-I_{inc} and A-C_i curves, i.e. low I_{inc} range of light response curves: 150, 100, 80, and 50 μmol m^{-2} s^{-1} for both 21% O_2 and 2% O_2 and high C_a range of CO_2 response curve: 650, 1000, and 1500 μmol mol^{-1}. J_{max}, V_{cmax}, and T_p were estimated from gas exchange data only based on pre-calculated δ by the g_m model.

Stage	Background	Genotype	FvCB model parameters						Other parameters	
			R_d	κ_{2LL}	δ [a]	J_{max}	V_{cmax}	T_p	Φ_{2LL}	s
Stem-elongating	GLXN	C	0.758	0.296	0.944 (0.060)	155.3 (3.6)	131.9 (5.3)	7.2 (0.08)	0.731 (0.006)	0.405 (0.006)
		G	0.612	0.258		135.1 (4.1)	101.8 (2.8)	6.5 (0.14)	0.728 (0.008)	0.354 (0.006)
	YD	C	0.673	0.280		171.1 (4.2)	139.5 (2.7)	8.7 (0.14)	0.696 (0.012)	0.403 (0.005)
		G	0.706	0.297		195.4 (4.6)	145.6 (2.1)	9.0 (0.14)	0.717 (0.007)	0.414 (0.010)
	WYJ	C	0.982	0.274		201.1 (5.1)	153.6 (2.9)	9.2 (0.14)	0.615 (0.035)	0.446 (0.015)
		G	0.790	0.275		202.1 (5.2)	150.0 (2.7)	8.5 (0.12)	0.704 (0.013)	0.391 (0.013)
		Y	0.824	0.154		203.3 (9.1)	153.8 (27.9)	7.5 (0.11)	0.594 (0.013)	0.259 (0.007)
	ZF	C	0.629	0.266		120.8 (4.2)	90.1 (2.1)	6.7 (0.18)	0.710 (0.005)	0.375 (0.006)
		Y	0.740	0.235		169.4 (4.2)	137.2 (4.1)	7.7 (0.11)	0.691 (0.007)	0.341 (0.005)
Flowering	GLXN	C	0.643	0.276	0.788 (0.056)	137.8 (5.0)	130.9 (4.2)	6.4 (0.09)	0.730 (0.005)	0.378 (0.009)
		G	0.468	0.246		126.4 (5.2)	114.0 (4.1)	5.7 (0.09)	0.711 (0.008)	0.346 (0.007)
	YD	C	0.769	0.310		228.4 (6.5)	193.8 (6.2)	9.7 (0.10)	0.673 (0.013)	0.461 (0.011)
		G	0.902	0.304		238.4 (6.8)	203.2 (6.3)	9.9 (0.09)	0.688 (0.003)	0.443 (0.009)
	WYJ	C	0.674	0.307		241.4 (6.9)	201.4 (5.2)	9.9 (0.09)	0.713 (0.006)	0.431 (0.004)
		G	0.883	0.298		254.5 (7.8)	198.2 (6.3)	9.9 (0.10)	0.708 (0.004)	0.421 (0.004)
		Y	0.757	0.182		232.8 (10.8)	200.9 (29.8)	9.0 (0.10)	0.619 (0.009)	0.294 (0.007)
	ZF	C	0.753	0.284		157.7 (5.4)	126.9 (2.8)	8.2 (0.16)	0.714 (0.007)	0.398 (0.005)
		Y	1.025	0.251		282.5 (9.8)	217.8 (11.9)	10.9 (0.10)	0.698 (0.004)	0.360 (0.004)
20 d after flowering	GLXN	C	0.557	0.246	1.200 (0.072)	70.0 (2.0)	48.6 (1.4)	4.5 (0.14)	0.725 (0.013)	0.339 (0.006)
		G	0.380	0.231		64.2 (2.1)	40.2 (1.3)	4.3 (0.20)	0.733 (0.020)	0.315 (0.006)
	YD	C	0.612	0.257		81.7 (2.1)	51.8 (1.4)	5.4 (0.23)	0.683 (0.027)	0.377 (0.012)
		G	0.531	0.282		96.0 (1.7)	65.5 (4.0)	5.4 (0.14)	0.675 (0.035)	0.418 (0.004)
	WYJ	C	0.464	0.252		80.7 (1.6)	62.9 (3.0)	4.8 (0.14)	0.703 (0.009)	0.359 (0.010)
		G	0.382	0.246		81.0 (2.0)	54.9 (1.5)	5.1 (0.20)	0.720 (0.011)	0.341 (0.010)
		Y	0.497	0.131		104.2 (2.8)	72.7 (2.5)	5.3 (0.16)	0.627 (0.020)	0.210 (0.013)
	ZF	C	0.486	0.204		58.7 (2.0)	37.1 (1.3)	4.2 (0.13)	0.650 (0.027)	0.314 (0.008)
		Y	0.576	0.188		95.4 (2.2)	67.7 (4.5)	5.4 (0.16)	0.680 (0.009)	0.277 (0.007)

[a] the estimate δ did not vary significantly among genotypes within each stage, so a common value was estimated for a given stage (see the text).

2.3.5 Leaf morphological traits and photosynthetic nitrogen-use efficiency

The specific leaf area (SLA) was little affected in G variants, but SLA was significantly higher in Y variants than in the C (Table 2.4). Similarly, there was no remarkable difference in specific leaf nitrogen (SLN) between G and C (Table 2.4). No consistent change in SLN across stages was found in WYJ-Y compared with its C, while SLN of ZF-Y was always higher than that of C at three stages with a significant effect shown after flowering. The variation in SLN, either across genotypes or across stages, was positively correlated with the A_{max} value ($R^2 = 0.89$) as shown in Fig. 2.7 – the plot that gives an estimate of base leaf nitrogen $n_b = 0.23$ g N m^{-2}. Based on this n_b, we calculated the values for photosynthetic nitrogen-use efficiency (PNUE) at a light intensity of 2000 μmol m^{-2} s^{-1} and a CO_2 level of 400 μmol mol^{-1}. As expected from the linear relation between A_{max} and SLN, most genotypes did not show a significant difference in PNUE, except for a decrease in GLXN-G (at stem-elongating and grain-filling stages) and WYJ-Y (at grain-filling stage) compared with their C genotypes. Conversely, despite some increase in SLN, the PNUE of ZF-Y had still been improved significantly at all stages.

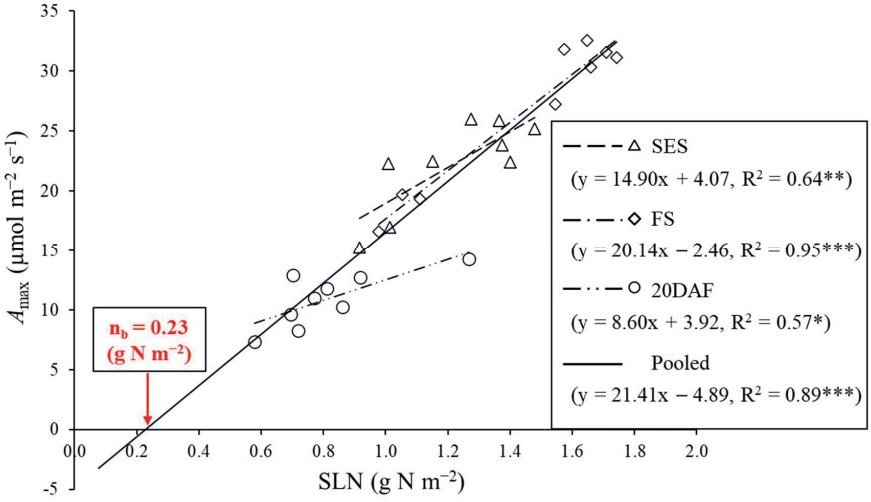

Fig. 2.7 Relationship between maximum photosynthesis rate (A_{max}) and specific leaf nitrogen (SLN). Data represented by different open shapes are from three stages (i.e. SES, stem-elongating stage; FS, flowering stage; 20DAF, 20 d after flowering) in greenhouse experiment. Each point represents the mean of three or four replicates. Linear regressions were fitted for data for each stage and for pooled data, with the significance shown by asterisks (* $P < 0.05$, ** $P < 0.01$, *** $P < 0.001$). The extrapolation of the regression for the pooled data gave an estimate of the base leaf N for photosynthesis (n_b).

Table 2.4 CO_2 diffusion parameters, specific leaf area (SLA, $m^2\ kg^{-1}$), specific leaf nitrogen (SLN, g N m^{-2}), and leaf photosynthetic nitrogen-use efficiency (PNUE, μmol $CO_2\ g^{-1}$ N s^{-1}) for four rice control (C) genotypes and their greener-leaf variants (G) or yellower-leaf variants (Y) at three stages.

Stage	Background	Genotype	g_s[a]	g_m[a]	SLA	SLN	PNUE[b]
Stem-elongating	GLXN	C	0.370 (0.028)	0.161 (0.006)	22.9 (0.20)	1.15 (0.02)	24.3 (0.76)
		G	**0.260 (0.015)***	**0.125 (0.005)***	23.5 (0.35)	**1.01 (0.03)***	**21.7 (0.84)***
	YD	C	0.401 (0.033)	0.169 (0.006)	26.4 (0.53)	1.37 (0.04)	20.8 (0.64)
		G	0.367 (0.030)	**0.192 (0.007)***	25.9 (0.74)	1.36 (0.08)	23.2 (1.86)
	WYJ	C	0.334 (0.006)	0.190 (0.007)	27.1 (1.24)	1.48 (0.06)	20.3 (1.21)
		G	0.346 (0.030)	0.195 (0.007)	26.4 (1.17)	**1.27 (0.05)***	**24.9 (1.20)***
		Y	**0.433 (0.045)***	**0.155 (0.005)***	**30.8 (0.28)***	1.40 (0.03)	19.2 (0.79)
	ZF	C	0.208 (0.023)	0.113 (0.004)	21.7 (0.72)	0.92 (0.03)	21.5 (0.79)
		Y	**0.442 (0.032)***	**0.154 (0.007)***	**28.7 (0.99)***	1.01 (0.06)	**29.1 (1.73)***
Flowering	GLXN	C	0.227 (0.015)	0.138 (0.003)	21.9 (0.32)	1.11 (0.03)	21.9 (0.47)
		G	0.203 (0.015)	**0.117 (0.005)***	22.2 (0.43)	**0.98 (0.05)***	22.2 (0.71)
	YD	C	0.516 (0.021)	0.204 (0.005)	23.4 (0.36)	1.66 (0.05)	21.3 (1.00)
		G	0.508 (0.012)	**0.227 (0.001)***	22.5 (0.54)	1.65 (0.02)	22.9 (0.43)
	WYJ	C	0.421 (0.031)	0.224 (0.002)	22.5 (0.65)	1.71 (0.05)	21.4 (1.00)
		G	0.451 (0.020)	0.218 (0.003)	23.3 (0.46)	1.74 (0.01)	20.6 (0.33)
		Y	**0.529 (0.024)***	**0.176 (0.004)***	**26.2 (0.46)***	**1.54 (0.06)***	20.8 (1.07)
	ZF	C	0.299 (0.019)	0.132 (0.007)	21.3 (0.39)	1.05 (0.03)	21.3 (0.63)
		Y	**0.583 (0.021)***	**0.214 (0.005)***	**24.0 (0.64)***	**1.57 (0.02)***	**23.6 (0.36)***
20 d after flowering	GLXN	C	0.191 (0.023)	0.073 (0.006)	22.6 (0.37)	0.69 (0.05)	21.0 (0.84)
		G	0.168 (0.009)	0.062 (0.003)	21.8 (0.36)	0.72 (0.02)	**17.0 (0.80)***
	YD	C	0.188 (0.018)	0.079 (0.008)	27.4 (0.67)	0.86 (0.05)	16.4 (1.81)
		G	0.226 (0.027)	0.100 (0.013)	26.7 (0.55)	0.92 (0.03)	18.3 (1.49)
	WYJ	C	0.190 (0.015)	0.092 (0.005)	27.2 (0.52)	0.81 (0.03)	20.3 (0.56)
		G	0.209 (0.033)	0.083 (0.006)	28.5 (1.15)	0.77 (0.04)	20.5 (1.58)
		Y	**0.284 (0.025)***	0.110 (0.005)	28.1 (0.93)	**1.27 (0.04)***	**13.8 (1.40)***
	ZF	C	0.150 (0.017)	0.056 (0.006)	20.4 (0.55)	0.58 (0.03)	19.9 (2.00)
		Y	**0.375 (0.061)***	**0.094 (0.002)***	**26.4 (0.99)***	**0.70 (0.01)***	**27.3 (1.17)***

[a] g_s refers to stomatal conductance for CO_2 diffusion, while g_m was derived from the fitted model, both for a light intensity of 2000 μmol $m^{-2}\ s^{-1}$ and a CO_2 concentration of 400 μmol mol^{-1};

[b] leaf photosynthetic nitrogen-use efficiency (PNUE) was defined as: $\text{PNUE} = \frac{A_{max}}{\text{SLN} - n_b}$, where A_{max} is the maximum net photosynthesis rate at a light intensity of 2000 μmol $m^{-2}\ s^{-1}$ and a CO_2 concentration of 400 μmol mol^{-1}, and n_b represents a base leaf nitrogen content; here an estimate of 0.23 g N m^{-2} for n_b was used (see Fig. 2.7).

Data (mean with standard error of three or four replicates in brackets) of a variant genotype significantly different from those of its control genotype (* $P < 0.05$) are shown in **bold**.

2.4 Discussion

2.4.1 Negligible impact of stay-green variants prior to the maturity stage

The G genotypes presented delays in chlorophyll catabolism only when the plants were approaching maturity, as shown by the SPAD values (Fig. 2.1A-D). Across all the earlier stages, there were negligible differences between G and C genotypes in leaf absorptance β (Fig. 2.1E-H), photosynthetic capacity (i.e. J_{max}, V_{cmax}, and T_p, Table 2.3), and even PNUE (Table 2.4). Such a result was also found in stay-green genotypes of other species, like wheat (Chen et al., 2010) and maize (Zheng et al., 2009). These results are not surprising given that stay-green traits are mainly meant to sustain leaf photosynthetic competence during later grain filling (Gregersen et al., 2013; Borrell et al., 2014). It is worthwhile to study whether the stay-green traits indeed delay declines in photosynthesis or just are cosmetic phenotypes, when approaching maturity.

2.4.2 Impact of restrained light-absorptance ability in yellow-leaf variants

Given the hyperbolic relation between β and SPAD (Fig. S2.2), the Y variants impacted leaf light-absorptance ability throughout the entire crop cycle with decreased SPAD values (Fig. 2.1A-D) and light-harvesting proteins (Fig. 2.5). Rotasperti et al. (2022) reported that the barley mutant with decreased leaf SPAD and truncated antenna size increased photosynthetic efficiency but this is not a universal case. Excessive suppression of β would be detrimental for plants in limiting-light environments (Ort et al., 2011). In our study, the average decline in leaf β of WYJ-Y was triple that of ZF-Y across the three stages, relative to their C genotypes (Fig. 2.1G-H). Overly reduced β values in WYJ-Y led to reduced photosynthetic parameters (s and Φ_{2LL}), which strongly decreased irradiance-to-electron conversion efficiency (i.e. κ_{2LL}, Table 2.3) and the quantum yield of photosynthesis (Table S2.2). By contrast, ZF-Y was less affected in this respect. Besides, the photosynthetic difference between Y and C in the WYJ background was mainly due to reduced β given the overlapping light response curves based on I_{abs} (Fig. 2.3) and similar photosynthetic capacity parameters (Table 2.3) when excluding the effects of leaf SLN. In addition, modifying leaf [CHL] changed not only light harvesting and resultant physiology, but also leaf morphology, as shown by the significantly increased SLA of Y variants (Table 2.4). This impact of restrained β on SLA could be analogous to the commonly observed thin leaves when plants grow under low-light conditions (Evans and Poorter, 2001). Xiao et al.

(2016) also showed that the leaf anatomical features, especially those controlling the light distribution inside a leaf, can influence the β value of a leaf.

2.4.3 Shift in balance between thermal dissipation and photochemical energy utilisation

Similar to previous reports (Li et al., 2013; Gu et al., 2017a,b), our results (Fig. 2.2A-H) for differences in either G or Y variants relative to C were observed for NPQ using conventional calculation, i.e. [= $F_m/F'_m - 1$], indicating the potential of thermal dissipation for variants was altered. However, as mentioned earlier, these calculated NPQ values can go beyond 1.0, which is not handy to evaluate the relative consumption of absorbed energy between NPQ and photochemistry. So, derived from the actual photochemical efficiency of PSII, F_{npq} is proposed (see Eqn 2.5) to describe the actual relative energy loss due to NPQ under fluctuating light environment (Fig. 2.2I-P). The method follows a similar consideration as Hendrickson et al. (2004) discussed – the relative energy loss via NPQ is presented by a value between 0 and 1, and the absolute energy loss primarily via NPQ was presented as an electron-equivalent flux (J_{NPQ}), which competed with the total PSII electron flux (J_2) (see Fig. S2.1b). With this method, we found that the difference in F_{npq} between G and C almost disappeared based on either I_{inc} or I_{abs}, indicating the distribution pattern of absorbed energy between J_2 and J_{NPQ} was not changed by G variants. The same result was found for WYJ-Y although a small deviation from the F_{npq} curve between WYJ-Y and WYJ-C under I_{inc} was caused by β. In contrast, ZF-Y had a lower F_{npq} compared with its C genotype, suggesting an increased energy demand for photosynthetic metabolisms.

The intersection point (I_{50}, J_{50}) of J_2 and J_{NPQ} curves represents a balance of coordination between photochemical reactions and the thermal dissipation (Gilmore et al., 1996). Based on the 'FvCB model', Eqn (2.6) was derived from estimated photosynthetic parameters, which not only avoids additional empirical equations applied in the analysis of Meacham et al. (2017), but also prevents an uncertain assumption made by Hendrickson (2004) and Meacham et al. (2017) that the proportion of I_{abs} partitioned to PSII is 0.5. Our formulae for the balance point (I_{50}, J_{50}) could be used for screening genotypes with greater potentials for improved light use efficiency. Through calculating this balance point, we examined the genotypic variation after modifying [CHL]. Both I_{50} were much higher in Y than in C genotypes (Fig. 2.2K-L), suggesting an enhanced high-light tolerance in Y genotypes. But only ZF-Y showed an increase in J_{50}, indicating an elevated energy utilisation efficiency. Our result suggests that manipulation of leaf

[CHL] alone could exert a certain influence on the light energy distribution between J_2 and J_{NPQ} by adjusting β, but it does not necessarily result in an improved energy use competence in leaves. Therefore, we concluded that only by improving the capacity of photochemical energy utilisation can the share of light energy allocated to NPQ be substantially reduced.

2.4.4 Dependence of nitrogen distribution strategy on genetic background

The positive correlation between SLN and A_{max} (Fig. 2.7) indicated that photosynthesis was mainly determined by leaf N content across either genotypes or stages, but when SLN was similar, variation in A_{max} among the same genetic background can be explained by different N investment patterns. There was a higher 'work efficiency' per unit [CHL] in Y variants than in control genotypes (Table S2.1). Among the two genetic backgrounds having the Y-variants, only the Y genotype from the ZF background showed an improved leaf N partitioning with higher photosynthetic capacity parameter values (i.e. J_{max}, V_{cmax}, and T_p) (Table 2.3) and increased protein expression levels of Cyt b_6/f and Rubisco (Fig. 2.5), compared with its control. A significant correlation as shown in Fig. 2.6 confirmed that higher Rubisco activity in the ZF-Y genotype came from more nitrogen investment in Rubisco-related proteins. Although leaf SLN of ZF-Y was increased obviously after stem-elongating stage, the significant increase in PNUE still confirmed the existence of this improvement (Table 2.4).

However, the process of improving N allocation was not observed in WYJ-Y. Given that both Y genotypes reduced N input to light-harvesting complexes (Fig. 2.5), where did the conserved N in WYJ-Y go? Medlyn (1996) suggested that leaf photosynthetic N content can be divided into four rate-limiting pools (i.e. chlorophyll, the electron transport system, Rubisco, and other soluble proteins). The four pools compete with each other for N in response to environmental changes (Yin et al., 2019). So the N resources saved from [CHL] in WYJ-Y are likely distributed over other soluble proteins that are not determining A_{max}, as no significant differences in components of the electron transport system and Rubisco were observed by our model- and proteomic-analysis (Table 2.3; Fig. 2.5). But photosynthetic N content generally differs among leaves and accounts for 50% ~80% of total leaf N content in C_3 plants (Makino and Osmond, 1991; Hikosaka and Terashima, 1995). The leaf N allocated to photosynthesis-independent organelles or cell walls (Evans and Clarke, 2019) may have been the investment route for conserved N in the leaves of WYJ-Y. Any increased investment on respiration-related processes cannot explain this as R_d was even lower in WYJ-Y than in WYJ-C (Table 2.3). Possible outlets concerning the saved N in WYJ-Y and whether the difference in photosynthetic

behaviours between WYJ-Y and ZF-Y was due to genetic background would need more studies to elucidate.

2.5 Concluding remarks

Altering leaf chlorophyll content can affect the photosynthetic physiology of the whole leaf. Overall, the G variants had little impact on photosynthesis until a very late stage towards maturity while larger effects were observed on Y variants due to significantly reduced [CHL]: increased SLA, g_s, and high-light tolerance in Y variants, compared with their controls. Moreover, reducing [CHL] can prevent excessive absorption of solar radiation energy, resulting in little need to operate NPQ (i.e. low F_{npq}), but the key to change the inherent energy use mode is to translate the reduced NPQ into the energy demand of photochemical quenching by an increased photosynthetic capacity. Of the two Y variants analysed in this study, only ZF-Y showed a leaf N partitioning with improved photosynthetic capacity parameters (i.e. J_{max}, V_{cmax}, and T_p) and increased protein expression levels of Cyt b_6/f and Rubisco. Thus, both A_{max} and PNUE of ZF-Y were improved under saturated I_{inc}. The difference between WYJ-Y and ZF-Y might reflect the effect of genetic background, and the impact as observed in ZF is desirable as the Y variant from ZF background had advantages in photosynthesis under high-light environments. The results of our ZF materials confirmed the feasibility of reducing [CHL] of leaves coupled with distributing saved N into more beneficial investments on proteins that determine V_{cmax} and J_{max}. This provides a direction for breeding programmes or genetic engineering to improve leaf photosynthesis.

Acknowledgements

Z.Z. thanks the China Scholar Council (CSC) for funding his PhD fellowship. We thank Dr. Changquan Zhang (Yangzhou University) and Prof. Fangmin Cheng (Zhejiang University) for providing seeds used in this study.

References

Arnon D. 1949. Copper enzymes in isolated chloroplasts. Polyphenol oxidase in Beta vulgaris. *Plant Physiology* 24, 1.

Bilger W, Björkman O. 1990. Role of the xanthophyll cycle in photoprotection elucidated by measurements of light-induced absorbance changes, fluorescence and photosynthesis in leaves of Hedera canariensis. *Photosynthesis Research* 25, 173−185.

Borrell AK, van Oosterom EJ, Mullet JE, George-Jaeggli B, Jordan DR, Klein PE, Hammer GL. 2014. Stay-green alleles individually enhance grain yield in sorghum under drought by modifying canopy development and water uptake patterns. *New Phytologist* 203, 817−830.

von Caemmerer S. 2000. Biochemical models of leaf photosynthesis. *CSIRO Publishing*.

Chen J, Liang Y, Hu X, Wang X, Tan F, Zhang H, Ren Z, Luo P. 2010. Physiological characterization of "stay green" wheat cultivars during the grain filling stage under field growing conditions. *Acta Physiologiae Plantarum* 32, 875−882.

Cousins AB, Ghannoum O, Von Caemmerer S, Badger MR. 2010. Simultaneous determination of Rubisco carboxylase and oxygenase kinetic parameters in Triticum aestivum and Zea mays using membrane inlet mass spectrometry. *Plant, Cell & Environment* 33, 444−452.

Cox J, Mann M. 2008. MaxQuant enables high peptide identification rates, individualized ppb-range mass accuracies and proteome-wide protein quantification. *Nature Biotechnology* 26, 1367−1372.

Cui C, Wang Z, Su Y, Wang T. 2021. New insight into the rapid growth of the Mikania micrantha stem based on DIA proteomic and RNA-Seq analysis. *Journal of Proteomics* 236, 104126.

Evans JR. 1996. Developmental constraints on photosynthesis: effects of light and nutrition. *Photosynthesis and the Environment, Springer. Dordrecht*. 281−304.

Evans JR, Clarke VC. 2019. The nitrogen cost of photosynthesis. *Journal of Experimental Botany* 70, 7−15.

Evans J, Poorter H. 2001. Photosynthetic acclimation of plants to growth irradiance: the relative importance of specific leaf area and nitrogen partitioning in maximizing carbon gain. *Plant, Cell & Environment* 24, 755−767.

Farquhar GD, von Caemmerer SV, Berry JA. 1980. A biochemical model of photosynthetic CO_2 assimilation in leaves of C_3 species. *Planta* 149, 78−90.

Genty B, Briantais JM, Baker NR. 1989. The relationship between the quantum yield of photosynthetic electron transport and quenching of chlorophyll fluorescence. *Biochimica et Biophysica Acta (BBA)-General Subjects* 990, 87−92.

Gilmore AM, Hazlett TL, Debrunner PG, Govindjee. 1996. Comparative time-resolved photosystem II chlorophyll a fluorescence analyses reveal distinctive differences between photoinhibitory reaction centre damage and xanthophyll cycle-dependent energy dissipation. *Photochemistry and Photobiology* 64, 552−563.

Gilmore AM, Ball MC. 2000. Protection and storage of chlorophyll in overwintering evergreens. *Proceedings of the National Academy of Sciences* 97, 11098−11101.

Glick RE, Melis A. 1988. Minimum photosynthetic unit size in system I and system II of barley chloroplasts. *Biochimica et Biophysica Acta (BBA)-Bioenergetics* 934, 151−155.

Gregersen PL, Culetic A, Boschian L, Krupinska K. 2013. Plant senescence and crop productivity. *Plant Molecular Biology* 82, 603−622.

Gu J, Zhou Z, Li Z, Chen Y, Wang Z, Zhang H. 2017a. Rice (*Oryza sativa* L.) with reduced chlorophyll content exhibit higher photosynthetic rate and efficiency, improved canopy light distribution, and greater yields than normally pigmented plants. *Field Crops Research* 200, 58−70.

Gu J, Zhou Z, Li Z, Chen Y, Wang Z, Zhang H, Yang J. 2017b. Photosynthetic properties and potentials for improvement of photosynthesis in pale green leaf rice under high light conditions. *Frontiers in Plant Science* 8, 1082.

Harley PC, Loreto F, Di Marco G, Sharkey TD. 1992. Theoretical considerations when estimating the mesophyll conductance to CO_2 flux by analysis of the response of photosynthesis to CO_2. *Plant Physiology* 98, 1429−1436.

Hendrickson L, Furbank RT, Chow WS. 2004. A simple alternative approach to assessing the fate of absorbed light energy using chlorophyll fluorescence. *Photosynthesis research* 82, 73−81.

Hikosaka K, Terashima I. 1995. A model of the acclimation of photosynthesis in the leaves of C_3 plants to sun and shade with respect to nitrogen use. *Plant, Cell & Environment* 18, 605−618.

Hossain M, Fischer KS. 1995. Rice research for food security and sustainable agricultural development in Asia: achievements and future challenges. *GeoJournal* 35, 286−298.

Khush GS. 1995. Breaking the yield frontier of rice. *GeoJournal* 35, 329−332.

Kirst H, Gabilly ST, Niyogi KK, Lemaux PG, Melis A. 2017. Photosynthetic antenna engineering to improve crop yields. *Planta* 245, 1009−1020.

Kirst H, Shen Y, Vamvaka E, Betterle N, Xu D, Warek U, Strickland J, Melis A. 2018. Downregulation of the CpSRP43 gene expression confers a truncated light-harvesting antenna (TLA) and enhances biomass and leaf-to-stem ratio in Nicotiana tabacum canopies. *Planta* 248, 139−154.

Krieger-Liszkay A, Fufezan C, Trebst A. 2008. Singlet oxygen production in photosystem II and related protection mechanism. *Photosynthesis Research* 98, 551−564.

Li Y, Ren B, Gao L, Ding L, Jiang D, Xu X, Shen Q, Guo S. 2013. Less chlorophyll does not necessarily restrain light capture ability and photosynthesis in a chlorophyll-deficient rice mutant. *Journal of Agronomy and Crop Science* 199, 49−56.

Liu D, Wang W, Cai X. 2014. Modulation of amylose content by structure-based modification of Os GBSS 1 activity in rice (*Oryza sativa* L.). *Plant Biotechnology Journal* 12, 1297−1307.

Loriaux SD, Avenson TJ, Welles JM, McDermitt DK, Eckles RD, Riensche B, Genty B. 2013. Closing in on maximum yield of chlorophyll fluorescence using a single multiphase flash of sub-saturating intensity. *Plant, Cell & Environment* 36, 1755−1770.

Makino A, Osmond B. 1991. Effects of nitrogen nutrition on nitrogen partitioning between chloroplasts and mitochondria in pea and wheat. *Plant Physiology* 96, 355−362.

Meacham K, Sirault X, Quick WP, von Caemmerer S, Furbank R. 2017. Diurnal solar energy conversion and photoprotection in rice canopies. *Plant Physiology* 173, 495−508.

Medlyn BE. 1996. The optimal allocation of nitrogen within the C_3 photosynthetic system at elevated CO_2. *Functional Plant Biology* 23, 593−603.

Melis A. 2009. Solar energy conversion efficiencies in photosynthesis: minimizing the chlorophyll antennae to maximize efficiency. *Plant Science* 177, 272−280.

Ort DR, Zhu X, Melis A. 2011. Optimizing antenna size to maximize photosynthetic efficiency. *Plant Physiology* 155, 79−85.

Polle JE, Kanakagiri S, Jin E, Masuda T, Melis A. 2002. Truncated chlorophyll antenna size of the photosystems—a practical method to improve microalgal productivity and hydrogen production in mass culture. *International Journal of Hydrogen Energy* 27, 1257−1264.

Rotasperti L, Tadini L, Chiara M, Crosatti C, Guerra D, Tagliani A, Forlani S, Ezquer I, Horner D, Hahns P, Gajek K, Pesaresi P. 2022. The barley mutant happy under the sun 1 (hus1): an additional contribution to pale green crops. *Environmental and Experimental Botany* 196, 104795.

Ruban AV. 2016. Nonphotochemical chlorophyll fluorescence quenching: mechanism and effectiveness in protecting plants from photodamage. *Plant Physiology* 170, 1903−1916.

Slattery RA, VanLoocke A, Bernacchi CJ, Zhu X, Ort DR. 2017. Photosynthesis, light use efficiency, and yield of reduced-chlorophyll soybean mutants in field conditions. *Frontiers in Plant Science* 8, 549.

Song Q, Zhang G, Zhu XG. 2013. Optimal crop canopy architecture to maximisecanopy photosynthetic CO_2 uptake under elevated CO_2–a theoretical studyusing a mechanistic model of canopy photosynthesis. *Functional Plant Biology* 40, 108–124.

Song Q, Wang Y, Qu M, Ort DR, Zhu XG. 2017. The impact of modifying photosystem antenna size on canopy photosynthetic efficiency—Development of a new canopy photosynthesis model scaling from metabolism to canopy level processes. *Plant, Cell & Environment* 40, 2946−2957.

Swain DK, Sandip SJ. 2010. Development of SPAD values of medium-and long-duration rice variety for site-specific nitrogen management. *Journal of Agronomy* 9, 38−44.

Takagi D, Takumi S, Hashiguchi M, Sejima T, Miyake C. 2016. Superoxide and singlet oxygen produced within the thylakoid membranes both cause photosystem I photoinhibition. *Plant Physiology* 171, 1626−1634.

Thomas H, Ougham H. 2014. The stay-green trait. *Journal of Experimental Botany* 65, 3889−3900.

Walker BJ, Drewry DT, Slattery RA, VanLoocke A, Cho YB, Ort DR. 2018. Chlorophyll can be reduced in crop canopies with little penalty to photosynthesis. *Plant Physiology* 176, 1215−1232.

Wood CW, Reeves DW, Himelrick DG. 1993. Relationships between chlorophyll meter readings and leaf chlorophyll concentration, N status, and crop yield: a review. *Proceedings of the Agronomy Society of New Zealand* 23, 1−9.

Yin X, Belay DW, van der Putten PEL, Struik PC. 2014. Accounting for the decrease of photosystem photochemical efficiency with increasing irradiance to estimate quantum yield of leaf photosynthesis. *Photosynthesis Research* 122, 323−335.

Yin X, van der Putten PEL, Belay D, Struik PC. 2020. Using photorespiratory oxygen response

to analyse leaf mesophyll resistance. *Photosynthesis Research* 144, 85−99.

Yin X, Schapendonk AH, Struik PC. 2019. Exploring the optimum nitrogen partitioning to predict the acclimation of C_3 leaf photosynthesis to varying growth conditions. *Journal of Experimental Botany* 70, 2435−2447.

Yin X, Struik PC, Romero P, Harbinson J, Evers JB, van der Putten PEL, Vos J. 2009. Using combined measurements of gas exchange and chlorophyll fluorescence to estimate parameters of a biochemical C_3 photosynthesis model: a critical appraisal and a new integrated approach applied to leaves in a wheat (Triticum aestivum) canopy. *Plant, Cell & Environment* 32, 448−464.

Yin X, Sun Z, Struik PC, Gu J. 2011. Evaluating a new method to estimate the rate of leaf respiration in the light by analysis of combined gas exchange and chlorophyll fluorescence measurements. *Journal of Experimental Botany* 62, 3489−3499.

Zheng HJ, Wu AZ, Zheng CC, Wang YF, Cai R, Shen XF, Xu RR, Liu P, Kong LJ, Dong ST. 2009. QTL mapping of maize (Zea mays) stay-green traits and their relationship to yield. *Plant Breeding* 128, 54−62.

Zhou Y, Tan Z, Xue P, Wang Y, Li X, Guan F. 2021. High-throughput, in-depth and estimated absolute quantification of plasma proteome using data-independent acquisition/mass spectrometry (“HIAP-DIA”). *Proteomics* 21, 2000264.

Supplementary Appendix A in Chapter 2

The Farquhar-von Caemmerer-Berry model for photosynthesis

The 'FvCB model' (Farquhar et al., 1980), as modified by Sharkey (1985), expresses net photosynthetic rate (A) as the minimum of the Rubisco carboxylation-limited rate (A_c), electron transport limited rate (A_j), and the triose phosphate utilisation limited rate (A_p):

$$A = \min(A_c, A_j, A_p) \quad \text{(A2.1)}$$

For the A_c-limited part: $$A_c = \frac{(C_c - \Gamma_*)V_{cmax}}{C_c + K_{mC}(1 + O/K_{mO})} - R_d \quad \text{(A2.2)}$$

where C_c and O are the chloroplast partial pressures of CO_2 and O_2, respectively. V_{cmax} is the maximum rate of Rubisco activity for carboxylation, while K_{mC} and K_{mO} are Michaelis-Menten constants of Rubisco for CO_2 and O_2, respectively. Γ_* is the CO_2 compensation point in the absence of day respiration (R_d), described by: $\Gamma_* = 0.5O/S_{c/o}$, where $S_{c/o}$ is the relative CO_2/O_2 specificity factor for Rubisco.

For the A_j-limited part: $$A_j = \frac{(C_c - \Gamma_*)J}{4(C_c + 2\Gamma_*)} - R_d \quad \text{(A2.3a)}$$

where J is the potential noncyclic PSII electron transport rate used for CO_2 fixation and photorespiration; it can be calculated as a function of incident light (I_{inc}):

$$J = \left[\kappa_{2LL} I_{inc} + J_{max} - \sqrt{(\kappa_{2LL} I_{inc} + J_{max})^2 - 4\theta J_{max} \kappa_{2LL} I_{inc}}\right] / (2\theta) \quad \text{(A2.3b)}$$

where J_{max} is the maximum value of J under saturated light; κ_{2LL} represents the conversion efficiency of incident light into J at strictly limiting light; θ is a dimensionless convexity factor for the response of J to I_{inc}.

For the A_p-limited part: $$A_P = 3T_P - R_d \quad \text{(A2.4)}$$

where T_P is the rate of triose phosphate utilisation.

Supplementary Appendix B in Chapter 2

Derivation of Eqn (2.6) in the main text

As shown in Figure S2.1a, J_{NPQ} (electron-equivalent flux for NPQ) can be expressed as:

$$J_{\mathrm{NPQ}} = \alpha_{2\mathrm{LL}} I_{\mathrm{abs}} - J_2 \tag{B2.1}$$

where I_{abs} is the irradiance absorbed by the two photosystems, α_{2LL} is the electron transport efficiency of PSII on the basis of irradiance absorbed by both photosystems under strictly limiting light conditions, and J_2 is the total electron flux passing through PSII, which can be expressed as $\alpha_2 I_{\mathrm{abs}}$, with α_2 being the electron transport efficiency of PSII on the basis of irradiance absorbed by the two photosystems at a given light level.

In order to use parameter values (κ_{2LL}, J_{max} and θ) of Eqn (A2.3b) which quantifies linear electron transport (J) as affected by incident irradiance (I_{inc}), Eqn (B2.1) is better to be expressed on the basis of I_{inc}, i.e.,

$$J_{\mathrm{NPQ}} = \alpha_{2\mathrm{LL}} \beta I_{\mathrm{inc}} - \alpha_2 \beta I_{\mathrm{inc}} \tag{B2.2}$$

where β is absorptance by leaf photosynthetic pigments.

According to the definitions, $\alpha_2 = J_2/(\beta I_{\mathrm{inc}})$, and $\kappa_2 = J/I_{\mathrm{inc}}$, with κ_2 being the efficiency of linear electron transport on the basis of incident irradiance at a given light level. The linear electron transport J is part of the total PSII electron flux J_2 after accounting for cyclic (f_{cyc}) and pseudocyclic (f_{pseudo}) electron fractions, and their relationship can be expressed as (Yin et al., 2009):

$$J = J_2 \left(1 - \frac{f_{\mathrm{pseudo}}}{1 - f_{\mathrm{cyc}}}\right) \tag{B2.3}$$

Therefore, α_2 can be expressed in relation to κ_2 as:

$$\alpha_2 = \frac{\kappa_2}{\beta\left(1 - \frac{f_{\mathrm{pseudo}}}{1 - f_{\mathrm{cyc}}}\right)} \tag{B2.4a}$$

Likewise, α_{2LL} can be expressed in relation to κ_{2LL} as:

$$\alpha_{2\mathrm{LL}} = \frac{\kappa_{2\mathrm{LL}}}{\beta\left(1 - \frac{f_{\mathrm{pseudo}}}{1 - f_{\mathrm{cyc}}}\right)} \tag{B2.4b}$$

Substituting Eqns (B2.4a) and (B2.4b) into Eqn (B2.2) gives:

$$J_{\mathrm{NPQ}} = \frac{\kappa_{2\mathrm{LL}}}{1 - \frac{f_{\mathrm{pseudo}}}{1 - f_{\mathrm{cyc}}}} I_{\mathrm{inc}} - \frac{\kappa_2}{1 - \frac{f_{\mathrm{pseudo}}}{1 - f_{\mathrm{cyc}}}} I_{\mathrm{inc}} \tag{B2.5}$$

If absorbed light energy is equally used between NPQ and driving electron transport, $J_{NPQ} = J_2$. Given that the last term of Eqn (B2.5) is J_2, Eqn (B2.5) can be rewritten for the condition that $J_{NPQ} = J_2$ as:

$$2\frac{\kappa_2}{1-\frac{f_{\text{pseudo}}}{1-f_{\text{cyc}}}}I_{50} = \frac{\kappa_{2\text{LL}}}{1-\frac{f_{\text{pseudo}}}{1-f_{\text{cyc}}}}I_{50} \quad \text{(B2.6)}$$

where I_{50} is the level of I_{inc} at which 50% of absorbed irradiance is consumed for NPQ and driving electron transport each. Eqn (B2.6) can be simplified to:

$$2\kappa_2 I_{50} = \kappa_{2\text{LL}} I_{50} \quad \text{(B2.7a)}$$

Note that $\kappa_2 I_{50}$, by definition, represents linear electron transport at I_{50}, i.e. J_{50}:

$$2J_{50} = \kappa_{2\text{LL}} I_{50} \quad \text{(B2.7b)}$$

J_{50} can be expressed by Eqn (A2.3b). Therefore, Eqn (B2.7b) can be rewritten as:

$$2\frac{\kappa_{2\text{LL}}I_{50}+J_{\text{max}}-\sqrt{(\kappa_{2\text{LL}}I_{50}+J_{\text{max}})^2-4\theta\kappa_{2\text{LL}}I_{50}J_{\text{max}}}}{2\theta} = \kappa_{2\text{LL}}I_{50} \quad \text{(B2.8)}$$

Eqn (B2.8) can be simplified and then transformed to:

$$(1-\theta)\kappa_{2\text{LL}}I_{50}+J_{\text{max}} = \sqrt{(\kappa_{2\text{LL}}I_{50}+J_{\text{max}})^2 - 4\theta\kappa_{2\text{LL}}I_{50}J_{\text{max}}} \quad \text{(B2.9a)}$$

Squaring up both sides of Eqn (B2.9a) and then further transforming give:

$$4\theta\kappa_{2\text{LL}}I_{50}J_{\text{max}} = (\kappa_{2\text{LL}}I_{50}+J_{\text{max}})^2 - [(1-\theta)\kappa_{2\text{LL}}I_{50}+J_{\text{max}}]^2 \quad \text{(B2.9b)}$$

According to the simple algebra that $a^2 - b^2 = (a+b)(a-b)$, the whole right side of Eqn (B2.9b) can be written as $[(2-\theta)\kappa_{2\text{LL}}I_{50}+2J_{\text{max}}](\theta\kappa_{2\text{LL}}I_{50})$. Thus, Eqn (B2.9b) becomes:

$$4\theta\kappa_{2\text{LL}}I_{50}J_{\text{max}} = [(2-\theta)\kappa_{2\text{LL}}I_{50}+2J_{\text{max}}](\theta\kappa_{2\text{LL}}I_{50}) \quad \text{(B2.9c)}$$

Removing the term $\theta\kappa_{2\text{LL}}I_{50}$ on both sides, Eqn (B2.9c) is simplified to:

$$4J_{\text{max}} = (2-\theta)\kappa_{2\text{LL}}I_{50}+2J_{\text{max}} \quad \text{(B2.9d)}$$

Solving for I_{50} gives:

$$I_{50} = \frac{2J_{\text{max}}}{(2-\theta)\kappa_{2\text{LL}}} \quad \text{(B2.10)}$$

This is Eqn (2.6) in the main text for calculating I_{50}.

Substituting Eqn (B2.10) into Eqn (B2.7b) gives:

$$J_{50} = \frac{J_{\text{max}}}{2-\theta} \quad \text{(B2.11)}$$

This is Eqn (2.6) in the main text for calculating J_{50}, the rate of linear electron transport at I_{50}.

Supplementary Tables in Chapter 2

Table S2.1 The ratio of photosynthetic capacity parameter values to SPAD for four rice control (C) genotypes and their greener-leaf variants (G) or yellower-leaf variants (Y) at three stages.

Background	Genotype	Stem-elongating stage			Flowering stage			20 d after flowering		
		J_{max}/SPAD	V_{cmax}/SPAD	T_p/SPAD	J_{max}/SPAD	V_{cmax}/SPAD	T_p/SPAD	J_{max}/SPAD	V_{cmax}/SPAD	T_p/SPAD
GLXN	C	4.04	3.43	0.188	3.98	3.78	0.186	2.38	1.65	0.154
	G	3.70	2.79	0.177	3.75	3.38	0.168	1.94	1.21	0.130
YD	C	4.05	3.30	0.207	4.73	4.01	0.202	2.00	1.27	0.132
	G	4.52	3.37	0.207	4.93	4.20	0.205	2.25	1.53	0.127
WYJ	C	4.48	3.42	0.205	4.91	4.10	0.201	2.21	1.72	0.133
	G	4.78	3.55	0.200	5.20	4.05	0.203	2.16	1.46	0.135
	Y	14.47	10.95	0.532	12.02	10.37	0.462	6.93	4.84	0.354
ZF	C	3.91	2.91	0.217	4.61	3.71	0.240	2.23	1.41	0.159
	Y	7.58	6.14	0.345	10.85	8.37	0.418	5.54	3.93	0.314

Table S2.2 Estimated values of quantum yield for CO_2 assimilation on the basis of incident light ($\Phi_{CO2LL(inc)}$) and absorbed light ($\Phi_{CO2LL(abs)}$) under both photorespiratory (PR) and non-photorespiratory (NPR) conditions calculated by the method described in Yin et al. (2014) for four rice control (C) genotypes and their greener-leaf variants (G) or yellower-leaf variants (Y) at three stages.

Background	Genotype		Stem-elongating stage		Flowering stage		20 d after flowering	
			$\Phi_{CO2LL(inc)}$	$\Phi_{CO2LL(abs)}$	$\Phi_{CO2LL(inc)}$	$\Phi_{CO2LL(abs)}$	$\Phi_{CO2LL(inc)}$	$\Phi_{CO2LL(abs)}$
GLXN	C	PR	0.050	0.061	0.042	0.053	0.035	0.045
		NPR	0.073	0.088	0.068	0.085	0.059	0.076
	G	PR	0.040	0.049	0.039	0.048	0.032	0.041
		NPR	0.063	0.078	0.061	0.075	0.052	0.065
YD	C	PR	0.048	0.057	0.055	0.064	0.043	0.051
		NPR	0.068	0.081	0.077	0.089	0.060	0.072
	G	PR	0.046	0.054	0.054	0.063	0.041	0.049
		NPR	0.072	0.086	0.074	0.085	0.058	0.070
WYJ	C	PR	0.049	0.058	0.054	0.062	0.039	0.049
		NPR	0.067	0.080	0.077	0.089	0.059	0.073
	G	PR	0.049	0.058	0.051	0.060	0.039	0.048
		NPR	0.066	0.079	0.073	0.086	0.059	0.072
	Y	PR	0.027	0.059	0.033	0.051	0.025	0.044
		NPR	0.037	0.079	0.044	0.070	0.033	0.057
ZF	C	PR	0.042	0.054	0.049	0.061	0.033	0.046
		NPR	0.064	0.081	0.070	0.087	0.050	0.070
	Y	PR	0.042	0.060	0.043	0.060	0.034	0.054
		NPR	0.057	0.082	0.062	0.086	0.047	0.075

Supplementary Figures in Chapter 2

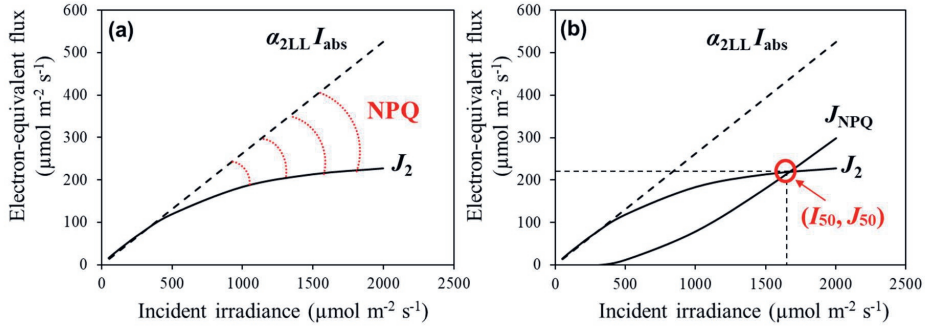

Fig. S2.1 (a) The relative energy loss due to non-photochemical quenching (NPQ) based on the deviation of J_2 from the dotted line of $\alpha_{2LL}I_{abs}$. (b) The intersection point (I_{50}, J_{50}) when the solar photons absorbed by plant leaves are evenly distributed between photochemical quenching and NPQ, i.e., $J_2 = J_{NPQ}$.

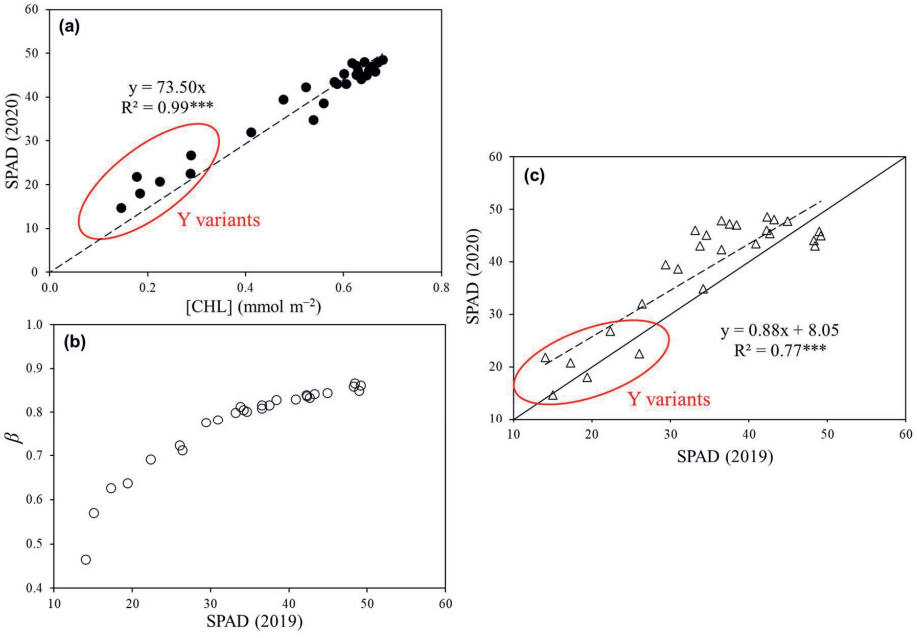

Fig. S2.2 Relationships (a) between SPAD value and chlorophyll content ([CHL]), data from field experiment in 2020 (filled circles); (b) between leaf absorptance (β) and SPAD value, data from greenhouse experiment in 2019 (open circles); (c) of SPAD between greenhouse experiment and field experiment (open triangles). Each point represents the mean of three or four replicates. Linear regressions were fitted for overall data of three stages: stem-elongating stage, flowering stage, and 20 d after flowering. The significance of each correlation is shown by asterisks: *** $P < 0.001$. The diagonal line (full line) in panel (c) is the 1:1 line.

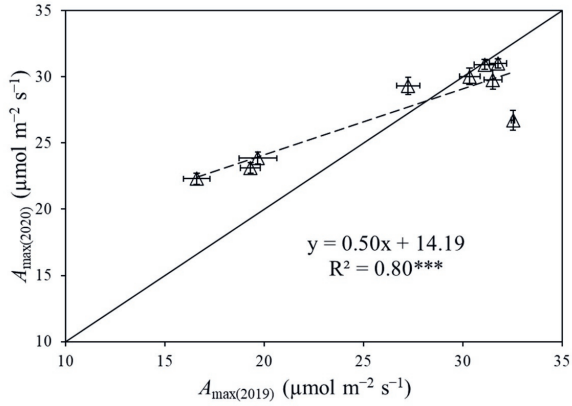

Fig. S2.3 Relationship of maximum photosynthesis rate (A_{max}) between greenhouse experiment (2019) and field experiment (2020) at flowering stage. Each point represents the mean of three or four replicates (± standard errors). Linear regression (dotted line) was fitted for overall data with its significance of correlation shown by asterisks: *** $P < 0.001$. The diagonal line (full line) is the 1:1 line.

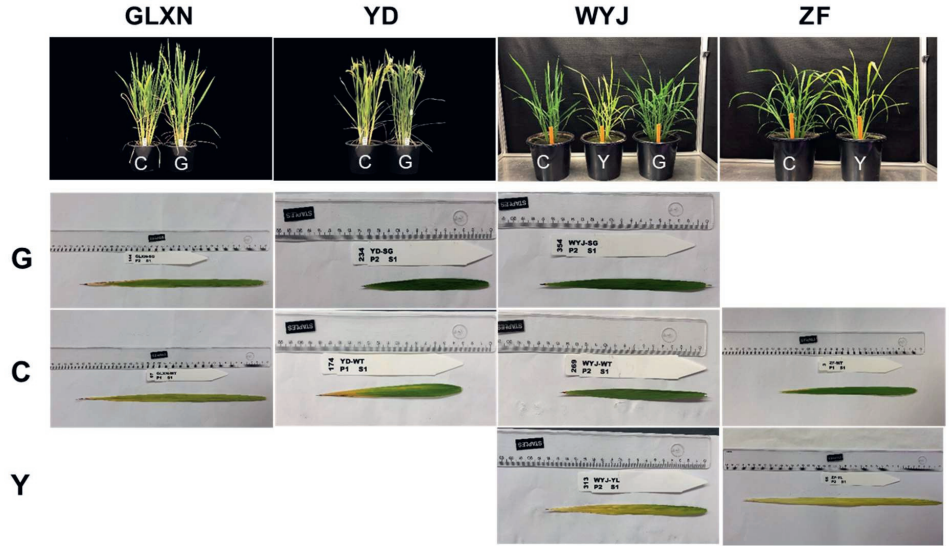

Fig. S2.4 Differences in leaf colour of four rice control (C) genotypes and their greener-leaf variants (G) or yellower-leaf variants (Y). Flag leaves were taken at late-flowering stage. Genotype-background abbreviations - GLXN: cv. Guanglingxiangnuo; YD: cv. Yandao 8; WYJ: cv. Wuyunjing 3; and ZF: cv. Zhefu 802.

References

Farquhar GD, von Caemmerer SV, Berry JA. 1980. A biochemical model of photosynthetic CO_2 assimilation in leaves of C_3 species. *Planta* 149, 78−90.

Sharkey TD. 1985. Photosynthesis in intact leaves of C_3 plants: physics, physiology and rate limitations. *The Botanical Review* 51, 53−105.

Yin X, Belay DW, van der Putten PEL, Struik PC. 2014. Accounting for the decrease of photosystem photochemical efficiency with increasing irradiance to estimate quantum yield of leaf photosynthesis. *Photosynthesis Research* 122, 323−335.

Yin X, Struik PC, Romero P, Harbinson J, Evers JB, van der Putten PEL, Vos J. 2009. Using combined measurements of gas exchange and chlorophyll fluorescence to estimate parameters of a biochemical C_3 photosynthesis model: a critical appraisal and a new integrated approach applied to leaves in a wheat (Triticum aestivum) canopy. *Plant, Cell & Environment* 32, 448−464.

Chapter 3

Leaf-colour modification affects canopy photosynthesis, dry-matter accumulation and yield traits in rice

Zhenxiang Zhou[1], Paul C. Struik[1], Junfei Gu[2], Peter E.L. van der Putten[1], Zhiqin Wang[2], Xinyou Yin[1] and Jianchang Yang[2]

[1] Centre for Crop Systems Analysis, Department of Plant Sciences, Wageningen University & Research, 6700 AK Wageningen, The Netherlands

[2] College of Agriculture, Yangzhou University, 48 Wenhui East Road, Yangzhou, Jiangsu 225009, China

This chapter has been published in *Field Crops Research* (2023), 290, 108746.

Abstract

Recent research has proposed to modify leaf-colour traits to improve canopy photosynthesis (A_c) by allowing light penetration to lower layers of a dense canopy. Whether and how enhanced light penetration can really increase A_c and whether leaf-colour modification influences other growth-related traits remain unclear. Canopy light and nitrogen profile parameters (i.e., the extinction coefficient for light, K_L; and for nitrogen, K_N; and their ratio, K_N/K_L), A_c, and agronomic yield traits were examined in nine rice genotypes comprising different genetic backgrounds and their leaf-colour variants. Compared with stay-green (G) variants, yellow-leaf (Y) variants caused larger effects on crop growth and development: altered growth duration (increased in one genetic background while decreased in the other), lower tiller number, and reduced leaf area. As with G traits, a delayed senescence at the post-flowering stage was observed in Y variants, which was associated with nitrogen dynamics in plants. Although Y variants expectedly allowed more light penetration into lower layers of the canopy (i.e., lower K_L), the leaf-nitrogen profile, and thus, the leaf photosynthetic capacity (i.e., A_{max}) profile, did not necessarily follow more closely the light profile. Improved A_c and higher daily crop growth rate (CGR) were observed in the Y variant of one genetic background but not of the other, and the higher A_c or CGR were associated with improved leaf photosynthetic nitrogen use efficiency and higher canopy K_N values. The higher CGR during the grain-filling phase and resulting increased harvest index of this Y variant contributed to its greater grain productivity. Multiple regression analysis of the data of all nine genotypes indicated that the K_N:K_L ratio was the most important factor determining A_c and CGR. Leaf-colour modification can improve A_c, CGR and crop productivity only if other traits (especially N profile in the canopy) are adjusted synergistically. However, the observed diversity in phenotypic variations of multiple traits caused by leaf-colour modification implies the potential of exploiting breeding or crop management to improve rice biomass and yield.

Keywords: agronomic trait, canopy photosynthesis, light and nitrogen profile, *Oryza sativa*, stay-green and yellow-leaf variants.

3.1 Introduction

Rice is one of the most important crops in meeting diversified social demands by humans. First, grain production of rice plant accounts for ca. 21% and ca. 50% of human food calories for global and Asian consumption, respectively (Awika, 2011; Muthayya et al, 2014). Second, utilisation of rice husk and straw has been considered as one of the most promising sources of renewable energy to address the rapidly growing needs for alternative energy (Lim et al., 2012; Dungani et al., 2016). However, as the world's population and economy expand, the gap between the need for agricultural production and the actual level of productivity is likely to widen further in the near future (Zhu et al., 2008). The stagnation of rice productivity in recent decades is partly associated with the low efficiency of converting photosynthetically active radiation (PAR) into biomass accumulation, which is currently far below the theoretical maximum value of solar energy conversion efficiency (Long et al., 2015; Ort et al., 2015; Yin and Struik, 2015). One possible strategy to overcome this is to improve canopy photosynthesis (A_c) by modifying leaf-colour traits (i.e., stay-green and yellow-leaf traits). Stay-green traits are mainly meant to sustain canopy photosynthetic competence during later grain filling (Gregersen et al., 2013; Borrell et al., 2014), while yellow-leaf traits are applied to increase light penetration to lower layers and thus improve A_c (Ort et al., 2011).

Rice productivity during its entire life cycle depends on the duration of complete canopy cover and the capacity of canopy photosynthesis. Accelerating canopy closure during vegetative growth (i.e., improving early leaf area growth rate) or slowing down canopy senescence during the grain filling phase (i.e., introducing stay-green traits) may enhance light capture (Yin and Struik, 2015). For a closed canopy, however, undue increases in leaf area index (LAI) enhance self-shading (leaves in the lower parts of the canopy may be shaded by the upper leaves that receive most of incoming PAR), and therefore, could be detrimental to canopy photosynthesis (Hirose et al., 1997). Green leaves in the upper canopy of typical C_3 crop plants are usually light-saturated under full sunlight, whereas leaves deep down the canopy contribute less to A_c due to light starvation (Zhu et al., 2008; Walker et al., 2018). Adopting rice genotypes with reduced canopy chlorophyll content (relatively yellower leaves) has been proposed to improve A_c and biomass production by allowing more light penetration into the lower layers of the canopy (Ort et al., 2011). This concept has been previously examined in soybean (Pettigrew et al., 1989; Slattery et al., 2017; Walker et al., 2018), but little relevant information is available for rice, because yellow-leaf variants are rare in rice.

Besides the canopy light profile, the profile of leaf photosynthetic resources (leaf nitrogen in particular) also affects the carbon gain of the canopy by influencing photosynthesis of each individual layer (Hikosaka, 2014). The physiological mechanism behind this is that leaf photosynthetic capacity is closely related to nitrogen content (Evans, 1988, 1989). In an actual plant canopy, the nitrogen distribution is normally not uniform, but may acclimate to the light profile in such a way that the upper sunlit leaves have more nitrogen content than the lower, shaded ones (Field, 1983; Evans, 1993; Li et al., 2013). This spatial nitrogen distribution pattern in a plant canopy can be more efficient in accumulating photosynthate compared with that under uniform nitrogen distribution (Hirose and Werger, 1987), since it serves as an adaptive response to the light distribution within the canopy (Field, 1983). In fact, mathematical optimisation analysis has shown that the A_c is maximised if the light-saturated maximum leaf-photosynthesis (A_{max}) profile follows the light profile (Anten et al., 1995; Goudriaan, 1995). This requires that the photosynthetically active nitrogen extinction coefficient (K_N, defining the extent to which nitrogen gradually decreases with canopy depth) equals the light extinction coefficient (K_L, defining the extent to which photon flux density gradually attenuates with canopy depth) if A_{max} is linearly correlated to leaf nitrogen content. However, typically, K_N in an actual canopy is considerably lower than K_L, e.g., only ~0.35 times K_L in kenaf (Archontoulis et al., 2011). Nevertheless, the expected decrease of K_L in yellow-leaf genotypes may make it possible to close the gap between light and nitrogen profile distribution, putting K_N closer to K_L, but whether this is the case and how leaf-colour traits would facilitate to maximize A_c remains to be investigated.

In addition to light and nitrogen profiles along the canopy depth, some agronomic and physiological characteristics of the canopy like LAI, tiller number, and canopy nitrogen content are variable among different genotypic backgrounds, growth stages, and even growing environments. These traits interact with each other and contribute to the variations in K_L and K_N (Yin et al., 2003; Ouyang et al., 2021). There is little information associated with investigating the impact of leaf-colour modification on these traits and exploring how these canopy traits affect biomass accumulation, grain production and yield components.

In this study, we used rice genotypes from different genetic backgrounds that had been modified to have either the stay-green trait or the yellow-leaf trait or both. We aimed (i) to examine whether and how A_c and dry matter accumulation can be improved by leaf-colour modification; (ii) to calculate the ratios of K_N to K_L among genotypes with contrasting chlorophyll content;

and (iii) to identify the beneficial traits improving the crop yield and biomass production after leaf-colour modification.

3.2 Materials and Methods

3.2.1 Plant material and growth conditions

Four genotypes of rice (*Oryza sativa* L.) were modified to have either the stay-green variant or the yellow-leaf variant, or both, creating a total of nine genotypes that were used in this study. The default genotypes belong to four different rice groups, representing four genetic backgrounds. Cv. Guanglingxiangnuo (GLXN) belonging to mid-season *japonica* rice material was modified via T-DNA insertion using the KOD-Plus-Mutagenesis Kit (Toyobo, Osaka, Japan) to substitute each position of the wild-type *Wx* gene sequence; then this gene fragment from the site-directed mutagenesis was inserted to construct the plasmids, which were introduced in EHA105 *Agrobacterium* strain cells by electroporation; finally, transgenic rice plants were generated by *Agrobacterium tumefaciens*-mediated transformation; the variant used in our study was selected from the homozygous single T-DNA insertion transgenic plant of Liu et al. (2014) as it holds a pleiotropic, stay-green trait. The other three rice materials were modified by radiation mutagenesis. To realise this, the seeds were incubated in a water bath at 33 °C for 48 h to induce germination to obtain high-frequency gene mutagenesis. Then they were irradiated with ^{60}Co γ-rays at 50 Gy; after 24 h, the seeds were sown under field conditions to obtain the first generation (M1); the leaf-colour traits were identified and screened from a population of M2 plants; the derived variants were genetically fixed through advancement to the M8 generation (Jiang et al., 2007). Mid-season *japonica* cv. Yandao 8 (YD) was modified to have a stay-green variant, an early *indica* cv. Zhefu 802 (ZF) was modified to have a yellow-leaf variant, and a *japonica* type cv. Wuyunjing 3 (WYJ) was modified to have both stay-green and yellow-leaf variants. Resulting stay-green and yellow-leaf genotypes are marked as G and Y, respectively, while the nonmodified or default genotypes are labelled as control (C). Seeds of GLXN, YD, and WYJ cultivars were from Yangzhou University, and seeds of the ZF background were from Zhejiang University, China. After multiplying for many generations, these genotypes showed stability of the G and Y variant lines.

Two independent experiments were conducted, one in a greenhouse at Wageningen University & Research, Wageningen, the Netherlands (51°58′N, 05°40′E), and one at the field farm of Yangzhou University, Jiangsu Province, China (32°30′N, 119°25′E), respectively. The

phenological information of days from sowing to different stages (i.e., beginning of stem elongation, heading, and maturity) of these genotypes in each experiment are listed in Table 3.1. The leaf chlorophyll contents of the nine genotypes in the field experiment are listed in Fig. S3.1.

Table 3.1 Duration of different phenological phases for rice genotypes of four genetic backgrounds, each including a control (C) genotype and its greener-leaf variant (G) and/or yellower-leaf variant (Y) genotype, in two experiments.

Experiment	Background	Genotype	Days from sowing to beginning of stem elongation (d)	Days from sowing to heading (d)	Days from heading to maturity (d)	Days from sowing to maturity (d)
Greenhouse	GLXN	C	68	74	58	132
Experiment		G	68	74	58	132
(2019)	YD	C	43	50	55	105
		G	45	52	55	107
	WYJ	C	47	55	48	103
		G	47	55	48	103
		Y	51	59	50	109
	ZF	C	90	100	50	150
		Y	58	65	47	112
Field	GLXN	C	86	96	77	173
Experiment		G	86	96	77	173
(2020)	YD	C	77	85	77	162
		G	79	87	77	164
	WYJ	C	85	95	64	159
		G	85	95	64	159
		Y	89	99	71	170
	ZF	C	78	88	56	144
		Y	71	78	49	127

The sowing date in the greenhouse experiment was 30 April in 2019 with seedlings transplanted 20 d later; the sowing date in the field experiment was 27 May in 2020 with seedlings transplanted 30 d later.

3.2.2 Greenhouse experiment

The environmental conditions of the greenhouse were controlled. Light intensity inside was kept within 400-500 W m^{-2}; temperature was set at 26 ± 0.5 °C for the 12 h light period and at 23 ± 0.5 °C for the 12 h dark period; the CO_2 level was about 400 μmol mol^{-1} and the relative humidity was set at 65~75%. Pre-germinated seeds of the nine genotypes were sown on 30 April 2019 in porous plastic trays, and then transplanted to pots (24 cm in diameter and 20 cm

in height, and 7 litres in volume) at the 3rd leaf stage with two seedlings per pot. All pots were placed on movable lorries according to a randomised complete block design, with three replications per genotype. The soil used was a sandy loam with 84.5 mg alkali-hydrolysable N, 6.5 mg Olsen-P, and 229.7 mg exchangeable K. 1.5 g KH_2PO_4 was applied and incorporated with soil just before transplanting as basal fertilizer. Nitrogen in the form of urea (totally 1 g urea per pot) was applied at pre-transplanting, early tillering, and panicle initiation stage with the proportions being 50%, 20% and 30%, respectively. Throughout the entire growth cycle, pots were frequently supplied with tap water, ensuring 2 cm of standing water on top of the soil surface. Drainage was only undertaken at a critical leaf-age stage to control non-productive tillers, in line with the local standard practices of the rice growing area, where our field experiment was conducted.

3.2.3 Field experiment

Pre-germinated seeds were first sown on 27 May 2020 in paddy seedbed field plots, and then seedlings of the 3rd leaf stage in the seedbed were transplanted to the experimental field with a hill spacing of 0.25 m × 0.16 m and two seedlings per hill. A split-plot design was used with genetic backgrounds as the main plots and genotypes as the split plots, in a randomised block arrangement with three replicates. The main plots were separated by ridges at a 1-m width covered by plastic film inserted in the soil at a depth of 0.5 m. Each split-plot area was 20 m^2, and, thus, the size of each main plot for the WYJ background (the only one having three genotypes) was 60 m^2 while it was 40 m^2 for each of the other three backgrounds (i.e., GLXN, YD, and ZF). The soil used in the experiment was also a sandy loam (Typic Fluvaquent, Etisols [U.S. taxonomy]) with 25.5 g kg^{-1} organic matter, 103 mg kg^{-1} alkali-hydrolysable N, 33.4 mg kg^{-1} Olsen-P, and 70.5 mg kg^{-1} exchangeable K. One day before transplanting, phosphorus (30 kg ha^{-1} as single superphosphate) and potassium (40 kg ha^{-1} as KCl) as basal fertiliser were applied. 240 kg N ha^{-1}, in the form of urea, was applied at pre-transplanting, early tillering, and panicle initiation stage with the same proportion as in the greenhouse experiment. Weather data for the average air temperature and sunshine hours during the rice growing season were monitored at a weather station close to the experimental site and are shown in Fig. S3.2.

3.2.4 Canopy light and nitrogen distribution measurements

In the field experiment, the level of photosynthetically active radiation at various canopy depths was measured by using a 100-cm linear ceptometer (SunScan Systems SS1, Delta-T devices,

Cambridge, UK) placed diagonally across the rows. The PAR measurements, at stem elongating, flowering (defined as 80% panicles fully emerged from flag-leaf sheath and began flowering, ca. 7 d after heading stage), and 20 d after flowering stage, were taken every 10 cm from the top of the canopy to the ground level with three to four replicates in each plot for each genotype. All measurements were restricted to the time span from 11:00 to 13:00 under a clear sky. Next, leaves of five plants in the same canopy were dissected at the same 10-cm interval from the top canopy downwards according to the stratified-clipping method (Monsi and Saeki, 2005). Leaf area of each horizontal layer of the canopy was determined by using an area meter (Li-3100; Li-Cor, Lincoln, Nebraska, USA). Afterwards, these leaf blades were placed in a forced air oven (UF 260, Memmert Corp., Germany) at 105 °C for 0.5 h and then dried at 75 °C for 72 h to a constant weight. After weighing, the leaf samples were ground into powder, which was then assessed for the leaf nitrogen concentration by the Kjeldahl apparatus (Kjeltec 8400, Foss Corp., Germany). The specific leaf nitrogen (SLN, leaf nitrogen content per unit leaf area) was then calculated.

3.2.5 Estimation of light and nitrogen extinction coefficients

Photon flux density was assumed to attenuate with the canopy depth according to the Lambert-Beer's law:

$$I_{\mathrm{i}} = I_0 \exp(-K_{\mathrm{L}} \mathrm{LAI}_{\mathrm{i}}) \tag{3.1}$$

where $\mathrm{LAI_i}$ (m^2 green leaves m^{-2} ground) is the cumulative surface area of green leaves per unit ground area from the top of the canopy; I_{i} and I_0 (μmol m^{-2} s^{-1}) are the incoming photon flux values at depth i and above the canopy, respectively; K_{L} is the light extinction coefficient.

Following Anten et al. (1995), the vertical gradient of the SLN in the canopy was expressed as:

$$\mathrm{SLN_i} = (\mathrm{SLN_0} - n_{\mathrm{b}}) \exp(-K_{\mathrm{N}} \mathrm{LAI_i}) + n_{\mathrm{b}} \tag{3.2}$$

where $\mathrm{SLN_i}$ is the SLN (g N m^{-2}) of the leaves at the ith layer of the canopy; $\mathrm{SLN_0}$ is the SLN of the leaves at the top of the canopy; K_{N} is the extinction coefficient for effective leaf nitrogen; n_{b} is the minimum leaf nitrogen for photosynthesis, at or below which photosynthesis is zero; an estimated value of 0.3 g N m^{-2} for n_{b} was adopted for all the rice genotypes from Yin and van Laar (2005). K_{N} and $\mathrm{SLN_0}$ were estimated by fitting Eqn (3.2) to the measured data.

3.2.6 Plant growth measurements

In the greenhouse experiment, tiller number and leaf area were measured at heading (defined as the moment the first panicle of the whole plant emerged from the flag-leaf sheath), 20 d after heading, and 40 d after heading with sampling size of three to five pots per genotype. Above-ground dry weight for each genotype at the same moments and at maturity (defined as the moment the rachis of panicle turned yellow) was determined after oven drying at 75 °C for 72 h to constant weight.

In the field experiment, three extra time points for measurements were added: at 20 d after transplanting, 35 d after transplanting, and at stem-elongating, to better examine the dynamics of traits throughout the whole crop cycle. Plants of five hills randomly selected from each plot were sampled as one replicate at each measurement. Daily average crop growth rate (CGR) was calculated for each genotype as the difference in above-ground dry weight divided by the number of days between samplings. After that, the leaf part of the sample at each stage was used to measure the nitrogen concentration using the Kjeldahl apparatus (Kjeltec 8400, Foss Corp., Germany). Total canopy nitrogen content (N_C, g N m^{-2} ground), and canopy-averaged nitrogen per leaf area (SLN_C, g N m^{-2} leaf) were then calculated.

3.2.7 Leaf chlorophyll content and photosynthesis measurement

In the field experiment, leaf chlorophyll concentration was measured at tillering, stem-elongating, heading, 20 d after heading, and 40 d after heading, according to the method of Arnon (1949). The uppermost newly expanded leaves were ground to extract chlorophyll with 95% ethanol at 60-65 °C, and then the chlorophyll content was determined using an ultraviolet spectrophotometer (Lambda 650, PerkinElmer, USA). Light-saturated leaf photosynthesis at ambient CO_2 level (A_{max}, μmol CO_2 m^{-2} s^{-1}) was measured on flag leaves at a light intensity of 2,000 μmol photons m^{-2} s^{-1} using an open-path gas exchange system (Li-Cor 6400XT; Li-Cor Inc., Lincoln, NE, USA) at the flowering stage (7 d after the first panicle tip emerged from the flag-leaf sheath), with the flow rate set at 400 μmol s^{-1}. All measurements were carried out at a leaf temperature of 25 °C and a leaf-to-air vapour pressure deficit between 1.0 and 1.6 kPa. The leaf segments used for photosynthesis measurements were cut out and used to determine leaf nitrogen concentration by an element analyser (Vario Macro cube, Elementar, Germany) based on the micro-Dumas combustion method.

Canopy photosynthesis was measured using a static-chamber method at the same day (i.e., the flowering stage) as leaf photosynthesis measurements, which has been applied and validated in many previous studies (Welker et al., 2004; Bubier et al., 2007; Xia et al., 2009; Niu et al., 2010). Transparent PVG plates (Transmittance > 95%) were used to make an assimilation chamber with dimensions 60 cm × 60 cm × 150 cm, and then connected with the gas exchange system (Li-Cor 6400XT; Li-Cor Inc., Lincoln, NE, USA) (Fig. S3.3; also see detailed information in Niu et al., 2008). Two electric fans (size: 120 mm × 120 mm × 25 mm) with rotation speeds of 6000-10000 rpm were built to promote air mixing continuously inside the chamber. Fifteen consecutive recordings of CO_2 and water vapour concentrations were taken on each frame at 10-s intervals during a 150-s period after steady-state conditions were achieved within the chamber. According to our field planting density, plants of totally eight hills (two rows × four hills) were enclosed in the chamber. We made this measurement for three to four times for each plot. All measurements were conducted from 10:00 to 12:00 am at a clear sky during flowering, when the incoming solar photosynthetic flux density was between 1000 and 1200 μmol photon m^{-2} s^{-1}. The variation in air temperature inside the chamber was less than 0.2 °C during an average measurement period. The flux rates were determined from the time-course of the CO_2 concentration in the assimilation chamber. To correct for the effect of soil respiration, the measurement was conducted at the same spot with all above-ground parts of the plants in the chamber cut off. The net canopy photosynthesis rate ($A_{c,net}$, μmol CO_2 m^{-2} ground s^{-1}) was then calculated as the difference between the two measurements according to the soil-flux calculation procedure in the LI-6400 gas exchange system manual (LiCor Inc., 2004) or LI-8100A soil gas flux system manual (LiCor Inc., 2015).

3.2.8 Calculation of photosynthetic nitrogen use efficiency

Leaf photosynthetic nitrogen-use efficiency (PNUE) was defined as:

$$\mathrm{PNUE} = \frac{A_{\max}}{\mathrm{SLN} - n_b} \tag{3.3}$$

where A_{max} (μmol CO_2 m^{-2} s^{-1}) is the maximum net photosynthesis rate of the flag leaf at a light intensity of 2000 μmol m^{-2} s^{-1} and a CO_2 concentration of 400 μmol mol^{-1}; SLN (g N m^{-2} leaf) is the specific leaf nitrogen, and n_b represents a base leaf nitrogen content as defined for Eqn (3.2) (n_b = 0.3 g N m^{-2} for rice; Yin and van Laar, 2005).

Canopy photosynthetic nitrogen-use efficiency ($PNUE_c$) was defined as:

$$\mathrm{PNUE_c} = \frac{A_c}{(\mathrm{SLN_c} - n_b)\mathrm{LAI}} \quad (3.4)$$

where A_c (μmol CO_2 m^{-2} ground s^{-1}) is the canopy photosynthesis; SLN_c (g N m^{-2} leaf) is the canopy-averaged specific leaf nitrogen (= N_c/LAI); and LAI (m^2 leaf m^{-2} ground) is the leaf area index.

3.2.9 Yield and yield-related traits at maturity

At maturity, yield, yield components, total above-ground biomass, and harvest index were determined in the greenhouse and field experiments. Grain yield and yield components were measured following the procedure as described by Yoshida et al. (1976). Aboveground plants sampled at maturity were separated into straw, filled and unfilled grains, and rachis. Dry weight of each component was determined by oven-drying to constant weight, then the harvest index was calculated as the ratio of filled grain weight to total above-ground weight. In the greenhouse experiment, plants of three pots were sampled as one replicate for each plot to determine the yield (g $hill^{-1}$) and yield components (i.e., number of panicles per hill, number of spikelets per panicle, filled-grain percentage, and 1000-grain weight). In the field experiment, grain yield (g m^{-2}) was determined from harvesting plants of 2 m^2 in each plot and adjusted to 14% moisture. The yield components (i.e., number of panicles per m^2, number of spikelets per panicle, filled-grain percentage, and 1000-grain weight) were determined from randomly selected plants of ten hills (excluding the border ones) in each plot. The number of spikelets per panicle was calculated as total number of spikelets divided by the number of panicles. The filled-grains percentage was defined as the percentage of filled grains (specific gravity $\geqslant$ 1.06 g cm^{-3}) to the total number of spikelets. The 1000-grain weight was calculated as the filled grain weight divided by the number of the filled grains, then multiplied by 1000. Harvest index was calculated as the ratio of filled grain weight to above-ground dry weight of plants. The daily average grain-filling rate was calculated as the final grain yield (14% moisture) divided by the days of duration from heading stage to maturity.

3.2.10 Data analysis

Nonlinear fitting was carried out using the GAUSS method in PROC NLIN of SAS (SAS Institute Inc., Cary, NC, USA) to estimate K_L and K_N in Eqns (3.1) and (3.2). Significance of differences between a variant genotype and its control genotype was assessed using SPSS (version 25.0; SPSS Inc) based on the computed *F* values in each figure or table if applicable.

Multiple linear regression analysis, where genetic backgrounds (GLXN, YD, WYJ, and ZF) were introduced as dummy variables, was conducted to identify which physiological variables (N_c versus K_N:K_L) was most important in determining A_c or CGR.

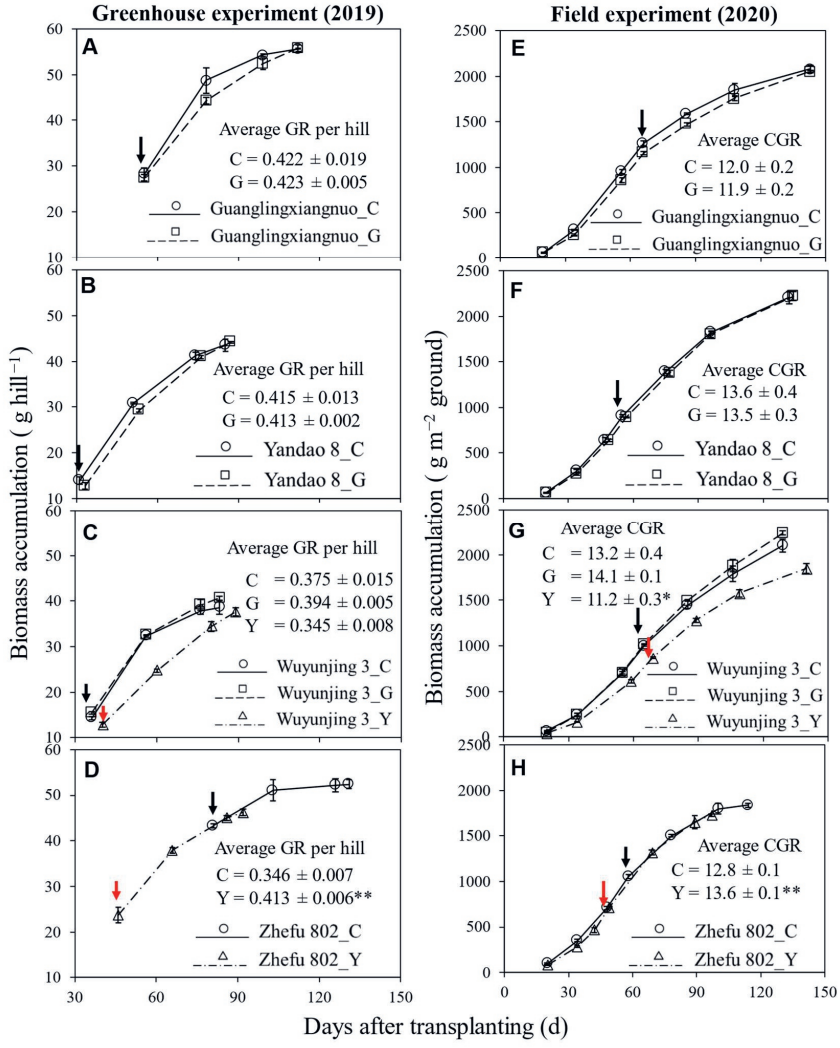

Fig. 3.1 The time course of above-ground biomass in two experiments. Rice genotypes comprised four rice control (C, circles) genotypes and their greener-leaf variant (G, squares) and/or yellower-leaf variant (Y, triangles) genotypes. Each data point is shown as mean ± standard error of three to four replicates. Daily average growth rate per hill (GR per hill, g hill^{-1} d^{-1} in greenhouse experiment) and daily average crop growth rate (CGR, g m^{-2} ground d^{-1} in field experiment) for the entire life cycle were listed in each panel with a significant difference between variant genotype and its control genotype shown by asterisks: * $P < 0.05$, ** $P < 0.01$. Black arrows indicate the heading dates of C genotypes and G genotypes, and red arrows represent those of Y genotypes.

3.3 Results

3.3.1 Phenology, growth traits and canopy nitrogen content

The comparison of variant genotypes with their control (C) genotypes showed that plant growth and development traits were more influenced by introducing yellow-leaf traits than introducing stay-green traits. The growth durations from sowing to maturity did not differ much between stay-green variants (G) and their C genotypes in both experiments (Table 3.1). However, introducing yellow-leaf traits resulted in a completely different effect on phenology, as the life cycle was prolonged in the yellow-leaf variant (Y) from the WYJ background whereas it was shortened in the Y genotype from the ZF background.

Fig. 3.1 presents time courses of above-ground dry weight and the daily average growth rate for the entire rice cycle in all genotypes. Overall, the patterns of the above-ground dry weight were similar in variants and their control genotypes, except for lower values in WYJ-Y compared with WYJ-C. In general, the daily growth rate (i.e., the slope between two sampling dates) declined after heading in all genotypes. To avoid the possible confounding effect of the changed growth durations, we analysed the daily average growth rate of the entire growth duration. The daily growth rate was significantly affected only in Y-variants, with an increase for ZF-Y in both experiments and a decrease in WYJ-Y in the field experiment.

Tiller number and leaf area were influenced more by the Y modification than by the G modification (Figs. 3.2 and 3.3). Across genetic backgrounds, tiller number was lower in Y variants than in their C genotypes (Fig. 3.2). Data from the field experiment indicated a similar growth of LAI for genotypes from the same background at early vegetative stage (Fig. 3.3). However, the peak of growth curves of LAI for Y variants was less sharp around flowering, followed by a slower decline when approaching maturity, compared with G variants and C genotypes.

The pattern of total canopy nitrogen content in green leaves (N_c) in the field experiment for each genotype across stages (Fig. 3.4) was similar to that of LAI, fast increasing at early stages and then decreasing after peaking around the heading stage. Canopy-averaged nitrogen per leaf area (SLN_c) was higher in the variants, especially in Y variants during the reproductive phase (Figs. 3.4G−H). It is worth mentioning that ZF-Y began to manifest a higher SLN_c at vegetative growth stage (ca. 30 d after transplanting).

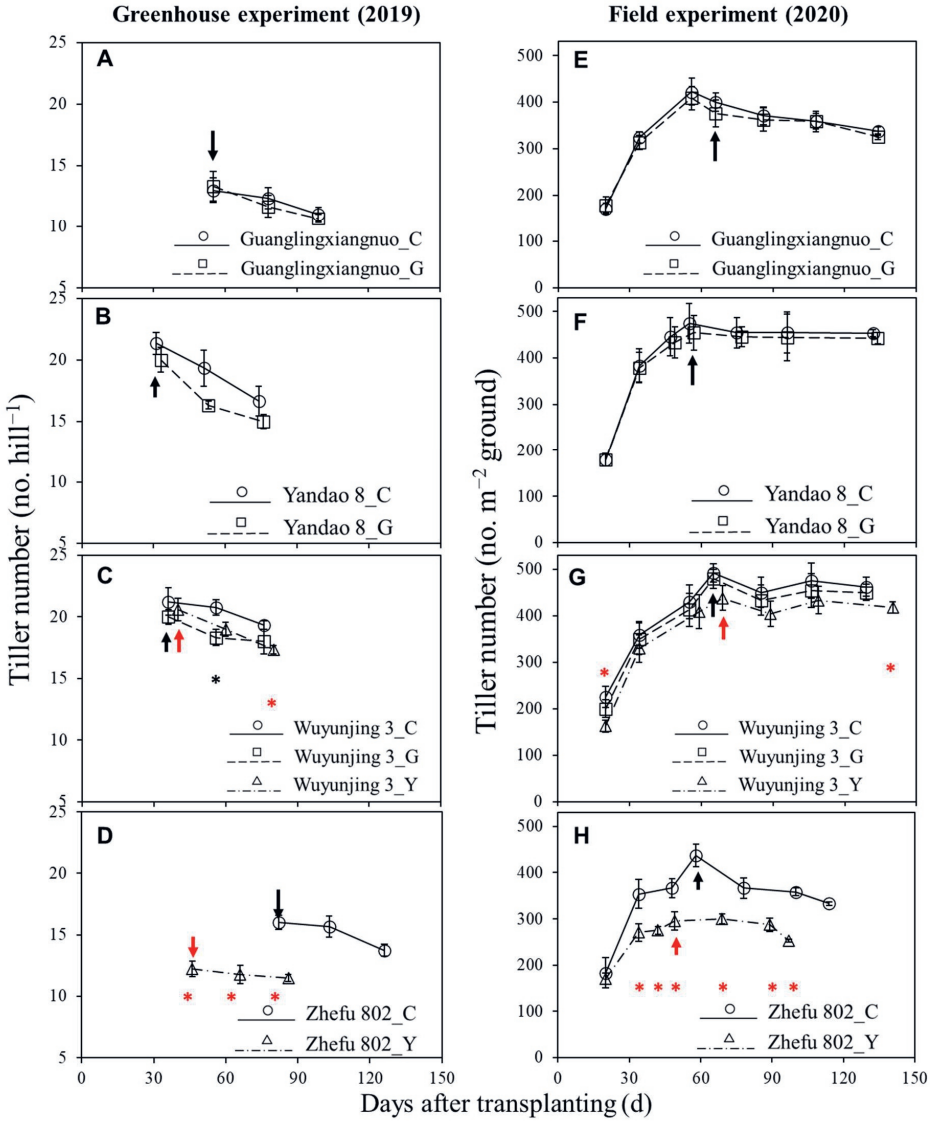

Fig. 3.2 The time course of tiller number of rice genotypes in two experiments. Genotypes comprised four control (C, circles) genotypes and their greener-leaf variant (G, squares) and/or yellower-leaf variant (Y, triangles) genotypes. Each data point is shown as mean ± standard error of three to four replicates. A significant difference ($P < 0.05$) between variant genotype and its control genotype at each sampling stage is shown by asterisks in different colours, with black and red for G variants and Y variants, respectively. Black arrows indicate the heading dates of C genotypes and G genotypes, and red arrows represent those of Y genotypes.

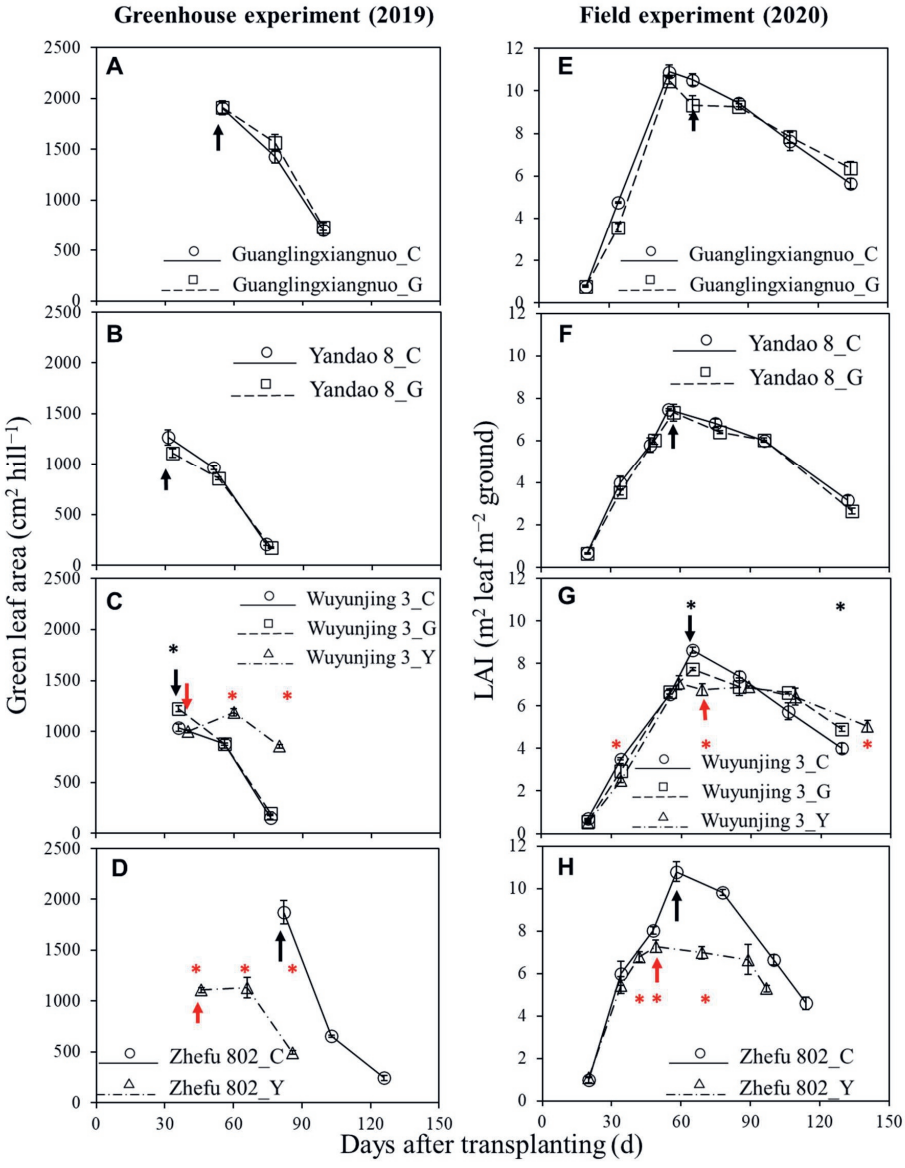

Fig. 3.3 The time course of leaf area in rice genotypes. Leaf area is shown in leaf area per hill for the greenhouse experiment (A-D) and in leaf area index (LAI) for the field experiment (E-H). Genotypes comprised four control (C, circles) genotypes and their greener-leaf variant (G, squares) and/or yellower-leaf variant (Y, triangles) genotypes. Each data point represents the mean ± standard error of three to four replicates. A significant difference ($P < 0.05$) between variant genotype and its control genotype at each sampling stage is shown by asterisks in different colours, with black and red for G variants and Y variants, respectively. Black arrows indicate the heading dates of C genotypes and G genotypes, and red arrows represent those of Y genotypes.

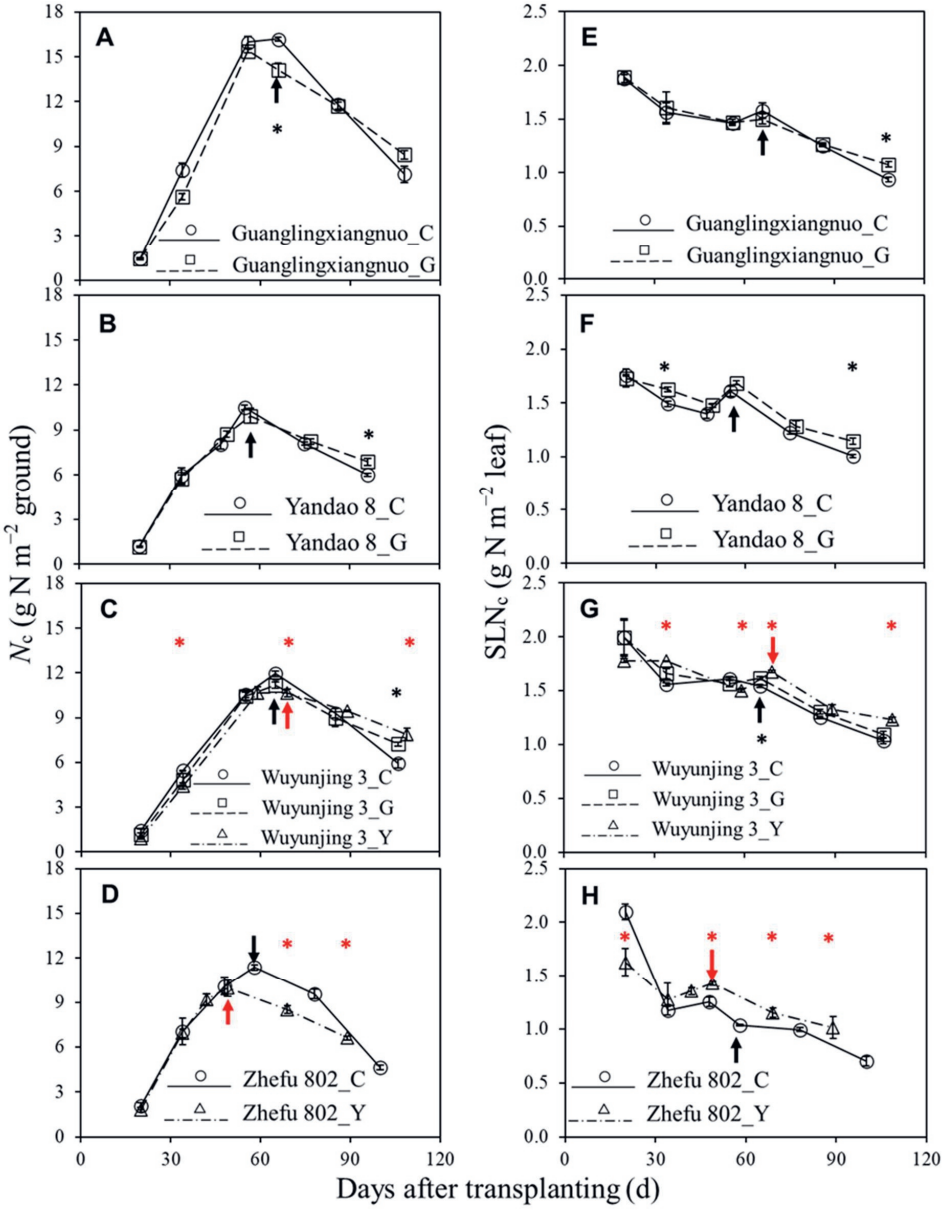

Fig. 3.4 The time course of crop nitrogen status in the field experiment. Canopy total nitrogen content (N_c, A-D) and canopy-averaged specific leaf nitrogen (SLN_c, E-H) of green leaves are shown for four rice control (C, circles) genotypes and their greener-leaf variant (G, squares) and/or yellower-leaf variant (Y, triangles) genotypes. Each data point represents the mean ± standard error of three to four replicates. A significant difference ($P < 0.05$) between variant genotype and its control genotype at each sampling stage is shown by asterisks in different colours, with black and red for G variants and Y variants, respectively. Black arrows indicate the heading dates of C genotypes and G genotypes, and red arrows represent those of Y genotypes.

3.3.2 Contrasting impact of yellow-leaf modification on yield and yield-related traits

In both experiments, yield and yield-related traits did not significantly differ between G and their C genotypes, except that the filled-grain percentage was significantly reduced in GLXN-G (Table 3.2). For Y variants, panicle number and filled-grain percentage were lower while number of spikelets per panicle was higher than for C counterparts across experiments. Compared with its C genotype, ZF-Y also showed significantly higher 1000-grain weight, daily grain-filling rate and harvest index, which contributed to a higher final yield, despite a lower total biomass. On the contrary, WYJ-Y exhibited lower daily grain-filling rate in both experiments, and a remarkably lower yield and total biomass gain in the field experiment.

3.3.3 Yellow-leaf variants had significantly higher K_N:K_L than control genotypes

Canopy extinction coefficients for light (K_L) and for nitrogen (K_N), and the specific leaf nitrogen at the top of the canopy (SLN_0) (Table 3.3) were derived from the vertical profile of relative values of photosynthetically active radiation and canopy leaf nitrogen, respectively (Fig. 3.5). Overall, G modification did not result in a significant change in light and nitrogen profiles in comparison with the C genotypes, although the K_N:K_L ratio was slightly higher in G than in C genotypes when approaching maturity. For Y variants, more light penetrated into the lower layers of the canopy, as reflected by an average of 33% and 42% lower K_L for Y variants than for the C genotypes from WYJ and ZF background, respectively, across stages. With the aging of canopy leaves, K_L increased and the rates of increase in Y variants were faster than those in their C counterparts towards the early grain-filling stage. SLN_0 and K_N did not significantly differ between Y and C genotypes for the WYJ background ($P > 0.05$), except for a slightly lower value of SLN_0 in the Y variant at the stem-elongating stage (Table 3.3). However, higher values of SLN_0 (20% increase) and K_N (25% increase) were observed for the ZF-Y genotype than its C genotype, across three stages (Fig. 3.5). Across stages, both Y variants had a significantly higher K_N:K_L ratio than their C counterparts (Table 3.3; Fig. S3.4).

To check the reliability of our estimates for canopy light and N profiles, we used the unpublished data collected from a pre-experiment using only ZF genotypes conducted under field conditions in 2016, in which we measured their light profile and N profile at the flowering stage. Parameters characterising the profiles, K_L and K_N, had very similar values (Fig. S3.5) to those we obtained from the 2020 full experiment for the two genotypes (Table 3.3).

Table 3.2 Yield and yield related traits (mean with its standard error of three or four replicates in brackets) for rice genotypes of four genetic backgrounds, each including a control (C) genotype and its greener-leaf variant (G) and/or yellower-leaf variant (Y) genotype, in two experiments.

Experiment	Background	Genotype	Yield components				Grain yield	Grain-filling rate	Total biomass	Harvest index
			Panicle number	Spikelets per panicle	Filled-grain	1000-grain weight				
Greenhouse			(no. hill^{-1})	(no.)	(%)	(g)	(g hill^{-1})	(g hill^{-1} d^{-1})	(g hill^{-1})	(g g^{-1})
Experiment	GLXN	C	10.3 (0.3)	93 (2)	98.2 (0.2)	27.8 (0.8)	26.1 (0.4)	0.450 (0.007)	60.0 (0.8)	0.374 (0.008)
(2019)		G	10.0 (0.4)	98 (4)	**97.3 (0.2)***	28.1 (0.2)	26.8 (0.7)	0.462 (0.012)	60.4 (1.0)	0.382 (0.010)
	YD	C	15.7 (0.7)	67 (3)	94.1 (2.1)	28.7 (0.1)	28.0 (0.4)	0.510 (0.008)	44.4 (1.3)	0.542 (0.006)
		G	14.7 (0.3)	73 (2)	91.9 (1.8)	28.0 (0.3)	27.5 (0.5)	0.500 (0.010)	43.0 (0.2)	0.559 (0.003)
	WYJ	C	17.3 (0.3)	53 (1)	90.0 (0.5)	29.9 (0.5)	24.5 (0.4)	0.510 (0.009)	40.4 (1.5)	0.521 (0.001)
		G	17.0 (0.6)	54 (1)	91.8 (0.8)	30.2 (0.1)	25.4 (0.5)	0.529 (0.010)	41.6 (0.5)	0.524 (0.003)
		Y	**15.7 (0.3)***	**58 (1)****	**87.9 (0.1)***	29.1 (0.5)	23.4 (0.6)	**0.468 (0.011)***	39.5 (0.9)	0.509 (0.009)
	ZF	C	14.3 (0.7)	92 (4)	97.6 (0.1)	24.7 (0.2)	31.2 (0.3)	0.612 (0.005)	59.3 (1.1)	0.453 (0.007)
		Y	**11.3 (0.7)***	**139 (2)*****	**80.6 (3.4)****	**25.6 (0.2)***	32.5 (1.2)	**0.690 (0.025)***	**52.2 (0.5)****	**0.534 (0.016)****
Field			(no. m^{-2} ground)	(no.)	(%)	(g)	(g m^{-2})	(g m^{-2} d^{-1})	(g m^{-2})	(g g^{-1})
Experiment	GLXN	C	338 (6)	107 (3)	87.4 (0.7)	27.1 (0.2)	823 (11)	10.7 (0.14)	2082 (37)	0.339 (0.004)
(2020)		G	325 (6)	113 (2)	**81.2 (0.7)****	26.9 (0.3)	800 (22)	10.4 (0.29)	2056 (40)	0.336 (0.006)
	YD	C	453 (2)	126 (3)	69.2 (1.2)	27.5 (0.1)	1076 (11)	14.0 (0.14)	2208 (67)	0.422 (0.011)
		G	443 (4)	127 (2)	74.3 (1.7)	27.4 (0.6)	1128 (32)	14.6 (0.42)	2222 (51)	0.441 (0.002)
	WYJ	C	462 (11)	94 (2)	87.6 (2.2)	29.2 (0.2)	1055 (6)	16.5 (0.10)	2104 (71)	0.446 (0.007)
		G	450 (8)	100 (1)	86.9 (0.6)	30.1 (0.2)	1117 (26)	17.5 (0.40)	2237 (22)	0.450 (0.005)
		Y	**417 (4)***	**102 (0)***	**72.8 (2.0)****	28.7 (0.4)	**857 (27)****	**12.1 (0.38)*****	**1846 (55)***	0.429 (0.012)
	ZF	C	373 (4)	110 (1)	74.1 (2.1)	24.0 (0.3)	704 (27)	12.6 (0.48)	1836 (20)	0.342 (0.013)
		Y	**293 (3)****	**176 (1)*****	**64.1 (1.4)***	**25.3 (0.2)***	**795 (7)***	**16.2 (0.14)****	**1686 (16)****	**0.417 (0.007)****

Data of a variant genotype significantly different from those of its control genotype (* $P < 0.05$, ** $P < 0.01$, *** $P < 0.001$) are shown in **bold**.

Table 3.3 Values (mean with its standard error in brackets) of leaf area index (LAI), and canopy light and nitrogen distribution parameters for rice genotypes of four genetic backgrounds, each including a control (C) genotype and its greener-leaf variants (G) and/or yellower-leaf variants (Y) genotype, measured at three stages in the field experiment.

Stage	Background	Genotype	LAI (m^2 leaf m^{-2} ground)	K_L (m^2 ground m^{-2} leaf)	SLN_0 (g N m^{-2} leaf)	K_N (m^2 ground m^{-2} leaf)	K_N/K_L (-)
Stem elongating stage	GLXN	C	10.92 (0.29)	0.384 (0.046)	1.69 (0.03)	0.026 (0.004)	0.067 (0.004)
		G	10.50 (0.17)	0.417 (0.053)	1.64 (0.01)	0.020 (0.002)	**0.048 (0.004)***
	YD	C	5.77 (0.35)	0.431 (0.004)	1.70 (0.03)	0.065 (0.001)	0.152 (0.004)
		G	6.04 (0.21)	0.459 (0.022)	1.79 (0.01)	0.060 (0.006)	0.132 (0.016)
	WYJ	C	6.57 (0.16)	0.382 (0.023)	1.85 (0.01)	0.041 (0.003)	0.108 (0.008)
		G	6.68 (0.12)	0.403 (0.027)	1.82 (0.04)	0.044 (0.002)	0.109 (0.004)
		Y	7.09 (0.31)	**0.291 (0.001)***	**1.76 (0.02)***	0.042 (0.003)	**0.150 (0.013)***
	ZF	C	7.21 (0.05)	0.517 (0.086)	1.77 (0.03)	0.099 (0.003)	0.202 (0.033)
		Y	6.78 (0.23)	**0.246 (0.002)***	**1.99 (0.03)****	0.113 (0.009)	**0.460 (0.035)****
Flowering stage	GLXN	C	10.53 (0.26)	0.460 (0.028)	1.85 (0.03)	0.033 (0.003)	0.073 (0.011)
		G	**9.32 (0.22)***	0.446 (0.050)	1.77 (0.01)	0.036 (0.007)	0.080 (0.006)
	YD	C	7.46 (0.05)	0.462 (0.041)	2.13 (0.04)	0.104 (0.012)	0.225 (0.007)
		G	7.33 (0.40)	0.448 (0.040)	2.17 (0.04)	0.098 (0.006)	0.223 (0.027)
	WYJ	C	8.62 (0.13)	0.451 (0.001)	1.97 (0.04)	0.081 (0.001)	0.180 (0.002)
		G	**7.72 (0.07)****	0.447 (0.034)	2.03 (0.02)	0.084 (0.004)	0.189 (0.012)
		Y	**6.77 (0.27)****	**0.237 (0.016)*****	2.07 (0.05)	0.079 (0.004)	**0.334 (0.028)****
	ZF	C	10.79 (0.47)	0.696 (0.062)	1.67 (0.07)	0.109 (0.002)	0.160 (0.018)
		Y	**7.28 (0.30)*****	**0.378 (0.017)****	**2.14 (0.06)****	**0.133 (0.005)***	**0.351 (0.005)*****
20 d after flowering stage	GLXN	C	9.44 (0.18)	0.529 (0.025)	1.54 (0.02)	0.044 (0.003)	0.083 (0.009)
		G	9.25 (0.14)	0.544 (0.018)	1.57 (0.03)	0.047 (0.001)	0.086 (0.002)
	YD	C	6.82 (0.20)	0.738 (0.023)	1.72 (0.03)	0.113 (0.005)	0.153 (0.007)
		G	6.41 (0.08)	0.717 (0.003)	1.68 (0.02)	0.118 (0.002)	0.164 (0.004)
	WYJ	C	7.40 (0.23)	0.627 (0.035)	1.69 (0.02)	0.084 (0.003)	0.134 (0.002)
		G	6.90 (0.42)	0.616 (0.024)	1.73 (0.01)	0.087 (0.009)	0.141 (0.009)
		Y	6.90 (0.05)	**0.458 (0.031)***	1.70 (0.04)	0.089 (0.008)	**0.198 (0.026)***
	ZF	C	9.82 (0.15)	0.823 (0.046)	1.41 (0.02)	0.084 (0.001)	0.103 (0.005)
		Y	**6.98 (0.29)*****	**0.591 (0.021)***	**1.69 (0.08)***	**0.116 (0.008)***	**0.197 (0.010)*****

LAI, Leaf area index; K_L, canopy light extinction coefficient; SLN_0, specific leaf nitrogen at the top of the canopy; K_N, canopy nitrogen extinction coefficient. Data of a variant genotype significantly different from those of its control genotype (* $P < 0.05$, ** $P < 0.01$, *** $P < 0.001$) are shown in **bold**.

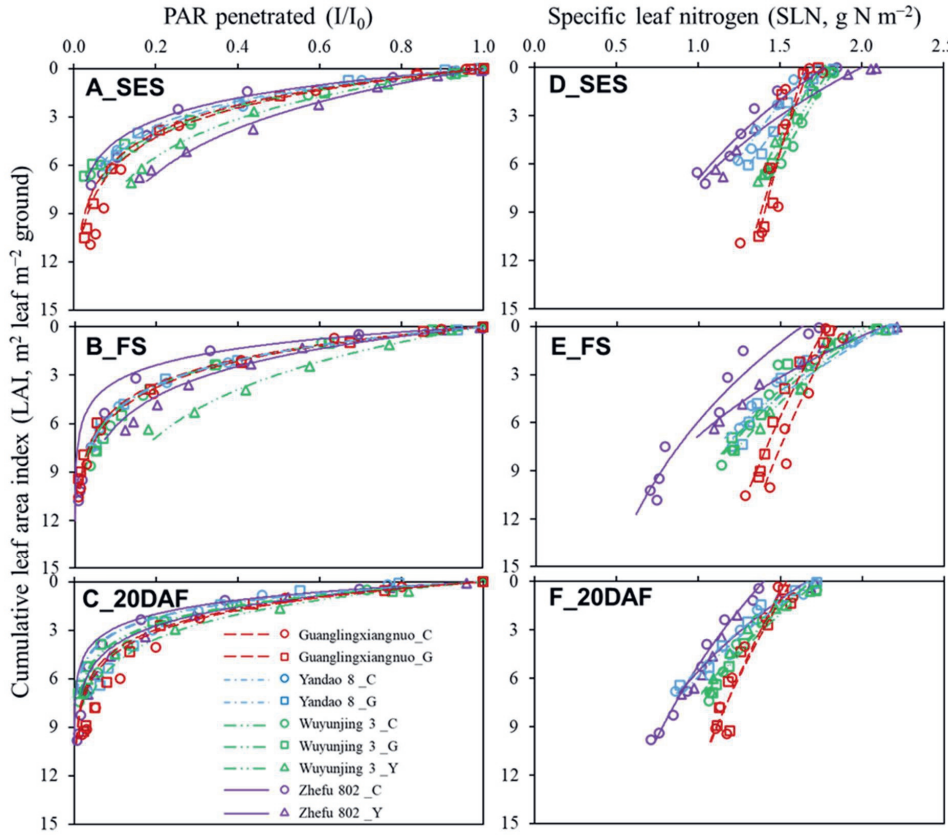

Fig. 3.5 Vertical light and nitrogen profile in canopies of rice genotypes in the field experiment. The canopy relative photosynthetically active radiation profile (PAR, A-C) and canopy leaf nitrogen profile (SLN, D-F) are plotted against cumulative leaf area index (LAI) counted from the top of the canopy for four rice control (C, circles) genotypes and their greener-leaf variant (G, squares) and/or yellower-leaf variant (Y, triangles) genotypes at three stages: SES, stem-elongating stage (A and D); FS, flowering stage (B and E); 20DAF, 20 d after flowering stage (C and F). Each data point represents the mean of three to four replicates. Curves for light profiles are drawn from Eqn (3.1) with parameter K_L fitted, while curves for nitrogen profiles are drawn from Eqn (3.2) with parameters SLN_0 and K_N fitted for each genotype. Cv. Guanglingxiangnuo is in red; cv. Yandao 8 is in blue; cv. Wuyunjing 3 is in green and cv. Zhefu 802 is in violet.

3.3.4 Differences in leaf and canopy photosynthesis among yellow-leaf variants

Light saturated net flag-leaf photosynthesis (A_{max}) and net canopy photosynthesis (A_c) were examined at flowering stage in the field experiment (Fig. 3.6). In general, variation in A_c across genotypes was significantly associated with variation in A_{max} ($R^2 = 0.68$; Fig. 3.7A), while A_{max} was highly correlated with its leaf nitrogen content ($R^2 = 0.60$; Fig. 3.7B). The photosynthetic performance at both leaf and canopy level were not changed much by G modification. However,

for Y modification, opposite trends were found relative to their C from different backgrounds: the modification caused ca. 12% decreases in both A_{max} and A_c in the WYJ background, while it caused ca. 32% and 38% increases in the ZF background, although leaf N content and canopy-averaged N content were increased in both Y variants. This difference in the effect of Y-modification between the two backgrounds is also directly reflected in Fig. 3.7A, where A_c is plotted against A_{max}. Because of this difference, the photosynthetic nitrogen use efficiencies (PNUE) at the leaf and canopy level were both significantly increased in ZF-Y, while the leaf PNUE was significantly decreased in WYJ-Y (Figs. 3.6C, F).

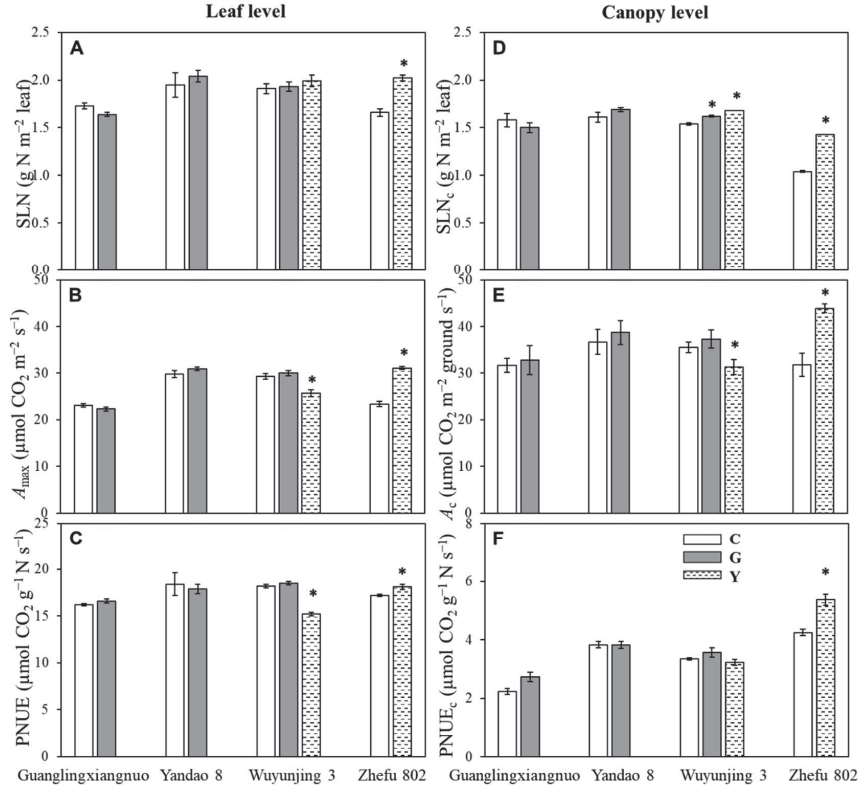

Fig. 3.6 Photosynthetic characteristics of rice genotypes at the flowering stage in the field experiment. Both leaf (A-C) and canopy (D-F) photosynthetic parameters for four rice control (C, white bars) genotypes and their greener-leaf variant (G, grey bars) and/or yellower-leaf variant (Y, dashed bars) genotypes are shown. Specific leaf nitrogen (SLN, A), light saturated leaf photosynthesis (A_{max}, B), leaf photosynthetic nitrogen-use efficiency (PNUE, C), canopy-averaged specific leaf nitrogen (SLN$_c$, D), canopy photosynthesis (A_c, E), and canopy photosynthetic nitrogen-use efficiency (PNUE$_c$, F) represent means ± standard errors of three or four replicates. PNUE and PNUE$_c$ were calculated based on Eqn (3.3) and Eqn (3.4), respectively. The asterisks (*) indicate statistical significance at the $P < 0.05$ level between variant genotype and its control genotype.

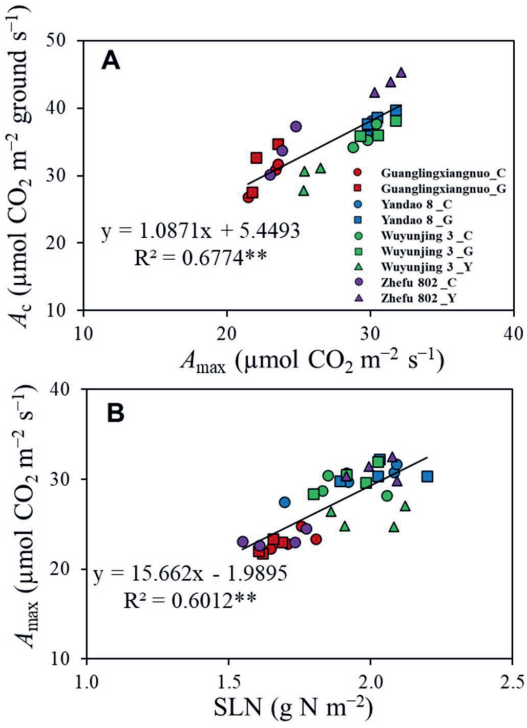

Fig. 3.7 Relations of photosynthetic parameters of rice genotypes in the field experiment. A: Relationship between canopy photosynthesis (A_c) and light saturated leaf photosynthesis (A_{max}) at the flowering stage. B: Relationship between A_{max} and specific leaf nitrogen (SLN). Linear regressions were fitted for all genotypes with three or four replicates. The significance of each correlation is shown by asterisks: ** $P < 0.01$. Cv. Guanglingxiangnuo is in red; cv. Yandao 8 is in blue; cv. Wuyunjing 3 is in green and cv. Zhefu 802 is in violet. C in circles represent control rice genotypes; G in squares represent greener-leaf variants and Y in triangles represent yellower-leaf variants.

3.3.5 K_N:K_L ratio as a main determinant of canopy photosynthesis and daily growth rate

We calculated daily CGR around flowering from measured biomass at two stages, i.e., heading and 20 d after heading. Across genotypes, CGR around flowering was positively correlated with A_c (measured at flowering) ($R^2 = 0.77$; Fig. 3.8). Theoretically, canopy productivity depends on: (i) overall canopy photosynthetic potential, represented here by N_c (which is the product of SLN_c and LAI), and (ii) the distribution of photosynthetic resources (nitrogen) in the canopy, represented by the K_N:K_L ratio (Yin and Struik, 2015). Our data showed that A_c or CGR was highly associated with the K_N:K_L ratio, although data points representing WYJ-Y clearly deviated from the linear relationships (Fig. 3.9). To examine which factor (i.e., N_c or K_N:K_L) contributed most to the variations in A_c and CGR (thus biomass gain) and whether the effect was caused by the genetic background, we conducted a multiple linear regression, where A_c or CGR was regressed against N_c and K_N:K_L with genetic backgrounds (GLXN, YD, WYJ-C&G, WYJ-Y, ZF) introduced as dummy variables (Table 3.4). The genotypes in the WYJ background

were divided into two groups (WYJ-C&G and WYJ-Y) to account for the earlier indicated negative effects of the Y modification on A_c or CGR in this WYJ background. Regression analysis showed that the variation in the K_N:K_L ratio contributed most to the variations in both A_c and CGR among all genotypes ($P < 0.001$), while N_c exerted some positive effect but was not the determining factor accounting for the variance in A_c and CGR in our study ($P > 0.05$). Nevertheless, the analysis also showed that CGR differed significantly among genetic backgrounds, with CGR of YD, WYJ-C&G and ZF being higher, and that of WYJ-Y being lower, than that of GLXN. Similar trends in genetic differences were found for A_c.

Table 3.4 Multiple regression analysis of canopy photosynthesis at flowering stage (A_c, μmol CO_2 m^{-2} ground s^{-1}) or daily crop growth rate (CGR, g m^{-2} ground d^{-1}) during flowering phase calculated from sampling intervals between heading and 20 d after heading stages as a function of genetic backgrounds (GLXN, YD, WYJ-C&G, WYJ-Y, ZF), total canopy nitrogen content in green leaves (N_c, g N m^{-2} leaf), and K_N:K_L ratio (A_c or CGR= $b_0 + b_1$GLXN + b_2YD + b_3WYJ-C&G + b_4WYJ-Y + b_5ZF + b_6N_c + b_7K_N:K_L), based on overall data of nine rice genotypes.

Dependent variable	Intercept b_0	Regression coefficient							R^2	No. of data points
		b_1§	b_2§	b_3§	b_4§	b_5§	b_6	b_7		
A_c	17.82	0	0.98	0.91	−12.70***	0.77	0.57	55.01***	0.87	27
CGR	4.51	0	4.14**	3.91**	−3.58	5.53**	0.56	40.07***	0.93	27

Significance level: ** $P < 0.01$, *** $P < 0.001$.

§ Genetic backgrounds (GLXN, YD, WYJ-C&G, WYJ-Y, ZF) as a category variable were quantified by introducing five dummy variables, with the GLXN as the reference level; so, the regression coefficient b_1 was nil while values of b_2, b_3, b_4, and b_5 indicate the effect on A_c or CGR in different genetic backgrounds, respectively, relative to the GLXN background; to differentiate the effects of Y trait from the C and G in the WYJ background on A_c and CGR (see the text), an additional dummy variable (WYJ-Y) was introduced in regression analysis.

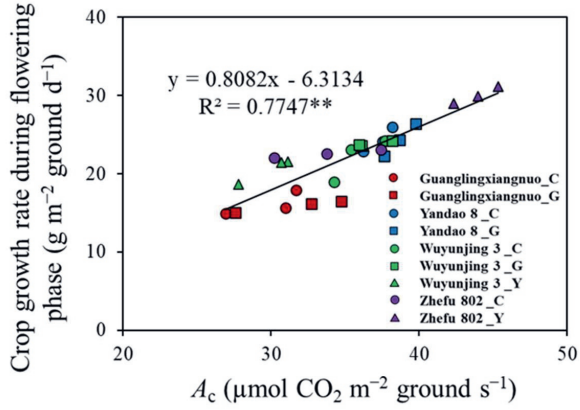

Fig. 3.8 Relationship between daily crop growth rate during flowering phase and canopy photosynthetic rate at the flowering stage (A_c). The daily average crop growth rate during flowering phase was calculated from dry weights obtained from sampling intervals between heading and 20 d after heading stages. Linear regressions were fitted for all genotypes, based on data of three individual replicates. The significance of correlation is shown by asterisks: ** $P < 0.01$.

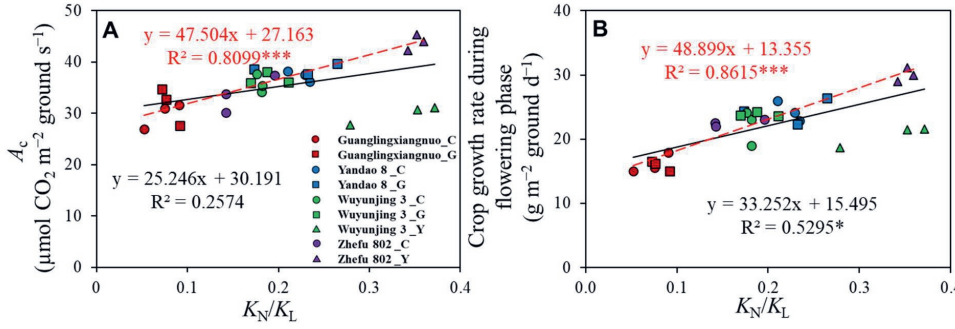

Fig. 3.9 Canopy photosynthesis or crop growth rate in relation to the canopy nitrogen to light extinction coefficient ratio (K_N/K_L). Canopy photosynthesis at flowering stage (A_c) is shown in Panel A, while daily average crop growth rate during flowering phase (shown in Panel B) was calculated from sampling intervals between heading and 20 d after heading stages in the field experiment. Linear regressions were fitted to pooled data of three replicates for all genotypes (black and full line). The red and dotted line represents the regression excluding the yellow-leaf variant from Wuyunjing background (see the text). The equation colours match the line colours. The significance of each correlation is shown by asterisks: * $P < 0.05$, *** $P < 0.001$. Cv. Guanglingxiangnuo is in red; cv. Yandao 8 is in blue; cv. Wuyunjing 3 is in green and cv. Zhefu 802 is in violet. C in circles represent control rice genotypes; G in squares represent greener-leaf variants and Y in triangles represent yellower-leaf variants.

3.4 Discussion

3.4.1 Variation in leaf photosynthesis as a result of leaf-colour modification affects canopy photosynthesis

Of the two kinds of leaf-colour modification, stay-green (G) modification had less influence on leaf photosynthesis than yellow-leaf (Y) modification (Fig. 3.6). In general, light-saturated leaf photosynthesis (A_{max}) is closely related to leaf nitrogen content (Hikosaka, 2010), in line with our result in Fig. 3.7B. To be more specific, A_{max} is related to the nitrogen invested in various photosynthetic enzymes that determine the photosynthetic capacity (Harley et al., 1992; Makino et al., 1994; Gu et al., 2012). Leaf-colour modification, as an artificial means to affect photosynthetic nitrogen distribution within the leaf, particularly alters the nitrogen investment in chlorophyll content (Fig. S3.1). This change in leaf chlorophyll content influences the photosynthetic competence by adjusting the light absorption (Evans, 1996). In this study, we examined the variation in leaf photosynthetic nitrogen use efficiency (PNUE), presented as A_{max} per unit nitrogen content (see Eqn 3.3), which resulted from the changes in the photosynthetic nitrogen content and photosynthetic nitrogen distribution within the leaf. For the two Y variants, an opposite effect on A_{max} and PNUE for the flag leaf was observed (decrease in WYJ-Y and increase in ZF-Y), suggesting discrepant effects of Y modification on the leaf nitrogen partitioning.

It was reported that exploiting the genetic variation in A_{max} can contribute to improving canopy photosynthesis (A_c) when other factors are constant (Teng et al., 2004; Gu et al., 2014). This is understandable since A_c is the spatial integration of leaf photosynthesis over canopy layers. Our results showed that leaf-colour modification similarly had an implication on canopy photosynthesis. In this case, the significantly different effects of Y modification on A_{max} were carried over to the canopy scale, as reflected by a good relationship among genotypes between A_{max} and A_c (R^2 = 0.68; Fig. 3.7A). However, the dependence of A_c on A_{max} appeared to be genetic background specific, on the basis of the understanding that A_c also depends on the relative nitrogen to light profiles in the canopy as discussed below.

3.4.2 Importance of the closeness between canopy nitrogen and light profiles in determining canopy photosynthesis

When upscaling photosynthesis from leaf to canopy level, factors like the extent to which photosynthetic N resources acclimate to light also matter (Yin and Struik, 2015). According to an optimization theory, A_c can be maximised when the leaf nitrogen distribution within the canopy is acclimated to the light distribution (i.e., K_N:K_L = 1) if A_{max} is linearly related to SLN (Field, 1983; Hirose and Werger, 1987; Goudriaan, 1995; Sands, 1995). For an actual canopy, nitrogen distribution is more uniform than light distribution, and the gradients of both light and nitrogen are highly affected by genotypic variation (Gu et al., 2017a; Ouyang et al., 2021). This was consistent with our results in that a clear difference was observed among different genetic backgrounds (Fig. 3.5). For example, compared with genotypes from other backgrounds, the ones from the GLXN background distributed more nitrogen resource to the lower layers of canopy (smaller K_N). Our results also showed an extremely steeper light gradient than the nitrogen gradient in a canopy. This gave rise to a severe mismatch in the distribution of light and nitrogen resources in the canopy, as indicated by a K_N:K_L ratio even below 0.1 for the GLXN background (Table 3.3). Overall, the observed K_N:K_L ratio, either across genotypes or across stages for our control genotypes, was not even close to the theoretical optimum (Table 3.3). Such low K_N:K_L ratios mainly resulted from the very low K_N. The low K_N:K_L ratios may reflect the possibilities that: (i) K_L varies diurnally and seasonally whereas the acclimation of nitrogen in the canopy always lags behind; (ii) A_{max} responds to leaf nitrogen content nonlinearly, in a diminishing-return manner as shown by Evans (1989); and (iii) the distribution of nitrogen in canopies is only partially driven by light distribution.

Lowering the canopy chlorophyll content proposed to improve light penetration to lower leaves has an implication on canopy photosynthesis as such manipulation decreases K_L, thereby increasing the K_N:K_L ratio. Our results with Y variants (especially with the ZF-Y genotype) confirmed this, as evidenced by higher K_N:K_L ratios in Y variants (especially in the ZF-Y genotype) (Table 3.3; Fig. S3.4). Compared with its C genotype, ZF-Y exhibited a phenotypic plasticity in nitrogen adaptation to the light environment with a steeper nitrogen gradient along the canopy (i.e., higher SLN_0 and K_N) (Figs. 3.5 and S3.5). This adaptive change in ZF-Y may partly result from its low tillering ability and LAI (Figs. 3.2 and 3.3), which overcame the weakness as occurred in its C genotype where high LAI diluted leaf nitrogen content after the stem-elongating stage (Fig. S3.6). This result supports the findings of Moreau et al. (2012) that

acclimation of the leaf nitrogen profile to the light profile is probably a whole-plant process as it was related to leaf canopy size. In our way, the resulting increase of K_N in ZF-Y, representing a higher efficiency in nitrogen use at the whole plant canopy, led to a further enhancement in A_c. This is supported by the multiple regression analysis showing that an increased K_N:K_L ratio was most significant parameter in improving A_c (Table 3.4). However, this effect was observed to a much less extent in the Y genotype from the WYJ background (Fig. 3.9). Therefore, reducing leaf and canopy chlorophyll alone (i.e., decline in K_L) may not necessarily contribute to A_c, unless a corresponding improvement in nitrogen partitioning is achieved at canopy level.

3.4.3 Opportunities for improving dry matter and yield by leaf-colour modification

The influence of leaf-colour modification on A_c eventually contributed to the dry matter accumulation, which was indicated by the high association between A_c and daily average CGR ($R^2 = 0.77$; Fig. 3.8). Leaf-colour modification is expected to improve dry matter accumulation either by extending the canopy duration (G traits) (Gregersen et al., 2013; Borrell et al., 2014) or by allowing more light penetrated into the lower canopy (Y traits) (Ort et al., 2011; Gu et al., 2017b). Given that reducing canopy chlorophyll alone may not necessarily resulted in an improved A_c, opportunities may exist by an optimization of the relevant photosynthetic traits. For example, our results from the multiple regression analysis (Table 3.4) suggested that A_c in the WYJ-Y genotype would have increased by some 13.47 (=12.7+0.77) μmol CO_2 m^{-2} ground s^{-1} if it had improved properties at leaf (higher A_{max} and PNUE) as well as canopy (e.g. K_N:K_L ratio) scales as the ZF-Y genotype. At this stage, we are not sure whether the ZF-Y genotype represents an absolutely optimised state, and it is highly likely that there is a room for the ZF-Y genotype to be further optimised for its photosynthetic characteristics.

Our study showed that leaf-colour modification not only affected leaf and canopy photosynthesis as discussed above, but also pleiotropically impacted other growth and developmental traits. In general, the impact of Y modification across the whole growth duration was more comprehensive than that of G modification as it affected other development or growth traits to a larger extent (Table 3.1). Opposite effect of Y variants on growth duration observed in WYJ vs ZF backgrounds (Table 3.1) indicated that the plant's developmental sensitivity to photoperiod or to temperature may also have been changed differently, as photoperiod and temperature are major environmental factors affecting rice phenology (Vergara et al., 1966; Yin

et al., 1997; Saito et al., 2009). The ZF-Y genotype showed fewer days to heading, indicating higher proportion of younger leaves, which could be beneficial for A_c and $PNUE_c$. On the other hand, less advantage of Y genotypes than their rice control genotype or G variants as a result of lower ability of light absorptance by leaf (Evans, 1996; Melis, 2009), may be responsible for the lower CGR of both Y variants before the establishment of a complete canopy (Fig. 3.1). In addition, the obvious decrease in number of tillers (Fig. 3.2) could also have contributed to the low CGR in Y variants, as the CGR can be significantly affected by tillers number (Hossain et al., 2011). Fewer tillers lead to lower leaf area index (LAI) (Zhong et al., 2002, 2003), and our data also showed that Y variants had a lower LAI although they reached their maximum LAI earlier (Fig. 3.3). Hence, one option to improve dry matter accumulation after Y modifications could be via crop management such as increasing planting density (e.g., a previous study of Gu et al., 2017b).

Y variants also showed a longer duration of its maximum LAI compared with their C genotypes (Fig. 3.3), which contributed to an efficient canopy light interception along the growing season for rice. A similar trend was observed for total canopy nitrogen content in green leaves (N_c) in the field experiment for each genotype across stages (Fig. 3.4), as expected given the close relationship between LAI and N_c (Fig. S3.6) as quantitatively described by Yin et al. (2003). Interestingly, both Y variants exhibited a slower decline of crop growth rate between two sampling dates during late grain-filling phase under abundant light environment (Fig. 3.1), suggesting a delayed senescence effect, which is expected in stay-green cases (Christopher et al., 2008; Wu et al., 2018; Zhao et al., 2019) and was also observed in our tested G variants (Fig. 3.1). Such a pattern in CGR could be related to nitrogen dynamics in Fig. 3.4. Among Y variants, only ZF-Y maintained a higher capacity of dry matter assimilation after the establishment of the canopy (due to the optimised nitrogen distribution at leaf and canopy level as discussed above). Such adjustment compensated for its relatively weaker dry matter accumulation in the early stages and led to a significantly enhanced CGR for the entire life cycle in relative to its C genotype (Fig. 3.1). Although total biomass gain of ZF-Y was constrained by the shortened growth duration (Table 3.1), its superior assimilate accumulation during the grain-filling phase and associated higher harvest index was responsible for its greater yield productivity (Table 3.2). The larger sink size (notably increased spikelet numbers) may also play a role as greater sink demanding for greater dry matter production can have a feedback effect on assimilate production (Dingkuhn et al., 2020). Further study on the impact of leaf-

colour modification on carbon and nitrogen source-sink balance is needed to explain our observed difference in yield and biomass accumulation during grain-filling phase.

3.5 Conclusion

In general, the impact of yellow-leaf (Y) modifications was greater than that of stay-green (G) ones. In the Y variants, light could penetrate more into the lower parts of the canopy (i.e., significantly reduced K_L), but the photosynthetic capacity (i.e., A_{max}) profile did not necessarily follow more closely to the light profile. Compared with its control genotype, the increase of A_c and CGR in ZF-Y was attributed to the higher nitrogen partitioning efficiency at both leaf (i.e., improved leaf PNUE) and canopy (i.e., steeper nitrogen gradient with more nitrogen content in the upper leaf layer of the canopy) level. The restricted leaf area and lower tiller number in Y variants maintained the higher nitrogen concentration per unit leaf area, which delayed senescence as occurred in the G variants. All these contributed to the higher CGR during the grain-filling phase and grain production per day in ZF-Y, although its total biomass accumulation was limited by shorter growth duration. Our results suggest that leaf-colour modification not only altered canopy light penetration, but also caused variations in phenology and other morpho-physiological characteristics. Whether this arose from genetic linkages or due to the randomness of radiation mutagenesis is unclear at this stage. Nevertheless, the altered traits appeared to be stable, which can be co-exploited by plant breeding for improving rice biomass and yield. Further studies are needed to understand the impact of leaf-colour modification on carbon and nitrogen source-sink relationships during grain filling.

Acknowledgements

Z.Z. thanks the China Scholar Council (CSC) for funding his PhD fellowship. We thank Dr. Changquan Zhang (Yangzhou University) and Prof. Fangmin Cheng (Zhejiang University) for providing seeds used in this study; Mr. Wendi Zhang and Mr. Yong Yang for assistance during experimentation; Dr. Kuanyu Zhu for help with canopy photosynthesis measurement and rice harvesting work. We thank reviewers for their critical comments that allowed us to improve the manuscript.

References

Anten NPR, Schieving F, Werger MJA. 1995. Patterns of light and nitrogen distribution in relation to whole canopy carbon gain in C_3 and C_4 mono- and dicotyledonous species. *Oecologia* 101, 504−513.

Archontoulis S V, Vos J, Yin X, Bastiaans L, Danalatos NG, Struik PC. 2011. Temporal dynamics of light and nitrogen vertical distributions in canopies of sunflower, kenaf and cynara. *Field Crops Research* 122, 186−198.

Arnon D. 1949. Copper enzymes in isolated chloroplasts. Polyphenoloxidase in Beta vulgaris. *Plant Physiology* 24, 1.

Awika JM. 2011. Chapter 1. Major cereal grains production and use around the world. *In: Awika, J.M., Piironen, V., Bean, S. (Eds), Advances in cereal science: implications to food processing and health promotion. American Chemical Society, ACS Symposium Series, vol 1089*. pp. 1−13.

Borrell AK, van Oosterom EJ, Mullet JE, George-Jaeggli B, Jordan DR, Klein PE, Hammer GL. 2014. Stay-green alleles individually enhance grain yield in sorghum under drought by modifying canopy development and water uptake patterns. *New Phytologist* 203, 817−830.

Bubier JL, Moore TR, Bledzki LA. 2007. Effects of nutrient addition on vegetation and carbon cycling in an ombrotrophic bog. *Global Change Biology* 13, 1168−1186.

Christopher JT, Manschadi AM, Hammer GL, Borrell AK. 2008. Developmental and physiological traits associated with high yield and stay-green phenotype in wheat. *Australian Journal of Agricultural Research* 59, 354−364.

Dingkuhn M, Luquet D, Fabre D, Muller B, Yin X, Paul MJ. 2020. The case for improving crop carbon sink strength or plasticity for a CO_2-rich future. *Current Opinion in Plant Biology* 56, 259−272.

Dungani R, Karina M, Subyakto, Sulaeman A, Hermawan D, Hadiyane A. 2016. Agricultural waste fibers towards sustainability and advanced utilization: A review. *Asian Journal of Plant Sciences* 15 , 42−55.

Evans JR. 1993. Photosynthetic acclimation and nitrogen partitioning within a lucerne canopy. II. stability through time and comparison with a theoretical optimum. *Functional Plant Biology* 20, 69−82.

Evans JR. 1988. Acclimation by the thylakoid membranes to growth irradiance and the partitioning of nitrogen between soluble and thylakoid proteins. *Functional Plant Biology* 15, 93−106.

Evans JR. 1996. Chapter: Developmental constraints on photosynthesis: effects of light and nutrition. *In: Baker, N.R. (ed), Photosynthesis and the Environment, Advances in Photosynthesis and Respiration, vol 5. Springer, Dordrecht.* pp. 281−304.

Evans JR. 1989. Photosynthesis and nitrogen relationships in leaves of C_3 plants. *Oecologia* 78, 9−19.

Field C. 1983. Allocating leaf nitrogen for the maximization of carbon gain: leaf age as a control on the allocation program. *Oecologia* 56, 341−347.

Goudriaan J. 1995. Optimization of nitrogen distribution and of leaf area index for maximum canopy photosynthesis rate. *In: Thiyagarajan, T.M., ten Berge, H.F.M., Wopereis, M.C.S. (Eds.), Nitrogen Management Studies in Irrigated Rice. AB-DLO and TPE-WAU, SARP Research Proceedings.* pp. 85−97 .

Gregersen PL, Culetic A, Boschian L, Krupinska K. 2013. Plant senescence and crop productivity. *Plant Molecular Biology* 82, 603−622.

Gu J, Chen Y, Zhang H, Li Z, Zhou Q, Yu C, Kong X, Liu L, Wang Z, Yang J. 2017a. Canopy light and nitrogen distributions are related to grain yield and nitrogen use efficiency in rice. *Field Crops Research* 206, 74−85.

Gu J, Yin X, Stomph TJ, Struik PC. 2014. Can exploiting natural genetic variation in leaf photosynthesis contribute to increasing rice productivity? A simulation analysis. *Plant, Cell & Environment* 37, 22−34.

Gu J, Yin X, Stomph TJ, Wang H, Struik PC. 2012. Physiological basis of genetic variation in leaf photosynthesis among rice (*Oryza sativa* L.) introgression lines under drought and well-watered conditions. *Journal of Experimental Botany* 63, 5137−5153.

Gu J, Zhou Z, Li Z, Chen Y, Wang Z, Zhang H. 2017b. Rice (*Oryza sativa* L.) with reduced chlorophyll content exhibit higher photosynthetic rate and efficiency, improved canopy light distribution, and greater yields than normally pigmented plants. *Field Crops Research* 200, 58−70.

Harley PC, Thomas RB, Reynolds JF, Strain BR. 1992. Modelling photosynthesis of cotton grown in elevated CO_2. *Plant, Cell & Environment* 15, 271−282.

Hikosaka K. 2014. Optimal nitrogen distribution within a leaf canopy under direct and diffuse light. *Plant, Cell & Environment* 37, 2077−2085.

Hikosaka K. 2010. Mechanisms underlying interspecific variation in photosynthetic capacity across wild plant species. *Plant Biotechnology* 27, 223−229.

Hirose T, Ackerly DD, Traw MB, Ramseier D, Bazzaz FA. 1997. CO_2 elevation, canopy photosynthesis, and optimal leaf area index. *Ecology* 78, 2339−2350.

Hirose T, Werger MJA. 1987. Maximizing daily canopy photosynthesis with respect to the leaf nitrogen allocation pattern in the canopy. *Oecologia* 72, 520−526.

Hossain MA, Sarkar MAR, Paul SK. 2011. Growth analysis of late transplant aman rice (cv. BR 23) raised from tiller seedlings. *Libyan Agriculture Research Center Journal International* 2, 265−273.

Jiang H, Li M, Liang N, Yan H, Wei Y, Xu X, Wu G. 2007. Molecular cloning and function analysis of the stay green gene in rice. *The Plant Journal* 52, 197−209.

Li H, Zhao C, Huang W, Yang G. 2013. Non-uniform vertical nitrogen distribution within plant canopy and its estimation by remote sensing: A review. *Field Crops Research* 142, 75−84.

Lim JS, Abdul Manan Z, Wan Alwi SR, Hashim H. 2012. A review on utilisation of biomass from rice industry as a source of renewable energy. *Renewable and Sustainable Energy Reviews* 16, 3084−3094.

Liu D, Wang W, Cai X. 2014. Modulation of amylose content by structure-based modification of Os GBSS 1 activity in rice (*Oryza sativa* L.). *Plant Biotechnology Journal* 12, 1297−1307.

Long SP, Marshall-Colon A, Zhu XG. 2015. Meeting the global food demand of the future by engineering crop photosynthesis and yield potential. *Cell* 161, 56−66.

Makino A, Nakano H, Mae T. 1994. Responses of ribulose-1,5-bisphosphate carboxylase, cytochrome f, and sucrose synthesis enzymes in rice leaves to leaf nitrogen and their relationships to photosynthesis. *Plant Physiology* 105, 173−179.

Melis A. 2009. Solar energy conversion efficiencies in photosynthesis: minimizing the chlorophyll antennae to maximize efficiency. *Plant Science* 177, 272−280.

Monsi M, Saeki T. 2005. On the factor light in plant communities and its importance for matter production. *Annals of Botany* 95, 549−567.

Moreau D, Allard V, Gaju O, le Gouis J, John Foulkes M, Martre P. 2012. Acclimation of leaf nitrogen to vertical light gradient at anthesis in wheat is a whole-plant process that scales with the size of the canopy. *Plant Physiology* 160, 1479−1490.

Muthayya S, Sugimoto JD, Montgomery S, Maberly GF. 2014. An overview of global rice production, supply, trade, and consumption. *Annals of the new york Academy of Sciences* 1324, 7−14.

Niu S, Wu M, Han Y, Xia J, Li L, Wan S. 2008. Water-mediated responses of ecosystem carbon fluxes to climatic change in a temperate steppe. *New Phytologist* 177, 209−219.

Niu S, Wu M, Han Y, Xia J, Zhang Z, Yang H, Wan S. 2010. Nitrogen effects on net ecosystem carbon exchange in a temperate steppe. *Global Change Biology* 16, 144−155.

Ort DR, Merchant SS, Alric J, Barkan A, Blankenship RE, Bock R, Croce R, Hanson MR, Hibberd JM, Long SP, Moore TA, Moroney J, Niyogi KK, Parry MAJ, Peralta-Yahya PP, Prince RC, Redding KE, Spalding MH, van Wijk KJ, Vermaas WFJ, von Caemmerer S, Weber APM, Yeates TO, Yuan JS, Zhu XG. 2015. Redesigning photosynthesis to sustainably meet global food and bioenergy demand. *Proceedings of the National Academy of Sciences* 112, 8529−8536.

Ort DR, Zhu X, Melis A. 2011. Optimizing Antenna Size to Maximize Photosynthetic Efficiency. *Plant Physiology* 155, 79−85.

Ouyang W, Yin X, Yang J, Struik PC. 2021. Roles of canopy architecture and nitrogen distribution in the better performance of an aerobic than a lowland rice cultivar under water deficit. *Field Crops Research* 271, 108257.

Pettigrew WT, Hesketh JD, Peters DB, Woolley JT. 1989. Characterization of canopy photosynthesis of chlorophyll-deficient soybean isolines. *Crop Science* 29, 1025−1029.

Saito H, Yuan Q, Okumoto Y, Doi K, Yoshimura A, Inoue H, Teraishi M, Tsukiyama T, Tanisaka T. 2009. Multiple alleles at Early flowering 1 locus making variation in the basic vegetative growth period in rice (*Oryza sativa* L.). *Theoretical and Applied Genetics* 119, 315−323.

Sands PJ. 1995. Modelling canopy production. I. Optimal distribution of photosynthetic resources. *Functional Plant Biology* 22, 593−601.

Slattery RA, Vanloocke A, Bernacchi CJ, Zhu XG, Ort DR. 2017. Photosynthesis, light use efficiency, and yield of reduced-chlorophyll soybean mutants in field conditions. *Frontiers in Plant Science* 8, 549.

Teng S, Qian Q, Zeng D, Kunihiro Y, Fujimoto K, Huang D, Zhu L. 2004. QTL analysis of leaf photosynthetic rate and related physiological traits in rice (*Oryza sativa* L.). *Euphytica* 135,

1−7.
Vergara BS, Tanaka A, Lilis R, Puranabhavung S. 1966. Relationship between growth duration and grain yield of rice plants. Soil Science and Plant Nutrition 12, 31−39.
Walker BJ, Drewry DT, Slattery RA, VanLoocke A, Cho YB, Ort DR. 2018. Chlorophyll can be reduced in crop canopies with little penalty to photosynthesis. *Plant Physiology* 176, 1215−1232.
Welker JM, Fahnestock JT, Henry GHR, O'Dea KW, Chimner RA. 2004. CO_2 exchange in three Canadian High Arctic ecosystems: response to long-term experimental warming. *Global Change Biology* 10, 1981−1995.
Wu H, Xiang J, Zhang Y, Zhang Y, Peng S, Chen H, Zhu D. 2018. Effects of post-anthesis nitrogen uptake and translocation on photosynthetic production and rice yield. *Scientific Reports* 8, 12891.
Xia J, Niu S, Wan S. 2009. Response of ecosystem carbon exchange to warming and nitrogen addition during two hydrologically contrasting growing seasons in a temperate steppe. *Global Change Biology* 15, 1544−1556.
Yin X, Kropff MJ, Horie T, Nakagawa H, Centeno HG, Zhu D, Goudriaan J. 1997. A model for photothermal responses of flowering in rice I. Model description and parameterization. *Field Crops Research* 51, 189−200.
Yin X, Lantinga EA, Schapendonk AHCM, Zhong X. 2003. Some quantitative relationships between leaf area index and canopy nitrogen content and distribution. *Annals of Botany* 91, 893−903.
Yin X, Struik PC. 2015. Constraints to the potential efficiency of converting solar radiation into phytoenergy in annual crops: from leaf biochemistry to canopy physiology and crop ecology. *Journal of Experimental Botany* 66, 6535−6549.
Yin X, van Laar HH. 2005. Crop systems dynamics: an ecophysiological simulation model of genotype-by-environment interactions. *Wageningen Academic Publishers, The Netherlands.*
Yoshida S, Forno DA, Cock JH, Gomez KA. 1976. Laboratory manual for physiological studies of rice. *International Rice Research Institute, The Philippines*. pp. 24–79.
Zhao Y, Qiang C, Wang X, Chen Y, Deng J, Jiang C, Sun X, Chen H, Li J, Piao W, Zhu X, Zhang Z, Zhang H, Li Z, Li J. 2019. New alleles for chlorophyll content and stay-green traits revealed by a genome wide association study in rice (*Oryza sativa*). *Scientific Reports* 9, 2541.
Zhong X, Peng S, Sanico AL, Liu H. 2003. Quantifying the interactive effect of leaf nitrogen and leaf area on tillering of rice. *Journal of Plant Nutrition* 26, 1203−1222.
Zhong X, Peng S, Sheehy JE, Visperas RM, Liu H. 2002. Relationship between tillering and leaf area index: Quantifying critical leaf area index for tillering in rice. *The Journal of Agricultural Science* 138, 269−279.
Zhu XG, Long SP, Ort DR. 2008. What is the maximum efficiency with which photosynthesis can convert solar energy into biomass? *Current Opinion in Biotechnology* 19, 153−159.

Supplementary materials in Chapter 3

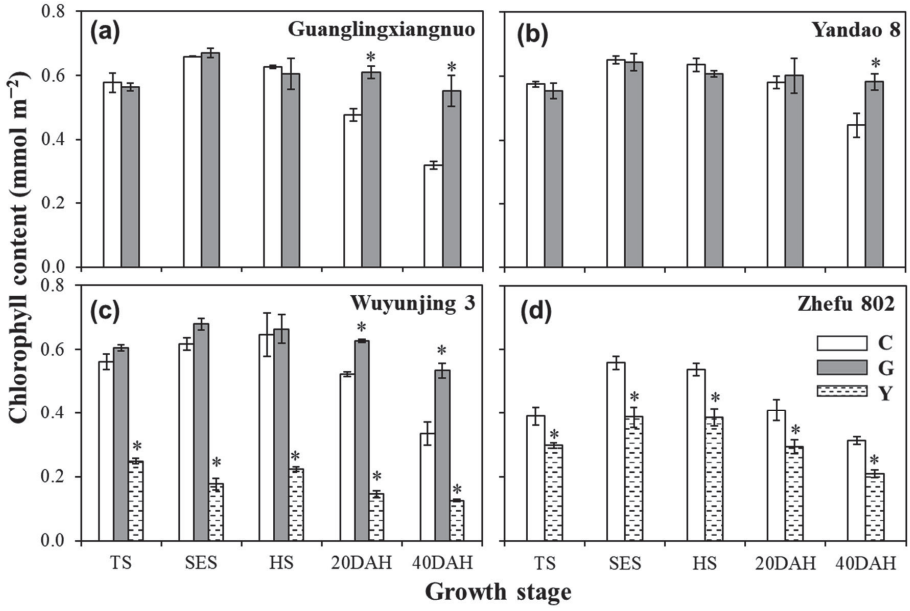

Fig. S3.1 Leaf chlorophyll content for four rice control (C, white bars) genotypes and their greener-leaf variant (G, grey bars) and/or yellower-leaf variant (Y, dashed bars) genotypes at different stages: tillering stage (TS), stem-elongating stage (SES), heading stage (HS), 20 d after heading (20DAH), and 40 d after heading stage (40DAH), in the field experiment. Vertical bars ± standard errors represent the means of four replicates. The asterisks (*) indicate statistical significance at the $P < 0.05$ level between variant genotype and its control genotype within a given stage.

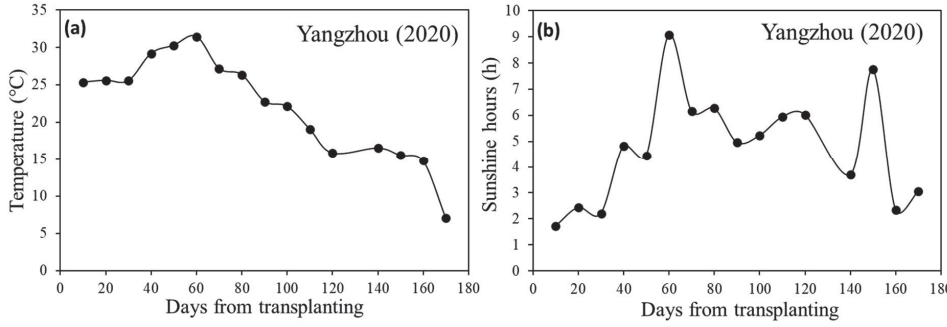

Fig. S3.2 The daily mean temperature (a) and sunshine hours (b) during the growing season of rice in 2020 at the experiment site of Yangzhou, Southeast China. Data are means per 10 days from transplanting.

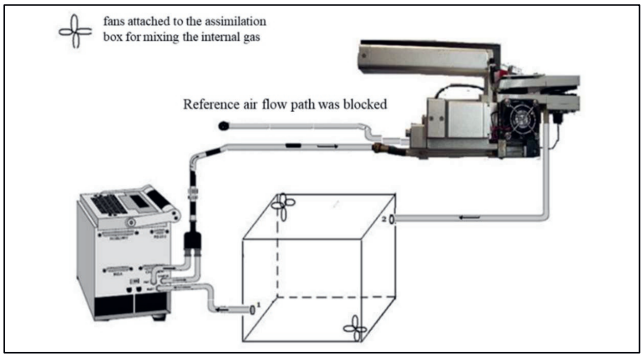

Fig. S3.3 Schematic diagram of canopy assimilation box installation (provided by Li-Cor company, Lincoln, NE, USA).

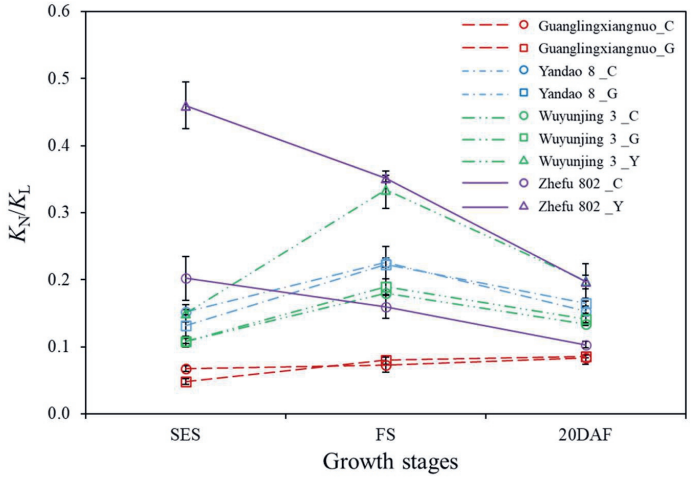

Fig. S3.4 The time course of the canopy nitrogen to light extinction coefficient ratio (K_N:K_L) for four rice control (C, circles) genotypes and their greener-leaf variant (G, squares) and/or yellower-leaf variant (Y, triangles) genotypes at three stages: SES, stem-elongating stage; FS, flowering stage; 20DAF, 20 d after flowering stage, in the 2020 field experiment. Each data point represents the mean ± standard error of three to four replicates. Cv. Guanglingxiangnuo is in red; cv. Yandao 8 is in blue; cv. Wuyunjing 3 is in green and cv. Zhefu 802 is in violet.

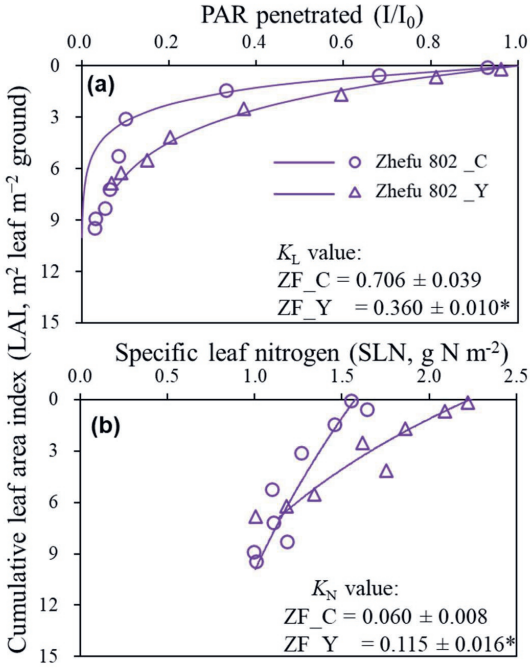

Fig. S3.5 Canopy light and nitrogen profiles, based on unpublished data from the 2016 field experiment. (a) The canopy relative photosynthetically active radiation profile (PAR) and (b) canopy leaf nitrogen profile (SLN) against cumulative leaf area index (LAI) counted from the top of the canopy for one rice control (C, circles) genotype and its yellower-leaf variant (Y, triangles) genotype at the flowering stage. Each data point is shown as mean of three to four replicates. Curves for light profiles are drawn from Eqn (3.1) while curves for nitrogen profiles are drawn from Eqn (3.2). Note: these additional data from 2016 was collected under the same crop management as in the 2020 experiment.

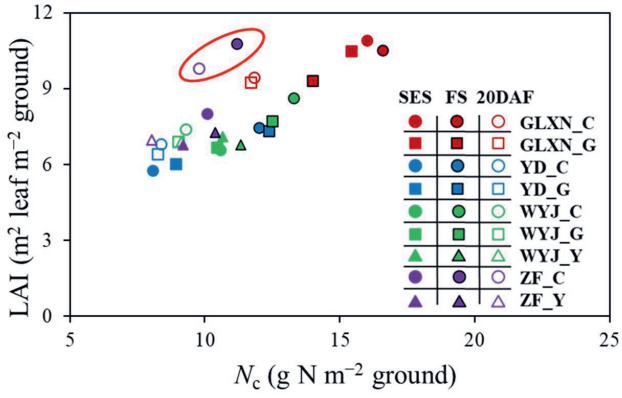

Fig. S3.6 Relationship between green leaf area index (LAI) and total canopy nitrogen content in green leaves (N_c). Data were from all genotypes at three stages: SES, stem-elongating stage; FS, flowering stage; 20DAF, 20 d after flowering stage in the field experiment in 2020. Each point represents the mean of three replicates. The symbols inside the ellipse represents the control genotype from ZF background at FS and 20DAF, respectively. Cv. Guanglingxiangnuo (GLXN) is in red; cv. Yandao 8 (YD) is in blue; cv. Wuyunjing 3 (WYJ) is in green and cv. Zhefu 802 (ZF) is in violet. Rice control (C) genotypes are in circles; greener-leaf variant (G) genotypes are in squares and yellower-leaf variant (Y) genotypes are in triangles.

Chapter 4

Quantifying source-sink relationships in leaf-colour modified rice genotypes during grain filling phase

Zhenxiang Zhou[1], Paul C. Struik[1], Junfei Gu[2], Peter E.L. van der Putten[1], Zhiqin Wang[2], Jianchang Yang[2] and Xinyou Yin[1]

[1] Centre for Crop Systems Analysis, Department of Plant Sciences, Wageningen University & Research, 6700 AK Wageningen, The Netherlands

[2] College of Agriculture, Yangzhou University, 48 Wenhui East Road, Yangzhou, Jiangsu 225009, China

This chapter has been submitted.

Abstract

Leaf-colour modification can affect the canopy photosynthesis (source), with a potential effect on rice yield and yield components (sink). Also, modulating source-sink relationships through crop management has been used to improve crop productivity. This study aims to investigate whether and how modifying leaf colour alters source-sink relationships and whether current crop cultivation practices remain applicable for leaf-colour modified genotypes. Periodically collected data of total biomass and nitrogen (N) accumulation in rice genotypes of four genetic backgrounds and their leaf-colour modified (greener or yellower) variants grown in a greenhouse experiment and a field experiment were analysed, using a recently established model method to quantify the source-sink (im)balance during grain filling. Additionally, data from a planting density experiment was also analysed. All variants prolonged the period from flowering to maturity while most of them decreased the rate of source activity and sink demand for both biomass and N. Stay-green variants did not differ, while yellow-leaf ones showed lower whole-plant biomass and N accumulation, compared with their respective normal genotypes. Of the two yellow-leaf variants, only one showed higher source capacity and sink growth than the normal genotype. The increased source capacity was associated with increased post-flowering N-uptake that prolonged functional leaf-N duration, and this increased post-flowering N-uptake was possible because of reduced pre-flowering N-uptake. The density experiment showed that current management practices (insufficient planting density accompanied with abundant N application) were unsuitable for the yellower-leaf genotype, ultimately limiting its yield potential. Leaf-colour modification affects source-sink relationships by regulating N trade-off between pre-flowering and post-flowering uptake, and N translocation between source and sink organs. To best exploit leaf-colour modification for an improved crop productivity, adjustments of crop management practices are required.

Keywords: source-sink relationship, biomass, nitrogen, *Oryza sativa*, leaf-colour modification.

4.1 Introduction

To increase rice productivity, researchers have long been studying the physiological factors that constrain the yield potential of rice, and one of these physiological constraints is source-sink relationships (Engels et al., 2011; Peng et al., 2000; Won et al., 2022; Zhang et al., 2020). Source activity (photosynthetic activity) and size (photosynthetic area and its duration) of the leaves determine crop source capacity for biomass production, while post-flowering grain growth in utilising available assimilates is the sink process (Burgess et al., 2023; Engels et al., 2011; Ohsumi et al., 2011; Peng et al., 2000; Shi et al., 2017). Source capacity and sink growth co-determine rice yield (Wardlaw, 1990; McCormick et al., 2006; Paul and Foyer, 2001; Reynolds et al., 2005; Zhang et al., 2021). Better coordination of source supply and sink demand has frequently been proposed as a viable approach to improve crop cultivation towards greater productivity (Li et al., 2020; Liu et al., 2022; Xu et al., 2018).

Leaf-colour modification has been proposed as an effective means to improve the crop source capacity of assimilate accumulation (Ort et al., 2011). Stay-green and yellow-leaf are two common traits derived from leaf-colour modification. Stay-green, delaying the onset of leaf senescence, extends the duration of canopy photosynthesis to achieve a larger post-flowering biomass accumulation (Kumar et al., 2019). By comparison, yellow-leaf traits with optimised chlorophyll content has been proposed to improve the photosynthetic carbon gain by allowing more light to penetrate to the lower part of the canopy (Ort et al., 2011; Slattery and Ort, 2021). Both traits can increase source capacity; but to be effective strategies to achieve high yields, sink traits, such as total amount of spikelets per area (Ohsumi et al., 2011; Ray et al., 2013), grain-filling ratio (Yang and Zhang, 2010), and 1000-grain weight (Liu et al., 2010), should be improved as well. Little information is available on whether and how leaf-colour modification affects sink growth and source-sink relationships.

The source-sink concept is mostly applied to analyse carbohydrate accumulation, but can equally applied to quantify nitrogen (N) budgets during grain filling (Shao et al., 2021; Sinclair et al., 2019). Both post-flowering N uptake of roots and N remobilisation from vegetative organs (leaf blades, leaf sheaths and stems) are the sources of grain N (Burgess et al., 2023; Ta and Weiland, 1992), but N remobilisation becomes progressively more important as N uptake begins to decline from flowering towards maturity (Rajcan and Tollenaar, 1999). Moreover, the more N is remobilised, the faster the photosynthetic function of vegetative organs declines. For example, Wei et al. (2018) demonstrated that rice genotypes with higher grain N concentrations,

requiring more N for grain growth, had a lower grain yield as a result of faster senescence caused by more N remobilisation. Therefore, coordinating pre-flowering N accumulation and post-flowering N remobilisation and uptake is crucial for determining both post-flowering canopy photosynthesis and grain yield (Nehe et al., 2020). The stay-green trait, delaying the degradation of chlorophyll into amino acids that could serve as a N source for the grains (Patra, 2020), can prolong the functional N duration of leaves and may enhance the rates of grain-filling and sink growth. Likewise, the yellow-leaf traits as a result of lower chlorophyll contents, may alter the remobilisation of N components from the leaves, thereby altering the source of the N supply to grains. How to maintain the dynamic relationship between N source capacity and sink demand in leaf-colour modified genotypes, and whether this relationship differs among genetic backgrounds, all remain largely unexploited.

The genotype-specific relationship between source and sink dynamics has been extensively investigated to develop strategies for achieving high crop yields (Asseng et al., 2017; Barnett and Pearce, 1983; Smith et al., 2018). These studies suggested that source-sink ratios or relationships could be further adjusted through effective management practices (Bonelli et al., 2016; Zhang et al., 2021, 2018). Among these practices, planting density plays a significant role as it can influence source-sink relationships by altering competition within the plant population for resource like light and N fertiliser (Zhang et al., 2020). Recent evidences showed that optimising the planting density of specific maize genotypes can result in increased production without the need for additional N input (Hou et al., 2020; Zhang et al., 2020). Since leaf-colour modification potentially alters source activity, it remains uncertain whether these variant genotypes can effectively adapt to current standard planting density, and if not, whether planting densities could be optimised.

We hypothesise that the source-sink balance may be shifted by leaf-colour modification and local standard plant density with abundant nitrogen supply currently in use may not be optimal for the leaf-colour variants, thus limiting their final yield potential. To test these hypotheses, we used rice genotypes from different genetic backgrounds, that had been modified to have either the stay-green trait or the yellow-leaf trait or both, to assess the source-sink (im)balance of carbohydrate and N during grain filling in these genotypes. We aimed to (i) examine the effect of leaf-colour modification on source-sink relationships for carbohydrate and N during grain filling; (ii) explore how source capacity and sink growth of biomass regulated by N budgets; and (iii) examine whether the source-sink relationships of leaf-colour variants could further be optimised via adjusting plant density.

4.2 Materials and Methods

Data for addressing the above questions came from three experiments that were previously described. Two of these experiments using the nine rice genotypes were conducted in a greenhouse at Wageningen University & Research, Wageningen, the Netherlands (51°58′N, 05°40′E), and at the field farm of Yangzhou University, Jiangsu Province, China (32°30′N, 119°25′E) and have been described by Zhou et al. (2023). A third experiment on the effect of plant density was reported by Gu et al. (2017). The data from these experiments used here for quantifying source-sink relationships were not published previously. Some information about these experiments is given below.

4.2.1 Plant materials

Rice (*Oryza sativa* L.) materials were obtained from four background groups: cv. Guanglingxiangnuo (GLXN; *japonica* type), cv. Yandao 8 (YD; *japonica* type), cv. Wuyunjing 3 (WYJ; *japonica* type), and cv. Zhefu 802 (ZF; *indica* type). The GLXN genotype was subjected to tissue culture to acquire a stay-green trait. The YD and ZF genotypes were modified via radiation mutagenesis (with ^{60}Co γ-rays) to hold a stay-green and a yellow-leaf trait, respectively. Only the WYJ genotype was modified via radiation mutagenesis to exhibit both the stay-green and yellow-leaf traits. Thus, there were a total of nine genotypes. These leaf-colour traits were identified from a larger population of phenotypes and these variant genotypes showed stability of the lines over generations. To distinguish the resulting variants, the stay-green and yellow-leaf genotype variants are coded as G and Y, respectively, while the nonmodified genotypes are labelled as control (C). The seeds of genotypes with GLXN, YD, and WYJ backgrounds were obtained from Yangzhou University, and those of ZF genotypes were from Zhejiang University, China. Detailed information about the modifications and nine genotypes can be found in Zhou et al. (2023).

As shown in our previous analysis (Zhou et al., 2023) and in the present study (see later), of all the leaf-colour modified genotypes, the Y variant of the ZF background is the most promising genotype to be exploited for improving leaf photosynthesis and crop productivity. So, additionally, we used data from a planting density experiment of 2015, as reported by Gu et al. (2017) for the two genotypes with the ZF background, to assess the suitability of the current crop density for the ZF-Y genotype.

4.2.2 Experimental environments

Greenhouse experiment (2019): Global irradiation was kept within 400-500 W m^{-2}. The day-time temperature was maintained at 26 ± 0.5 °C and night-time temperature at 23 ± 0.5 °C, each lasting 12 hours per day. The CO_2 level was ca. 400 μmol mol^{-1}. The relative humidity was within 65~75%. Pre-germinated seeds of the nine genotypes were sown in porous plastic trays (filled with nutrition-rich substrate) on 10 April 2019. Two seedlings were then transplanted at the 3rd leaf stage to each pot that contained 6.5 kg of sandy loam soil with 84.5 mg alkali-hydrolysable N, 6.5 mg Olsen-P, and 229.7 mg exchangeable K. Totally 1.5 g KH_2PO_4 and 1 g urea was applied in each pot. All pots were placed on movable lorries according to a randomised complete block design, with three replications per genotype.

Field experiment (2020): During the rice growing season (from June to October), the average air temperature was 23.8 °C and average daily sunshine hours were 5.1 h. The soil in the experimental field was also a sandy loam (Typic Fluvaquent, Etisols [U.S. taxonomy]) with 25.5 g kg^{-1} organic matter, 103 mg kg^{-1} alkali-hydrolysable N, 33.4 mg kg^{-1} Olsen-P, and 70.5 mg kg^{-1} exchangeable K. Pre-germinated seeds were first sown in paddy seedbed field plots on 27 May 2020. The seedlings of the 3rd leaf stage were then transplanted to the experimental field with a hill spacing of 25 cm × 16 cm and two seedlings per hill. A split-plot design was used with genetic backgrounds as the main plots and genotypes as the split plots, in a randomised block arrangement with three replicates. The experimental plot received a total of 30 kg ha^{-1} of phosphorus (as single superphosphate), 40 kg ha^{-1} of potassium (as KCl), and 240 kg ha^{-1} of N (as urea).

According to the local standard practices in Yangzhou, the phosphorus and potassium nutrients were applied adequately as basal fertiliser before the transplanting process, and N was applied at pre-transplanting, early tillering, and panicle initiation stage with the ratio of 5:2:3 at these stages, for both greenhouse and field experiments. Throughout the growth cycle, the plants received sufficient water, and drainage was only implemented during a critical leaf-age stage.

For the plant-density experiment, the growth conditions and crop management practices (except for the density-treatments) were consistent with those outlined in our 2020 experiment. The four density levels were: control (hill spacing of 25 × 15 cm^2), 30% higher density (hill spacing of 25 × 11.5 cm^2), 50% higher density (hill spacing of 25 × 10 cm^2), and 70% higher density (hill spacing of 25 × 8.8 cm^2), corresponding to 27, 35, 40, and 45 hills per m^2, respectively.

4.2.3 Sampling and measurements

Flowering date of each rice genotype was observed as the moment when the first panicle of the whole plant emerged from the flag-leaf sheath, while maturity date was defined as the moment when 98% grains or the rachis of the panicle turned yellow. The flowering and maturity dates of each rice genotype in these experiments are listed in Table S4.1. Starting from flowering stage, aboveground rice materials of one pot in the greenhouse experiment and of five plants per plot in the field experiments were sampled 8-13 times per replicate per genotype, depending on genotypes' grain-filling duration. These sampled plants were separated into panicle, leaf, and stem (including leaf sheath) parts, and then transferred to a forced air oven (UF 260, Memmert Corp., Germany) at 105 °C for 0.5 h. After further oven-drying at a constant temperature (75 °C) for at least 72 hours, biomass of these organs was weighed and ground into powder to determine the N concentration using the Kjeldahl apparatus (Kjeltec 8400, Foss Corp., Germany). The N accumulation for each organ was calculated by multiplying N concentration with biomass weight, while the total aboveground N accumulation was the sum of the N accumulation of all the organs (i.e., panicle, leaf, and stem).

4.2.4 Quantifying carbon and nitrogen source–sink relationships during grain filling

As carbon fraction in biomass is quite conserved among rice organs (~45%; Penning de Vries et al., 1974, 1989), we then used biomass data to indicate the carbon source-sink relationships. We use W and N to describe biomass and nitrogen data, respectively. To differentiate sink parameters from source parameters, we add subscript i to indicate all sink parameters and subscript o for all source parameters (see Table S4.2 for all model symbol definitions and units).

For estimating parameters values of sink for biomass (W_{i}), the time course of panicle weight can be described by a sigmoid function (Yin et al., 2003) as:

$$W_{\mathrm{i}} = \begin{cases} (W_{\mathrm{x,i}} - W_{\mathrm{b,i}})\left(1 + \frac{t_{\mathrm{e,i}} - t}{t_{\mathrm{e,i}} - t_{\mathrm{m,i}}}\right)\left(\frac{t - t_{\mathrm{b}}}{t_{\mathrm{e,i}} - t_{\mathrm{b}}}\right)^{\frac{t_{\mathrm{e,i}} - t_{\mathrm{b}}}{t_{\mathrm{e,i}} - t_{\mathrm{m,i}}}} + W_{\mathrm{b,i}} & if\ t_{\mathrm{b}} \le t \le t_{\mathrm{e,i}} \\ W_{\mathrm{x,i}} & if\ t > t_{\mathrm{e,i}} \end{cases} \quad (4.1)$$

where $W_{\mathrm{b,i}}$ represents the initial panicle weight at the initial time point (t_{b}), $W_{\mathrm{x,i}}$ represents the maximum panicle weight reached at the moment when the grain-filling rate is decreased to zero ($t_{\mathrm{e,i}}$), $t_{\mathrm{m,i}}$ represents the moment when the maximum grain-filling rate is achieved, and t is the time after flowering.

After these parameters was estimated, the sink activity (s_{iW}) representing the temporal course of the rate of increase in panicle weight was calculated through the differential form of eqn (4.1) (Yin et al., 2003, 2009):

$$s_{iW} = s_{m,iW}\left(\frac{t_{e,i}-t}{t_{e,i}-t_{m,i}}\right)\left(\frac{t-t_b}{t_{m,i}-t_b}\right)^{\frac{t_{m,i}-t_b}{t_{e,i}-t_{m,i}}} \tag{4.2}$$

where $s_{m,iW}$ is the maximum rate of increase in panicle weight at time $t_{m,i}$, which was given by Yin et al. (2003):

$$s_{m,iW} = \left(W_{x,i} - W_{b,i}\right)\left[\frac{2t_{e,i}-t_{m,i}-t_b}{(t_{e,i}-t_b)(t_{e,i}-t_{m,i})}\right]\left(\frac{t_{m,i}-t_b}{t_{e,i}-t_b}\right)^{\frac{t_{m,i}-t_b}{t_{e,i}-t_{m,i}}} \tag{4.3}$$

In contrast to the eqn (4.2) described bell-shape dynamics of sink activity, source activity (s_{oW}) after flowering declines, which can be described by a reversed sigmoid function (Yin et al., 2009):

$$s_{oW} = \begin{cases} s_{m,oW}\left[1-\left(1+\frac{t_{e,o}-t}{t_{e,o}-t_{m,o}}\right)\left(\frac{t}{t_{e,o}}\right)^{\frac{t_{e,o}}{t_{e,o}-t_{m,o}}}\right] & if\ t < t_{e,o} \\ 0 & if\ t \geq t_{e,o} \end{cases} \tag{4.4}$$

where $t_{m,o}$ represents the moment when the decrease of s_{oW} is fastest, and $t_{e,o}$ represents the moment when the s_{oW} is decreased to zero; $s_{m,oW}$ represents the maximum rate of s_{oW}, which occurs at flowering. Integrating eqn (4.4) over time from flowering to $t_{e,o}$ gives an equation describing the time course of aboveground biomass during grain filling (Shi et al., 2017):

$$W_o = s_{m,oW}t\left\{1-\left(\frac{1}{2t_{e,o}-t_{m,o}}\right)\left(\frac{t}{t_{e,o}}\right)^{\frac{t_{e,o}}{t_{e,o}-t_{m,o}}}\left[\left(2t_{e,o}-t_{m,o}-t\right)+\frac{(t_{e,o}-t_{m,o})t}{3t_{e,o}-2t_{m,o}}\right]\right\} + W_{b,o} \tag{4.5}$$

So, the maximum aboveground biomass, $W_{x,o}$, which is achieved at time $t = t_{e,o}$, can be expressed from eqn (4.5) as (see Shi et al., 2017):

$$W_{x,o} = W_{b,o} + s_{m,oW}\frac{{t_{e,o}}^2}{3t_{e,o}-2t_{m,o}} \tag{4.6}$$

where $W_{b,o}$ is the initial aboveground biomass at flowering. Solving parameter $s_{m,oW}$ from eqn (4.6) and substituting it into eqn (4.5) give an equation describing the time course of aboveground biomass from flowering to maturity:

$$W_o = \begin{cases} \frac{(W_{x,o}-W_{b,o})t}{{t_{e,o}}^2}\left[\left(3t_{e,o}-2t_{m,o}\right)-\left(3t_{e,o}-2t_{m,o}-t\right)\left(\frac{t}{t_{e,o}}\right)^{\frac{t_{e,o}}{t_{e,o}-t_{m,o}}}\right]+W_{b,o} & if\ t < t_{e,o} \\ W_{x,o} & if\ t \geq t_{e,o} \end{cases} \tag{4.7}$$

Commonly, these parameters of source (i.e. $W_{b,o}$, $W_{x,o}$, $t_{m,o}$, and $t_{e,o}$) and sink (i.e. $W_{b,i}$, $W_{x,i}$, $t_{m,i}$, and $t_{e,i}$) could be estimated by fitting eqn (4.1) and eqn (4.7) to periodically sampled data for

aboveground biomass weight and panicle weight, respectively. Here, we followed the fitting procedure of Shao et al. (2021) by introducing two dummy variables Z_1 and Z_2 as: $W = Z_1 W_o + Z_2 W_i$, where $Z_1 = 1$ and $Z_2 = 0$ were set for aboveground biomass and $Z_1 = 0$ and $Z_2 = 1$ were for panicle biomass. Using this dummy variable method can estimate all parameters for sink and source part in a single procedure (as a full model). The total amount of sink growth or of source capacity during grain-filling can be expressed as:

$$\text{Total sink growth} = W_{x,i} - W_{b,i} \tag{4.8a}$$

$$\text{Total source capacity} = W_{x,o} - W_{b,o} \tag{4.8b}$$

And the mean rate ($\bar{s}_W$) of sink demand or of source activity during this phase can also be calculated as:

$$\bar{s}_{iW} = \frac{W_{x,i} - W_{b,i}}{t_{e,i} - t_b} \tag{4.9a}$$

$$\bar{s}_{oW} = \frac{W_{x,o} - W_{b,o}}{t_{e,o} - t_b} \tag{4.9b}$$

The advantage of using the dummy variable approach is to allow a statistical test if total post-flowering source meets the demand for total sink growth. For that, we conducted an additional fitting step, in which we introduced the following source-sink equilibrium formula to reduce one estimated parameter (i.e. $W_{x,o}$) to be fitted (as a reduced model):

$$W_{x,o} = \left(W_{x,i} - W_{b,i}\right) + W_{b,o} \tag{4.10}$$

By comparing the residual sum of squares and degrees of freedom between the full model and reduced model, the *F* test was conducted to examine the null hypothesis (H_0) that total post-flowering source and total sink growth are equal. A significant *F*-value ($P < 0.05$) indicates the rejection of the H_0, namely, total source supply during grain-filling differs significantly from the demand for total sink growth.

For describing the source and sink dynamics of N accumulation, the same procedures from eqn (4.1) to eqn (4.10) were applied in observed data for the time course of N accumulation in panicles and aboveground components, with all the symbol *W* in these equations (i.e. dry weight accumulation) being replaced by symbol *N* (i.e. N accumulation) (see Table S4.2).

After getting these fitted parameter values for biomass and N, respectively, the source–sink difference was calculated as the difference between total source supply and total sink growth,

and the source/sink ratio is defined as total source supply divided by total sink growth. If total source supply is larger than or equal to total sink growth (i.e. source-sink difference ≥ 0), it means no need to translocate pre-flowering carbohydrates or N accumulation to support grain filling; otherwise, the carbohydrates produced or the N uptake after flowering are insufficient, contribution from pre-flowering assimilates (remobilised from vegetative organs) is necessary to meet the demand for grain growth, which can be quantified as:

$$\text{Pre-F (\%)} = \frac{\text{Sink−source difference}}{\text{total sink growth}} \times 100. \tag{4.11}$$

4.2.5 Data analysis

Ambient temperature fluctuated both diurnally and seasonally during grain filling, especially under field conditions. To reduce the impact of the temperature variations, we converted the actual grain-filling days (d) into thermal days (td) according to the bell-shaped function of Yin et al. (1995), describing developmental rate in response to temperature, g(T), as:

$$g(T) = \begin{cases} \left(\frac{T_c - T}{T_c - T_o}\right)\left(\frac{T - T_b}{T_o - T_b}\right)^{\frac{T_o - T_b}{T_c - T_o}} & \text{if } T_b < T < T_c \\ 0 & \text{if } T \le T_b \text{ or } T \ge T_c \end{cases} \tag{4.12}$$

where T_b, T_o, and T_c are the base, the optimum, and the ceiling temperature for phenological development, respectively (in fact, the above eqn 4.2 where the x-axis is time is mathematically equivalent to eqn 4.12 where the x-axis is temperature – both equations generate the same bell-shaped curves, Yin et al., 2003). Based on Yin and van Laar (2005), we assumed T_b = 8°C, T_o = 30°C and T_c = 42°C for rice. The value of $g(T)$ was calculated using every 30-min temperature and the daily thermal unit was calculated as the average of the values of these $g(T)$ values within the day (i.e. 24 h). One thermal unit, by definition, should be less than one actual day, unless the temperature at each 30 min of the day is at the optimum.

Data for the time course of biomass weight and N as function of thermal days were fitted to the model described in the preceding section, using a nonlinear fitting procedure the Gauss method in PROC NLIN of SAS (SAS Institute Inc., Cary, NC, USA). Simple linear regressions wherever is required in data analysis were conducted using Microsoft Excel.

4.3 Results

4.3.1 Effects of leaf-colour modification on biomass and nitrogen accumulation

The dynamics of panicle biomass accumulation and N accumulation (as sink) after flowering in the two experiments were accurately as described by eqn (4.1) while those of aboveground biomass accumulation and N accumulation (as source) were fitted well by eqn (4.7) (Fig. 4.1 and Fig. S4.1), using these estimated parameter values of sink and source ($R^2 \geq 0.98$) (Tables S4.3 and S4.4). There was little difference in whole-plant and panicle biomass or N accumulation during grain filling between G variants and their C genotypes in both experiments. For yellow-leaf (Y) modification, both variants showed lower whole-plant biomass and N accumulation, as indicated by lower estimated values in maximum aboveground biomass ($W_{x,o}$) and N ($N_{x,o}$), compared with their respective C genotypes. However, an opposite trend was observed in sink parameters between two Y genotypes: lower values of maximum panicle biomass ($W_{x,i}$) and N ($N_{x,i}$) in WYJ-Y, and higher $W_{x,i}$ and $N_{x,i}$ in ZF-Y, compared with their C genotypes. The duration from flowering to maturity for both source ($t_{e,o}$) and sink ($t_{e,i}$) was increased by leaf-colour modification, implying a delayed leaf senescence and prolonged grain filling.

4.3.2 Effects of leaf-colour modification on source activity and sink demand

Using the estimated parameter values in Tables S4.3-S4.4, we derived rate parameter values (Table S4.5) and drew curves for the dynamics of daily biomass (Fig. 4.2) or N (Fig. S4.2) sink demand and source activity during grain filling by eqns (4.2) and (4.4), respectively. The rate of sink demand exhibited an initial increase followed by a subsequent decrease after reaching its peak. On the other hand, the rate of source activity remained relatively constant initially and then gradually declined over time.

For most of the genetic backgrounds (except ZF), the dynamic curves of the rate of source activity for biomass were lower during the initial phase and higher for a brief duration towards maturity in leaf-colour modified genotypes, as indicated by lower values of the maximum rate ($s_{m,oW}$) and the mean rate ($\bar{s}_{oW}$) of source activity (Table S4.5). The dynamic curves of sink demand for biomass showed lower peaks but higher values during the initial and late phases, resulting from decreased parameter values of the maximum rate ($s_{m,iW}$) and the mean rate ($\bar{s}_{iW}$) of sink demand, in leaf-colour modified genotypes compared with their C genotypes.

In the ZF background, the Y-variant genotype exhibited higher source activity and sink demand than its C genotype after flowering (Figs 4.2D,H), and the extent of increase in $s_{m,oW}$ and $\bar{s}_{oW}$ was much higher than that in $s_{m,iW}$ and $\bar{s}_{iW}$.

Patterns for N sink demand and source activity were observed to be similar to those for biomass in each genotype, as shown in Fig. S4.2.

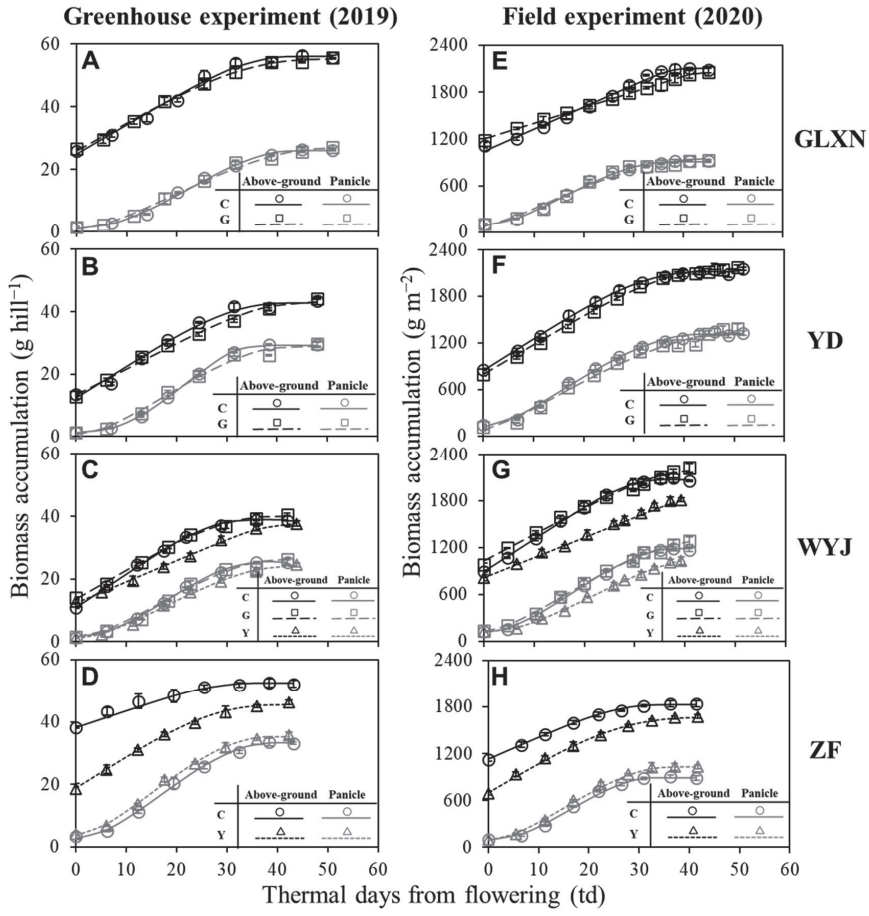

Fig. 4.1 The time course of above-ground biomass (dark symbols) and panicle biomass (grey symbols) in two experiments. Rice genotypes comprised four rice control (C, circles) genotypes and their greener-leaf variant (G, squares) and/or yellower-leaf variant (Y, triangles) genotypes. Each data point is shown as mean ± standard error of three to four replicates. The curves were drawn from eqns (4.1) and (4.7) for panicle and whole aboveground biomass accumulation, respectively, using parameter values in Table S4.3. Genotype-background abbreviations: GLXN, cv. Guanglingxiangnuo; YD, cv. Yandao 8; WYJ, cv. Wuyunjing 3; and ZF, cv. Zhefu 802.

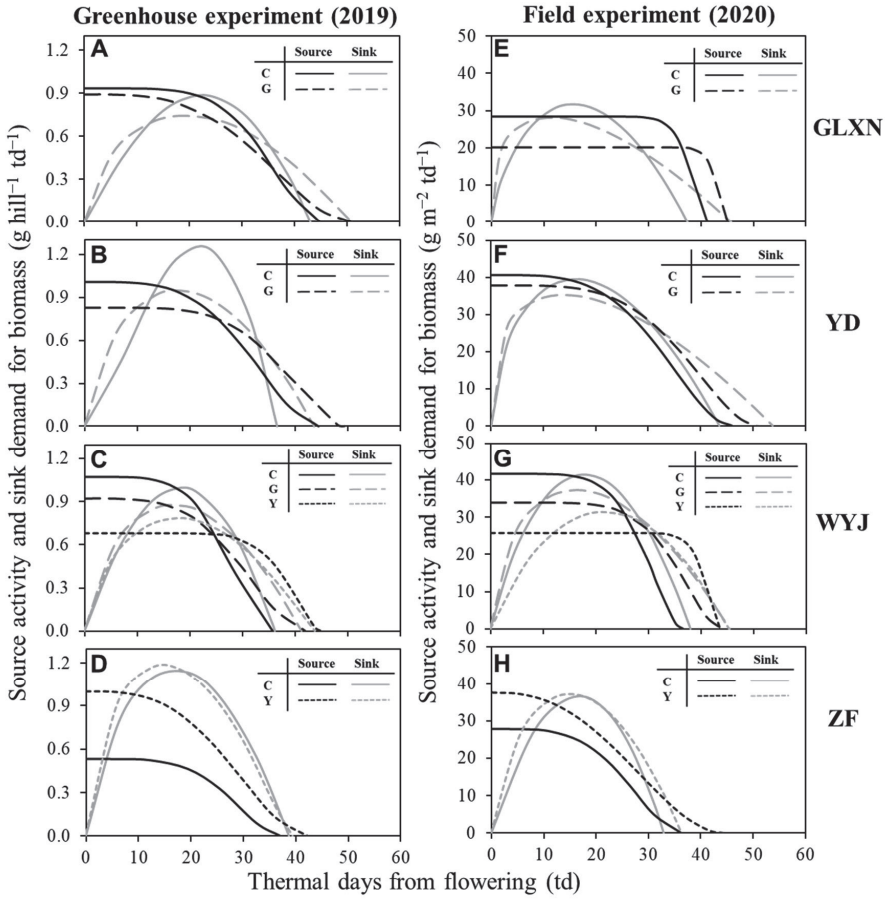

Fig. 4.2 Dynamics of source activity and sink demand for biomass in two experiments. Rice genotypes comprised four rice control (C, full curves) genotypes and their greener-leaf variant (G, long-dashed curves) and/or yellower-leaf variant (Y, short-dashed curves) genotypes. The curves were drawn from eqns (4.2) and (4.4) for biomass sink and source activity, respectively, using parameter values in Table S4.3. Genotype-background abbreviations: GLXN, cv. Guanglingxiangnuo; YD, cv. Yandao 8; WYJ, cv. Wuyunjing 3; and ZF, cv. Zhefu 802.

Table 4.1 The source-sink relationships for biomass (W) and nitrogen (N) accumulation during grain filling in three experiments.

Experiment	Background	Genotype	Density	Source-sink relationship for biomass					Source-sink relationship for nitrogen				
				Source capacity	Sink growth	Source-sink difference	Source/sink ratio	Pref-F [a]	Source capacity	Sink growth	Source-sink difference	Source/sink ratio	Pre-F [a]
				(g hill^{-1})	(g hill^{-1})	(g hill^{-1})	(−)	(%)	(g hill^{-1})	(g hill^{-1})	(g hill^{-1})	(−)	(%)
Greenhouse experiment (2019)	GLXN	C		31.2	25.0	6.1**	1.24	0	0.071	0.189	-0.119***	0.37	63
		G		29.4	26.0	3.3	1.13	0	0.071	0.198	-0.127***	0.36	64
	YD	C		30.5	28.3	2.3	1.08	0	0.127	0.249	-0.122***	0.51	49
		G		29.8	28.5	1.3	1.04	0	0.139	0.257	-0.119***	0.54	46
	WYJ	C		28.0	23.9	4.1*	1.17	0	0.108	0.216	-0.108***	0.50	50
		G		26.4	24.8	1.6	1.06	0	0.117	0.222	-0.105***	0.53	47
		Y		25.5	23.3	2.2	1.10	0	0.123	0.211	-0.088***	0.58	42
	ZF	C		14.2	30.5	-16.2***	0.47	53	0.077	0.231	-0.154***	0.34	66
		Y		26.6	31.5	-4.9*	0.85	15	0.138	0.262	-0.124***	0.53	47
				(g m^{-2})	(g m^{-2})	(g m^{-2})	(−)	(%)	(g m^{-2})	(g m^{-2})	(g m^{-2})	(−)	(%)
Field experiment (2020)	GLXN	C		1058.6	817.4	241.2***	1.30	0	6.0	8.8	-2.8***	0.68	32
		G		854.7	872.4	-17.7	0.98	2	5.5	9.5	-4.0***	0.57	43
	YD	C		1274.6	1197.5	77.1	1.06	0	11.0	15.4	-4.4***	0.72	28
		G		1354.5	1295.5	59.0	1.05	0	12.0	16.2	-4.2***	0.74	26
	WYJ	C		1178.6	1064.8	113.8*	1.11	0	8.9	12.6	-3.7***	0.71	29
		G		1159.1	1172.6	-13.5	0.99	1	9.1	14.1	-5.1***	0.64	36
		Y		1039.7	964.0	75.7	1.08	0	7.6	11.8	-4.3***	0.64	36
	ZF	C		696.1	800.6	-104.5*	0.87	13	6.6	11.0	-4.4***	0.60	40
		Y		963.8	933.4	30.4	1.03	0	9.2	12.9	-3.6***	0.72	28
Field density experiment	ZF	C	Local	725.0	802.3	-77.3	0.90	10	6.9	11.1	-4.2***	0.63	37
			+30%	844.2	845.2	-1.0	1.00	0	7.6	11.5	-3.9***	0.66	34
			+50%	739.7	789.9	-50.2	0.94	6	6.7	10.8	-4.1***	0.62	38
			+70%	620.1	730.8	-110.7*	0.85	15	5.4	9.9	-4.5***	0.55	45
		Y	Local	911.8	851.3	60.5	1.07	0	9.4	12.8	-3.4***	0.73	27
			+30%	967.8	918.9	48.9	1.05	0	10.3	13.5	-3.2***	0.77	23
			+50%	1002.1	958.6	43.5	1.05	0	10.7	13.8	-3.1***	0.78	22
			+70%	1005.6	974.6	31.0	1.03	0	11.0	14.0	-2.9***	0.79	21

[a] Contribution from pre-flowering assimilates (remobilised from vegetative organs) to grain growth, as defined by eqn (4.11);

Genotype-background abbreviations: GLXN, cv. Guanglingxiangnuo; YD, cv. Yandao 8; WYJ, cv. Wuyunjing 3; and ZF, cv. Zhefu 802. C is rice control genotypes; G is greener leaf variant genotypes; and Y is yellower-leaf variant genotypes. Local, +30%, +50%, and +70% represent plants at local normal plant density (25 × 15 cm), 30% higher density (25 × 11.5 cm), 50% higher density (25 × 10 cm), and 70% higher density (25 × 8.8 cm), respectively. Total source capacity and sink growth for biomass and N were calculated from eqn (4.8), using parameter values in Tables S4.3 and S4.4, respectively. The significance of source-sink difference for biomass and N of each genotype is shown by asterisks: * $P < 0.05$, ** $P < 0.01$, *** $P < 0.001$.

4.3.3 Source-sink relationships among leaf-colour modified genotypes

Table 4.1 shows the total source and the total sink during grain filling, as well as the contribution of pre-flowering carbohydrate or N to grain yield. For biomass, most genotypes exhibited higher post-flowering source capacity than sink growth (except for those from the ZF background), resulting in values of source/sink ratio higher than 1.0. Any significant source-sink difference, based on the *F*-test, was primarily observed in C genotypes rather than in leaf-colour variant genotypes. Among all genotypes, only ZF-Y showed an increase in both biomass source capacity and sink demand compared to its C genotype. Notably, the increase in the source capacity outweighs the increase in the sink demand. The contributions of pre-flowering carbohydrates to grain yield were primarily observed in the ZF background in the greenhouse experiment. An exceptionally high requirement for pre-flowering remobilisation (53%) in ZF-C in the greenhouse was associated with the delayed flowering observed in this genotype (Zhou et al., 2023).

As expected, compared with biomass, the N accumulation in source capacity was much lower than that in sink demand for all genotypes, leading to source/sink ratios significantly lower than 1.0 (Table 4.1). The contributions of pre-flowering N uptake to grain N accumulation were lower in the field experiment than in the greenhouse experiment. Among all genotypes, only ZF-Y increased both N source capacity and sink growth relative to its control genotype, particularly with increased source capacity.

Overall, there were close correlations between source capacity and sink growth for both biomass and N accumulation across genotypes (Fig. S4.3a-d). Negative correlations were observed between the loss of vegetative-organ biomass and the biomass source-sink difference, and between the loss of vegetative-organ N accumulation and the N source-sink difference during grain filling (Fig. S4.4).

4.3.4 Correlations of biomass source capacity with nitrogen budgets

Rice plants had higher levels of pre-flowering N uptake ($N_{pre\text{-}F}$) than post-flowering N uptake ($N_{post\text{-}F}$) (Fig. 4.3). While the same amount of N was applied for genotypes in each experiment, a negative relationship between $N_{pre\text{-}F}$ and $N_{post\text{-}F}$ was observed across genotypes (Fig. 4.3). Contribution of pre-flowering N uptake to grain N accumulation was negatively correlated with $N_{post\text{-}F}$ (Fig. 4.4).

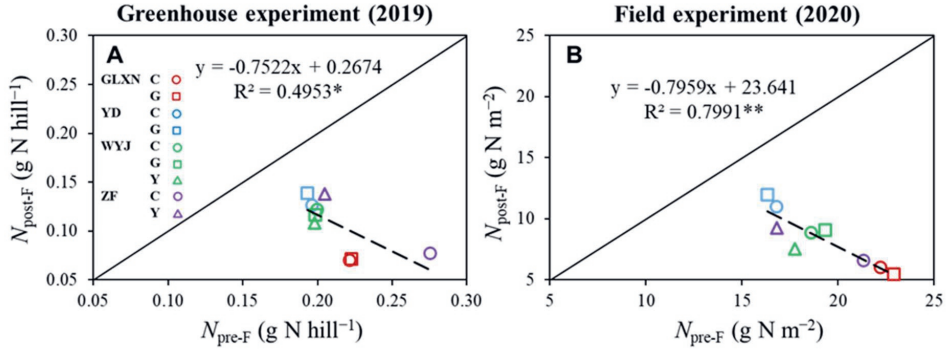

Fig. 4.3 Relationships between pre-flowering nitrogen uptake ($N_{pre\text{-}F}$) and post-flowering nitrogen uptake ($N_{post\text{-}F}$) in two experiments. $N_{pre\text{-}F}$ represents the initial aboveground N accumulation at the onset of grain filling (i.e., $N_{b,so}$), and $N_{post\text{-}F}$ represents the total N source capacity during grain filling, calculated from eqn (4.8). Linear regression was fitted for overall data with its significance of correlation shown by asterisks: * $P < 0.05$, ** $P < 0.01$. Genotype-background abbreviations: GLXN, cv. Guanglingxiangnuo; YD, cv. Yandao 8; WYJ, cv. Wuyunjing 3; and ZF, cv. Zhefu 802. C is rice control genotypes; G is greener-leaf variant genotypes; and Y is yellower-leaf variant genotypes. The diagonal line is the 1:1 line.

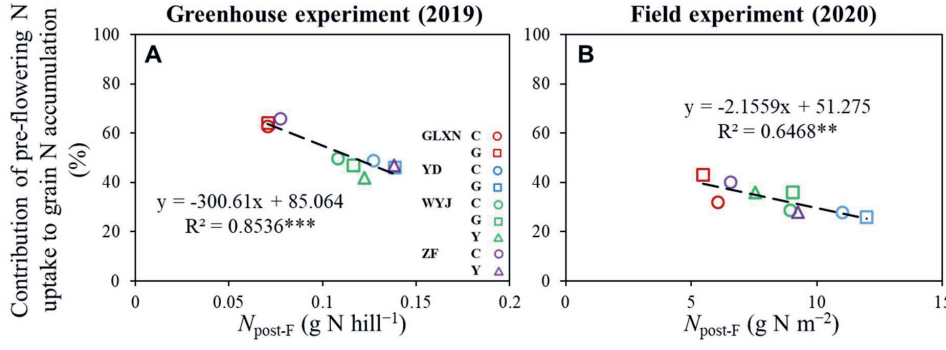

Fig. 4.4 Relationships between post-flowering nitrogen uptake ($N_{post\text{-}F}$) and contribution of pre-flowering N uptake to grain N accumulation in two experiments. Linear regression was fitted for overall data with its significance of correlation shown by asterisks: ** $P < 0.01$, *** $P < 0.001$. Genotype-background abbreviations: GLXN, cv. Guanglingxiangnuo; YD, cv. Yandao 8; WYJ, cv. Wuyunjing 3; and ZF, cv. Zhefu 802. C is rice control genotypes; G is greener-leaf variant genotypes; and Y is yellower-leaf variant genotypes.

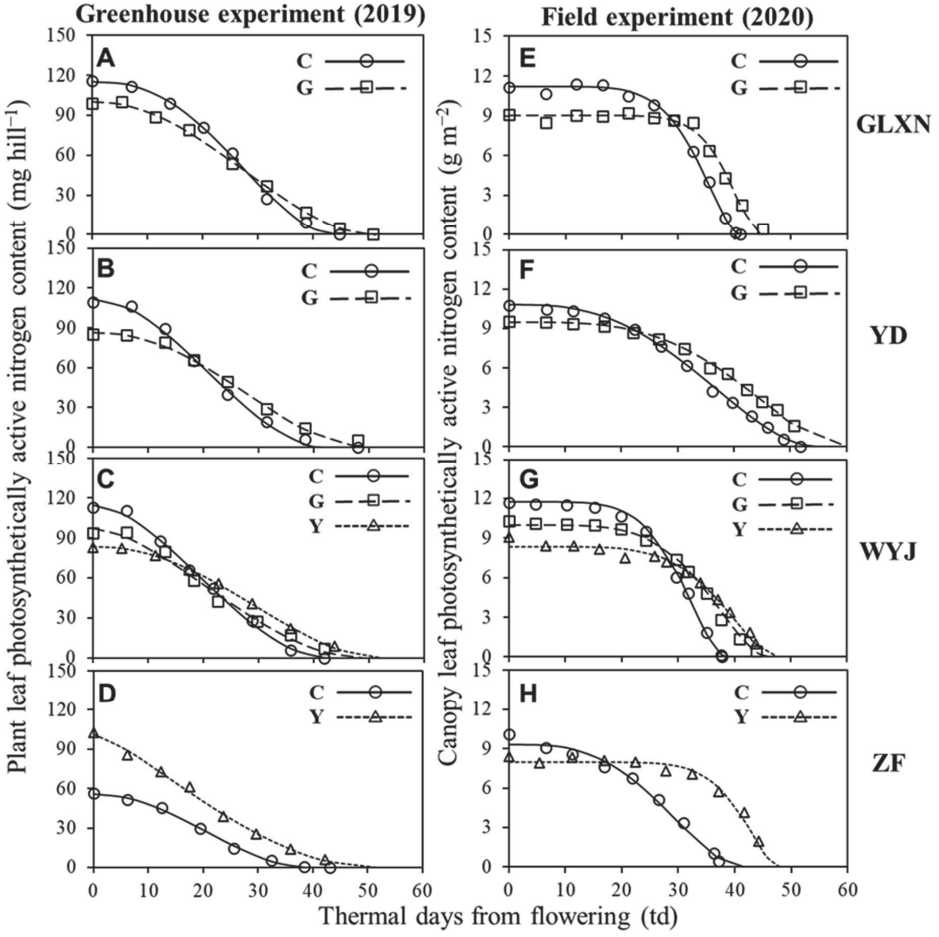

Fig. 4.5 The time course of total leaf photosynthetically active nitrogen (N) content in two experiments. Rice genotypes comprised four rice control (C, circles) genotypes and their greener-leaf variant (G, squares) and/or yellower-leaf variant (Y, triangles) genotypes. Each data point is shown as mean of three to four replicates. Plant or canopy leaf photosynthetically active N content was calculated as: $\text{total leaf N content} - \text{leaf area} \times n_b$, where n_b represents a base leaf N content for photosynthesis with an estimate of 0.23 g N m^{-2} from Zhou et al. (2023). Given a similar shape to the function describing the dynamics of source activity, the curves for the time course of N content were drawn using parameter values of eqn (4.4) fitted to the data. The thermal days were calculated from recorded temperatures of every 30 min, based on eqn (4.12). Genotype-background abbreviations: GLXN, cv. Guanglingxiangnuo; YD, cv. Yandao 8; WYJ, cv. Wuyunjing 3; and ZF, cv. Zhefu 802.

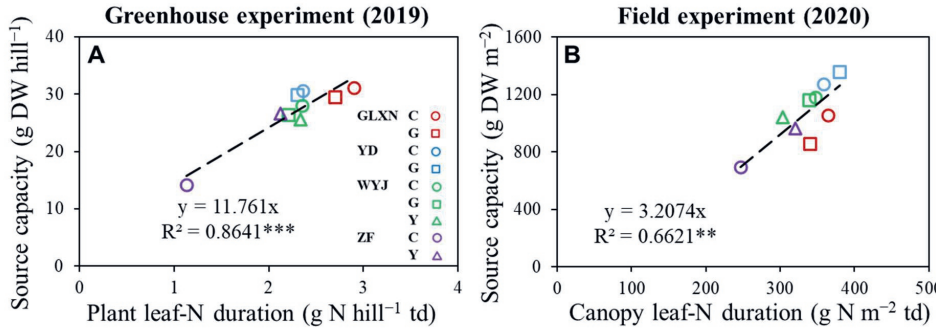

Fig. 4.6 Correlations of biomass source capacity with plant (A) and canopy (B) leaf-N duration during grain filling in two experiments. Plant and canopy leaf-N duration were calculated from the cumulative increment of leaf photosynthetically active N content during grain filling, i.e. the area under the curve in Fig. 4.5, based on eqn (4.6) when applied to N. Linear regression was fitted for overall data with its significance of correlation shown by asterisks: ** $P < 0.01$, *** $P < 0.001$. Genotype-background abbreviations: GLXN, cv. Guanglingxiangnuo; YD, cv. Yandao 8; WYJ, cv. Wuyunjing 3; and ZF, cv. Zhefu 802. C is rice control genotypes; G is greener-leaf variant genotypes; and Y is yellower-leaf variant genotypes.

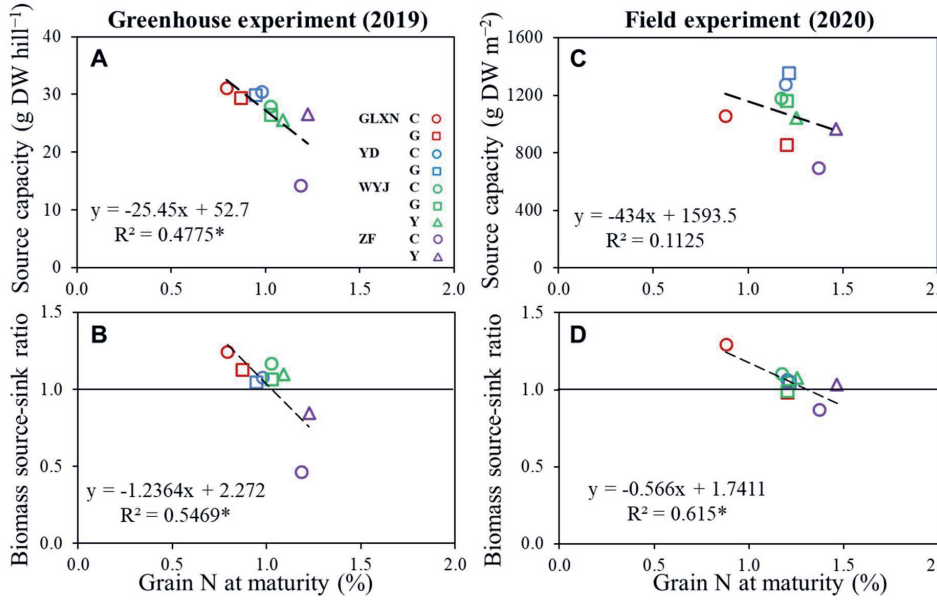

Fig. 4.7 Correlations of biomass source capacity (A, C) and source-sink ratio (B, D) during grain filling with grain nitrogen (N) concentration at maturity in two experiments. Linear regression was fitted for overall data with its significance of correlation shown by asterisks: * $P < 0.05$. Genotype-background abbreviations: GLXN, cv. Guanglingxiangnuo; YD, cv. Yandao 8; WYJ, cv. Wuyunjing 3; and ZF, cv. Zhefu 802. C is rice control genotypes; G is greener leaf variant genotypes; and Y is yellower-leaf variant genotypes. The black horizontal line (y = 1.0) in panels B and D represents the biomass source-sink ratio being 1.0, i.e., the balance between source supply and sink growth during grain filling.

After flowering, leaf photosynthetically active N content started to decline over time (Fig. 4.5), while significantly positive correlations between biomass source capacity and leaf-N duration were observed ($P < 0.01$; Fig. 4.6). Notably, the slope of this correlation was more than three times steeper in the greenhouse experiment compared to the field experiment (Fig. 4.6), probably due to wider-space effects associated with higher radiation interception per leaf area in the greenhouse than in the field.

There was a negative correlation between biomass source capacity and grain N concentration at maturity, and between biomass source-sink ratio and grain N concentration ($P < 0.05$; Fig. 4.7).

4.3.5 Source-sink parameters in the density experiment

In the density experiment in the field of using the genotypes with the ZF background, for biomass, both the source capacity and sink demand in the control genotype increased initially and then decreased after peaking at 30% higher density, whereas the ZF-Y genotype exhibited a continuously steady increase with planting density (Fig. 4.8A). Source-sink ratio of ZF-C was close to 1.0 at 30% higher density, while that of ZF-Y presented a continuous decrease, approaching a balance between source supply and sink growth (Fig. 4.8B). For N, the response of source capacity and sink demand to planting density followed a similar pattern to that observed for biomass (Fig. 4.8C). Source-sink ratios for both genotypes were lower than 1.0, but ZF-Y showed relatively higher values and increasing ratios in response to increasing plant density (Fig. 4.8D). Across different planting densities, source capacity and sink growth were correlated for both biomass and N ($P < 0.001$; Fig. S4.3e-f). With the increase in planting density, canopy leaf photosynthetically active N content decreased at an earlier stage and faster pace in ZF-C, whereas it maintained a high value for most of the post-flowering phase in the ZF-Y genotype (Fig. S4.5).

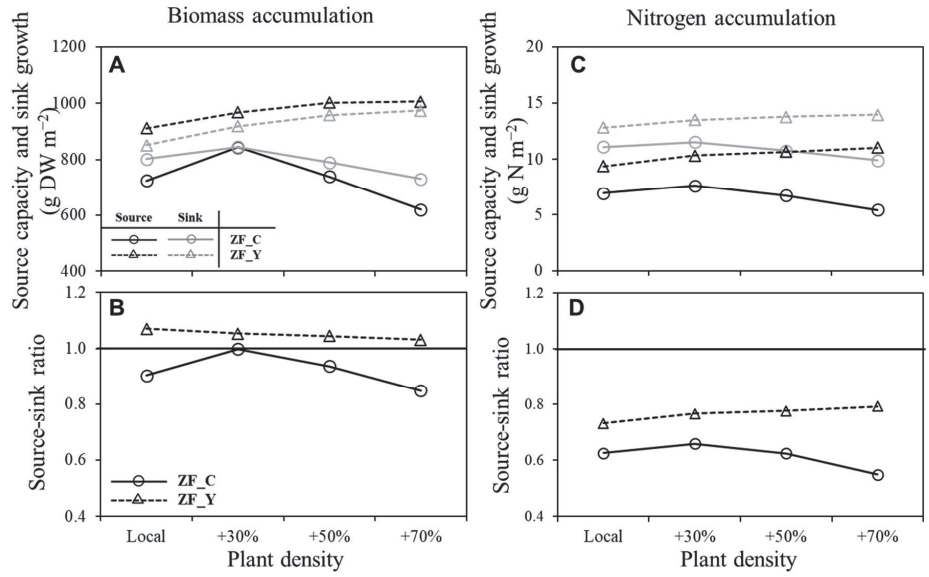

Fig. 4.8 Effects of planting density on biomass and nitrogen (N) source-sink relationship for one rice control genotype (C) and its yellower-leaf variant (Y) genotype from cv. Zhefu 802 (ZF) background in the field density experiment (Gu et al., 2017). Source capacity and sink growth (A, C), and their ratio (B, D) for biomass and N at four levels of planting density: local, +30%, +50%, and +70%, each of them representing plants at local normal plant density (25 × 15 cm), 30% higher density (25 × 11.5 cm), 50% higher density (25 × 10 cm), and 70% higher density (25 × 8.8 cm), respectively. The black horizontal lines (y = 1.0) in panels B and D represent the biomass source-sink ratio being 1.0, i.e., the balance between source supply and sink growth during grain filling.

4.4 Discussion

The coordination of source supply and sink growth during grain filling is crucial for improving rice yields. The source supply to grain growth (sink) come either from the remobilisation of stored pre-flowering assimilates or from post-flowering assimilation, and the relative contribution of the two has been investigated through isotope-labelling techniques (Deléens et al., 1994; Gebbing et al., 1999). However, it is impractical to apply this technique to study the source-sink relationships of many genotypes under field conditions (Wichern et al., 2008). Furthermore, studying this for both C and N would need different techniques for labelling C and N, which are hard to implement in the same experiment. Therefore, a model-fitting method offers advantages in quantifying differences in source-sink (im)balance among genotypes. This method allows for the analysis of experimental data obtained from periodic sampling measurements of aboveground biomass and N accumulation (Fig. 4.1 and Fig. S4.1), eliminating the need for sophisticated labelling techniques. This approach employs the

determinate sigmoid growth function developed by Yin et al. (2003), which has been successfully applied in previous studies on annual crops such as wheat and rice (Liu et al., 2023; Shao et al., 2021; Shi et al., 2017; Wei et al., 2018; Zhang et al., 2022). Each parameter derived from this model (eqns 4.1-4.11) holds its own biological significance (Table S4.2). By estimating the parameters of this model, we examined our hypotheses regarding the effects of leaf-colour modification on source-sink relationships, yield formation, and the development of strategies to improve crop productivity as discussed below.

4.4.1 The relative significance of source and sink among diverse genetic backgrounds

During grain filling, panicle growth (sink) is primarily driven by the assimilates produced (source), but when the post-flowering source supply is inadequate, the assimilates accumulated in vegetative organs before flowering are reallocated to fulfil the demand for panicle development (Asseng et al., 2017; Fu et al., 2011). The quantitative framework we used define source capacity specifically in terms of the carbohydrates produced (or N accumulated) after flowering. This allowed for a direct comparison with the total sink growth within the same period, and served as a means to quantify the difference between post-flowering source and sink, as well as the contribution of remobilisation of the stored pre-flowering assimilates.

Using this approach, we observed positive biomass source-sink differences (i.e., source capacity > sink growth) in most genetic backgrounds, such as GLXN, YD, and WYJ (Table 4.1 and Fig. S4.3). This indicated that the carbohydrates produced after flowering was sufficient to fill the grains without the necessity for significant remobilisation of assimilates reserved from the pre-flowering phase (Table 4.1), representing great photosynthetic source capacities in local conventional rice varieties. These genotypes may have evolved in an environment of long-term high-N fertilisation created by farmers' excessive application rates, with the aims to ensure a high rice productivity, yet without considering potential reductions in N use efficiency or the environmental consequences (Dobermann and Cassman, 2004; Ladha et al., 2020). Only genotypes from the ZF background showed a significantly negative source-sink difference, particularly in the greenhouse experiment, necessitating reallocation of pre-flowering accumulations (Table 4.1; Fig. S4.4). Although for this case, the model cannot guarantee that the potential grain yield of ZF genotypes was limited by insufficient source availability (as the actual available pre-flowering reserves cannot not be determined), the actual contributions of pre-flowering reserves were quantified based on model calculations (Table 4.1). Overall, our

results suggest that rice control genotypes are in a state of source-sink imbalance and most of them are mainly sink-limited.

Compared with small biomass remobilisation, higher contributions of pre-flowering N reserves for yield formation were expectedly observed in all genotypes, aligning with previous results (Fan et al., 2023; Shao et al., 2021). The reliance on pre-flowering N remobilisation in the field experiment (26~43%) was relatively lower than in the greenhouse experiment (42~66%) (Table 4.1) and in other studies (Maltese et al., 2019; Wei et al., 2018), which indicated a higher N-uptake from soil after flowering in the field experiment. However, this high N availability from soil may increase the amount of residual N in vegetative organs at maturity and cause N loss to the environment. All of these reconfirmed the presumably high N fertilizer involved in the local rice management practices.

4.4.2 Leaf-colour modification contributed to biomass source-sink balance

Previous studies have reported that stay-green (G) traits could enhance biomass source capacity and thus sink growth, because they extend the lifespan of the canopy (Christopher et al., 2018; Patra, 2020; Thomas and Ougham, 2014). We observed that G genotypes really postponed the end of crop growth ($t_{e,o}$) and grain filling ($t_{e,i}$), relative to their C genotypes (Table S4.3). However, we also found a decrease in the rates of source activity ($s_{m,oW}$ and $\bar{s}_{oW}$), as well as in the rates of sink demand ($s_{m,iW}$ and $\bar{s}_{iW}$) in these G genotypes (Table S4.5). These effects are clearly reflected in the dynamic changes of source activity and sink demand (Fig. 4.2). For source, the G modification decreased the rates of source activity during the initial phase after flowering, and increased these rates during the final phase of grain filling due to the extended $t_{e,o}$. Despite this late increase, the initial decrease in the cumulative increment of source activity was not fully compensated for, resulting in a decline in total source capacity. The total sink growth slightly increased across all G variants relative to their C genotypes, as the initial and late rate of sink demand was increased due to delayed $t_{e,i}$ and advanced $t_{m,i}$.

Yellow-leaf (Y) traits have been proposed to increase source capacity by allowing the distribution of light to deeper layers in the canopy (Long et al., 2006; Ort et al., 2011). The two Y genotypes exhibited the same extended grain-filling duration (i.e., $t_{e,o}$ and $t_{e,i}$) as the G variants (Table S4.3), possibly reflecting an increased assimilate production by leaves in the lower parts of the canopy by optimised light environment. Despite the extended source activity, the impact of the Y modification on source capacity was inconsistent between the WYJ and ZF

backgrounds. The WYJ-Y variant, with decreased $s_{m,oW}$ and $\bar{s}_{oW}$, had a lower source capacity. In contrast, the ZF-Y variant, with increased $s_{m,oW}$ and $\bar{s}_{oW}$, showed a higher source capacity (Table 4.1). This difference in source activity may be related to the acclimation of the canopy N profile to the light profile, as our previous study revealed that a phenotypic plasticity in N adaptation to the light environment only happened in ZF-Y with a steeper N gradient and more N in the upper leaf layer of the canopy, which contributed to the higher canopy photosynthetic activity (Zhou et al., 2023). The variation in sink growth, across these two Y-genotypes, was consistent with that of source capacity, supported by a positive correlation between them (Fig. S4.3). Both Y variants altered post-flowering source capacity, thus indirectly affected sink growth. It was likely that the biomass source-sink balances caused by leaf-colour modification were primarily determined by the altered biomass source capacity during grain filling.

4.4.3 Post-flowering N budgets involved in regulation of biomass source capacity

Significantly negative relationships between pre-flowering N uptake ($N_{pre\text{-}F}$) and post-flowering N uptake ($N_{post\text{-}F}$) (Fig. 4.3) indicated that under a given N application, there was a trade-off for N resources between pre-flowering and post-flowering phases. It appeared that different genotypes had contrasting N-uptake abilities. In the present study, several genotypes (like GLXN-C, GLXN-G, and ZF-C) had an ability to quickly take up N (higher $N_{pre\text{-}F}$), resulting in a decreased N supply from soil after flowering. The lower post-flowering N availability increased the need for N remobilisation from vegetative organs to fill in the grains (Table 4.1 and Fig. 4.4). However, increased N remobilisation led to a faster decline in the photosynthetic function of vegetative organs, such as leave blades (Derkx et al., 2012; Mu et al., 2018). This view is supported by our findings of an early and rapid decline in leaf photosynthetically active N content in these genotypes when the crop approached maturity under field conditions (Fig. 4.5). This phenomenon was particularly apparent for genotypes like ZF-C with high grain N requirement (Fig. 4.7). The resulting decreased post-flowering leaf-N duration accounted for the lower biomass production during grain filling, as evidenced by the positive correlation between source capacity and canopy leaf-N duration (Fig. 4.6). Of the leaf-colour modified genotypes, the ZF-Y genotype showed an obviously decreased accumulation for $N_{pre\text{-}F}$, which overcame the weakness as occurred in its C genotype (despite a similar grain-N% in ZF-C and ZF-Y genotypes, Fig. 4.7). This altered characteristic in ZF-Y led to increased post-flowering N availability and more N-uptake from soil to support grain growth, which reduced the reliance on N remobilisation from leaves. This was observed by more stable leaf-N content and

prolonged functional leaf-N duration particularly in N-rich field condition (Fig. 4.5H; Fig. S4.5b). All of these contributed to higher aboveground and panicle biomass accumulation during grain filling in ZF-Y.

Across all genotypes, grain N accumulation generally increased with post-flowering N uptake (Table 4.1 and Fig. S4.3). Previous studies have reported that grain N requirements could impact source-sink relationships (Gaju et al., 2014; Wei et al., 2018), and our results confirm that this impact also persisted for leaf-colour modified genotypes, as evidenced by the negative correlations of biomass source capacity and source-sink ratio with grain N concentration at maturity (Fig. 4.7). Overall, our study provides insights into how biomass source capacity and source-sink relationships are influenced by post-flowering N budgets. These findings suggest that effectiveness of leaf-colour modification varies depending on genetic backgrounds, and increased biomass accumulation after flowering necessitates optimal N allocation between the pre-flowering and post-flowering phases, along with a balanced N remobilisation between source and sink organs.

4.4.4 Applying source-sink relationships to guide management practices for higher crop productivity of leaf-colour modified genotypes

It is widely recognised for a long time that rice plants with high leaf-greenness possess a significant advantage in canopy light interception, leading to enhanced biomass accumulation and accelerated canopy closure (Gu et al., 2017; Ort et al., 2015). Nevertheless, the early and fast growth of organs, driven by leaf greenness, is always associated with high N uptake (Liao et al., 2004), which could be a liability under a field condition with a given N application. Too much N uptake during vegetative growth will result in lower post-flowering N availability and lower biomass capacity as discussed above. In this circumstance, opting for rice plants with reduced canopy chlorophyll, as observed in the Y-variant genotypes exhibiting decreased pre-flowering N accumulation (Table S4.4), may be a wise choice. Previous reports also confirmed that reducing leaf-greenness did not necessarily decrease the radiation use efficiency and biomass accumulation (Malnou et al., 2008; Tillier et al., 2023; Walker et al., 2018). These Y-variant genotypes, characterised by reduced light absorption capacity, have a decreased competition for both light and N resources in field conditions, which could allow an increase in planting density for higher crop productivity without need for extra N supply. However, it is important to note that the current N application and planting density have primarily been developed and optimised for local conventional green-leaf rice varieties, such as the C

genotypes, and the effectiveness of these cultivation practices may not translate directly and suitably to the leaf-colour variants. To investigate this, we conducted a similar analysis on ZF genotypes using data from a density experiment. The experiment revealed that as the post-flowering source-sink ratio approached to a balanced state, the crop productivity (including both source capacity and sink growth) for ZF-C was maximised at 30% higher density (i.e., optimal planting density), while that for ZF-Y showed a continuous increase with increasing planting density, exceeding the maximum density used (Fig. 4.8). Moreover, increasing planting density caused a faster and earlier decrease in canopy leaf-N content in ZF-C (Fig. S4.5), indicating that the effect of increasing plant density exacerbates the need for post-flowering N remobilisation. However, this effect was observed to a much less extent in its ZF-Y variant (Fig. S4.5). These findings suggest that for the Y-variant genotype, the current local cultivation management system may involve superfluous N application and insufficient planting density, which prevents the Y genotype from attaining its maximum yield.

Taken together, our results underscore the importance of adjusting planting density to fully exploit the increased crop yield potential in response to the impact of leaf colour modification. Further research is essential to better understand the source-sink relationships under integrative cultivation management, particularly within the context of genotype-environment interactions. These insights will contribute to the development of more effective and genotype-dependent crop management strategies. By tailoring cultivation practices to the specific requirements of leaf-colour variants and considering their genotype-environment interactions, the source-sink relationships and crop productivity might be optimised further.

Acknowledgements

Z.Z. thanks the China Scholar Council (CSC) for funding his PhD fellowship. We thank Dr. Changquan Zhang (Yangzhou University) and Prof. Fangmin Cheng (Zhejiang University) for providing seeds used in this study; Mr. Wendi Zhang and Mr. Yong Yang for assistance during experimentation.

References

Asseng S, Kassie BT, Labra MH, Amador C, Calderini DF. 2017. Simulating the impact of source-sink manipulations in wheat. *Field Crops Research* 202, 47−56.

Barnett KH, Pearce RB. 1983. Source-sink ratio alteration and its effect on physiological parameters in maize. *Crop Science* 23, 294−299.

Bonelli LE, Monzon JP, Cerrudo A, Rizzalli RH, Andrade FH. 2016. Maize grain yield components and source-sink relationship as affected by the delay in sowing date. *Field Crops Research* 198, 215−225.

Burgess AJ, Masclaux-Daubresse C, Strittmatter G, Weber APM, Taylor SH, Harbinson J, Yin X, Long S, Paul MJ, Westhoff P, Loreto F, Ceriotti A, Saltenis VLR, Pribil M, Nacry P, Scharff LB, Jensen PE, Muller B, Cohan JP, Foulkes J, Rogowsky P, Debaeke P, Meyer C, Nelissen H, Inzé D, Klein Lankhorst R, Parry MAJ, Murchie EH, Baekelandt A. 2023. Improving crop yield potential: Underlying biological processes and future prospects. *Food and Energy Security* 12, 1−29.

Christopher M, Chenu K, Jennings R, Fletcher S, Butler D, Borrell A, Christopher J. 2018. QTL for stay-green traits in wheat in well-watered and water-limited environments. *Field Crops Research* 217, 32−44.

De Vries FWTP, Brunsting AHM, Van Laar HH. 1974. Products, requirements and efficiency of biosynthesis a quantitative approach. *Journal of theoretical Biology* 45, 339−377.

Deléens E, Cliquet JB, Prioul JL. 1994. Use of ^{13}C and ^{15}N plant label near natural abundance for monitoring carbon and nitrogen partitioning. *Functional Plant Biology* 21, 133−146.

Derkx AP, Orford S, Griffiths S, Foulkes MJ, Hawkesford MJ. 2012. Identification of differentially senescing mutants of wheat and impacts on yield, biomass and nitrogen partitioning. *Journal of Integrative Plant Biology* 54, 555−566.

Dobermann A, Cassman KG. 2004. Environmental dimensions of fertilizer nitrogen: What can be done to increase nitrogen use efficiency and ensure global food security? *Agriculture and the Nitrogen Cycle: Assessing the Impacts of Fertilizer Use on Food Production and the Environment.* 65, 261.

Engels C, Kirkby E, White P. 2011. Mineral nutrition, yield and source-sink relationships. *In: Marschner's mineral nutrition of higher plants. Academic Press*. pp. 85−133.

Fan P, Ming B, Evers JB, Li Y, Li S, Xie R, Anten NPR. 2023. Nitrogen availability determines the vertical patterns of accumulation, partitioning, and reallocation of dry matter and nitrogen in maize. *Field Crops Research* 297, 108927.

Fu J, Huang Z, Wang Z, Yang J, Zhang J. 2011. Pre-anthesis non-structural carbohydrate reserve in the stem enhances the sink strength of inferior spikelets during grain filling of rice. *Field Crops Research* 123, 170−182.

Gaju O, Allard V, Martre P, Le Gouis J, Moreau D, Bogard M, Hubbart S, Foulkes MJ. 2014. Nitrogen partitioning and remobilization in relation to leaf senescence, grain yield and grain nitrogen concentration in wheat cultivars. *Field Crops Research* 155, 213−223.

Gebbing T, Schnyder H, Kühbauch W. 1999. The utilization of pre-anthesis reserves in grain filling of wheat. Assessment by steady-state $^{13}CO_2/^{12}CO_2$ labelling. *Plant, Cell &*

Environment 22, 851−858.

Gu J, Zhou Z, Li Z, Chen Y, Wang Z, Zhang H. 2017. Rice (*Oryza sativa* L.) with reduced chlorophyll content exhibit higher photosynthetic rate and efficiency, improved canopy light distribution, and greater yields than normally pigmented plants. *Field Crops Research* 200, 58−70.

Hou P, Liu Y, Liu W, Liu G, Xie R, Wang K, Ming B, Wang Y, Zhao R, Zhang W, Wang Y, Bian S, Ren H, Zhao X, Liu P, Chang J, Zhang G, Liu J, Yuan L, Zhao H, Shi L, Zhang L, Yu L, Gao J, Yu X, Shen L, Yang S, Zhang Z, Xue J, Ma X, Wang X, Lu T, Dong B, Li G, Ma B, Li J, Deng X, Liu Y, Yang Q, Fu H, Liu X, Chen X, Huang C, Li S. 2020. How to increase maize production without extra nitrogen input. *Resources, Conservation and Recycling* 160, 104913.

Kumar R, Bishop E, Bridges WC, Tharayil N, Sekhon RS. 2019. Sugar partitioning and source–sink interaction are key determinants of leaf senescence in maize. *Plant, Cell & Environment* 42, 2597−2611.

Ladha JK, Jat ML, Stirling CM, Chakraborty D, Pradhan P, Krupnik TJ, Sapkota TB, Pathak H, Rana DS, Tesfaye K, Gerard B. 2020. Achieving the sustainable development goals in agriculture: The crucial role of nitrogen in cereal-based systems. *Advances in Agronomy* 163, 39−116.

Li G, Cheng G, Li L, Lu D, Lu W. 2020. Effects of slow-released fertilizer on maize yield, biomass production, and source-sink ratio at different densities. *Journal of Plant Nutrition* 43, 725−738.

Liao M, Fillery IRP, Palta JA. 2004. Early vigorous growth is a major factor influencing nitrogen uptake in wheat. *Functional Plant Biology* 31, 121−129.

Liu G, Yang Y, Guo X, Liu W, Xie R, Ming B, Xue J, Wang K, Li S, Hou P. 2022. Coordinating maize source and sink relationship to achieve yield potential of 22.5 Mg ha^{-1}. *Field Crops Research* 283, 108544.

Liu K, Meng M, Zhang T, Chen Y, Yuan H, Su T. 2023. Quantitative analysis of source-sink relationships in two potato varieties under different nitrogen application rates. *Agronomy* 13, 1–19.

Liu T, Shao D, Kovi MR, Xing Y. 2010. Mapping and validation of quantitative trait loci for spikelets per panicle and 1,000-grain weight in rice (*Oryza sativa* L.). *Theoretical and Applied Genetics* 120, 933−942.

Long SP, Zhu XG, Naidu SL, Ort DR. 2006. Can improvement in photosynthesis increase crop yields? *Plant, Cell & Environment* 29, 315−330.

Malnou CS, Jaggard KW, Sparkes DL. 2008. Nitrogen fertilizer and the efficiency of the sugar beet crop in late summer. *European Journal of Agronomy* 28, 47−56.

Maltese NE, Melchiori RJM, Maddonni GA, Ferreyra JM, Caviglia OP. 2019. Nitrogen economy of early and late-sown maize crops. *Field Crops Research* 231, 40−50.

McCormick AJ, Cramer MD, Watt DA. 2006. Sink strength regulates photosynthesis in sugarcane. *New Phytologist* 171, 759−770.

Mu X, Chen Q, Chen F, Yuan L, Mi G. 2018. Dynamic remobilization of leaf nitrogen components in relation to photosynthetic rate during grain filling in maize. *Plant*

Physiology and biochemistry 129, 27−34.

Nehe AS, Misra S, Murchie EH, Chinnathambi K, Singh Tyagi B, Foulkes MJ. 2020. Nitrogen partitioning and remobilization in relation to leaf senescence, grain yield and protein concentration in Indian wheat cultivars. *Field Crops Research* 251, 107778.

Ohsumi A, Takai T, Ida M, Yamamoto T, Arai-Sanoh Y, Yano M, Ando T, Kondo M. 2011. Evaluation of yield performance in rice near-isogenic lines with increased spikelet number. *Field Crops Research* 120, 68−75.

Ort DR, Merchant SS, Alric J, Barkan A, Blankenship RE, Bock R, Croce R, Hanson MR, Hibberd JM, Long SP, Moore TA, Moroney J, Niyogi KK, Parry MAJ, Peralta-Yahya PP, Prince RC, Redding KE, Spalding MH, van Wijk KJ, Vermaas WFJ, von Caemmerer S, Weber APM, Yeates TO, Yuan JS, Zhu XG. 2015. Redesigning photosynthesis to sustainably meet global food and bioenergy demand. *Proceedings of the National Academy of Sciences* 112, 8529−8536.

Ort DR, Zhu X, Melis A. 2011. Optimizing antenna size to maximize photosynthetic efficiency. *Plant Physiology* 155, 79−85.

Patra M. 2020. A review : Stay-green trait and its physiological and genetic basis of yield variation in rice. *Journal of Pharmacognosy and Phytochemistry* 9, 1311−1321.

Paul MJ, Foyer CH. 2001. Sink regulation of photosynthesis. *Journal of Experimental Botany* 52, 1383−1400.

Peng S, Laza RC, Visperas RM, Sanico AL, Cassman KG, Khush GS. 2000. Grain yield of rice cultivars and lines developed in the Philippines since 1966. *Crop Science* 40, 307−314.

Rajcan I, Tollenaar M. 1999. Source : sink ratio and leaf senescence in maize:: II. Nitrogen metabolism during grain filling. *Field Crops Research* 60, 255−265.

Ray DK, Mueller ND, West PC, Foley JA. 2013. Yield trends are insufficient to double global crop production by 2050. *PLoS One* 8.

Reynolds MP, Pellegrineschi A, Skovmand B. 2005. Sink-limitation to yield and biomass: A summary of some investigations in spring wheat. *Annals of Applied Biology* 146, 39−49.

Shao L, Liu Z, Li H, Zhang Y, Dong M, Guo X, Zhang H, Huang B, Ni R, Li G, Cai C, Chen W, Luo W, Yin X. 2021. The impact of global dimming on crop yields is determined by the source–sink imbalance of carbon during grain filling. *Global Change Biology* 27, 689−708.

Shi W, Xiao G, Struik PC, Jagadish KSV, Yin X. 2017. Quantifying source-sink relationships of rice under high night-time temperature combined with two nitrogen levels. *Field Crops Research* 202, 36−46.

Sinclair TR, Rufty TW, Lewis RS. 2019. Increasing photosynthesis: Unlikely solution for world food problem. *Trends in Plant Science* 24, 1032−1039.

Slattery RA, Ort DR. 2021. Perspectives on improving light distribution and light use efficiency in crop canopies. *Plant Physiology* 185, 34−48.

Smith MR, Rao IM, Merchant A. 2018. Source-sink relationships in crop plants and their influence on yield development and nutritional quality. *Frontiers in Plant Science* 9, 1889.

Ta CT, Weiland RT. 1992. Nitrogen Partitioning in Maize during Ear Development. *Crop Science* 32, 443−451.

Thomas H, Ougham H. 2014. The stay-green trait. *Journal of Experimental Botany* 65,

3889−3900.
Tillier LC, Murchie EH, Sparkes DL. 2023. Does canopy angle influence radiation use efficiency of sugar beet? *Field Crops Research* 293, 108841.
Walker BJ, Drewry DT, Slattery RA, VanLoocke A, Cho YB, Ort DR. 2018. Chlorophyll can be reduced in crop canopies with little penalty to photosynthesis. *Plant Physiology* 176, 1215−1232.
Wardlaw IF. 1990. The control of carbon partitioning in plants. *New Phytologist* 116, 341−381.
Wei H, Meng T, Li X, Dai Q, Zhang H, Yin X. 2018. Sink-source relationship during rice grain filling is associated with grain nitrogen concentration. *Field Crops Research* 215, 23−38.
Wichern F, Eberhardt E, Mayer J, Joergensen RG, Müller T. 2008. Nitrogen rhizodeposition in agricultural crops: Methods, estimates and future prospects. *Soil Biology and Biochemistry* 40, 30−48.
Won PLP, Kanno N, Banayo NPM, Bueno CS, Sta Cruz P, Kato Y. 2022. Source–sink relationships in short-duration and hybrid rice cultivars in tropical Asia. *Field Crops Research* 282, 108485.
Xu X, Zhang Y, Li J, Zhang M, Zhou X, Zhou S, Wang Z. 2018. Optimizing single irrigation scheme to improve water use efficiency by manipulating winter wheat sink-source relationships in Northern China Plain. *PLoS One* 13.
Yang J, Zhang J. 2010. Grain-filling problem in “super” rice. *Journal of Experimental Botany* 61, 1−5.
Yin X, Goudriaan J, Lantinga EA, Vos J, Spiertz HJ. 2003. A flexible sigmoid function of determinate growth. *Annals of Botany* 91, 361−371.
Yin X, Guo W, Spiertz JH. 2009. A quantitative approach to characterize sink-source relationships during grain filling in contrasting wheat genotypes. *Field Crops Research* 114, 119−126.
Yin X, Kropff MJ, McLaren G, Visperas RM. 1995. A nonlinear model for crop development as a function of temperature. *Agricultural and Forest Meteorology* 77, 1−16.
Yin X, van Laar HH. 2005. Crop Systems Dynamics: An ecophysiological simulation model of genotype-by-environment interactions. *Wageningen Academic Publishers, The Netherlands*.
Zhang D, Sun Z, Feng L, Bai W, Yang N, Zhang Z, Du G, Feng C, Cai Q, Wang Q, Zhang Y, Wang R, Arshad A, Hao X, Sun M, Gao Z, Zhang L. 2020. Maize plant density affects yield, growth and source-sink relationship of crops in maize/peanut intercropping. *Field Crops Research* 257, 107926.
Zhang H, Jing W, Zhao B, Wang W, Xu Y, Zhang W, Gu J, Liu L, Wang Z, Yang J. 2021. Alternative fertilizer and irrigation practices improve rice yield and resource use efficiency by regulating source-sink relationships. *Field Crops Research* 265, 108124.
Zhang H, Yu C, Kong X, Hou D, Gu J, Liu L, Wang Z, Yang J. 2018. Progressive integrative crop managements increase grain yield, nitrogen use efficiency and irrigation water productivity in rice. *Field Crops Research* 215, 1−11.
Zhang L, Zhang Z, Luo Y, Cao J, Li Z. 2020. Optimizing genotype-environment-management interactions for maize farmers to adapt to climate change in different agro-ecological zones

across China. *Science of the Total Environment* 728, 1−12.

Zhang S, Wang H, Fan J, Zhang F, Cheng M, Yang L, Ji Q, Li Z. 2022. Quantifying source-sink relationships of drip-fertigated potato under various water and potassium supplies. *Field Crops Research* 285, 108604.

Zhou Z, Struik PC, Gu J, van der Putten PEL, Wang Z, Yin X, Yang J. 2023. Leaf-colour modification affects canopy photosynthesis, dry-matter accumulation and yield traits in rice. *Field Crops Research* 290, 108746.

Supplementary materials in Chapter 4

Table S4.1 The flowering and maturity dates, reproductive growth duration, and total growth duration for rice genotypes of four genetic backgrounds, each including a control (C) genotype and its greener-leaf variant (G) and/or yellower-leaf variant (Y) genotype, in three experiments.

Experiment	Background	Genotype	Flowering date (month/day)	Maturity date (month/day)	Grain-filling duration[a] (d)	Total growth duration (d)
Greenhouse (2019)	GLXN	C	6/23	8/19	58	132
		G	6/23	8/19	58	132
	YD	C	5/30	7/23	55	105
		G	6/1	7/25	55	107
	WYJ	C	6/4	7/21	48	103
		G	6/4	7/21	48	103
		Y	6/8	7/27	50	109
	ZF	C	7/20	9/7	50	150
		Y	6/14	7/30	47	112
Field (2020)	GLXN	C	8/31	11/15	77	173
		G	8/31	11/15	77	173
	YD	C	8/20	11/4	77	162
		G	8/22	11/6	77	164
	WYJ	C	8/30	11/1	64	159
		G	8/30	11/1	64	159
		Y	9/3	11/12	71	170
	ZF	C	8/23	10/17	56	144
		Y	8/14	9/30	49	127
Field (Density)[b]	ZF	C	8/9	9/29	52	133
		Y	8/2	9/19	49	123

[a] days from flowering to maturity.

[b] Note: since there is no difference in the observed growth period of ZF materials under different density treatments in the 2015 field experiment, only one set of growth period data is listed here.

The duration from flowering to maturity and total growth duration are expressed as actual days. Genotype-background abbreviations: GLXN, cv. Guanglingxiangnuo; YD, cv. Yandao 8; WYJ, cv. Wuyunjing 3; and ZF, cv. Zhefu 802. C is rice control genotypes; G is greener leaf variant genotypes; and Y is yellower-leaf variant genotypes.

Table S4.2 List of parameters for source and sink of biomass and nitrogen.

Category		Parameter	Definition	Unit (Greenhouse)	Unit (Field)
Biomass (W)	Source	W_o	Aboveground biomass	g hill^{-1}	g m^{-2}
		$W_{x,o}$	The maximum aboveground biomass	g hill^{-1}	g m^{-2}
		$W_{b,o}$	The initial aboveground biomass at flowering	g hill^{-1}	g m^{-2}
		$t_{m,o}$	The moment when the decrease of s_{oW} is fastest	td	td
		$t_{e,o}$	The moment when s_{oW} is decreased to zero	td	td
		s_{oW}	The rate of biomass source activity	g hill^{-1} td^{-1}	g m^{-2} td^{-1}
		$s_{m,oW}$	The maximum value of s_{oW}	g hill^{-1} td^{-1}	g m^{-2} td^{-1}
		$\bar{s}_{oW}$	The mean rate of s_{oW} during grain filling	g hill^{-1} td^{-1}	g m^{-2} td^{-1}
	Sink	W_i	Panicle biomass	g hill^{-1}	g m^{-2}
		$W_{x,i}$	The maximum panicle biomass	g hill^{-1}	g m^{-2}
		$W_{b,i}$	The initial panicle biomass at flowering	g hill^{-1}	g m^{-2}
		t_b	Time point at flowering, here $t_b = 0$	td	td
		$t_{m,i}$	The moment when $s_{m,iW}$ is achieved	td	td
		$t_{e,i}$	The moment when s_{iW} is decreased to zero	td	td
		s_{iW}	The rate of biomass sink demand	g hill^{-1} td^{-1}	g m^{-2} td^{-1}
		$s_{m,iW}$	The maximum value of s_{iW}	g hill^{-1} td^{-1}	g m^{-2} td^{-1}
		$\bar{s}_{iW}$	The mean rate of s_{iW} during grain filling	g hill^{-1} td^{-1}	g m^{-2} td^{-1}
Nitrogen (N)	Source	N_o	Aboveground N accumulation	g hill^{-1}	g m^{-2}
		$N_{x,o}$	The maximum aboveground N accumulation	g hill^{-1}	g m^{-2}
		$N_{b,o}$	The initial aboveground N accumulation at flowering	g hill^{-1}	g m^{-2}
		$t_{m,o}$	The moment when the decrease of s_{oN} is fastest	td	td
		$t_{e,o}$	The moment when s_{oN} is decreased to zero	td	td
		s_{oN}	The rate of N source activity	mg hill^{-1} td^{-1}	g m^{-2} td^{-1}
		$s_{m,oN}$	The maximum value of s_{oN}	mg hill^{-1} td^{-1}	g m^{-2} td^{-1}
		$\bar{s}_{oN}$	The mean rate of s_{oN} during grain filling	mg hill^{-1} td^{-1}	g m^{-2} td^{-1}
	Sink	N_i	Panicle N accumulation	g hill^{-1}	g m^{-2}
		$N_{x,i}$	The maximum panicle N accumulation	g hill^{-1}	g m^{-2}
		$N_{b,i}$	The initial panicle N accumulation at flowering	g hill^{-1}	g m^{-2}
		t_b	Time point at flowering, here $t_b = 0$	td	td
		$t_{m,i}$	The moment when $s_{m,iN}$ is achieved	td	td
		$t_{e,i}$	The moment when s_{iN} is decreased to zero	td	td
		s_{iN}	The rate of N sink demand	mg hill^{-1} td^{-1}	g m^{-2} td^{-1}
		$s_{m,iN}$	The maximum value of s_{iN}	mg hill^{-1} td^{-1}	g m^{-2} td^{-1}
		$\bar{s}_{iN}$	The mean rate of s_{iN} during grain filling	mg hill^{-1} td^{-1}	g m^{-2} td^{-1}

The unit 'td' in the table refers to the thermal days, calculated from recorded temperatures of every 30-min, based on eqn (4.12) (see the text).

Table S4.3 Estimated parameter values (standard error in parentheses) using the full model (see the text) for source and sink for biomass during grain filling in three experiments.

Experiment	Background	Genotype	Density	Estimated parameter values of source				Estimated parameter values of sink				Other parameter values	
				$W_{x,o}$	$W_{b,o}$	$t_{m,o}$	$t_{e,o}$	$W_{x,i}$	$W_{b,i}$	$t_{m,i}$	$t_{e,i}$	R^2	Data points
				(g hill^{-1})	(g hill^{-1})	(td)	(td)	(g hill^{-1})	(g hill^{-1})	(td)	(td)		
Greenhouse experiment (2019)	GLXN	C		56.0 (0.53)	24.9 (0.74)	37.2 (1.4)	44.8 (1.2)	26.2 (0.61)	1.2 (0.78)	22.3 (1.6)	43.0 (2.6)	0.994	54
		G		55.2 (0.60)	25.8 (0.78)	37.1 (2.7)	50.8 (0.9)	26.9 (0.90)	0.9 (0.84)	19.5 (2.9)	50.4 (4.0)	0.992	54
	YD	C		42.9 (0.51)	12.3 (0.65)	34.1 (1.6)	44.5 (0.5)	29.5 (0.53)	1.2 (0.63)	21.9 (0.8)	36.6 (1.5)	0.992	48
		G		43.2 (0.60)	13.4 (0.58)	40.3 (1.5)	49.3 (0.6)	29.1 (0.48)	0.6 (0.63)	17.8 (1.4)	43.6 (4.1)	0.992	48
	WYJ	C		38.8 (0.36)	10.8 (0.50)	29.2 (0.9)	35.7 (0.9)	25.3 (0.43)	1.4 (0.52)	18.3 (1.0)	36.2 (1.6)	0.994	48
		G		39.9 (0.47)	13.5 (0.58)	32.2 (1.5)	41.8 (0.9)	26.2 (0.49)	1.4 (0.63)	16.9 (1.5)	41.2 (4.2)	0.990	48
		Y		37.8 (0.67)	12.3 (0.52)	40.6 (1.2)	45.1 (0.8)	24.3 (0.70)	1.0 (0.63)	17.8 (1.7)	43.1 (2.5)	0.988	48
	ZF	C		52.5 (0.66)	38.3 (1.03)	29.9 (16.2)	37.2 (0.6)	33.1 (0.49)	2.7 (0.64)	17.0 (2.0)	38.7 (2.1)	0.990	48
		Y		45.4 (0.48)	18.8 (0.81)	29.9 (3.1)	42.3 (0.4)	35.2 (0.79)	3.7 (0.86)	14.8 (1.8)	38.5 (2.5)	0.986	48
				(g m^{-2})	(g m^{-2})	(td)	(td)	(g m^{-2})	(g m^{-2})	(td)	(td)		
Field experiment (2020)	GLXN	C		2104.6 (15.6)	1046.0 (17.8)	39.1 (0.6)	41.2 (1.6)	907.8 (13.6)	90.4 (23.6)	15.7 (1.6)	37.4 (1.8)	0.996	72
		G		2056.8 (25.8)	1202.1 (17.3)	43.8 (0.9)	45.1 (1.6)	947.9 (15.0)	75.5 (27.8)	11.6 (2.3)	45.7 (2.4)	0.995	72
	YD	C		2119.9 (14.0)	845.3 (27.2)	35.3 (1.4)	46.0 (2.1)	1312.7 (16.3)	115.2 (30.6)	16.2 (1.8)	43.6 (1.9)	0.992	78
		G		2150.9 (15.8)	796.4 (25.4)	40.1 (1.3)	51.1 (1.2)	1367.7 (37.6)	72.2 (30.3)	13.9 (2.6)	53.8 (3.8)	0.992	78
	WYJ	C		2071.4 (16.5)	892.8 (25.9)	31.3 (0.9)	36.6 (0.6)	1182.9 (22.9)	118.1 (27.9)	17.8 (1.4)	38.0 (1.9)	0.992	66
		G		2186.3 (22.0)	1027.2 (23.0)	37.7 (1.2)	43.9 (1.7)	1298.2 (62.0)	125.6 (28.7)	16.4 (2.0)	45.5 (4.5)	0.993	66
		Y		1854.2 (65.1)	814.5 (21.3)	41.8 (1.7)	43.7 (3.5)	1080.2 (89.0)	116.2 (27.9)	21.7 (1.6)	45.4 (5.9)	0.990	66
	ZF	C		1830.1 (11.4)	1134.0 (18.0)	28.0 (1.3)	36.3 (1.1)	888.5 (11.7)	87.9 (18.7)	16.6 (0.9)	32.9 (1.2)	0.997	54
		Y		1665.1 (16.6)	701.3 (25.0)	28.2 (3.1)	44.2 (0.6)	1028.3 (18.7)	94.9 (25.7)	15.1 (1.5)	36.4 (2.0)	0.990	54
Field density experiment	ZF	C	Local	1747.8 (13.2)	1022.8 (18.5)	27.1 (3.7)	43.4 (4.9)	883.0 (11.1)	80.7 (18.4)	15.8 (1.1)	33.1 (1.3)	0.999	42
			+30%	1881.9 (13.2)	1037.7 (18.0)	31.7 (1.1)	39.2 (4.3)	945.4 (11.5)	100.2 (19.1)	15.6 (1.1)	32.9 (1.4)	0.999	42
			+50%	1833.7 (12.8)	1094.0 (18.5)	30.8 (1.4)	38.3 (5.3)	901.7 (12.0)	111.8 (20.3)	15.3 (1.1)	31.2 (1.6)	0.999	42
			+70%	1735.2 (13.5)	1115.1 (20.3)	29.9 (1.7)	37.3 (6.2)	852.6 (12.2)	121.8 (21.4)	14.3 (1.3)	30.4 (1.8)	0.995	42
		Y	Local	1502.0 (11.9)	590.2 (16.3)	29.3 (1.9)	43.9 (3.7)	927.0 (9.9)	75.7 (16.4)	17.2 (0.9)	35.1 (1.2)	0.999	42
			+30%	1580.4 (19.4)	612.6 (28.9)	29.6 (3.2)	43.2 (5.8)	995.7 (17.3)	76.8 (28.9)	16.2 (1.6)	34.5 (2.0)	0.998	42
			+50%	1674.5 (18.0)	672.4 (23.6)	28.8 (1.4)	42.6 (4.9)	1047.4 (13.0)	88.8 (21.5)	16.6 (1.1)	34.9 (1.5)	0.999	42
			+70%	1686.1 (11.6)	680.5 (16.7)	29.2 (1.2)	41.1 (3.1)	1061.4 (10.1)	86.8 (16.9)	16.7 (0.8)	35.0 (1.1)	0.999	42

Genotype-background abbreviations: GLXN, cv. Guanglingxiangnuo; YD, cv. Yandao 8; WYJ, cv. Wuyunjing 3; and ZF, cv. Zhefu 802. C is rice control genotypes; G is greener-leaf variant genotypes; and Y is yellower-leaf variant genotypes. Local, +30%, +50%, and +70% represent plants at local normal plant density (25 × 15 cm), 30% higher density (25 × 11.5 cm), 50% higher density (25 × 10 cm), and 70% higher density (25 × 8.8 cm), respectively. Source parameters (estimated from eqn 4.7): $W_{x,o}$, the maximum aboveground biomass; $W_{b,o}$, the initial aboveground biomass at flowering; $t_{m,o}$, the moment when the decrease of source activity is fastest; $t_{e,o}$, the moment when source activity is decreased to zero. Sink parameters (estimated from eqn 4.1): $W_{x,i}$, the maximum panicle biomass; $W_{b,i}$, the initial panicle biomass at flowering; $t_{m,i}$, the moment when maximum sink demand is achieved; $t_{e,i}$, the moment when sink demand is decreased to zero. The unit day in the table is the thermal days calculated from recorded temperatures of every 30 min, based on eqn (4.12).

Table S4.4 Estimated parameter values (standard error in parentheses) using the full model (see the text) for source and sink for nitrogen during grain filling in three experiments.

Experiment	Background	Genotype	Density	Estimated parameter values of source				Estimated parameter values of sink				Other parameter values	
				$N_{x,o}$	$N_{b,o}$	$t_{m,o}$	$t_{e,o}$	$N_{x,i}$	$N_{b,i}$	$t_{m,i}$	$t_{e,i}$	R^2	Data points
				(g hill^{-1})	(g hill^{-1})	(td)	(td)	(g hill^{-1})	(g hill^{-1})	(td)	(td)		
Greenhouse experiment (2019)	GLXN	C		0.292 (0.002)	0.222 (0.004)	26.3 (3.9)	38.7 (0.3)	0.203 (0.003)	0.013 (0.004)	20.7 (1.0)	41.6 (1.5)	0.993	54
		G		0.294 (0.003)	0.223 (0.004)	26.4 (2.0)	44.5 (0.3)	0.211 (0.004)	0.013 (0.004)	18.7 (1.6)	45.9 (2.2)	0.991	54
	YD	C		0.323 (0.003)	0.196 (0.004)	32.6 (1.0)	34.2 (2.0)	0.270 (0.004)	0.021 (0.005)	20.7 (0.7)	34.9 (1.2)	0.992	48
		G		0.332 (0.005)	0.193 (0.004)	43.2 (1.8)	48.0 (0.5)	0.271 (0.003)	0.014 (0.005)	16.3 (1.2)	42.4 (1.2)	0.993	48
	WYJ	C		0.306 (0.002)	0.198 (0.002)	29.6 (1.4)	30.9 (1.2)	0.237 (0.002)	0.021 (0.002)	17.0 (0.4)	32.2 (0.7)	0.995	48
		G		0.315 (0.004)	0.199 (0.004)	35.4 (2.6)	40.0 (1.9)	0.242 (0.003)	0.020 (0.003)	16.7 (0.7)	36.7 (1.2)	0.991	48
		Y		0.322 (0.004)	0.200 (0.004)	38.0 (1.8)	46.3 (4.8)	0.227 (0.004)	0.016 (0.004)	16.6 (1.4)	40.5 (2.0)	0.991	48
	ZF	C		0.353 (0.002)	0.276 (0.002)	36.1 (1.1)	38.4 (1.0)	0.264 (0.002)	0.033 (0.003)	17.3 (0.8)	39.0 (1.0)	0.985	48
		Y		0.343 (0.002)	0.205 (0.002)	31.7 (1.8)	43.8 (1.0)	0.304 (0.003)	0.042 (0.003)	14.7 (0.7)	39.3 (1.0)	0.976	48
				(g m^{-2})	(g m^{-2})	(td)	(td)	(g m^{-2})	(g m^{-2})	(td)	(td)		
Field experiment (2020)	GLXN	C		28.2 (0.09)	22.2 (0.16)	31.3 (1.7)	35.5 (0.1)	10.2 (0.11)	1.4 (0.19)	16.3 (1.1)	37.3 (1.3)	0.996	72
		G		28.4 (0.13)	22.9 (0.23)	31.5 (3.2)	40.3 (0.2)	10.7 (0.13)	1.2 (0.33)	15.1 (2.1)	42.2 (1.5)	0.996	72
	YD	C		27.8 (0.15)	16.8 (0.30)	27.2 (4.2)	44.9 (2.6)	16.9 (0.23)	1.6 (0.42)	17.7 (1.8)	43.2 (2.0)	0.991	78
		G		28.3 (0.20)	16.3 (0.34)	35.8 (3.2)	54.8 (3.9)	17.3 (0.45)	1.1 (0.38)	14.9 (2.5)	53.4 (3.6)	0.993	78
	WYJ	C		27.5 (0.13)	18.6 (0.16)	29.2 (1.4)	39.4 (0.9)	14.2 (0.13)	1.6 (0.16)	19.1 (1.4)	38.1 (2.1)	0.993	66
		G		28.4 (0.18)	19.4 (0.24)	34.5 (1.6)	42.4 (0.6)	15.7 (0.90)	1.6 (0.27)	18.2 (1.5)	48.2 (3.0)	0.994	66
		Y		25.3 (0.12)	17.7 (0.09)	39.2 (0.5)	42.8 (0.6)	13.4 (0.59)	1.5 (0.11)	23.4 (0.6)	48.8 (2.0)	0.995	66
	ZF	C		27.9 (0.13)	21.3 (0.21)	25.6 (1.5)	32.3 (1.4)	12.6 (0.13)	1.6 (0.20)	17.9 (0.6)	30.6 (0.9)	0.997	54
		Y		26.0 (0.13)	16.8 (0.22)	24.7 (2.8)	38.9 (0.4)	14.6 (0.15)	1.7 (0.21)	16.9 (0.8)	33.5 (1.1)	0.993	54
Field density experiment	ZF	C	Local	26.8 (0.11)	19.8 (0.19)	23.4 (2.0)	32.2 (4.3)	12.5 (0.11)	1.4 (0.18)	17.3 (0.7)	32.3 (1.0)	0.999	42
			+30%	28.0 (0.14)	20.4 (0.23)	24.0 (1.8)	25.5 (5.6)	13.4 (0.14)	1.8 (0.22)	18.1 (0.7)	31.7 (1.1)	0.999	42
			+50%	27.7 (0.15)	20.9 (0.28)	23.3 (2.0)	24.6 (5.8)	12.8 (0.17)	2.0 (0.29)	16.7 (1.0)	30.6 (1.5)	0.997	42
			+70%	26.9 (0.15)	21.4 (0.28)	22.3 (1.9)	24.9 (5.9)	11.8 (0.20)	1.9 (0.29)	14.8 (1.3)	30.0 (1.8)	0.999	42
		Y	Local	25.0 (0.16)	15.6 (0.23)	31.9 (1.6)	41.2 (4.9)	13.9 (0.13)	1.1 (0.20)	16.8 (0.8)	36.5 (1.1)	0.999	42
			+30%	26.2 (0.18)	15.8 (0.25)	31.3 (2.5)	44.1 (5.0)	14.7 (0.21)	1.2 (0.34)	16.1 (1.4)	36.8 (1.4)	0.999	42
			+50%	26.9 (0.16)	16.2 (0.22)	31.2 (1.6)	43.5 (4.2)	15.2 (0.14)	1.4 (0.23)	16.4 (0.9)	36.3 (1.2)	0.999	42
			+70%	27.1 (0.15)	16.0 (0.21)	31.9 (1.7)	43.8 (3.8)	15.4 (0.13)	1.5 (0.21)	17.0 (0.7)	35.1 (1.0)	0.998	42

Genotype-background abbreviations: GLXN, cv. Guanglingxiangnuo; YD, cv. Yandao 8; WYJ, cv. Wuyunjing 3; and ZF, cv. Zhefu 802. C is rice control genotypes; G is greener-leaf variant genotypes; and Y is yellower-leaf variant genotypes. Local, +30%, +50%, and +70% represent plants at local normal plant density (25 × 15 cm), 30% higher density (25 × 11.5 cm), 50% higher density (25 × 10 cm), and 70% higher density (25 × 8.8 cm), respectively. Source parameters (estimated from eqn 4.7): $N_{x,o}$, the maximum aboveground N accumulation; $N_{b,o}$, the initial aboveground N accumulation at flowering; $t_{m,o}$, the moment when the decrease of source activity is fastest; $t_{e,o}$, the moment when source activity is decreased to zero. Sink parameters (estimated from eqn 4.1): $N_{x,i}$, the maximum panicle N accumulation; $N_{b,i}$, the initial panicle N accumulation at flowering; $t_{m,i}$, the moment when maximum sink demand is achieved; $t_{e,i}$, the moment when sink demand is decreased to zero. The unit day in the table is the thermal days calculated from recorded temperatures of every 30 min, based on eqn (4.12).

Table S4.5 The maximum rate and the mean rate of source activity and sink demand for biomass (W) and nitrogen (N) accumulation during grain filling in three experiments.

Experiment	Background	Genotype	Density	Biomass dynamics				Nitrogen dynamics			
				$s_{m,oW}$	$\bar{s}_{oW}$	$s_{m,iW}$	$\bar{s}_{iW}$	$s_{m,oN}$	$\bar{s}_{oN}$	$s_{m,iN}$	$\bar{s}_{iN}$
				(g hill^{-1} td^{-1})	(g hill^{-1} td^{-1})	(g hill^{-1} td^{-1})	(g hill^{-1} td^{-1})	(mg hill^{-1} td^{-1})	(mg hill^{-1} td^{-1})	(mg hill^{-1} td^{-1})	(mg hill^{-1} td^{-1})
Greenhouse	GLXN	C		0.93	0.70	0.88	0.58	2.99	1.82	6.81	4.55
experiment		G		0.89	0.58	0.75	0.52	2.89	1.59	6.26	4.32
(2019)	YD	C		1.01	0.69	1.26	0.77	4.06	3.71	11.48	7.12
		G		0.83	0.60	0.95	0.65	3.47	2.89	8.77	6.07
	WYJ	C		1.07	0.78	0.99	0.66	3.79	3.49	10.23	6.70
		G		0.92	0.63	0.87	0.60	3.58	2.92	8.88	6.05
		Y		0.68	0.57	0.78	0.54	3.59	2.64	7.55	5.21
	ZF	C		0.53	0.38	1.15	0.79	2.26	2.02	8.68	5.93
		Y		1.00	0.63	1.18	0.82	4.88	3.15	9.63	6.67
				(g m^{-2} td^{-1})	(g m^{-2} td^{-1})	(g m^{-2} td^{-1})	(g m^{-2} td^{-1})	(g m^{-2} td^{-1})	(g m^{-2} td^{-1})	(g m^{-2} td^{-1})	(g m^{-2} td^{-1})
Field	GLXN	C		28.3	25.7	31.8	21.9	0.21	0.17	0.35	0.24
experiment		G		20.0	18.9	28.0	19.1	0.19	0.14	0.32	0.22
(2020)	YD	C		40.6	27.7	39.7	27.5	0.44	0.25	0.52	0.36
		G		37.9	26.5	35.3	24.1	0.37	0.22	0.44	0.30
	WYJ	C		41.5	32.2	41.4	28.0	0.34	0.23	0.50	0.33
		G		33.9	26.4	37.2	25.8	0.29	0.21	0.42	0.29
		Y		25.8	23.8	31.5	21.2	0.21	0.18	0.36	0.24
	ZF	C		27.9	19.2	36.6	24.4	0.29	0.20	0.58	0.36
		Y		37.6	21.8	37.3	25.7	0.41	0.24	0.58	0.38
Field	ZF	C	Local	29.2	16.7	36.0	24.3	0.33	0.22	0.53	0.34
density			+30%	29.7	21.5	38.0	25.7	0.33	0.30	0.58	0.36
experiment			+50%	26.9	19.3	37.7	25.3	0.30	0.27	0.55	0.35
			+70%	23.2	16.6	35.5	24.1	0.26	0.22	0.49	0.33
		Y	Local	34.6	20.8	36.2	24.2	0.33	0.23	0.52	0.35
			+30%	36.5	22.4	39.3	26.6	0.37	0.23	0.54	0.37
			+50%	38.7	23.5	40.7	27.5	0.39	0.25	0.56	0.38
			+70%	38.7	24.5	41.3	27.9	0.39	0.25	0.59	0.40

Genotype-background abbreviations: GLXN, cv. Guanglingxiangnuo; YD, cv. Yandao 8; WYJ, cv. Wuyunjing 3; and ZF, cv. Zhefu 802. C is rice control genotypes; G is greener-leaf variant genotypes; and Y is yellower-leaf variant genotypes. Local, +30%, +50%, and +70% represent plants at local normal plant density (25 × 15 cm), 30% higher density (25 × 11.5 cm), 50% higher density (25 × 10 cm), and 70% higher density (25 × 8.8 cm), respectively. Source parameters: $s_{m,oW}$ and $s_{m,oN}$ are the maximum rate of source activity for biomass and N, respectively; $\bar{s}_{oW}$ and $\bar{s}_{oN}$ are the mean rate of source activity for biomass and N, respectively. Sink parameters: $s_{m,iW}$ and $s_{m,iN}$ are the maximum rate of sink demand for biomass and N, respectively; $\bar{s}_{iW}$ and $\bar{s}_{iN}$ are the mean rate of sink demand for biomass and N, respectively.

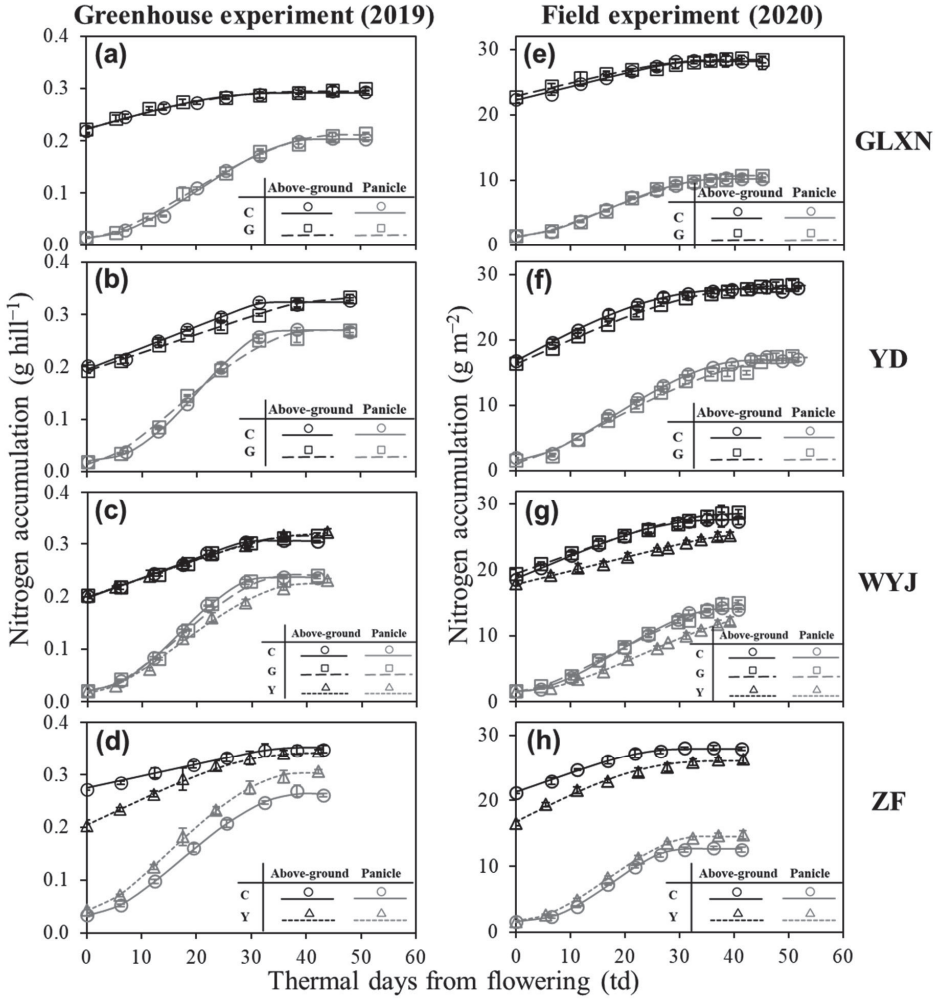

Fig. S4.1 The time course of above-ground N (dark symbols) and panicle nitrogen (grey symbols) accumulation in two experiments. Rice genotypes comprised four rice control (C, circles) genotypes and their greener-leaf variant (G, squares) and/or yellower-leaf variant (Y, triangles) genotypes. Each data point is shown as mean ± standard error of three to four replicates. The curves were drawn from eqns (4.1) and (4.7) for panicle and whole aboveground N accumulation, respectively, using parameter values in Table S4.4. Genotype-background abbreviations: GLXN, cv. Guanglingxiangnuo; YD, cv. Yandao 8; WYJ, cv. Wuyunjing 3; and ZF, cv. Zhefu 802.

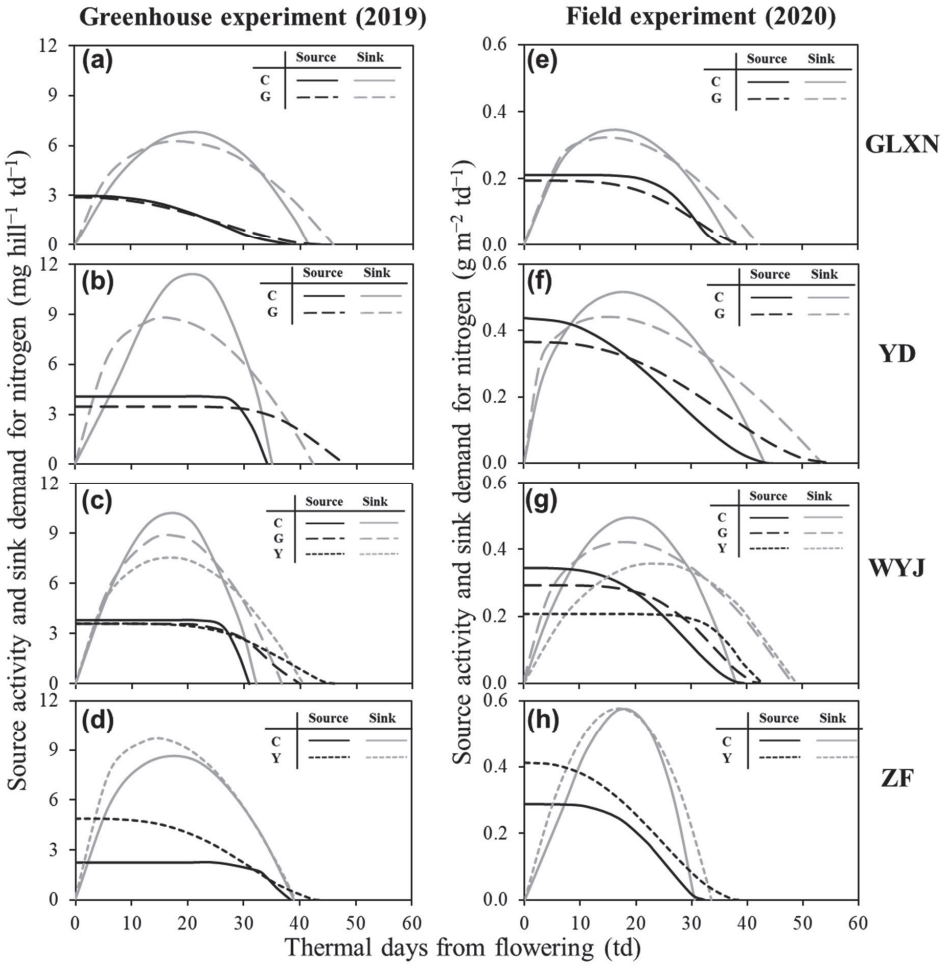

Fig. S4.2 Dynamics of source activity and sink demand for nitrogen (N) in two experiments. Rice genotypes comprised four rice control (C, full curves) genotypes and their greener-leaf variant (G, long-dashed curves) and/or yellower-leaf variant (Y, short-dashed curves) genotypes. The curves were drawn from eqns (4.2) and (4.4) for N sink and source activity, respectively, using parameter values in Table S4.4. Genotype-background abbreviations: GLXN, cv. Guanglingxiangnuo; YD, cv. Yandao 8; WYJ, cv. Wuyunjing 3; and ZF, cv. Zhefu 802.

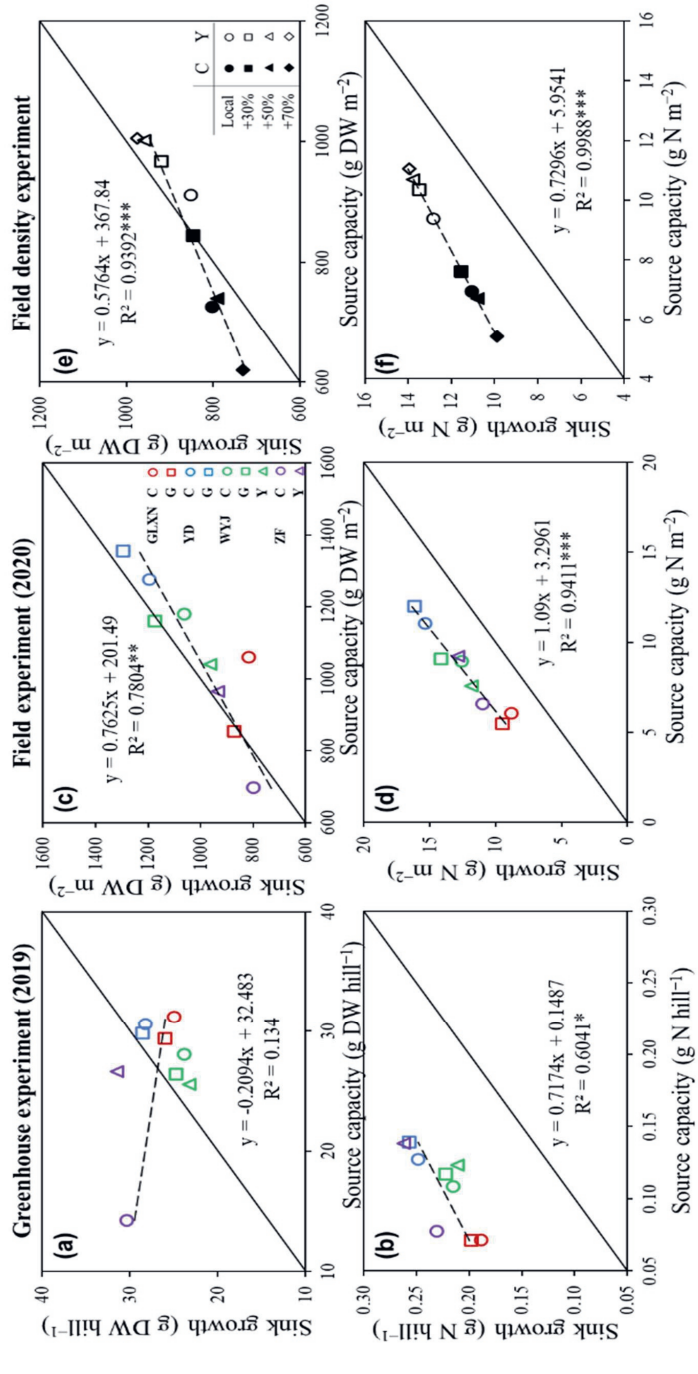

Fig. S4.3 Relationships between source capacity and sink growth for biomass (a, c, e) and nitrogen (b, d, f) in three experiments. Total source capacity and sink growth were calculated from eqn (4.8), using parameter values in Tables S4.3 and S4.4, respectively. Linear regression was fitted for overall data with its significance of correlation shown by asterisks: * $P < 0.05$, ** $P < 0.01$, *** $P < 0.001$. Genotype-background abbreviations: GLXN, cv. Guanglingxiangnuo; YD, cv. Yandao 8; WYJ, cv. Wuyunjing 3; and ZF, cv. Zhefu 802. C is rice control genotypes; G is greener-leaf variant genotypes; and Y is yellower-leaf variant genotypes. Local, +30%, +50%, and +70% represent plants at local normal plant density (25 × 15 cm), 30% higher density (25 × 11.5 cm), 50% higher density (25 × 10 cm), and 70% higher density (25 × 8.8 cm), respectively. The diagonal line is the 1:1 line. Note, only genotypes from ZF background was used in the field density experiment (Gu et al., 2017).

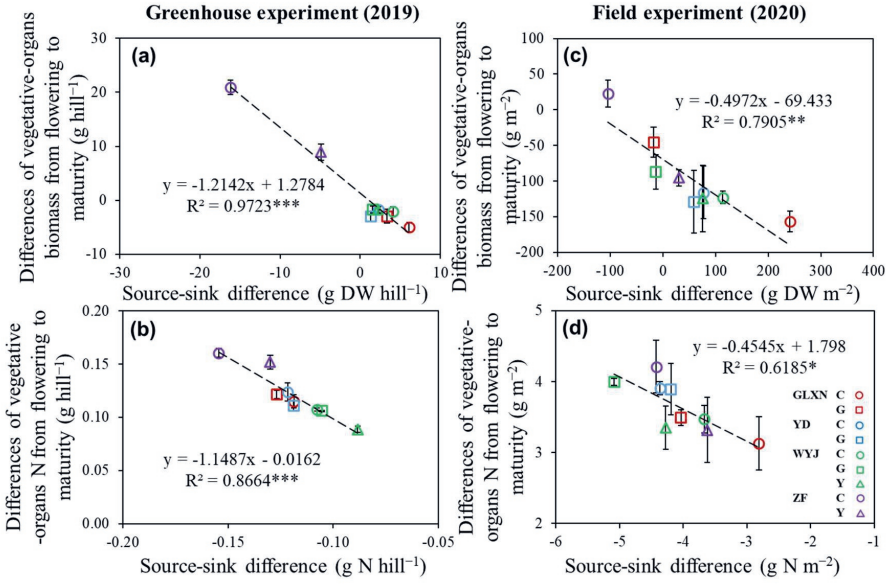

Fig. S4.4 Relationships of loss of vegetative-organ biomass versus biomass source-sink difference (a, c) and of loss of vegetative-organ nitrogen (N) accumulation versus N source-sink difference (b, d) during grain filling. Loss of vegetative-organ biomass was defined as the difference in biomass of leaf and stem between flowering and maturity stage, and loss of vegetative-organ N was defined as the difference in N accumulation of leaf and stem between flowering and maturity stage. Each data point for loss of vegetative-organ biomass (or N) represents the mean ± standard error of three to four replicates. Linear regression was fitted for overall data with its significance of correlation shown by asterisks: * $P < 0.05$, ** $P < 0.01$, *** $P < 0.001$. Genotype-background abbreviations: GLXN, cv. Guanglingxiangnuo; YD, cv. Yandao 8; WYJ, cv. Wuyunjing 3; and ZF, cv. Zhefu 802. C is rice control genotypes; G is greener-leaf variant genotypes; and Y is yellower-leaf variant genotypes.

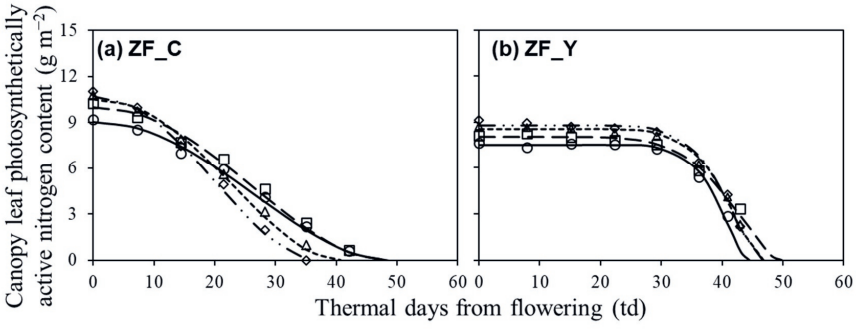

Fig. S4.5 The time course of canopy leaf photosynthetically active nitrogen (N) content for one rice control (C) genotype and its yellower-leaf variant (Y) genotype from cv. Zhefu 802 (ZF) background in the field density experiment (Gu et al., 2017). Each data point is shown as mean of three to four replicates. The thermal days were calculated from recorded temperatures of every 30 min, based on eqn (4.12). Local, +30%, +50%, and +70% represent plants at local normal plant density (25 × 15 cm), 30% higher density (25 × 11.5 cm), 50% higher density (25 × 10 cm), and 70% higher density (25 × 8.8 cm), respectively.

Chapter 5

Triose phosphate utilisation in leaves is modulated by whole-plant sink-source ratios and nitrogen budgets in rice

Zhenxiang Zhou[1], Zichang Zhang[1,2], Peter E.L. van der Putten[1], Denis Fabre[3,4], Michael Dingkuhn[3,4], Paul C. Struik[1] and Xinyou Yin[1]

[1] Centre for Crop Systems Analysis, Department of Plant Sciences, Wageningen University & Research, 6700 AK Wageningen, The Netherlands

[2] Institute of Plant Protection, Jiangsu Academy of Agricultural Sciences, Nanjing, Jiangsu, China

[3] CIRAD, UMR AGAP Institut, F-34398 Montpellier, France

[4] UMR AGAP Institut, Univ Montpellier, CIRAD, INRAE, Institut Agro, Montpellier, France

This chapter has been published in *Journal of Experimental Botany* (2023) erad329.

Abstract

The triose phosphate utilisation (TPU) is a biochemical process indicating carbon sink-source (im)balance within leaves. When TPU limits leaf photosynthesis, photorespiration-associated amino-acid exports probably provide an additional carbon outlet and increase leaf CO_2 uptake. However, whether this process is modulated by whole-plant sink-source relations and nitrogen (N) budgets remains unclear. We address this question by model analyses of gas-exchange data measured on leaves at three growth stages of rice plants grown at two N levels. Sink-source ratio was manipulated by panicle pruning, by using yellow-leaf variant genotypes, and by measuring photosynthesis on adaxial and abaxial leaf sides. Across all these treatments, higher leaf N content resulted in the occurrence of TPU limitation at lower intercellular CO_2 concentrations. Photorespiration-associated amino-acid export was greater in high-N leaves, but was smaller in yellower-leaf genotypes, panicle-pruned plants, and for abaxial measurement. The feedback inhibition of panicle pruning on rates of TPU was not always observed, presumably because panicle pruning blocked N remobilisation from leaves to grains and the increased leaf N content masked feedback inhibition. The leaf-level TPU limitation was thus modulated by whole-plant sink-source relations and N budgets during rice grain filling, suggesting a close link between within-leaf and whole-plant sink limitations.

Keywords: Adaxial vs abaxial measurement, *Oryza sativa*, panicle pruning, triose phosphate utilisation, photorespiration-associated nitrogen assimilation, sink limitation, yellower-leaf modification

5.1 Introduction

CO_2 response curves of leaf photosynthesis as obtained from gas exchange analysis are typically described by the canonical Farquhar–von Caemmerer–Berry (FvCB) biochemical photosynthesis model (Farquhar et al., 1980). This model predicts that leaf photosynthetic rates under the current environment conditions are determined by two main parameters, Rubisco carboxylation capacity (V_{cmax}) and maximum linear electron transport rate (J_{max}). The transition from Rubisco limitation to electron-transport limitation occurs around a leaf internal CO_2 level when the equivalent ambient-air CO_2 concentration (C_a) is about 400 μmol mol^{-1} (e.g. Mathan et al., 2021). However, the internal CO_2 inside a leaf can attain a high level at which leaf photosynthesis is limited by a third parameter T_p, the rate of triose phosphate utilisation (TPU). Until now, compared with the first two biochemical components (i.e., V_{cmax} and J_{max}), T_p has received less attention since observable TPU limitations only occur occasionally and are highly variable, depending on species, genotype, growth conditions, and measurement conditions (e.g., Kumarathunge et al., 2019). Also, the TPU-limited condition is observed only temporarily, because it can be removed quickly as other parameters like V_{cmax} and J_{max} may be regulated to a level where T_p is no longer "apparently" limiting (McClain et al., 2023). Nevertheless, with the increase of atmospheric CO_2 (to roughly 600 μmol mol^{-1}; Lombardozzi et al., 2018), TPU limitation will probably become increasingly important for predicting photosynthesis and yield.

TPU refers to the rate at which triose phosphates exit from the photosynthetic Calvin–Benson-Bassham (CBB) cycle and are used as sugar precursors for processes like the synthesis of sucrose and starch. As triose-phosphates are phosphorylated carbon, any TPU requires the returns of inorganic phosphate (P_i) to the chloroplast, since the quantity of phosphate in the chloroplast is finite and under tight homeostasis (McClain & Sharkey, 2019). A limitation of TPU on photosynthesis is triggered when carbon exports from (with the accompanying P_i import to) the cycle cannot keep pace with carbon fixation, which is in essence a local sink-source disequilibrium. TPU limitation causes unresponsiveness to CO_2 (Sharkey, 1985), or sometimes, reversed sensitivity of photosynthesis to increasing CO_2 (e.g. von Caemmerer & Farquhar 1981; Harley & Sharkey 1991). The TPU limitation is considered to be a biochemical mechanism for sink limitation on photosynthesis, expressed at a sub-foliar scale (Sharkey, 2019). This differs from the sink (panicles) limitation on source (leaves) activity agronomists commonly define at the whole-plant or crop scale. While sink limitations at sub-foliar and

whole-plant scales are not necessarily independent (Yin et al., 2022), few studies have been conducted on their connections.

Agronomists commonly manipulate sink-source ratios at the whole-plant scale by pruning leaves or panicles during the grain filling process, which modifies the transport of assimilates between source and sink organs (Li et al., 2017; He et al., 2019). Many reports (Rossi et al., 2015; Dingkuhn et al., 2020; Fabre et al., 2020) have also demonstrated that genotypes with larger crop carbon sink capacity can benefit more from future CO_2-rich climate. Conversely, a smaller sink (e.g., small-panicle genotypes, or plants with panicles pruned) reduces phloem loading, forcing assimilate accumulation in leaves or stems that may exert a feedback inhibition on leaf photosynthetic source activity (Burnett et al., 2016; White et al., 2016), and even on values of TPU (Fabre et al., 2019).

Carbon metabolism generally interacts with nitrogen (N) assimilation. In fact, Harley & Sharkey (1991) hypothesised that the reversed sensitivity of photosynthesis to increasing CO_2 under TPU limitation resulted from diverting a fraction of N-containing glycine from the photorespiratory pathway and this glycine is used elsewhere for other amino-acid or protein synthesis. Glycine is derived from the photorespiratory glycolate carbon; normally, 25% of the glycolate carbon is lost as CO_2 as a result of glycine decarboxylation, and the remaining 75% is recycled to glycerate and further to 3-phosphoglycerate to rejoin the CBB cycle (Fig. S5.1). With the exit of glycine, the P_i normally used in converting glycerate to 3-phosphoglycerate is made available for phosphorylation, thereby, stimulating photosynthesis (Harley & Sharkey, 1991). Busch et al. (2018) extended this hypothesis by considering the exit of both glycine and serine from the photorespiratory pathway. The export of N from the photorespiratory pathway requires *de novo* N assimilation and amino-acid synthesis (Fig. S5.1). They proposed that a large proportion of N assimilation in leaves accomplished *via* the photorespiratory pathway is innately linked with TPU. The exported amino acids represent an additional sink for carbon, and decrease P_i consumption for phosphorylating glycerate to 3-phosphoglycerate, thereby explaining the increased photosynthetic rate with decreasing CO_2 levels (with increasing photorespiration) within TPU-limited range (Busch et al., 2018; Yin et al., 2021). The extent of increase in photosynthesis depends on the proportion of glycolate carbon exported from the photorespiratory pathway. It is conceivable that the proportion of amino-acid carbon export may be associated with the availability of NO_3^- for N assimilation. Crop N assimilation occurs throughout the life cycle, but varies with NO_3^- availability and leaf N content. We hypothesise that values of a parameter related to TPU limitation (i.e., the fraction of the glycolate carbon

exported from the photorespiratory pathway) increase with leaf N content, and thus, vary among growth stages and N treatments.

In this study, we aim to (i) quantify how TPU-limited photosynthetic carbon uptake is affected by nitrogen assimilation via the photorespiratory pathway; and (ii) analyse how the local sink-source mechanisms of TPU limitation within leaves are regulated by the whole-plant physiological source and sink relationships. We address these aims in the context of our recent effort to examine the impact of leaf-colour modification on photosynthesis, using rice genotypes of different leaf colour based on our previous finding that genotypic leaf yellowness affects leaf photosynthetic rate via several mechanisms including altered leaf morphology (Zhou et al., 2023). As adaxial and abaxial photosynthetic rates are known to differ (e.g., Soares et al., 2008), gas exchange measurements with the local illumination on either leaf side may result in a varied leaf-scale source activity but with a constant sink demand. Thus, in our experimental set-up, we use three means to vary carbon sink-source ratios (genotypic leaf-colour variants, panicle pruning, and adaxial *vs* abaxial illumination while measuring gas exchange), and two means to vary nitrogen status (N treatments and plant developmental stages). In addition, we use 21% O_2 vs 2% O_2 conditions to alter photorespiration, likely modifying the amount of glycine and serine export. We hoped to obtain information on how TPU limitation is related to photorespiration-associated N assimilation and affected by altered sink-source ratios within the leaf and at the whole-plant scale.

5.2 Materials and Methods

5.2.1 Plant material and growth conditions

Rice (*Oryza sativa* L.) materials were based on two background genotypes: japonica type cv. Wuyunjing 3 (WYJ) and early indica type cv. Zhefu 802 (ZF). Both were modified by radiation mutagenesis with ^{60}Co γ-rays, and the yellower-leaf variants were identified from a larger population of phenotypes. These genotypes showed stability of the lines over generations (Zhou et al., 2023). Hereafter, yellower genotypes are denoted as Y and the wild type as control (C).

Two experiments were conducted in a climate-controlled glasshouse in Wageningen, the Netherlands in 2019 and 2022. The growth conditions were the same as described in our earlier study (Zhou et al., 2023): incident global radiation outside the greenhouse was kept within 400−500 W m^{-2} (resulting in a photosynthetic photon flux density measured at plant height of

~500 μmol m^{-2} s^{-1}), temperature was set at 26 °C for the 12-h light period and at 23 °C for the 12-h dark period, the CO_2 level was about 400 μmol mol^{-1}, and the relative humidity was 65−75%. The 2019 experiment was to examine if genotypes differ in the extent of photosynthetic differences between adaxial and abaxial illumination.

In the 2022 experiment, nitrogen supply and panicle pruning treatments were added as factors. Nitrogen was applied as urea at two levels: N1 (in total 0.7 g urea per pot) and N2 (in total 1.4 g urea per pot). All pots were evenly divided into four blocks (corresponding to four experimental replicates), and each block contained 64 pots, representing all combinations of four genotypes, two nitrogen levels, and two pruning levels. The four pots per treatment combination were used for measurements at three developmental stages (see below), with one pot as reserve in case of plant damage. Plants to be pruned were randomly selected and pre-labelled, and panicles of these plants were pruned at the moment when the first panicle of the plant had emerged from the flag-leaf sheath. This operation lasted a week to ensure that no new heads were produced from any culms.

5.2.2 Leaf photosynthesis measurements

Pre-labelled and fully expanded main-stem leaves in each experimental treatment per replicate were measured using an open-path gas exchange system integrated with a fluorescence chamber head (LI-COR 6800; LI-COR Inc., Lincoln, NE, USA) to simultaneously obtain gas exchange and chlorophyll fluorescence parameters. All measurements were carried out at a leaf temperature of 25 °C and a vapour pressure difference of 1.0−1.6 kPa between the leaf and air outside of the leaf, with a flow rate of 400 μmol s^{-1}.

For both 2019 and 2022 experiments, measurements were conducted on the same leaf segment at both adaxial and abaxial sides. It should be noted that measurements on “adaxial or abaxial sides” always integrated the gas exchange occurring on both sides, as both sides were exposed to the chamber air. However, the light was only received by the side that faced the light source. Strictly speaking, it was not the gas exchange measurement but the light orientation that varied, causing inverted light gradients through the leaf.

For the 2019 experiment, measurements were conducted only at the tillering stage. Light and CO_2 response curves were measured at the same position at both adaxial and abaxial sides of the leaves. The curves for net photosynthetic rate (A) response to incident irradiance (I_{inc}) were obtained with I_{inc} in a decreasing series of 2000, 1500, 1000, 500, 280, 150, 100, 80, and 50

μmol m^{-2} s^{-1} (6−8 min per step), while maintaining ambient CO_2 level (C_a) at 400 μmol mol^{-1}. The CO_2 response curves were measured at I_{inc} of 1000 μmol m^{-2} s^{-1}, with the C_a steps of 400, 250, 150, 80, 50, 400, 400, 400, 650, 1000, and 1500 μmol mol^{-1} (3−5 min per step; note that using the three repeated 400 μmol mol^{-1} steps was merely to re-adapt leaves and the data from these three points were excluded in the analysis). Both curves were measured at ambient O_2 (21%) level. To estimate day respiration (R_d) and establish a calibration factor (s) that converts chlorophyll fluorescence-based electron transport efficiency of Photosystem II (PSII) into linear electron transport rate (see Yin et al., 2009), we also conducted half of the light response curve (with I_{inc} being 280, 150, 100, 80, and 50 μmol m^{-2} s^{-1}) under non-photorespiratory conditions (2% O_2 combined with C_a at 1000 μmol mol^{-1}). These low light levels were applied to ensure that data for calibration were within the range where A is limited by electron transport. The low O_2 level was realised by using a cylinder containing a gas mixture of 2% O_2 and 98% N_2.

For the 2022 experiment, photosynthesis was measured on both adaxial and abaxial leaf surfaces at three stages: tillering stage (TS), flowering stage (FS), and grain-filling (~15 days after flowering, 15 DAF). The panicle-pruned plants were only measured at grain filling because these plants were supposed to function the same as the non-pruned plants at tillering and flowering. As this experiment was meant to examine the TPU limitation, only CO_2 response curves (where A is likely limited by TPU) were measured at I_{inc} of 1500 μmol m^{-2} s^{-1} under both 21% and 2% O_2 conditions, with the C_a in an increasing series: 400, 500, 600, 700, 800, 900, 1000, 1200, 1400, 1600, and 1800 μmol mol^{-1}. These C_a levels were chosen to ensure that part of the curve could reach the TPU-limited range. As with the 2019 experiment, we additionally measured the light-response curve with I_{inc} being 300, 150, 100, 80, and 40 μmol m^{-2} s^{-1} under non-photorespiratory conditions to estimate R_d and s.

For each irradiance or CO_2 step in both experiments, F_s (the steady-state fluorescence) was recorded after A reached the steady state. The maximum fluorescence (F'_m) was determined using a three-phase flash method (Loriaux et al., 2013): each phase went through a duration of 300 ms, and flash intensity of 6500 μmol m^{-2} s^{-1} in the second phase was attenuated by 40%. The apparent operating photochemical efficiency of PSII was assessed from chlorophyll fluorescence measurements: $\Phi_2 = 1 - F_s/F'_m$ (Genty et al., 1989).

All gas exchange data were corrected for any small basal leakage of CO_2 into and out of the leaf cuvette, based on measurements on boiled leaves across the CO_2 levels, and intercellular CO_2 levels (C_i) were then re-calculated.

5.2.3 Leaf SPAD and nitrogen content

All leaf segments used for measuring photosynthesis curves were cut out and used immediately to measure the leaf area with a LI-3100 area meter (LI-COR, Lincoln, NE, USA), and the values for SPAD indicating chlorophyll content (SPAD-502, Minolta Camera Co., Japan). SPAD was measured at both adaxial and abaxial sides of these leaf segments. Leaf materials were then oven-dried at 70 °C for 48 h to constant weight. Specific leaf area (SLA, $m^2\ kg^{-1}$) was calculated as the leaf area to dry leaf mass ratio. Each leaf segment was ground into powder in a 2-ml centrifuge tube, which was used to measure the N concentration by an element analyser based on the micro-Dumas combustion method. Specific leaf nitrogen (SLN, g N m^{-2}) was then calculated.

5.2.4 Plant growth measurements

At grain-filling stage in the 2022 experiment, the aboveground parts were sampled and separated. Dry weight of each part was determined after oven drying at 75 °C for 72 h to constant weight. The leaf samples were ground into powder, which was then assessed for nitrogen concentration with a Kjeldahl apparatus (Kjeltec 8400, Foss Corp., Germany). Total leaf-nitrogen per pot was calculated by leaf nitrogen concentration multiplied by total leaf dry weight. We counted the fertile spikelet number for each culm, and then measured the flag leaf area (just after photosynthesis measurement) and total leaf area by a LI-3100 area meter (LI-COR, Lincoln, NE, USA). Following Fabre et al. (2020), the ratio of flag leaf area (source) to the fertile spikelet number of the panicle (sink) on the culm was used as an indicator of the single-culm sink-source ratio, while total spikelet number divided by total leaf area of the whole plant was used as an indicator of the whole-plant sink-source ratio.

5.2.5 Estimating photosynthetic parameters

We estimated parameters of the 'FvCB model' (Farquhar et al., 1980), which expresses net photosynthetic rate (A) as the minimum of the Rubisco carboxylation-limited rate (A_c), electron-transport limited rate (A_j), and the triose phosphate utilisation (TPU) limited rate (A_p):

$$A = \min\left(A_c, A_j, A_p\right) \tag{5.1}$$

For A_c:

$$A_c = \frac{(C_c - \Gamma_*)V_{cmax}}{C_c + K_{mC}(1 + O/K_{mO})} - R_d \tag{5.2}$$

where C_c and O are the chloroplast partial pressures of CO_2 and O_2, respectively. V_{cmax} is the maximum rate of Rubisco activity for carboxylation, and K_{mC} and K_{mO} are Michaelis-Menten constants of Rubisco for CO_2 and O_2, respectively. $\Gamma*$ is the CO_2 compensation point in the absence of day respiration (R_d), described by: $\Gamma* = 0.5O/S_{c/o}$, where $S_{c/o}$ is the relative CO_2/O_2 specificity factor for Rubisco. Values of these Rubisco parameters vary significantly, depending on techniques used to measure them; here, we used the representative values of Rubisco parameters measured *in vitro* at 25 °C by Cousins et al. (2010) for wheat: i.e. 291 μbar for K_{mC}, 194 mbar for K_{mO}, and 3.022 mbar μbar^{-1} for $S_{c/o}$, given that values of these Rubisco parameters are believed to be conserved among C_3 species (von Caemmerer, 2000).

For A_j: $$A_j = \frac{(C_c-\Gamma_*)J}{4(C_c+2\Gamma_*)} - R_d \quad (5.3a)$$

where J is the potential linear electron transport rate supporting the CBB cycle and the photorespiratory cycle. J can be calculated using the calibration factor s, incident irradiance (I_{inc}), and fluorescence-based photochemical efficiency of PSII (Φ_2) as: $J = sI_{inc}\Phi_2$, where parameters s and R_d can be estimated from the slope and intercept of a linear plot of A_j against ($I_{inc}\Phi_2/4$) measured under non-photorespiratory conditions (Yin et al., 2009). The calculated J can be fitted according to:

$$J = \left[\kappa_{2LL}I_{inc} + J_{max} - \sqrt{(\kappa_{2LL}I_{inc} + J_{max})^2 - 4\theta J_{max}\kappa_{2LL}I_{inc}}\right]/(2\theta) \quad (5.3b)$$

where J_{max} is the maximum value of J under saturated light; κ_{2LL} represents the conversion efficiency of incident light into J at strictly limiting light; and θ is a dimensionless convexity factor for the response of J to I_{inc}, and here a common value of 0.76 for θ was adopted for all rice genotypes from Zhou et al. (2023).

For A_p, the widely used algorithm (Harley & Sharkey, 1991; von Caemmerer, 2000) assumes that glycine is taken out from the photorespiratory pathway. However, this algorithm does not consider the required change of the CO_2 compensation point, as a result of the glycine export, to $(1-\alpha_G)\Gamma*$ (Busch et al., 2018; Yin et al., 2021, also see Fig. S5.1; where α_G is the proportion of glycolate carbon exported from the photorespiratory pathway in the form of glycine). Model fitting results of Busch et al. (2018) suggested that the proportion of glycolate carbon exported as glycine is lower than the proportion exported as serine. Isotope-labelling measurements (Abadie et al., 2016; Fu et al., 2022) more convincingly confirmed little export in the form of glycine. As serine export causes no change in the CO_2 compensation point, here for the purpose

of simplicity, we assumed only the serine export, for which the model becomes (Yin et al., 2021; see their eqn 17b):

$$A_{\mathrm{p}} = \frac{(C_{\mathrm{c}} - \Gamma_*)(3T_{\mathrm{p}})}{C_{\mathrm{c}} - (1+4\alpha_{\mathrm{S}})\Gamma_*} - R_{\mathrm{d}} \tag{5.4}$$

where α_{S} is the proportion of glycolate carbon exported from photorespiratory pathway in the form of serine (with $\alpha_{\mathrm{S}} \leq 0.75$). This guarantees the same term in the numerator, (C_{c}–Γ_*), which is consistent with Rubisco- or electron transport-limited forms. Such consistency simplifies the modelling algorithms for the next steps of analysis (eqns 5.5–5.6). The simple model in eqn (5.4) also generates the TPU-limited rate A_{p} similar to the full model with both glycine and serine export if the total fraction of glycolate carbon export remains the same (Yin et al., 2021). Note that the coefficient in front of the term for the proportion of glycolate carbon export in the denominator of eqn (5.4) is 4, whereas this is 3 in the commonly used old equation assuming the glycine exit (von Caemmerer, 2000; Ellsworth et al., 2015; Busch & Sage, 2017; Kumarathunge et al., 2019; also see Fig. S5.1). As a result, the old equation, when applied to fit gas-exchange data, overestimates the glycolate carbon export fraction by a factor of 4/3 (Yin et al. 2021).

The method of Harley et al. (1992) was first applied to examine whether mesophyll conductance g_{m} varied with intercellular CO_2 level (C_{i}) or I_{inc}, and we found that g_{m} is variable and declines with increasing C_{i} or with decreasing I_{inc}, with g_{m} = 0 as I_{inc} approaches to zero (results not shown). To describe this pattern of variable g_{m}, we used an equation of Yin et al. (2009):

$$g_{\mathrm{m}} = \delta\,(A + R_{\mathrm{d}})/(C_{\mathrm{c}} - \Gamma_*) \tag{5.5}$$

where parameter δ represents the carboxylation resistance to mesophyll resistance ratio (Yin et al., 2020). Then, this equation (5) was combined with eqns (5.2), (5.3a), and (5.4), and C_{c} was replaced by ($C_{\mathrm{i}} - A/g_{\mathrm{m}}$) to solve for A (Yin et al., 2020):

$$A = \left(-b \pm \sqrt{b^2 - 4ac}\right)/(2a) \tag{5.6}$$

where

$$a = x_2 + \Gamma_* + \delta(C_{\mathrm{i}} + x_2)$$

$$b = -(x_2 + \Gamma_*)(x_1 - R_{\mathrm{d}}) - \delta(C_{\mathrm{i}} + x_2)(x_1 - R_{\mathrm{d}}) - \delta[x_1(C_{\mathrm{i}} - \Gamma_*) - R_{\mathrm{d}}(C_{\mathrm{i}} + x_2)]$$

$$c = \delta(x_1 - R_\mathrm{d})[x_1(C_\mathrm{i} - \Gamma_*) - R_\mathrm{d}(C_\mathrm{i} + x_2)]$$

where $For\ A_\mathrm{c}\ part \begin{cases} x_1 = V_\mathrm{cmax} \\ x_2 = K_\mathrm{mC}(1 + O/K_\mathrm{mO}) \end{cases}$

$For\ A_\mathrm{j}\ part \begin{cases} x_1 = J/4 \\ x_2 = 2\Gamma_* \end{cases}$

$For\ A_\mathrm{p}\ part \begin{cases} x_1 = 3T_\mathrm{p} \\ x_2 = -(1 + 4\alpha_\mathrm{S})\Gamma_* \end{cases}$

Note when calculating A in eqn (5.6), the − sign in front of the $\sqrt{b^2 - 4ac}$ term was applied for either the A_c- or A_j-limited part while the + sign was required for A_p-limited part (see Yin et al., 2020).

For analysing the 2019 data where light-response curves were measured, we first estimated J_max by fitting eqn (5.3b) to data points of light response of J derived from chlorophyll fluorescence parameters Φ_2 (i.e. $J = sI_\mathrm{inc}\Phi_2$). Then photosynthetic parameters δ, V_cmax, T_p, and α_S can be estimated simultaneously by fitting combined eqn (5.1), eqn (5.3b) and eqn (5.6) to all CO_2 exchange data from both light- and CO_2-response curves. For data from 2022, as only CO_2 response curves were measured yet starting with C_a from 400 μmol mol^{-1} onwards that only covered A_j- and A_p-limited parts, we thus combined $J = sI_\mathrm{inc}\Phi_2$ and A_j- and A_p-parts of eqn (5.6) to estimate parameters δ, T_p, and α_S simultaneously.

Once photosynthetic parameters were estimated, the transition point from A_j- to A_p-limited rates can be solved. We also estimated the transition point by solving the second-order polynomial regression equations that were fitted to A_j- and A_p-ranges, respectively, of A-C_i curves. The estimated threshold C_i was highly consistent (see Results); thus, we used the polynomial-based values for showing the transition.

5.2.6 Statistical analyses and curve fitting

Simple linear regressions were conducted using Microsoft Excel. Non-linear regressions were performed using the Gauss method in PROC NLIN of SAS (SAS Institute Inc., Cary, NC, USA). An analysis of variance (ANOVA) of multiple experimental factors (i.e. genotype, adaxial vs abaxial, pruning, N level, stage), and their interaction effects on each parameter was performed

in the 2022 experiment. A multiple comparison of means was then performed using the LSD (least significant difference) test.

5.3 Results

5.3.1 Effect of adaxial vs abaxial measurements on leaf source activity

In the 2019 experiment, the two Y-variant genotypes exhibited an opposite trend in leaf photosynthetic rate (A): relative to their control (C) genotypes, a decrease in A and estimated parameters (J_{max}, V_{cmax}, and T_p) was obtained in WYJ-Y whereas an increase in these parameters was observed in ZF-Y (Fig. 5.1). In addition, the parameter α_S was also altered by the Y modification: it became lower ($P < 0.05$), particularly in the WYJ background.

The difference in photosynthetic rates between the two sides of the same leaf depended on genotypes. For light response curves (Figs. 5.1A-D), a great reduction (ca. 8−10%) in A at a light intensity of 2000 μmol m^{-2} s^{-1} (A_{2000}) was observed on the abaxial side in C genotypes, resulting in a lower estimated J_{max} on the abaxial surface compared with that on the adaxial surface. In contrast, the light response curves were similar on both sides of leaves in Y-variant genotypes (difference of A_{2000} less than 2%). Similar patterns were observed for CO_2 response curves (Figs. 5.1E-H), with greater differences between adaxial and abaxial values for parameters V_{cmax}, T_p, and α_S in C genotypes than in Y-variant genotypes.

5.3.2 Overview of A-C_i curves from the 2022 experiment

Given the above differences between adaxial and abaxial measurements in the 2019 experiment, we continued in the 2022 experiment to use adaxial *vs* abaxial measurements for all nitrogen × pruning combinations as a means to manipulate within-leaf sink-source ratios. In addition, measurements were made for three different stages and at two O_2 levels. All the A-C_i curves obtained are shown in Fig. S5.2.

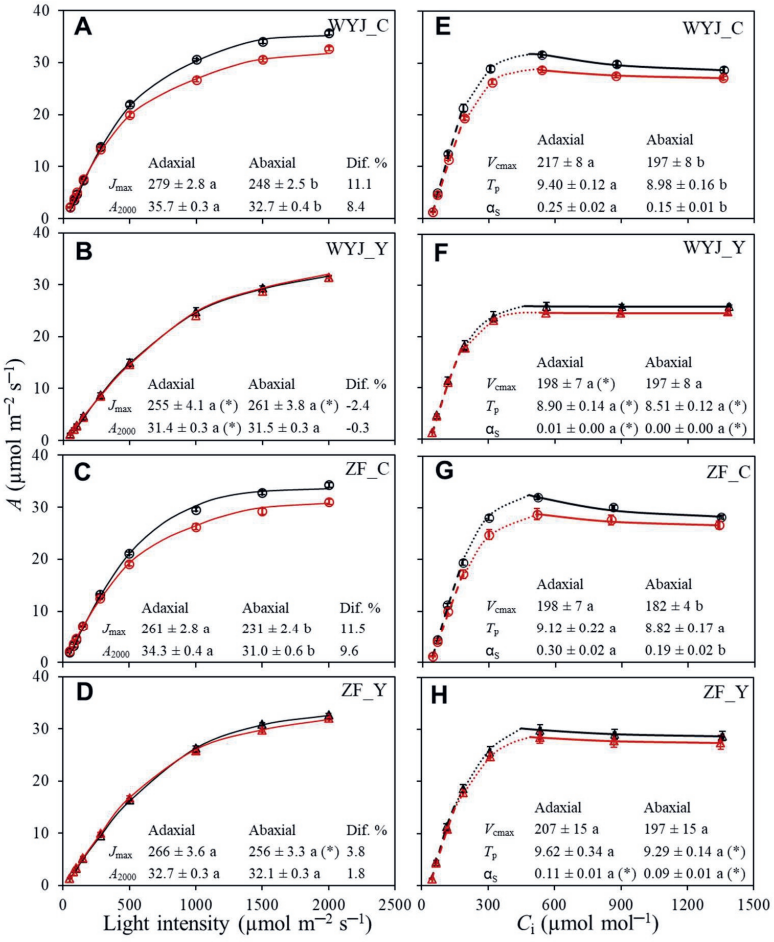

Fig. 5.1 Effects of adaxial vs abaxial measurement on the photosynthetic parameters in four rice genotypes (data measured at the tillering stage in the 2019 experiment). **A-D**, light-response curves of photosynthesis (A) at the CO_2 concentration of 400 μmol mol^{-1}; **E-H**, CO_2-response curves at the light intensity of 1000 μmol m^{-2} s^{-1}, for rice control (C) genotypes (circles) and their yellower-leaf (Y) variant genotypes (triangles). Data shown as means of four replicates (± standard errors) for each genotype are with black symbols representing measurement on adaxial surface of leaves and red symbols representing measurement on abaxial surface of leaves. WYJ and ZF are the abbreviations of two genetic backgrounds Wuyunjing 3 and Zhefu 802, respectively. For Panels A-D, the curves are drawn from Eqn (5.6) using fitted parameter values. The estimated maximum linear electron transport under saturating light (J_{max}, μmol m^{-2} s^{-1}), net photosynthesis rate under light intensity of 2000 μmol m^{-2} s^{-1} (A_{2000}, μmol m^{-2} s^{-1}), and the percentage difference in the J_{max} and A_{2000} (calculated as: $\frac{Adaxial-Abaxial}{Adaxial} \times 100$) are listed. For Panels E-H, the curves representing A_c- (dashed curve), A_j- (dotted curve), and A_p-limited (full curve) parts are drawn from Eqn (5.6) using fitted values of the parameters: the estimated maximum rate of Rubisco carboxylation (V_{cmax}, μmol m^{-2} s^{-1}), rate of triose phosphate utilisation (T_p, μmol m^{-2} s^{-1}), and the proportion of glycolate carbon exported from the photorespiratory pathway in the form of serine (α_S). The different letters indicate statistical significance at the $P < 0.05$ level for the estimated parameters between adaxial and abaxial measurements, and the asterisks (*) represent significant differences ($P < 0.05$) between C genotype and its Y variant.

Differences in measured A-C_i curves and in the estimated A_j-to-A_p transition point between 21% and 2% O_2 (Fig. S5.2) agreed with those theoretically expected for TPU limitation either with (Fig. S5.2A) or without (Fig. S5.2B) glycolate carbon exit from the photorespiratory pathway (Harley & Sharkey 1991; Busch et al. 2018). Thus, combined data from the two O_2 levels were fit to estimate TPU parameters.

5.3.3 Estimated TPU capacity

Values of T_p estimated for pruned and non-pruned plants under two nitrogen levels (N1 and N2) and at three growth stages in the 2022 experiment are shown in Fig. 5.2. As expected, the rate of TPU (T_p; Figs. 5.2A-D and Table S5.1) and photosynthetic rate at a light intensity of 1500 μmol m^{-2} s^{-1} (A_{1500}; Table S5.2) increased with the addition of N fertiliser and decreased with advancing growth stage. Significant effects mainly occurred from flowering onwards. At 15DAF, there were no significant effects of panicle pruning on T_p except for an increase of T_p in WYJ-C at N1 (Fig. 5.2A). In line with the results of the 2019 experiment (Fig. 5.1), values of T_p from the adaxial measurements were generally higher than those from the abaxial measurements (Fig. 5.2E).

5.3.4 Estimated proportion of photorespiratory carbon exited as serine (α_S)

The effects of N treatments on the values of α_S are shown in Fig. 5.3. The high N level generally increased α_S ($P < 0.05$). But growth-stage effects were more complex, as α_S varied more among growth stages in C genotypes than in Y variants (Figs. 5.3A-D). The estimated α_S of WYJ-C declined significantly ($P < 0.05$) at 15DAF after an increase at FS, whereas that of ZF-C decreased along all growth stages. The estimated α_S was negatively correlated with SLA, an indicator of leaf thinness (Fig. S5.3).

Unlike T_p, α_S was greatly decreased by pruning in all genotypes, especially at N2. There was a significant interaction between pruning and N level on α_S ($P<0.001$; Table S5.3). In addition, compared with T_p, α_S differed more between adaxial and abaxial measurements (by ~24%), with larger differences in C genotypes than in Y-variant genotypes, especially at TS and FS stages (Fig. 5.3E). No interactions of measurement side with N level or growth stage were found for α_S (Table S5.3).

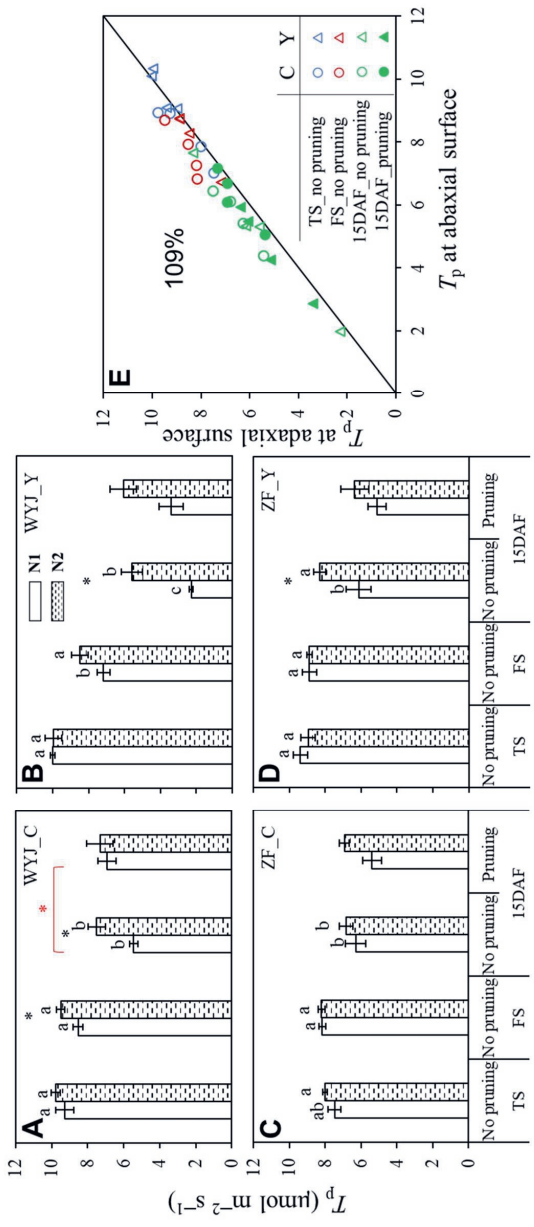

Fig. 5.2 Effects of altered sink-source ratios on parameter T_p (the 2022 experiment). **A-D**, The rate of triose phosphate utilisation (T_p, based on measurements on the adaxial leaf surface) for rice control (C) genotypes and their yellower-leaf (Y) variant genotypes of intact or panicle-pruned plants at tillering (TS), flowering (FS), and 15d after flowering (15DAF) stages under low-nitrogen (N1, white bars) and high-nitrogen (N2, dashed bars) levels. The value of each bar representing mean ± standard error of four replicates was estimated by fitting curves to CO_2 exchange data (see Fig S5.2). For intact plants (no pruning), different letters indicate statistical significance at the $P < 0.05$ level between three stages within each genotype-nitrogen combination, and the asterisks (*) in black represent significant differences ($P < 0.05$) between N1 and N2 levels within each genotype and stage. The asterisk (*) in red represents significant difference ($P < 0.05$) for a given genotype-nitrogen combination between pruned and un-pruned plants at 15DAF stage. WYJ and ZF are the abbreviations of two genetic backgrounds: cv. Wuyunjing 3 and cv. Zhefu 802. **E**, Comparisons of the values of T_p measured at adaxial surface vs those measured at abaxial surface. The percentage is the average of adaxial relative to abaxial parameters and the diagonal line is the 1:1 line. Data represented by different colours and symbols are from C genotypes (circles) and Y-variant genotypes (triangles) of intact (open symbols) and panicle-pruned (filled symbols) plants at TS (blue), FS (red), and 15DAF (green) stage. Each point represents the mean of three or four replicates.

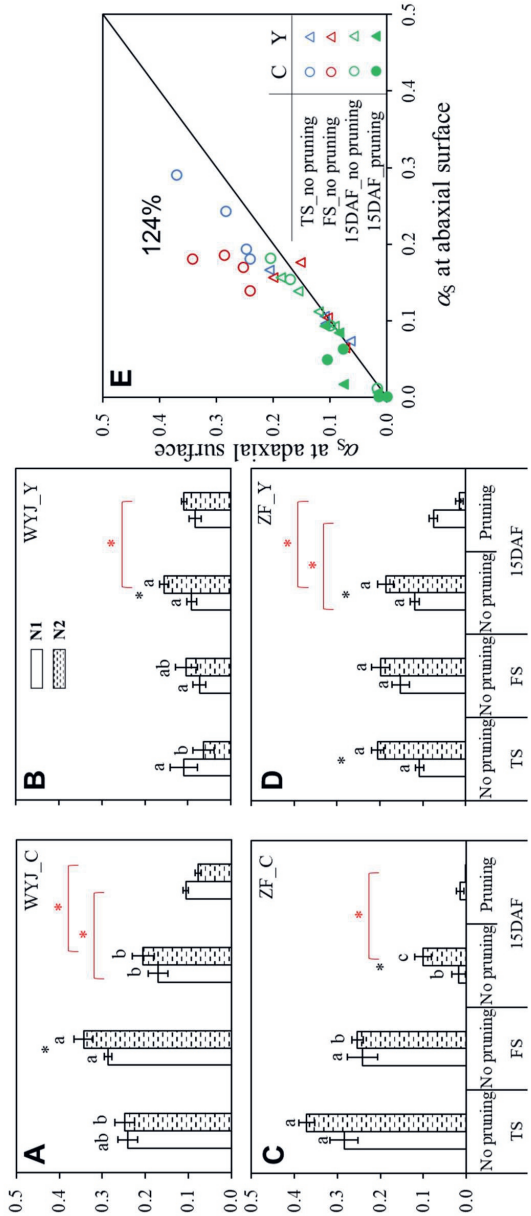

Fig. 5.3 Effects of various growth stages and nitrogen levels on parameter α_S, the proportion of glycolate carbon exported from the photorespiratory pathway in the form of serine (the 2022 experiment). **A-D**, α_S (based on measurements on the adaxial leaf surface) for rice control (C) genotypes and their yellower-leaf (Y) variant genotypes of intact or panicle-pruned plants at tillering (TS), flowering (FS), and 15d after flowering (15DAF) stages under low-nitrogen (N1, white bars) and high-nitrogen (N2, dashed bars) levels. The value of each bar representing mean ± standard error of four replicates was estimated by fitting curves to CO_2 exchange data (see Fig S5.2). For intact plants (no pruning), different letters indicate statistical significance at the $P < 0.05$ level between three stages within each genotype-nitrogen combination, and the asterisks (*) in black represent significant differences ($P < 0.05$) between N1 and N2 levels within each genotype and stage. The asterisks (*) in red represent significant differences ($P < 0.05$) for a given genotype-nitrogen combination between pruned and un-pruned plants at 15DAF stage. WYJ and ZF are the abbreviations of two genetic backgrounds: cv. Wuyunjing 3 and cv. Zhefu 802. **E**, Comparison of the values of α_S measured at adaxial surface vs those measured at abaxial surface. The percentage is the average of adaxial relative to abaxial parameters and the diagonal line is the 1:1 line. Data represented by different colours and symbols are from C genotypes (circles) and Y-variant genotypes (triangles) of intact (open symbols) and panicle-pruned (filled symbols) plants at TS (blue), FS (red), and 15DAF (green) stage. Each point represents the mean of three or four replicates.

5.3.5 Correlations between TPU parameters and leaf nitrogen content

In general, T_p and α_S were positively correlated with SLN across all N levels and growth stages, but correlations were genotype-dependent (Fig. 5.4). Given the smaller α_S values in Y genotypes (Figs. 5.1 and 5.3), slopes were smaller and correlations were poorer, particularly when measuring the abaxial leaf side, compared with the C genotypes.

The threshold C_i values (at which TPU became limiting) estimated by the two methods were highly consistent (Fig. S5.4). The threshold C_i increased with advancing growth stage. It was negatively correlated with T_p ($R^2 = 0.51$, $P < 0.001$; Fig. 5.5A) and with SLN ($R^2 = 0.42$, $P < 0.001$; Fig. 5.5B).

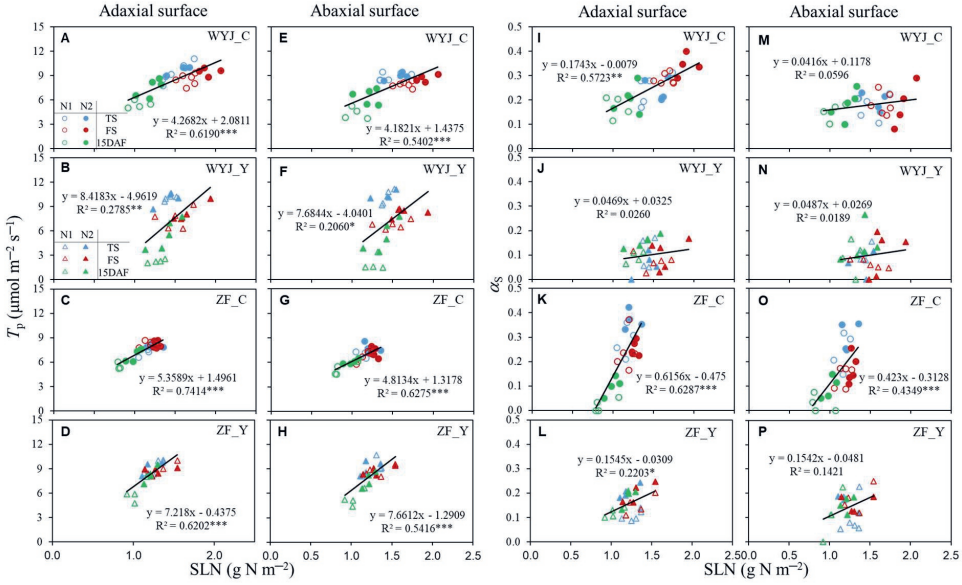

Fig. 5.4 Relationship between photosynthetic parameters and leaf nitrogen content (based on measurements on the un-pruned plants in the 2022 experiment). **A-H**, Relationship between triose phosphate utilisation rate (T_p) and specific nitrogen content (SLN). **I-P**, Relationship between the proportion of glycolate carbon exported from photorespiratory pathway in the form of serine (α_S) and SLN. Data represented by different colours and symbols are from tillering (TS, blue), flowering (FS, red), and 15 d after flowering (15DAF, green) stage under low-nitrogen (N1, open symbols) and high-nitrogen (N2, filled symbols) levels, with circles for rice control (C) genotypes and triangles for their yellower-leaf (Y) variant genotypes. Linear regressions were fitted for each genotype with four or five replicates across two nitrogen levels and three stages. The significance of each correlation is shown by asterisks: * $P < 0.05$, ** $P < 0.01$, *** $P < 0.001$. WYJ and ZF are the abbreviations of two genetic backgrounds: cv. Wuyunjing 3 and cv. Zhefu 802.

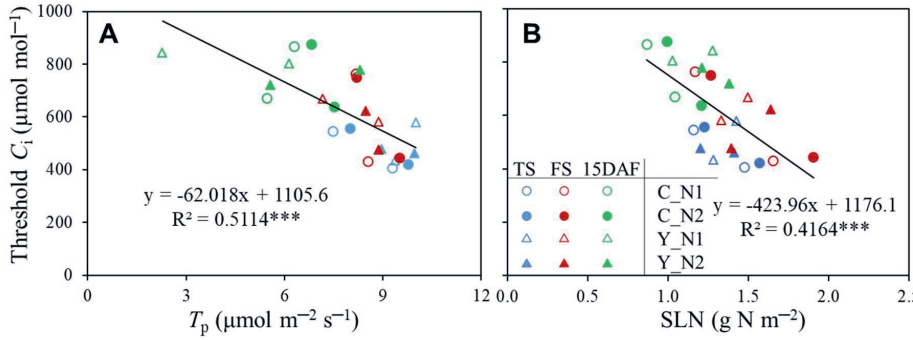

Fig. 5.5 The threshold C_i values in relation to leaf physiological parameters. **A**, Relationship between threshold C_i and the rate of triose phosphate utilisation (T_p) (data based on measurements on the adaxial surface of leaves in the 2022 experiment); **B**, Relationship between threshold C_i and specific leaf nitrogen (SLN). The threshold C_i represents the transition point where photosynthesis-limiting process was changed from electron transport into TPU, derived from CO_2 response curves (see Fig. S5.2). Data represented by different colours and symbols are from tillering (TS, blue), flowering (FS, red), and 15 d after flowering (15DAF, green) stage under low-nitrogen (N1, open symbols) and high-nitrogen (N2, filled symbols) levels, with circles for rice control (C) genotypes and triangles for their yellower-leaf (Y) variant genotypes. Linear regressions were fitted for overall data with the significance of each correlation shown by asterisks: *** $P < 0.001$.

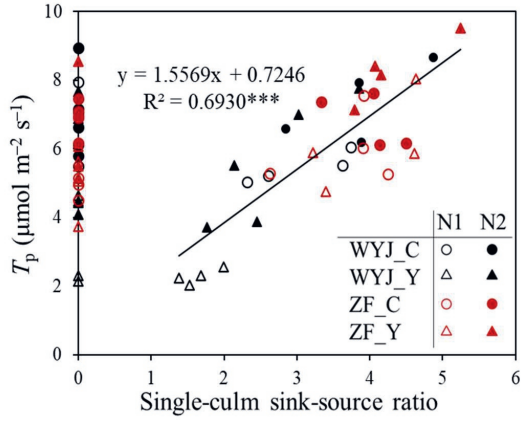

Fig. 5.6 Relationship between the rate of triose phosphate utilisation (T_p, based on measurements on the adaxial leaf surface) and single-culm sink-source ratio. Here, following Fabre et al. (2020), the ratio of flag leaf area (source) to the fertile spikelet number of the panicle (sink) on the culm was used as an indicator of the single-culm sink-source ratio (also see the text). Data are for rice control (C) genotypes (circles) and yellower-leaf (Y) variant genotypes (triangles) from grain-filling stage under low-nitrogen (N1, open symbols) and high-nitrogen (N2, filled symbols) levels in the 2022 experiment, with cv. Wuyunjing 3 (WYJ) in black and cv. Zhefu 802 (ZF) in red. For those plants with panicle pruning, we define their sink-source ratio to be zero, so all their data points fall on the Y axis. Linear regression was

fitted for data (representing no pruning) with the significance of the correlation shown by asterisks: *** $P < 0.001$.

5.3.6 TPU-limited photosynthesis in relation to whole-plant sink limitation

The variation in A_{1500} of each genotype-nitrogen combination, either across stages or across pruning levels, was positively correlated with T_p for adaxial (Fig. S5.5a) or abaxial surfaces (Fig. S5.5b) of leaves. A positive linear correlation of T_p with single-culm sink-source ratio (R^2 = 0.69; Fig. 5.6) or whole-plant sink-source ratio (R^2 = 0.60; Fig. S5.6) was observed at the grain-filling stage. Note that data points presented on the line $x = 0$ in these figures for panicle-pruned plants (thus, panicle sink was zero) were in a similar range of T_p (ca. 2–9 μmol m^{-2} s^{-1}) of those plants without pruning. This suggests that, overall, there was little observable effect of panicle pruning on T_p. We then compared the correlation between T_p and SLN for non-pruned and panicle-pruned plants separately in Figs. 5.7A-D. The pruned plants still had close T_p correlations with SLN, but the relationship deviated from (e.g. the slope became smaller in most cases) that of the non-pruned plants.

Sink limitation caused by panicle pruning also exerted significant impacts on whole-plant traits, such as increased leaf area, leaf and stem dry weight, and total leaf-nitrogen (Table 5.1). As a result of increased N accumulation in the flag leaf (Figs. 5.7E-H), panicle pruning lowered leaf photosynthetic nitrogen-use efficiency (PNUE) for each combination of genotype and N level (Figs. 5.7I–M; $P < 0.001$, Table S5.3).

5.4 Discussion

In response to sink-source (im)balance, plants can adjust physiological processes at different scales, and these scales can be inter-connected involving dynamic feedback. We hypothesised that the sub-foliar sink-source (im)balance involving triose phosphate utilisation (TPU) is regulated by whole-plant sink-source relationships. We used yellow-leaf (Y) modification and adaxial vs abaxial illumination, and 21% vs 2% O_2 gas mixture to alter the leaf-scale source activity. Panicle pruning was used to alter whole-plant sink/source ratios. The factorial design involving these two scales enabled linking them. By observing plants under different N supply conditions and at three growth stages, we introduced additional variation of source and sink capacity, and enabled the establishment of parameter relationships, notably including TPU-limited photosynthesis and photorespiration-associated N assimilation.

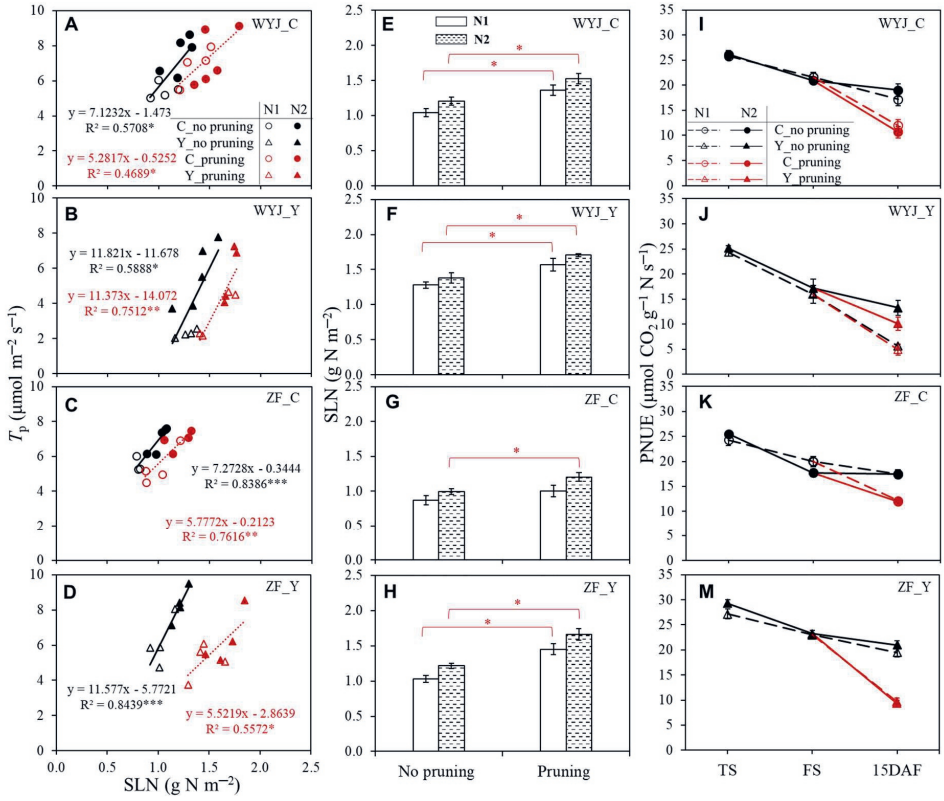

Fig. 5.7 The effects of panicle pruning on leaf photosynthetic parameters (based on measurements on the adaxial leaf surface in the 2022 experiment). **A-D**, Relationship between the rate of triose phosphate utilisation (T_p) and specific leaf nitrogen (SLN) for the intact and panicle-pruned plants; **E-H**, Effect of panicle pruning on SLN; **I-M**, Leaf photosynthetic nitrogen-use efficiency (PNUE) at tillering (TS), flowering (FS), and 15 d after flowering (15DAF) stage (see Table S5.2 for the definition of PNUE). Linear regressions in A-D were fitted for each genotype with four or five replicates under two-nitrogen levels; the significance of each correlation is shown by asterisks: * $P < 0.05$, ** $P < 0.01$, *** $P < 0.001$. Data in E-M represent means ± standard errors of four replicates; the asterisks (*) represent significant differences ($P < 0.05$) within each genotype-nitrogen combination between un-pruned and pruned plants. The data in A-H are from 15DAF stage, and the data in A-D and I-M represent the values for rice control (C) genotypes (circles) and their yellower-leaf (Y) variant genotypes (triangles) of the intact (black) and panicle-pruned (red) plants under low-nitrogen (N1, open symbols) and high-nitrogen (N2, filled symbols) levels. WYJ and ZF are the abbreviations of two genetic backgrounds: cv. Wuyunjing 3 and cv. Zhefu 802.

Table 5.1 Values (mean ± standard error of the mean among four replicates) of rice sink and source organs for single culm and whole plant in the control (C) genotypes and the yellower-leaf variant (Y) genotypes at 15 d after flowering stage in the 2022 experiment.

			Single culm		Whole plant				
N level	Background	Genotype	Spikelets per culm (no.)	Flag leaf area (cm^2)	Total spikelet (no.)	Leaf area (cm^2 pot^{-1})	Leaf dry weight (g)	Stems dry weight (g)	Total leaf nitrogen (g N pot^{-1})
No pruning									
N1	WYJ	C	47 ± 5	15.5 ± 0.7	543 ± 49	1259.5 ± 27.8	4.8 ± 0.1	17.7 ± 0.8	0.098 ± 0.003
	WYJ	Y	30 ± 3	18.1 ± 0.7	336 ± 24	1361.5 ± 73.0	4.3 ± 0.3	8.2 ± 0.5	0.130 ± 0.007
	ZF	C	101 ± 9	28.7 ± 4.6	811 ± 21	1400.8 ± 59.0	7.7 ± 0.5	34.6 ± 0.9	0.082 ± 0.006
	ZF	Y	114 ± 7	29.7 ± 4.1	893 ± 55	2158.3 ± 97.5	9.4 ± 0.6	19.4 ± 1.2	0.168 ± 0.008
N2	WYJ	C	70 ± 14	17.8 ± 2.8	827 ± 55	1597.7 ± 30.7	6.2 ± 0.1	23.5 ± 1.5	0.129 ± 0.004
	WYJ	Y	46 ± 6	19.7 ± 1.4	797 ± 86	1665.5 ± 86.3	5.9 ± 0.3	12.2 ± 1.0	0.186 ± 0.006
	ZF	C	105 ± 5	26.7 ± 2.7	1324 ± 23	1898.0 ± 50.1	9.0 ± 0.6	34.9 ± 1.1	0.100 ± 0.009
	ZF	Y	132 ± 12	31.2 ± 4.1	1421 ± 54	2702.5 ± 50.8	11.6 ± 0.6	21.8 ± 1.9	0.232 ± 0.020
Pruning									
N1	WYJ	C	-	13.3 ± 2.1	-	1304.6 ± 43.4	5.6 ± 0.1	24.8 ± 1.0	0.106 ± 0.005
	WYJ	Y	-	15.7 ± 1.2	-	1569.5 ± 33.7	5.8 ± 0.2	15.5 ± 1.1	0.179 ± 0.005
	ZF	C	-	29.1 ± 2.4	-	1684.0 ± 76.4	10.5 ± 0.6	43.9 ± 2.6	0.101 ± 0.007
	ZF	Y	-	28.2 ± 3.4	-	2324.6 ± 97.0	10.5 ± 0.5	25.2 ± 1.5	0.186 ± 0.009
N2	WYJ	C	-	19.3 ± 2.2	-	1633.3 ± 31.5	7.1 ± 0.1	28.1 ± 0.3	0.150 ± 0.002
	WYJ	Y	-	17.3 ± 1.3	-	1736.9 ± 86.3	6.6 ± 0.3	16.5 ± 1.3	0.247 ± 0.009
	ZF	C	-	30.9 ± 2.7	-	2240.9 ± 70.5	14.7 ± 0.3	58.6 ± 0.7	0.145 ± 0.004
	ZF	Y	-	35.3 ± 2.5	-	3174.8 ± 88.1	14.3 ± 0.3	27.2 ± 0.8	0.288 ± 0.010
Analysis of variance									
Genotype			46.9***	33.0***	56.9***	214.2***	235.7***	392.6***	167.1***
N level			6.9*	3.6	135.5***	167.8***	114.4***	43.9***	171.4***
Panicle pruning			-	0.1	-	34.4***	105.8***	177.0***	72.8***
Genotype × N level			0.5	0.7	2.1	8.9***	5.2**	3.6*	8.5***
Genotype × panicle pruning			-	0.7	-	3.58*	14.5***	17.7***	4.3**
N level × panicle pruning			-	1.6	-	0.6	6.2*	2.8	7.4**
Genotype × N level × panicle pruning			-	0.2	-	1.8	4.4**	10.4***	0.6

In the analysis of variance, the significance is shown by asterisks: * $P < 0.05$, ** $P < 0.01$, *** $P < 0.001$, according to the LSD test. Note, we use "genotype" rather than "Y modification" as a fixed factor mainly because Y modification produces different effects on leaf photosynthetic physiology between WYJ (cv. Wuyunjing 3) and ZF (cv. Zhefu 802) backgrounds (see Results).

5.4.1 Adaxial vs abaxial measurements on leaf-colour genotypes as a means to alter leaf source activity

In the 2019 experiment using rice genotypes of contrasting leaf colour, a TPU limitation on leaf photosynthesis was observed (Fig. 5.1). The yellow-leaf variants (Y) differed from their control (C) genotypes in photosynthetic capacity (i.e., A_{2000}) and underlying parameters (J_{max}, V_{cmax}, and T_p), and the difference was mostly expressed when comparing response curves measured under adaxial vs abaxial illumination (Fig. 5.1). Zhou et al. (2023) demonstrated differences in leaf photosynthetic capacity between C and Y genotypes were associated with intra-leaf photosynthetic N reallocation of the surplus N resources liberated by decreased investment in chlorophyll. However, modifying leaf colour changed not only intra-leaf N partitioning but also leaf morphology, such as increased SLA (i.e., thinner leaves) in Y-genotypes (Table S5.2).

This genotypic difference in leaf thickness probably contributed to our result that when light illuminated the abaxial surface, the decrease in leaf photosynthetic capacity parameters was small in Y genotypes but greater in C genotypes (Fig. 5.1). This suggests that our C genotypes, like plants in previous reports (e.g., Soares et al., 2008), had an adaptive advantage to the adaxial illumination, which is the predominant condition occurring in the field. As the carbon sinks of the leaf and the whole plant were unchanged, altered leaf photosynthetic capacity via adaxial vs abaxial illumination during gas exchange measurement will alter the sink-source ratio, and this was particularly the case in the C genotypes.

5.4.2 Effects of altered sink-source ratios on leaf TPU limitation

The occurrence of the TPU limitation requires a high photosynthetic rate (Yang et al., 2016). We chose a saturating light intensity (1500 μmol m^{-2} s^{-1}) and CO_2 levels up to 1800 μmol mol^{-1} for measuring A-C_i curves in the 2022 experiment. In our study, A_{1500} was highly correlated with T_p in all cases (Fig. S5.5), reflecting a parallel change between them. Y modification reduced leaf T_p and A_{1500} in WYJ background but increased them in ZF background (Figs. 5.2A-D; Tables S5.1 and S5.2); adaxial illumination gave higher T_p than abaxial, especially for C genotypes (Fig. 5.2E and Table S5.1). Strong correlations between T_p and SLN in each genotype (Fig. 5.4) suggested that N always exerted a positive effect on T_p. We also found that the higher the leaf N content was (resulting in higher A_{1500}), the lower was the threshold C_i where leaf photosynthesis became TPU-limited (Fig. S5.2), as shown by the negative relationship between the threshold C_i and T_p or SLN ($P < 0.001$; Fig. 5.5). This relationship was built from data

across three growth stages, reflecting dynamic changes in the TPU limitation during rice development.

During the vegetative phase, there is no sink demand from panicles or grains, and all assimilates are used for vegetative organ growth (i.e., absence of a dominant sink like the panicle). In this phase, growing leaves rich in N resources serve as both source and sink organs. The high photosynthetic potential of young plants feeds a plastic (partly facultative) demand exerted by organ development, probably explaining why TPU limitation occurred at a lower C_i level (ca. 400 μmol mol^{-1}; Fig. 5.5). After flowering, carbon assimilates are exclusively used to support grain growth, and N resources are mobilised from vegetative organs, particularly from leaves (Sinclair & de Wit, 1975). The resulting decrease in A_{1500} and T_p (Fig. 5.2; Tables S5.1 and S5.2), coupled with increased sink demand, alleviated the extent of TPU limitation.

Our study provides insights on how altered sink-source relationships influence T_p and thus leaf source activity. The estimated T_p and the C_i threshold for the onset of TPU limitation were associated with leaf N content across growth stages. Thus, leaf N content not only determines leaf photosynthetic capacity (Nakano et al., 1995), but also modulates TPU limitation in response to sink-source imbalance.

5.4.3 Nitrogen assimilation increases photosynthesis under potential TPU limitation

Assimilating NO_3^- via exporting glycolate carbon from the photorespiratory pathway in the form of amino acids can contribute to photosynthetic carbon uptake (Busch et al., 2018; Busch, 2020; Fu et al., 2022). Our A-C_i curves, indicating A was higher under 21% O_2 than under 2% O_2 conditions, confirmed this - although this advantage from photorespiration diminished with advancing growth stages (Fig. S5.2). The increase in A largely depends on the extent of glycolate carbon exported from the photorespiratory pathway (Bauwe et al., 2010; Busch et al. 2018; Yin et al. 2021; also see Figs. S5.2A,B). Fu et al. (2022) demonstrated that the carbon flow out of the pathway was primarily in the form of serine, with a proportion of 23-41% in tobacco plants. Our estimates of parameter α_S from model analysis (up to 0.37; Table S5.1) are in line with the measured values of Fu et al. (2022) as well as with the modelling results of Busch et al. (2018). Based on modelled α_S, we further assessed the effect of various experimental factors on photorespiration-associated N assimilation. We found that similar to the effect on T_p, leaf N content is also critical to α_S, as evidenced by correlations between α_S

and SLN (Figs. 5.4I-P). However, this positive effect of N level disappeared under Y modification (Table S5.3), since both Y genotypes had lower α_S than their corresponding C genotypes (Figs. 5.1 and 5.3; Table S5.1). In conjunction with this, there was a negative relationship between α_S and SLA (Fig. S5.3), suggesting that the thinner leaves associated with Y modification may have limited NO_3^- assimilation. This limiting effect was enhanced by illuminating the abaxial surface of leaves during measurements (Fig. 5.3E and Table S5.3).

In our experiment, urea was used as the N source in fertilising plants. Busch et al. (2018) found that α_S was higher in sunflower plants fertilised with NO_3^--N than those with NH_4^+-N. Whether this is also the case when applied to our rice plants of different leaf-colours remains to be investigated. Previous studies (Reich et al., 2006; Bloom et al., 2012, 2014) reported that elevated growth CO_2 (resulting in increased source) inhibited the NO_3^- assimilation in C_3 plants. Here, we found a similar result with a significant drop in α_S for the plants after panicle pruning (resulting in decreased sink) (Fig. 5.3). However, the underlying mechanisms might differ. Elevated growth CO_2 not only decreased photorespiration but also diluted leaf N concentration *via* increased biomass (Yin, 2013; Igarashi et al., 2021). In contrast, panicle pruning resulted in an increased N content in leaves (Table 5.1; Figs. 5.7E-H). Nevertheless, despite higher leaf N, a lower α_S (thus, probably less N assimilation) was observed in leaves of panicle-pruned plants, suggesting a dominating role of whole-plant sink-source ratio in the control of leaf N metabolism.

5.4.4 Feedback inhibition of whole-plant sink limitation on leaf photosynthesis

It has long been observed that the plant sink-source ratio can affect leaf photosynthesis (Tanaka & Fujita, 1974; Crafts-Brandner & Egli, 1987; Arp, 1991; Li et al., 2015; Aslani et al., 2020). In line with this, studies indicated that a larger sink capacity can increase the effect of elevated atmospheric CO_2 on photosynthesis and yield (Erice et al., 2011; Hasegawa et al., 2013; Rossi et al., 2015; Kikuchi et al., 2017; Dingkuhn et al. 2020). Our finding of a positive correlation between T_p and the sink-source ratio for single culm (Fig. 5.6) or for the whole plant (Fig. S5.6) confirmed the role of sink size in modulating source activity of leaves. The reduced T_p under sink limitation is probably associated with the accumulation of sucrose in leaf photosynthetic tissues (Fabre et al. 2019, 2020). This may give a signal regulating the activity of sucrose-phosphate synthase (SPS) through transduction of SnRK1 protein kinases (Halford & Hey, 2009), and the SPS feedback inhibition on sucrose synthesis can decrease export of triose

phosphates from the chloroplast (McClain & Sharkey, 2019). Our results also showed that panicle pruning dramatically increased the dry matter accumulation in leaves and stems (Table 5.1).

Given these considerations, one would expect that for the 15DAF stage, panicle-pruned plants would have lower T_p compared with intact plants where the TPU limitation was alleviated. Surprisingly, distinct from previous findings (Fabre et al., 2019; Nomura et al., 2022), T_p was little affected under this apparently sink-limited state (Figs. 5.2 and 5.6). In the study of Fabre et al. (2019), elevated CO_2 (increased source) coupled with pruning treatment (decreased sink) imposed a dual effect on T_p, which might contribute to more significant sink limitation and feedback effect in their study than in our study. However, the mechanism behind this difference could also be attributed to larger amount of N accumulated in the leaves of our panicle-pruned plants (Figs. 5.7E-H). After removal of all panicles, no N was required to be remobilised from leaves to support grain growth and more N remained in leaves. Leaf N is the most important resource for the photosynthetic machinery (Nakano et al., 1995), as shown by our close relationship between T_p and SLN, even in pruned plants (Figs. 5.7A-D). Thus, we posit that the feedback inhibition of sink limitation on T_p still occurred in our panicle-pruned plants, but the inhibitory effects from sink limitation were offset by the increased SLN as a consequence of the smaller N remobilisation from leaves, thereby resulting in no observable impact of pruning on T_p in leaves. The increased SLN did not result in higher N assimilation as α_S was lower in panicle-pruned plants (Fig. 5.3; Table S5.1); as a result, these plants might not benefit from amino-acid export for higher CO_2-uptake rates, but instead, had similar or lower A_{1500} compared with the control plants (Table S5.2). Because of the increased SLN (Figs. 5.7E-H) accompanied with no or little increase in A_{1500}, leaf PNUE decreased in the panicle-pruned plants (Figs. 5.7I-M). Taken these together, our results suggest that T_p and leaf photosynthesis during grain filling are controlled by the whole-plant sink demand and N budgets.

5.5 Concluding remarks

We have shown that the differences in photosynthetic rates between adaxially and abaxially illuminated leaves and the extent of such differences depends on leaf colours of the genotypes. Based on this finding, we further assessed how TPU limitation of photosynthesis, involving photorespiration-associated N assimilation, can be affected by altered sink-source ratios at different scales. We found:

1) Higher leaf N (observed at early growth stages or high N inputs) caused TPU limitation at relatively low intercellular CO_2 concentration.
2) The proportion of photorespiratory glycolate-carbon exported as serine (α_S) was positively correlated with leaf N content, suggesting that photorespiration was involved in leaf N assimilation more in high-N than low-N leaves. However, values of α_S were smaller in yellow-leaf genotypes, under illumination of abaxial leaf sides, and when panicles were removed.
3) Absence of observable effect of panicle pruning on the rate of TPU (T_p) suggested that the feedback inhibition of photosynthesis by whole-plant sink limitation was offset by the positive effect of increased leaf N content, caused by lesser N remobilisation.

Thus, our results revealed the crucial role of leaf N in affecting photosynthetic parameters T_p and α_S, and thus TPU limitation of photosynthesis. Likewise, N resources modulate the link between leaf-level TPU limitation and whole-plant sink limitation during rice grain filling. The latter link could be masked by the whole-plant N budget, providing a contributing factor (additional to what has been stated in Introduction) about why the sink feedback on, and TPU limitation to, leaf photosynthesis cannot always be observed experimentally. This also adds the complication of disentangling the interaction and causality between observed A_{1500} and T_p in relation to leaf N content. Our results have important implications for modelling crop production in response to a future high-CO_2 environment, where a delicate balance between source and sink in plants becomes increasingly altered, leaf photosynthesis is expected to be increasingly limited by TPU, and plant N resources tend to be diluted by the greater biomass (Dingkuhn et al., 2020). This warrants more research for better understanding of the N regulatory mechanism in this context so as to effectively screen adaptive traits in rice genotypes for improved crop productivity and nutritional value under futural climatic conditions.

Acknowledgements

Z.Z. thanks the China Scholar Council (CSC) for funding his PhD fellowship. We thank Profs Jianchang Yang and Junfei Gu (Yangzhou University), Dr. Changquan Zhang (Yangzhou University), and Prof. Fangmin Cheng (Zhejiang University) for providing seeds used in this study.

References

Abadie C, Boex-Fontvieille ERA, Carroll AJ, Tcherkez G. 2016. In vivo stoichiometry of photorespiratory metabolism. *Nature Plants* 2, 1−4.

Arp WJ. 1991. Effects of source-sink relations on photosynthetic acclimation to elevated CO_2. *Plant, Cell & Environment* 14, 869−875.

Aslani L, Gholami M, Mobli M, Sabzalian MR. 2020. The influence of altered sink-source balance on the plant growth and yield of greenhouse tomato. *Physiology and Molecular Biology of Plants* 26, 2109−2123.

Bauwe H, Hagemann M, Fernie AR. 2010. Photorespiration: players, partners and origin. *Trends in Plant Science* 15, 330−336.

Bloom AJ, Asensio JSR, Randall L, Rachmilevitch S, Cousins AB, Carlisle EA. 2012. CO_2 enrichment inhibits shoot nitrate assimilation in C_3 but not C_4 plants and slows growth under nitrate in C_3 plants. *Ecology* 93, 355−367.

Bloom AJ, Burger M, Kimball BA, Pinter PJ. 2014. Nitrate assimilation is inhibited by elevated CO_2 in field-grown wheat. *Nature Climate Change* 4, 477−480.

Burnett AC, Rogers A, Rees M, Osborne CP. 2016. Carbon source–sink limitations differ between two species with contrasting growth strategies. *Plant, Cell & Environment* 39, 2460−2472.

Busch FA. 2020. Photorespiration in the context of Rubisco biochemistry, CO_2 diffusion and metabolism. *The Plant Journal* 101, 919−939.

Busch FA, Sage RF. 2017. The sensitivity of photosynthesis to O_2 and CO_2 concentration identifies strong Rubisco control above the thermal optimum. *New Phytologist* 213, 1036−1051.

Busch FA, Sage RF, Farquhar GD. 2018. Plants increase CO_2 uptake by assimilating nitrogen via the photorespiratory pathway. *Nature Plants* 4, 46−54.

Cousins AB, Ghannoum O, Von Caemmerer S, Badger MR. 2010. Simultaneous determination of Rubisco carboxylase and oxygenase kinetic parameters in Triticum aestivum and Zea mays using membrane inlet mass spectrometry. *Plant, Cell & Environment* 33, 444−452.

Crafts-Brandner SJ, Egli DB. 1987. Sink removal and leaf senescence in soybean: cultivar effects. *Plant Physiology* 85, 662−666.

Dingkuhn M, Luquet D, Fabre D, Muller B, Yin X, Paul MJ. 2020. The case for improving crop carbon sink strength or plasticity for a CO_2-rich future. *Current Opinion in Plant Biology* 56, 259−272.

Ellsworth DS, Crous KY, Lambers H, Cooke J. 2015. Phosphorus recycling in photorespiration maintains high photosynthetic capacity in woody species. *Plant, Cell & Environment* 38, 1142−1156.

Erice G, Sanz-Sáez A, Aranjuelo I, Irigoyen JJ, Aguirreolea J, Avice JC, Sánchez-Díaz M. 2011. Photosynthesis, N_2 fixation and taproot reserves during the cutting regrowth cycle of alfalfa under elevated CO_2 and temperature. *Journal of Plant Physiology* 168, 2007−2014.

Fabre D, Dingkuhn M, Yin X, Clément-Vidal A, Roques S, Soutiras A, Luquet D. 2020. Genotypic variation in source and sink traits affects the response of photosynthesis and

growth to elevated atmospheric CO_2. *Plant, Cell & Environment* 43, 579−593.

Fabre D, Yin X, Dingkuhn M, Clément-Vidal A, Roques S, Rouan L, Soutiras A, Luquet D. 2019. Is triose phosphate utilization involved in the feedback inhibition of photosynthesis in rice under conditions of sink limitation? *Journal of Experimental Botany* 70, 5773−5785.

Farquhar GD, von Caemmerer S, Berry JA. 1980. A biochemical model of photosynthetic CO_2 assimilation in leaves of C_3 species. *Planta* 149, 78−90.

Fu X, Gregory LM, Weise SE, Walker BJ. 2022. Integrated flux and pool size analysis in plant central metabolism reveals unique roles of glycine and serine during photorespiration. *Nature Plants* 9, 169−178.

Genty B, Briantais JM, Baker NR. 1989. The relationship between the quantum yield of photosynthetic electron transport and quenching of chlorophyll fluorescence. *Biochimica et Biophysica Acta - General Subjects* 990, 87−92.

Halford NG, Hey SJ. 2009. Snf1-related protein kinases (SnRKs) act within an intricate network that links metabolic and stress signalling in plants. *Biochemical Journal* 419, 247−259.

Harley PC, Loreto F, Marco G Di, Sharkey TD. 1992. Theoretical considerations when estimating the mesophyll conductance to CO_2 flux by analysis of the response of photosynthesis to CO_2. *Plant Physiology* 98, 1429−1436.

Harley PC, Sharkey TD. 1991. An improved model of C_3 photosynthesis at high CO_2: Reversed O_2 sensitivity explained by lack of glycerate reentry into the chloroplast. *Photosynthesis Research* 27, 169−178.

Hasegawa T, Sakai H, Tokida T, Nakamura H, Zhu C, Usui Y, Yoshimoto M, Fukuoka M, Wakatsuki H, Katayanagi N et al. 2013. Rice cultivar responses to elevated CO_2 at two free-air CO_2 enrichment (FACE) sites in Japan. *Functional Plant Biology* 40, 148−159.

He A, Wang W, Jiang G, Sun H, Jiang M, Man J, Cui K, Huang J, Peng S, Nie L. 2019. Source-sink regulation and its effects on the regeneration ability of ratoon rice. *Field Crops Research* 236, 155−164.

Igarashi M, Yi Y, Yano K. 2021. Revisiting Why Plants Become N Deficient Under Elevated CO_2: Importance to Meet N Demand Regardless of the Fed-Form. *Frontiers in Plant Science* 12, 726186.

Kikuchi S, Bheemanahalli R, Jagadish KSV, Kumagai E, Masuya Y, Kuroda E, Raghavan C, Dingkuhn M, Abe A, Shimono H. 2017. Genome-wide association mapping for phenotypic plasticity in rice. *Plant, Cell & Environment* 40, 1565−1575.

Kumarathunge DP, Medlyn BE, Drake JE, Rogers A, Tjoelker MG. 2019. No evidence for triose phosphate limitation of light-saturated leaf photosynthesis under current atmospheric CO_2 concentration. *Plant, Cell & Environment* 42, 3241−3252.

Li T, Heuvelink E, Marcelis LFM. 2015. Quantifying the source-sink balance and carbohydrate content in three tomato cultivars. *Frontiers in Plant Science* 6, 416.

Li G, Pan J, Cui K, Yuan M, Hu Q, Wang W, Mohapatra PK, Nie L, Huang J, Peng S. 2017. Limitation of unloading in the developing grains is a possible cause responsible for low stem non-structural carbohydrate translocation and poor grain yield formation in rice through verification of recombinant inbred lines. *Frontiers in Plant Science* 8, 1369.

Lombardozzi DL, Smith NG, Cheng SJ, Dukes JS, Sharkey TD, Rogers A, Bonan GB. 2018. Triose phosphate limitation in photosynthesis models reduces leaf photosynthesis and global terrestrial carbon storage. *Environmental Research Letters* 13, 074025.

Loriaux SD, Avenson TJ, Welles JM, Mcdermitt DK, Eckles RD, Riensche B, Genty B. 2013. Closing in on maximum yield of chlorophyll fluorescence using a single multiphase flash of sub-saturating intensity. *Plant, Cell & Environment* 36, 1755−1770.

Mathan J, Singh A, Jathar V, Ranjan A. 2021. High photosynthesis rate in two wild rice species is driven by leaf anatomy mediating high Rubisco activity and electron transport rate. *Journal of Experimental Botany* 72, 7119-7135.

McClain AM, Cruz JA, Kramer DM, Sharkey TD. 2023. The time course of acclimation to the stress of triose phosphate use limitation. *Plant, Cell & Environment* 46, 64−75.

McClain AM, Sharkey TD. 2019. Triose phosphate utilization and beyond: From photosynthesis to end product synthesis. *Journal of Experimental Botany* 70, 1755−1766.

Nakano H, Makino A, Mae T. 1995. Effects of panicle removal on the photosynthetic characteristics of the flag leaf of rice plants during the ripening stage. *Plant and Cell Physiology* 36, 653−659.

Nomura K, Saito M, Ito M, Yamane S, Iwao T, Tada I, Yamazaki T, Ono S, Yasutake D, Kitano M. 2022. Diurnal decline in the photosynthetic capacity of uppermost leaves in an eggplant canopy grown in a horticultural greenhouse. *Photosynthetica* 60, 457−464.

Reich PB, Hobbie SE, Lee T, Ellsworth DS, West JB, Tilman D, Knops JMH, Naeem S, Trost J. 2006. Nitrogen limitation constrains sustainability of ecosystem response to CO_2. *Nature* 440, 922−925.

Rossi M, Bermudez L, Carrari F. 2015. Crop yield: Challenges from a metabolic perspective. *Current Opinion in Plant Biology* 25, 79−89.

Sharkey TD. 1985. Photosynthesis in intact leaves of C_3 plants: Physics, physiology and rate limitations. *The Botanical Review* 51, 53−105.

Sharkey TD. 2019. Is triose phosphate utilization important for understanding photosynthesis? *Journal of Experimental Botany* 70, 5521−5525.

Sinclair TR, De Wit CT. 1975. Photosynthate and nitrogen requirements for seed production by various crops. *Science* 189, 565−567.

Soares AS, Driscoll SP, Olmos E, Harbinson J, Arrabaça MC, Foyer CH. 2008. Adaxial/abaxial specification in the regulation of photosynthesis and stomatal opening with respect to light orientation and growth with CO_2 enrichment in the C_4 species Paspalum dilatatum. *New Phytologist* 177, 186−198.

Tanaka A, Fujita K. 1974. Nutrio-physiological studies on the tomato plant IV. Source-sink relationship and structure of the source-sink unit. *Soil Science and Plant Nutrition* 20, 305−315.

von Caemmerer S. 2000. *Biochemical models of leaf photosynthesis*. CSIRO publishing.

von Caemmerer S, Farquhar GD. 1981. Some relationships between the biochemistry of photosynthesis and the gas exchange of leaves. *Planta* 153, 376−387.

White AC, Rogers A, Rees M, Osborne CP. 2016. How can we make plants grow faster? A source-sink perspective on growth rate. *Journal of Experimental Botany* 67, 31−45.

Yang JT, Preiser AL, Li Z, Weise SE, Sharkey TD. 2016. Triose phosphate use limitation of photosynthesis: short-term and long-term effects. *Planta* 243, 687−698.

Yin X. 2013. Improving ecophysiological simulation models to predict the impact of elevated atmospheric CO_2 concentration on crop productivity. *Annals of Botany* 112, 465−475.

Yin X, Busch FA, Struik PC, Sharkey TD. 2021. Evolution of a biochemical model of steady-state photosynthesis. *Plant, Cell & Environment* 44, 2811−2837.

Yin X, Gu J, Dingkuhn M, Struik PC. 2022. A model-guided holistic review of exploiting natural variation of photosynthesis traits in crop improvement. *Journal of Experimental Botany* 73, 3173−3188.

Yin X, van der Putten PEL, Belay D, Struik PC. 2020. Using photorespiratory oxygen response to analyse leaf mesophyll resistance. *Photosynthesis Research* 144, 85−99.

Yin X, Struik PC, Romero P, Harbinson J, Evers JB, van der Putten PEL, Vos J. 2009. Using combined measurements of gas exchange and chlorophyll fluorescence to estimate parameters of a biochemical C_3 photosynthesis model: A critical appraisal and a new integrated approach applied to leaves in a wheat (Triticum aestivum) canopy. *Plant, Cell & Environment* 32, 448−464.

Zhou Z, Struik PC, Gu J, van der Putten PEL, Wang Z, Yin X, Yang J. 2023. Enhancing leaf photosynthesis from altered chlorophyll content requires optimal partitioning of nitrogen. *Crop and Environment* 2, 24−36.

Supplementary materials in Chapter 5

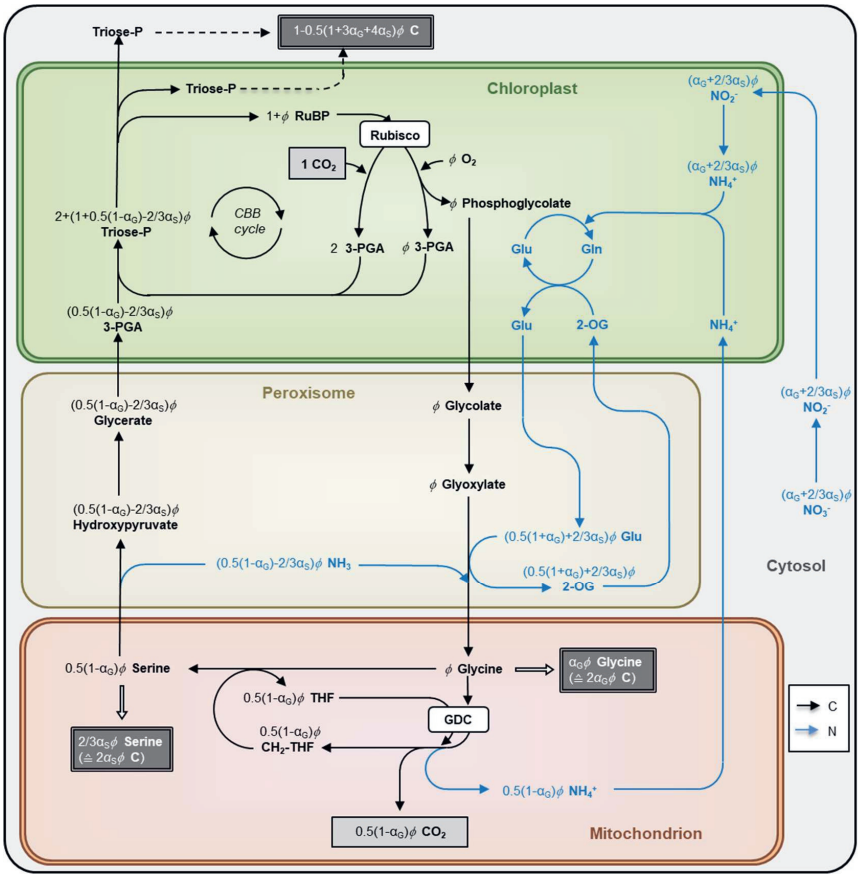

Fig. S5.1 The photorespiratory pathway (involving chloroplast, peroxisome, and mitochondrion), and its connection with the Calvin-Benson-Bassham (CBB) cycle and nitrogen (N) assimilation (revised from Busch, 2020). The scheme assumes certain fractions of glycolate-carbon exit in the form of either glycine (α_G) or serine (α_S) from the pathway for other uses in plant metabolism. All carbon (in black) and N (in blue) fluxes are scaled relative to the rate of RuBP carboxylation (the first step of the CBB cycle) while the ratio of RuBP oxygenation (the first step of the photorespiratory pathway) to RuBP carboxylation is denoted as ϕ. The amount of NO_3^- needed to enter the leaf via *de novo* N assimilation equals the total flux of glycine- and serine-nitrogen leaving the photorespiratory pathway (α_G+2/3α_S)ϕ. Regardless of triose-P used as sugar precursors for processes like starch synthesis in chloroplasts or like sucrose synthesis in cytosol (indicated by dashed arrows), the sum of individual sinks for assimilated carbon (indicated by double-bordered black boxes including those for glycine and serine exits) equals CO_2 taken up by RuBP carboxylation minus CO_2 released by glycine decarboxylase (GDC) in the mitochondrion (the source of "photorespiration") indicated by single-bordered grey boxes. Note that the CO_2 release by GDC will be decreased (by a factor of α_G) if glycine exits, whereas this is not the case if serine exits, from the pathway. This difference has implications for the CO_2-compensation point and thus for modelling leaf photosynthesis. For example, TPU-limited photosynthesis (A_p) can be modelled by eqn (5.4) in the main text if serine exits, whereas the model has to be changed to: $A_p = \frac{[C_c - \Gamma_*(1-\alpha_G)](3T_p)}{C_c - (1+3\alpha_G)\Gamma_*} - R_d$ if glycine exits (Busch et al., 2018; Yin et al., 2021). These two equations give a similar A_p when T_p and the glycolate-carbon exit fraction stay the same, whereas the commonly used algorithm $A_p = \frac{(C_c - \Gamma_*)(3T_p)}{C_c - (1+3\alpha_G)\Gamma_*} - R_d$ would underpredict A_p (Yin et al., 2021). Abbreviations: 2-OG, 2-oxoglutarate; 3-PGA, 3-phosphoglycerate; CH_2-THF, 5,10-methylene-tetrahydrofolate; Gln, glutamine; Glu, glutamate; RuBP, ribulose 1,5-bisphosphate; THF, tetrahydrofolate; triose-P, triose phosphate.

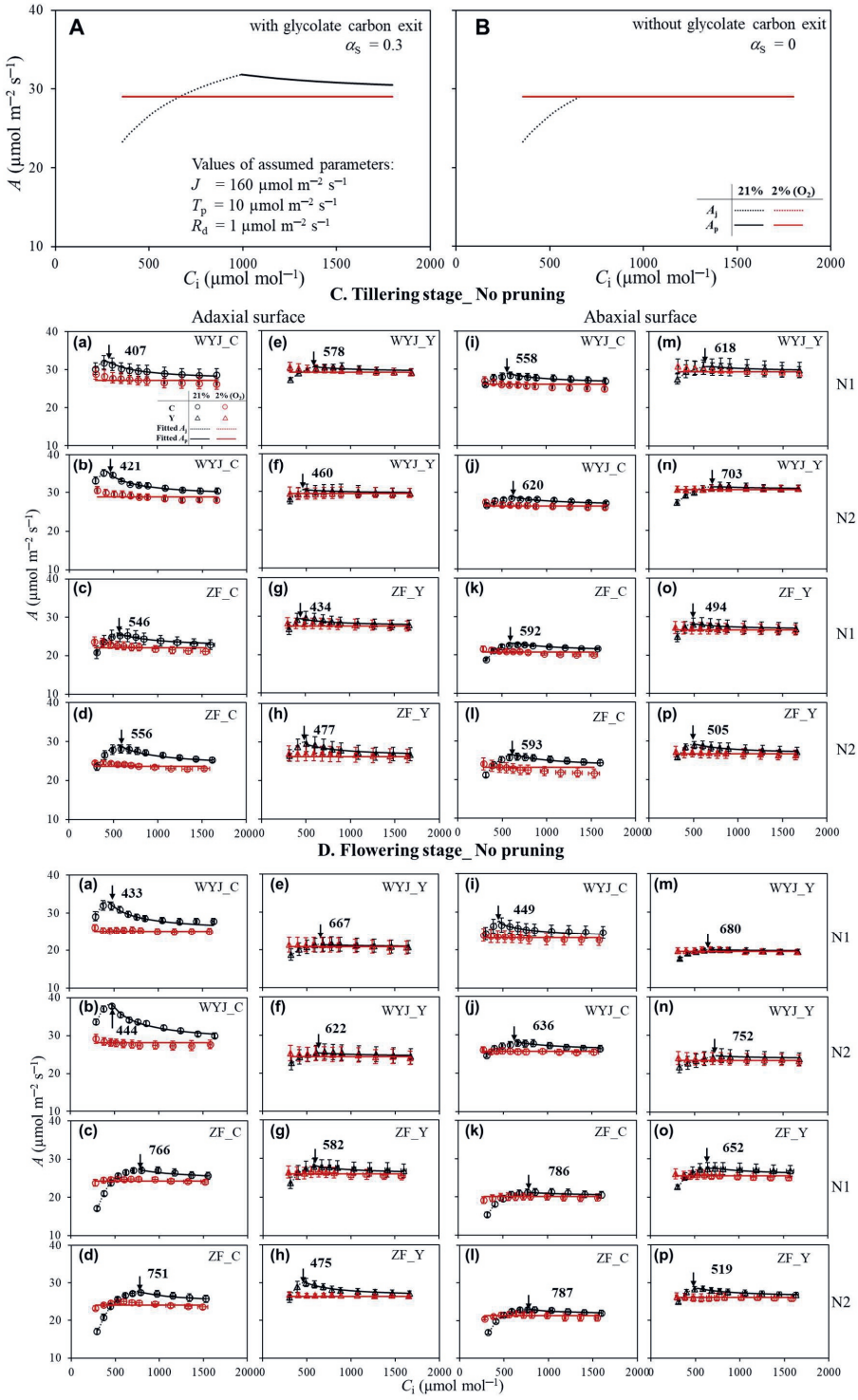
A
with glycolate carbon exit
α_s = 0.3
Values of assumed parameters:
J = 160 μmol m^{-2} s^{-1}
T_p = 10 μmol m^{-2} s^{-1}
R_d = 1 μmol m^{-2} s^{-1}
B
without glycolate carbon exit
α_s = 0
21% 2% (O_2)
A_j
A_p
A (μmol m^{-2} s^{-1})
C_i (μmol mol^{-1})
C. Tillering stage_ No pruning
Adaxial surface
Abaxial surface
(a) 407 WYJ_C
(e) 578 WYJ_Y
(i) 558 WYJ_C
(m) 618 WYJ_Y
N1
(b) 421 WYJ_C
(f) 460 WYJ_Y
(j) 620 WYJ_C
(n) 703 WYJ_Y
N2
(c) 546 ZF_C
(g) 434 ZF_Y
(k) 592 ZF_C
(o) 494 ZF_Y
N1
(d) 556 ZF_C
(h) 477 ZF_Y
(l) 593 ZF_C
(p) 505 ZF_Y
N2
D. Flowering stage_ No pruning
(a) 433 WYJ_C
(e) 667 WYJ_Y
(i) 449 WYJ_C
(m) 680 WYJ_Y
N1
(b) 444 WYJ_C
(f) 622 WYJ_Y
(j) 636 WYJ_C
(n) 752 WYJ_Y
N2
(c) 766 ZF_C
(g) 582 ZF_Y
(k) 786 ZF_C
(o) 652 ZF_Y
N1
(d) 751 ZF_C
(h) 475 ZF_Y
(l) 787 ZF_C
(p) 519 ZF_Y
N2

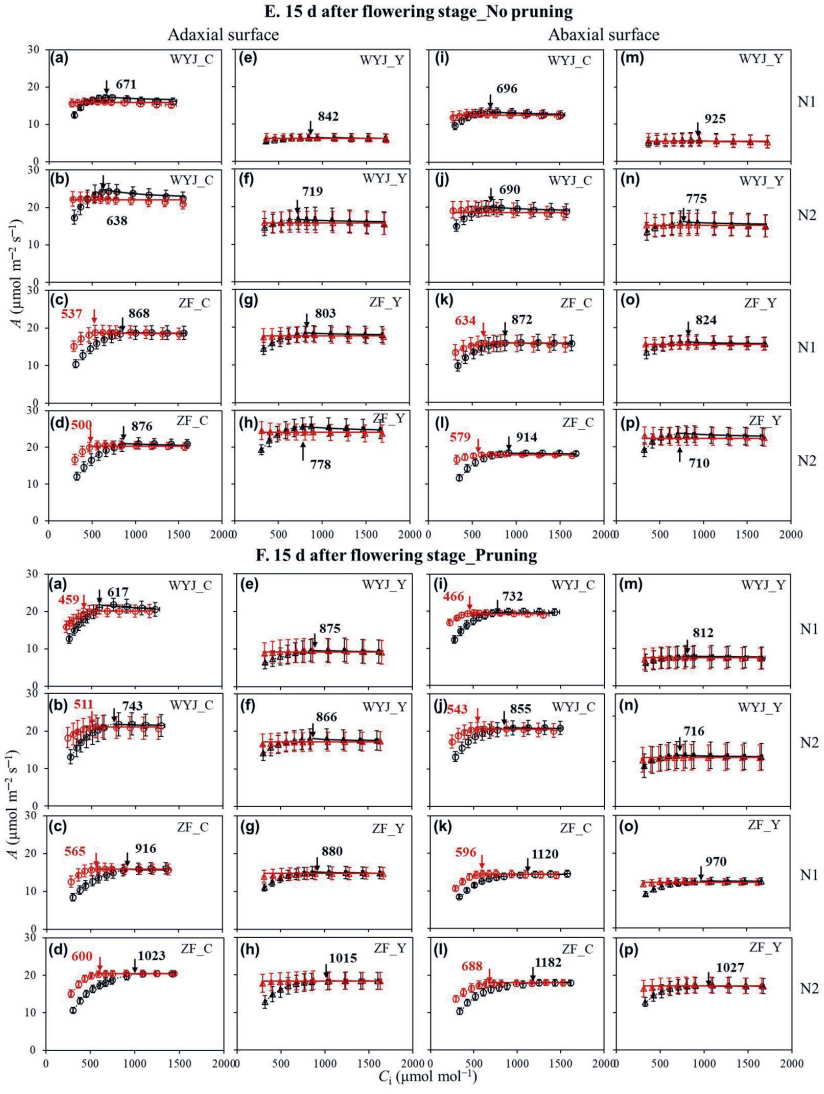

Fig. S5.2 A-C_i curves with black and red representing trends under 21% O_2 and 2% O_2 conditions, respectively. **A-B,** Theoretical curves with (A; $\alpha_S = 0.3$) or without (B; $\alpha_S = 0$) glycolate carbon exit from the photorespiratory pathway, drawn using assumed parameters (listed in Panel A; note that in Panel B, the black curve under 21% O_2 within the range of TPU limitation is invisible, because it is overlapped by the red one under 2% O_2). **C-F,** Measured A-C_i curves in the 2022 experiment for rice control (C) genotypes (circles) and their yellower-leaf (Y) variant genotypes (triangles), on both sides of the leaves at three stages. Data are shown as means of four replicates (± standard errors) for each genotype. The curves are drawn from eqn (5.6) using fitted parameter values (see Table S5.1), representing fitted A_j (dotted lines) and A_p (full lines). The transition points (termed "threshold C_i", see Fig. 5.6) shown with arrows (black for 21% and red for 2% O_2 conditions) in each panel are the intersection points of A_j and A_p curves (those red curves without an arrow means that the TPU limitation was already reached at a lower C_i out of the measured range). WYJ and ZF are the abbreviations of two genetic backgrounds: cv. Wuyunjing 3 and cv. Zhefu 802.

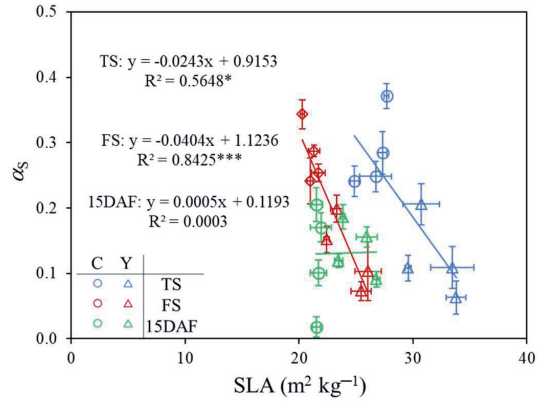

Fig. S5.3 Relationship between the proportion of glycolate carbon exported from photorespiratory pathway in the form of serine (α_S, based on measurements on the adaxial leaf surface) and specific leaf area (SLA). Data represented by different colours and symbols are the values for rice control (C) genotypes (circles) and yellower-leaf (Y) variant genotypes (triangles) of these un-pruned plants from tillering (TS, blue), flowering (FS, red), and 15 d after flowering (15DAF, green) stage in the 2022 experiment. Each point represents the mean of three or four replicates. Linear regressions were fitted for each stage with the significance of each correlation shown by asterisks: * $P < 0.05$, *** $P < 0.001$.

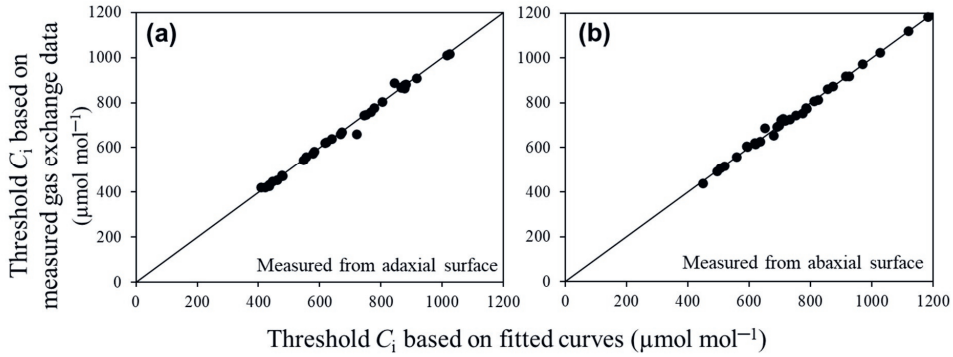

Fig. S5.4 Comparisons of the threshold C_i derived from two methods under adaxial (a) and abaxial (b) measurements, respectively (data based on the 2022 experiment). The first method for threshold C_i (the y-axis) was solved as the intersection point of second-order polynomial regression ($y = ax^2 + bx + c$) equations that best fitted to measured gas exchange data representing A_j- and A_p-ranges. The second method for threshold C_i (the x-axis) was obtained from the extrapolated intersection point of A_j- and A_p-part fitted curves drawn from eqn (5.6) based on the estimated parameters. The diagonal line is the 1:1 line.

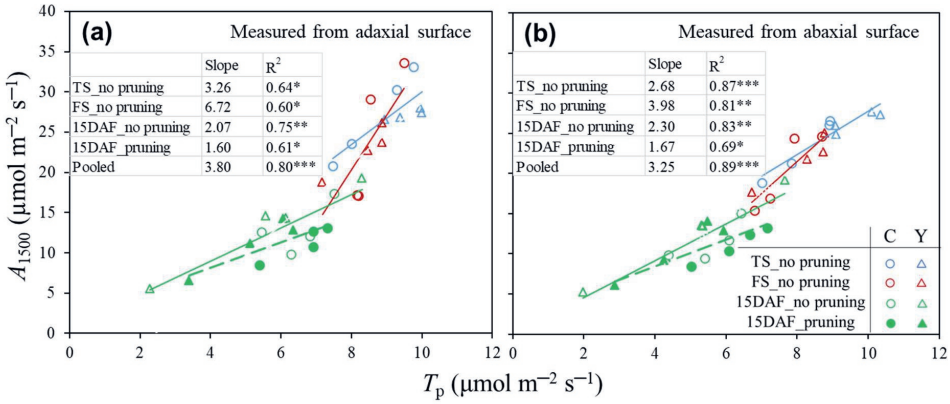

Fig. S5.5 Relationship between light-saturated leaf photosynthesis rate (A_{1500}) and the rate of triose phosphate utilisation (T_p) based on adaxial (a) and abaxial (b) measurements. Data represent the values for rice control (C) genotypes (circles) and yellower-leaf (Y) variant genotypes (triangles) of these intact (open symbols) and panicle-pruned (filled symbols) plants from tillering (TS, blue), flowering (FS, red), and 15 d after flowering (15DAF, green) stage in the 2022 experiment. Each point represents the mean of three or four replicates. Linear regressions were fitted for each stage and pooled data with the significance of correlation shown by asterisks: * $P < 0.05$, ** $P < 0.01$, *** $P < 0.001$.

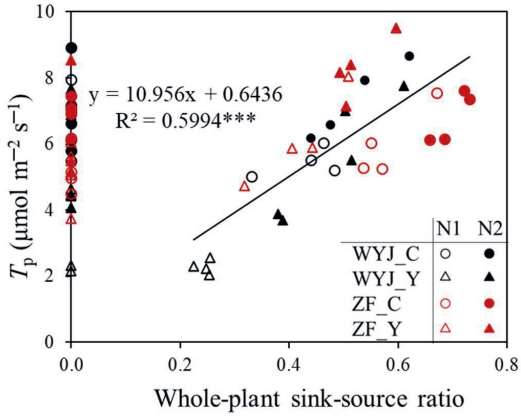

Fig. S5.6 Relationship between the rate of triose phosphate utilisation (T_p, based on measurements on the adaxial leaf surface) and whole-plant sink-source ratio. Here, following Fabre et al. (2020), the ratio of flag leaf area (source) to the fertile spikelet number of the panicle (sink) on the culm was used as an indicator of the whole-plant sink-source ratio (also see the text). Data are for rice control (C) genotypes (circles) and yellower-leaf (Y) variant genotypes (triangles) from grain-filling stage under low-nitrogen (N1, open symbols) and high-nitrogen (N2, filled symbols) levels in the 2022 experiment, with cv. Wuyunjing 3 (WYJ) in black and cv. Zhefu 802 (ZF) in red. For those plants with panicle pruning, we define their sink-source ratio to be zero, so all their data points fall on the Y axis. Linear regression was fitted for data (representing no pruning) with the significance of correlation shown by asterisks: *** $P < 0.001$.

Table S5.1 Modelled photosynthetic parameters (δ – the ratio of carboxylation resistance to mesophyll resistance; T_p – the rate of TPU; α_S – the proportion of glycolate carbon exported from photorespiratory pathway in the form of serine) for rice control (C) genotypes and their yellower-leaf (Y) variant genotypes at three stages under low-nitrogen (N1) and high-nitrogen (N2) levels measured from both sides of the leaves in the 2022 experiment.

Stage	Pruning level	N level	Background	Genotype	Adaxial surface			Abaxial surface		
					δ	T_p	α_S	δ	T_p	α_S
						μmol m^{-2} s^{-1}	–		μmol m^{-2} s^{-1}	–
Tillering	No pruning	N1	WYJ	C	1.13 ± 0.12	9.28 ± 0.49	0.241 ± 0.023	0.95 ± 0.15	8.90 ± 0.19	0.180 ± 0.019
			WYJ	Y	1.49 ± 0.28	10.00 ± 0.14	0.109 ± 0.032	1.07 ± 0.11	10.10 ± 0.51	0.107 ± 0.018
			ZF	C	1.16 ± 0.18	7.46 ± 0.36	0.284 ± 0.032	1.26 ± 0.19	7.02 ± 0.17	0.242 ± 0.039
			ZF	Y	1.22 ± 0.17	9.39 ± 0.39	0.108 ± 0.010	1.10 ± 0.15	9.09 ± 0.44	0.097 ± 0.033
		N2	WYJ	C	0.95 ± 0.10	9.76 ± 0.25	0.248 ± 0.024	1.31 ± 0.14	8.93 ± 0.22	0.193 ± 0.018
			WYJ	Y	1.74 ± 0.17	9.96 ± 0.45	0.063 ± 0.025	1.37 ± 0.09	10.35 ± 0.24	0.073 ± 0.027
			ZF	C	1.15 ± 0.18	7.99 ± 0.12	0.371 ± 0.019	1.14 ± 0.09	7.85 ± 0.24	0.290 ± 0.027
			ZF	Y	1.28 ± 0.15	8.96 ± 0.41	0.206 ± 0.014	1.20 ± 0.15	9.08 ± 0.44	0.166 ± 0.016
Flowering	No pruning	N1	WYJ	C	0.73 ± 0.05	8.54 ± 0.28	0.287 ± 0.009	0.73 ± 0.09	7.92 ± 0.14	0.185 ± 0.018
			WYJ	Y	1.28 ± 0.14	7.17 ± 0.35	0.073 ± 0.015	1.90 ± 0.25	6.73 ± 0.22	0.064 ± 0.008
			ZF	C	0.72 ± 0.07	8.16 ± 0.19	0.242 ± 0.035	1.01 ± 0.07	6.80 ± 0.27	0.138 ± 0.020
			ZF	Y	1.00 ± 0.12	8.87 ± 0.42	0.152 ± 0.020	1.00 ± 0.08	8.74 ± 0.33	0.176 ± 0.028
		N2	WYJ	C	0.72 ± 0.04	9.50 ± 0.23	0.344 ± 0.022	0.86 ± 0.04	8.69 ± 0.23	0.180 ± 0.045
			WYJ	Y	1.59 ± 0.18	8.48 ± 0.48	0.103 ± 0.026	1.67 ± 0.12	8.29 ± 0.23	0.105 ± 0.041
			ZF	C	0.63 ± 0.04	8.20 ± 0.19	0.254 ± 0.013	0.74 ± 0.09	7.24 ± 0.27	0.169 ± 0.026
			ZF	Y	0.97 ± 0.11	8.88 ± 0.14	0.199 ± 0.021	1.11 ± 0.08	8.77 ± 0.28	0.156 ± 0.017
15 d after flowering	No pruning	N1	WYJ	C	1.11 ± 0.15	5.45 ± 0.22	0.170 ± 0.023	1.06 ± 0.11	4.37 ± 0.36	0.153 ± 0.018
			WYJ	Y	1.08 ± 0.09	2.28 ± 0.11	0.091 ± 0.012	1.13 ± 0.13	1.98 ± 0.46	0.094 ± 0.035
			ZF	C	1.26 ± 0.11	6.29 ± 0.58	0.018 ± 0.015	1.16 ± 0.14	5.40 ± 0.38	0.011 ± 0.009
			ZF	Y	0.95 ± 0.22	6.14 ± 0.69	0.119 ± 0.010	0.98 ± 0.15	5.35 ± 0.48	0.112 ± 0.046
		N2	WYJ	C	0.72 ± 0.12	7.51 ± 0.48	0.205 ± 0.026	1.17 ± 0.13	6.42 ± 0.42	0.181 ± 0.026
			WYJ	Y	1.26 ± 0.20	5.57 ± 0.81	0.156 ± 0.011	0.77 ± 0.10	5.31 ± 0.82	0.138 ± 0.033
			ZF	C	1.02 ± 0.04	6.82 ± 0.39	0.101 ± 0.019	1.90 ± 0.25	6.09 ± 0.16	0.093 ± 0.023
			ZF	Y	1.15 ± 0.22	8.31 ± 0.49	0.187 ± 0.018	1.07 ± 0.18	7.66 ± 0.47	0.156 ± 0.016
	Pruning	N1	WYJ	C	0.53 ± 0.06*	6.92 ± 0.51*	0.105 ± 0.006*	0.92 ± 0.10	6.66 ± 0.21*	0.048 ± 0.021*
			WYJ	Y	0.55 ± 0.21*	3.40 ± 0.67	0.084 ± 0.014	0.46 ± 0.22*	2.87 ± 0.88	0.085 ± 0.014
			ZF	C	1.18 ± 0.22	5.39 ± 0.53	0.015 ± 0.009	1.50 ± 0.19	5.03 ± 0.41	0.000 ± 0.000
			ZF	Y	0.96 ± 0.12	5.12 ± 0.51	0.075 ± 0.010*	0.83 ± 0.08	4.26 ± 0.37	0.017 ± 0.017
		N2	WYJ	C	0.78 ± 0.22	7.33 ± 0.71	0.077 ± 0.007*	1.40 ± 0.28	7.16 ± 0.45	0.062 ± 0.008*
			WYJ	Y	0.92 ± 0.19	6.06 ± 0.75	0.109 ± 0.007*	1.27 ± 0.26	5.48 ± 0.74	0.093 ± 0.013
			ZF	C	0.82 ± 0.07	6.92 ± 0.27	0.000 ± 0.000*	1.10 ± 0.12*	6.07 ± 0.16	0.000 ± 0.000*
			ZF	Y	0.91 ± 0.23	6.35 ± 0.76	0.015 ± 0.009*	0.95 ± 0.15	5.94 ± 0.70	0.006 ± 0.006*

The asterisks (*) represent significant differences ($P < 0.05$) for a given genotype-nitrogen combination between pruned and un-pruned plants at 15 d after flowering.

Table S5.2 Leaf photosynthetic characteristics (mean ± standard error of four replicates) for rice control (C) genotypes and their yellower-leaf (Y) variant genotypes at three stages under low-nitrogen (N1) and high-nitrogen (N2) levels measured from both sides of leaves in the 2022 experiment.

Stage	Pruning level	N level	Background	Genotype	Adaxial surface			Abaxial surface			SLA ($m^2\ kg^{-1}$)	SLN (g N m^{-2})
					SPAD	A_{1500} (μmol $m^{-2}\ s^{-1}$)	PNUE (μmol g^{-1} N s^{-1})	SPAD	A_{1500} (μmol $m^{-2}\ s^{-1}$)	PNUE (μmol g^{-1} N s^{-1})		
Tillering	No pruning	N1	WYJ	C	42.9 ± 0.7	30.3 ± 1.6	25.8 ± 0.8	42.9 ± 0.5	26.1 ± 0.6	22.5 ± 1.2	24.9 ± 0.4	1.48 ± 0.06
			WYJ	Y	18.1 ± 1.1	27.4 ± 0.4	24.3 ± 0.7	18.5 ± 1.3	27.6 ± 1.3	24.4 ± 0.6	33.4 ± 1.9	1.43 ± 0.03
			ZF	C	30.9 ± 0.9	20.9 ± 1.6	24.3 ± 1.1	30.4 ± 0.9	18.8 ± 0.3	22.2 ± 1.1	27.3 ± 0.4	1.16 ± 0.04
			ZF	Y	21.2 ± 1.0	26.8 ± 1.5	27.2 ± 1.0	21.2 ± 0.9	24.8 ± 1.3	25.3 ± 1.1	29.6 ± 0.3	1.28 ± 0.04
		N2	WYJ	C	43.9 ± 0.9	33.2 ± 0.9	26.2 ± 0.7	43.2 ± 0.9	26.6 ± 0.5	21.1 ± 0.8	26.7 ± 1.4	1.57 ± 0.06
			WYJ	Y	18.2 ± 0.8	28.0 ± 1.3	25.2 ± 0.5	17.6 ± 1.0	27.3 ± 0.7	24.7 ± 1.6	33.8 ± 0.9	1.41 ± 0.07
			ZF	C	33.8 ± 1.1	23.6 ± 1.0	25.5 ± 0.5	33.4 ± 0.9	21.3 ± 0.6	23.3 ± 1.0	27.7 ± 0.2	1.23 ± 0.04
			ZF	Y	21.1 ± 0.6	26.5 ± 1.5	29.3 ± 0.7	21.0 ± 0.3	25.9 ± 0.6	28.8 ± 1.4	30.7 ± 1.6	1.21 ± 0.05
Flowering	No pruning	N1	WYJ	C	45.7 ± 0.7	29.1 ± 1.2	21.6 ± 1.0	45.5 ± 0.8	24.4 ± 1.7	18.0 ± 1.1	21.3 ± 0.5	1.65 ± 0.04
			WYJ	Y	12.6 ± 0.6	18.7 ± 1.5	15.9 ± 1.8	12.7 ± 0.5	17.6 ± 0.5	14.9 ± 1.0	25.4 ± 0.9	1.50 ± 0.08
			ZF	C	33.9 ± 0.1	17.2 ± 0.6	20.0 ± 1.0	33.8 ± 0.2	15.4 ± 0.7	17.8 ± 0.2	21.0 ± 0.3	1.17 ± 0.04
			ZF	Y	16.7 ± 0.7	23.7 ± 1.5	23.0 ± 0.4	16.6 ± 1.0	22.7 ± 0.6	22.4 ± 1.9	22.4 ± 0.2	1.33 ± 0.08
		N2	WYJ	C	49.7 ± 0.6	33.6 ± 0.7	21.0 ± 0.5	49.6 ± 0.7	24.6 ± 0.5	15.4 ± 0.5	20.3 ± 0.2	1.91 ± 0.06
			WYJ	Y	14.9 ± 0.8	22.7 ± 1.9	17.2 ± 1.8	15.2 ± 0.9	21.8 ± 1.5	16.3 ± 1.2	26.0 ± 1.1	1.64 ± 0.08
			ZF	C	35.9 ± 0.3	17.1 ± 0.8	17.7 ± 0.7	35.7 ± 0.3	16.9 ± 0.6	17.5 ± 0.5	21.7 ± 0.6	1.27 ± 0.02
			ZF	Y	20.2 ± 1.4	26.1 ± 1.4	23.2 ± 0.7	19.9 ± 1.5	25.0 ± 0.7	23.1 ± 1.8	23.3 ± 0.5	1.40 ± 0.06
15 d after flowering	No pruning	N1	WYJ	C	42.2 ± 1.0	12.6 ± 0.8	17.2 ± 1.3	41.8 ± 1.0	9.9 ± 1.3	13.8 ± 2.3	21.9 ± 0.9	1.04 ± 0.06
			WYJ	Y	4.6 ± 1.3	5.5 ± 0.6	5.6 ± 0.4	4.4 ± 1.2	5.2 ± 1.3	5.3 ± 1.2	26.8 ± 0.3	1.28 ± 0.05
			ZF	C	29.3 ± 1.0	9.9 ± 0.9	17.5 ± 0.9	30.0 ± 0.9	9.4 ± 1.1	16.6 ± 1.2	21.5 ± 0.4	0.87 ± 0.07
			ZF	Y	11.2 ± 1.4	14.4 ± 1.7	19.5 ± 0.9	10.7 ± 1.4	13.4 ± 1.7	18.2 ± 1.4	23.5 ± 0.4	1.03 ± 0.05
		N2	WYJ	C	45.5 ± 0.9	17.4 ± 1.9	19.1 ± 1.3	45.2 ± 0.7	15.1 ± 1.5	16.9 ± 1.8	21.5 ± 0.5	1.21 ± 0.06
			WYJ	Y	10.2 ± 1.9	14.5 ± 2.2	13.2 ± 1.5	10.7 ± 1.8	13.5 ± 2.4	12.3 ± 1.7	25.9 ± 0.9	1.38 ± 0.07
			ZF	C	34.2 ± 0.5	12.1 ± 1.1	17.4 ± 0.7	34.3 ± 0.4	11.7 ± 0.8	16.8 ± 0.6	21.7 ± 0.7	0.99 ± 0.04
			ZF	Y	17.9 ± 1.2	19.3 ± 1.3	21.0 ± 0.8	18.0 ± 1.5	19.2 ± 1.9	20.8 ± 1.3	23.8 ± 0.2	1.22 ± 0.03
	Pruning	N1	WYJ	C	45.3 ± 1.5	12.7 ± 1.3	12.0 ± 1.1*	45.4 ± 1.5	12.4 ± 1.0	11.9 ± 1.4	18.2 ± 0.8*	1.36 ± 0.07*
			WYJ	Y	8.1 ± 2.4	6.5 ± 1.8	4.9 ± 1.1	7.0 ± 2.5	6.0 ± 2.4	4.4 ± 1.5	22.8 ± 0.8*	1.57 ± 0.09*
			ZF	C	31.2 ± 0.9	8.5 ± 1.0	12.1 ± 0.3*	30.8 ± 0.9	8.5 ± 0.5	12.3 ± 0.8*	18.8 ± 0.4*	1.00 ± 0.08
			ZF	Y	12.0 ± 1.0	11.1 ± 0.9	9.7 ± 0.8*	11.9 ± 0.7	9.2 ± 0.6	8.0 ± 0.6*	19.0 ± 0.8*	1.45 ± 0.08*
		N2	WYJ	C	48.6 ± 0.3*	13.1 ± 1.9	10.6 ± 1.2*	49.1 ± 0.5*	13.2 ± 1.3	10.8 ± 0.9*	18.4 ± 0.5*	1.52 ± 0.07*
			WYJ	Y	10.3 ± 2.2	14.2 ± 2.1	10.0 ± 1.3	10.7 ± 2.0	14.0 ± 2.6	9.9 ± 1.7	23.5 ± 0.3*	1.71 ± 0.02*
			ZF	C	34.4 ± 0.8	10.7 ± 0.7	11.9 ± 0.4*	33.8 ± 0.9	10.3 ± 0.9	11.5 ± 0.7*	18.3 ± 0.7*	1.20 ± 0.06*
			ZF	Y	13.0 ± 1.5*	12.8 ± 1.7*	9.3 ± 0.7*	12.5 ± 1.3*	12.8 ± 1.2*	9.4 ± 0.5*	19.4 ± 0.4*	1.66 ± 0.08*

A_{1500}, photosynthetic rate at saturated light of 1500 μmol $m^{-2}\ s^{-1}$ and ambient CO_2 level; PNUE, leaf photosynthetic nitrogen-use efficiency, defined as: PNUE $= \frac{A_{1500}}{SLN - n_b}$, where SLN is specific leaf nitrogen, and n_b represents a base leaf nitrogen content (a value of 0.23 g N m^{-2} for all the rice genotypes from Zhou et al., 2023); SLA, specific leaf area. The asterisks (*) represent significant differences ($P < 0.05$) for a given genotype-nitrogen combination between pruned and un-pruned plants at 15 d after flowering.

Table S5.3 Summary of analysis of variance of leaf photosynthetic variables: the rate of TPU (T_p), the proportion of glycolate carbon exported from photorespiratory pathway in the form of serine (α_S), the ratio of carboxylation resistance to mesophyll resistance (δ), photosynthetic rate at saturated light of 1500 μmol m^{-2} s^{-1} and ambient CO_2 level (A_{1500}), leaf photosynthetic nitrogen-use efficiency (PNUE), chlorophyll content indicator (SPAD), specific leaf nitrogen (SLN), and specific leaf area (SLA), in response to genotype, panicle pruning, abaxial vs adaxial measurements, N level, three-stages' measurements, and their interactions (if applicable). Data are from the 2022 experiment, with values of these parameters shown in Tables S5.1 and S5.2.

Variable	T_p	α_S	δ	A_{1500}	PNUE	SPAD	SLN	SLA
Genotype	***	***	***	***	***	***	***	***
Pruning	ns	***	**	***	***	ns	***	***
Adaxial vs Abaxial	***	***	*	***	***	ns	-	-
N level	***	***	ns	***	***	***	***	ns
Stage	***	ns	***	***	***	ns	***	***
Genotype × Pruning	***	***	ns	**	***	***	*	ns
Genotype × Adaxial vs Abaxial	ns	***	*	**	*	ns	-	-
Genotype × N level	***	ns	ns	**	***	ns	ns	ns
Genotype × Stage	***	***	***	***	**	***	ns	*
Pruning × Adaxial vs Abaxial	ns	ns	ns	ns	ns	ns	-	-
Pruning × N level	ns	***	ns	ns	*	**	ns	ns
Adaxial vs Abaxial × N level	ns	ns	ns	ns	ns	ns	-	-
Adaxial vs Abaxial × Stage	ns	ns	*	ns	ns	ns	-	-
N level × Stage	ns	ns	ns	ns	ns	**	*	ns

In the analysis of variance, the significance is shown by asterisks: ns – no significance, * $P < 0.05$, ** $P < 0.01$, *** $P < 0.001$, according to the LSD test. Note, we use "genotype" rather than "yellow-leaf modification" as a fixed factor mainly because yellow-leaf modification produces different effects on leaf photosynthetic physiology between WYJ and ZF backgrounds (see Results).

References

Busch FA. 2020. Photorespiration in the context of Rubisco biochemistry, CO_2 diffusion and metabolism. *The Plant Journal* 101, 919−939.

Busch FA, Sage RF, Farquhar GD. 2018. Plants increase CO_2 uptake by assimilating nitrogen via the photorespiratory pathway. *Nature Plants* 4, 46−54.

Fabre D, Dingkuhn M, Yin X, Clément-Vidal A, Roques S, Soutiras A, Luquet D. 2020. Genotypic variation in source and sink traits affects the response of photosynthesis and growth to elevated atmospheric CO_2. *Plant, Cell & Environment* 43, 579−593.

Yin X, Busch FA, Struik PC, Sharkey TD. 2021. Evolution of a biochemical model of steady-state photosynthesis. *Plant, Cell & Environment* 44, 2811−2837.

Zhou Z, Struik PC, Gu J, van der Putten PEL, Wang Z, Yin X, Yang J. 2023. Enhancing leaf photosynthesis from altered chlorophyll content requires optimal partitioning of nitrogen. *Crop and Environment* 2, 24-36.

Chapter 6

General discussion

Since the Green Revolution in the 1960s, which significantly increased the yield of major crops by introducing cultivars with a high harvest index and increasing inputs, further increases in productivity of crop cultivars have been stagnant. With the recognition that the harvest index has more or less reached a plateau and input levels should not be increased further for reasons of sustainability, the next advance in crop yields will come from improvement in biomass production, most likely via improving photosynthesis (Long et al., 2006; Ray et al., 2013). The current humble rate of photosynthesis in crops, even under favourable growth conditions, is caused by a series of energy losses during the conversion of incoming global solar radiation into photosynthetic assimilates (Yin and Struik, 2015; Zhu et al., 2010). Leaf-colour modification (involving changes into "stay-green" and "yellow-leaf") has been recognised as a promising strategy for enhancing photosynthesis (Chapter 1). By fine-tuning the light-absorbing capacity of leaves, this approach holds the potential to reduce the efficiency loss during the light energy conversion from leaf to canopy and to whole-crop scales.

Leaf-colour modification, specifically a change in chlorophyll content, affects carbon assimilation not only through chlorophyll synthesis and catabolism and related light absorption but also via nitrogen (N) metabolism and remobilisation processes (Fu et al., 2021; Thomas and Ougham, 2014). The underlying mechanism is that the leaf carbon assimilation rate is closely related to the amount of leaf photosynthetic N content and its allocation to the different compartments such as the light-harvesting complex, the electron transport system, Rubisco and other photosynthesis-related enzymes (Makino et al., 1985, 1984; Yin et al., 2018). As awareness grows regarding the significance of N resources for photosynthesis physiology and yield formation, it becomes increasingly important to comprehend how the N budgets are adjusted by leaf-colour modification at different scales, from cellular level to crop level. This understanding is of utmost importance as this N allocation has substantial regulatory effects on the crop's photosynthesis and associated source-sink relationships, as well as on the dynamic feedforward or feedback between these processes across different scales (Chapter 1). However, the existing knowledge in this area is still limited.

This thesis used rice genotypes of different genetic backgrounds and their leaf-colour variants as test materials, with the main aim to explore the potential of applying leaf-colour modifications (making the leaves of the rice plant greener or yellower) to enhance crop photosynthesis and thereby increase yield of rice. To achieve this aim, I first introduced the subject about the potential effects of leaf-colour modification on rice photosynthesis and

source-sink relationships at different scales in Chapter 1. Then, I conducted experiments on the rice genotypes with modified leaf colour to examine these potential effects on photosynthesis at both leaf level (described in Chapter 2) and canopy level (described in Chapter 3). I also investigated the impact of leaf-colour modification on source-sink relationships at crop level (described in Chapter 4). Finally, based on the understanding of the N-regulatory mechanisms, the interconnection of sink limitations across scales was experimentally unravelled (Chapter 5).

In this general discussion, main findings of each research chapter will be presented in Section 6.1, and the multifaceted roles of N in modifying leaf colour, enhancing leaf and canopy photosynthesis, and optimising source-sink relations will be highlighted in Section 6.2. Thereafter, the implications of leaf-colour modification for crop breeding and cultivation will be discussed in Section 6.3. Finally, I will make some concluding remarks in Section 6.4.

6.1 Research findings of this thesis

6.1.1 Effects of leaf-colour modification on rice photosynthesis

Leaf-colour modification, mainly referring to alteration of leaf chlorophyll content, can affect rice photosynthesis at both leaf and canopy scales. Stay-green (G) and yellow-leaf (Y) are two common traits derived from leaf-colour modification. The G-variant genotypes showed delays in chlorophyll catabolism only when rice approached maturity, resulting in enhanced leaf longevity. The Y-variant ones demonstrated lower leaf chlorophyll throughout the entire crop cycle. Earlier and larger effects were observed for Y variants than for G variants as presented below:

- At leaf level (from Chapter 2): Compared with their corresponding default or control (C) genotypes, the Y-variant genotypes showed lower light absorptance at the leaf level and efficiency of converting incident irradiance into linear electron transport, but higher stomatal conductance and high-light tolerance. Despite lower values of non-photochemical quenching (NPQ) in both Y variants, only in the one from the ZF (cv. Zhefu 802) background there was lower relative energy loss via reduced NPQ. This smaller loss was associated with its higher photosynthetic capacity parameters (V_{cmax}, the maximum carboxylation capacity of Rubisco, and J_{max}, the maximum rate of linear electron transport under saturated light) and higher photosynthetic N-use efficiency. Proteomic analyses indicated that this Y-variant genotype from ZF background notably

decreased the relative abundance of light-harvesting proteins while increased the relative abundance of the Cytochrome *b6/f* complex and Rubisco-related proteins compared with its C genotype.

- At canopy level (from Chapter 3): Compared with their C genotypes, both Y-variant genotypes showed lower above-ground biomass accumulation during the early growth phase because of lower ability to intercept light. Although the Y-variant genotypes allowed more light penetration down into the lower parts of the canopy, as indicated by a significantly reduced light extinction coefficient (K_L), the profile of leaf photosynthetic resources (i.e., leaf N) did not necessarily follow more closely the light profile than in the C genotypes. Of the two Y-variant genotypes, only the one from the ZF background exhibited a steeper N gradient along the canopy than its C genotype, evidenced by a higher N extinction coefficient (K_N) and more N content in the upper leaf layers of the canopy. This Y-variant genotype with increased $K_{N,}$ and thus with an increased K_N/K_L ratio, showed an improvement in the canopy photosynthesis (A_c), in line with the theoretical expectation based on optimisation. For example, Goudriaan (1995) indicated that the A_c can be maximised if the profile of photosynthetic resource (i.e., leaf N that determines the light-saturated maximum leaf-photosynthesis) follows the light profile. This experimental and theoretical result for A_c was supported by its higher daily average crop growth rate (and thus grain yield) compared with its control genotype.

6.1.2 Effects of leaf-colour modification on rice source-sink relationships

While the potential capacity of photosynthesis (source) determines the overall biomass accumulation of the rice plant, it is the allocation and distribution of photosynthetic assimilates to the panicles (sink) that ultimately determines the grain yield (e.g. Venkateswarlu and Visperas, 1987). Although my initial research (Chapter 3) showed that leaf-colour modification can affect the canopy photosynthesis A_c (source activity), whether it also influences sink growth and source-sink relationships was still unclear. In Chapter 4, the source-sink dynamics for carbohydrate and N during rice grain filling were examined among different leaf-colour modified genotypes based on a model-fitting method. Furthermore, I investigated whether and how the altered source-sink relations by leaf-colour modification were associated with N budgets.

Compared with the C genotypes, all G-variant genotypes exhibited an extended grain-filling period from flowering to maturity, along with a decrease in both biomass sink and source activity, which resulted in little difference in whole-plant and panicle biomass (or N) accumulation. In comparison, although the Y-variant genotypes exhibited similar increases in grain-filling duration as the G-variant genotypes, they displayed reduced whole-plant biomass and N accumulation. Results indicated that leaf-colour modification affected biomass source-sink relationships, predominantly through the adjustment of post-flowering source capacity, but the approach to attaining this differed among genetic backgrounds. Among all variants, only one Y-variant genotype from the ZF background showed a simultaneous increase in source capacity and sink growth when compared to its corresponding C genotype. This increase in source capacity was associated with its prolonged leaf-N duration, resulting from more post-flowering N uptake and less N remobilisation from leaves to grains.

6.1.3 Unveiling the connection: leaf-level sink limitation and whole-plant sink limitation

It is commonly observed that the feedback effect of sink on source activity occurs at the whole-plant scale, as suggested by crop physiologists (White et al., 2016). Also, this feedback effect of sink occurs at the (sub)foliar scale, as proposed by photosynthesis biologists (Sharkey, 2019) within the context of triose phosphate utilisation (TPU) limitation, in which N assimilation via the photorespiratory pathway can increases CO_2 uptake. This is because a proportion of amino acids exported from the pathway represents an additional sink for carbon (Busch et al., 2018). These processes at two different scales may not be independent (Yin et al., 2021). Yet, little effort has been devoted to unravelling the connection between them and to exploring its inherent regulatory mechanism if the connection is associated with whole-plant N budgets. In Chapter 5, this issue was addressed by model analyses of gas-exchange data measured on leaves at three growth stages of rice plants grown at two N levels, where three experimental approaches (leaf-colour modification, comparison of adaxial vs abaxial measurements, and panicle pruning) were explored to alter source-sink ratios. Also, the amount of photorespiration was controlled by O_2 conditions (21% vs 2%), which helped quantify the amount of amino-acid export associated with the photorespiratory pathway. With this experimental set-up in combination with model analysis, I investigated:

i) how leaf photosynthetic carbon uptake under TPU limitation is affected by photorespiration-associated N assimilation;
ii) how the biochemical sink-source mechanism, reflected in TPU limitation, responds to altered sink-source ratios;
iii) how this process is regulated by whole-plant N budgets.

Results confirmed that N assimilation via exporting glycolate carbon from the photorespiratory pathway in the form of amino acids can increase the leaf photosynthetic rate. Photorespiration-associated N assimilation was involved more in high-N leaves, while it was less in the leaves from Y-variant genotypes, under abaxial measurement, and the leaves from panicle-pruned plants. In all conditions, the light-saturated maximum leaf photosynthesis was highly correlated with the rate of TPU (T_p); and both were positively correlated with leaf N content, while higher leaf N (observed at early growth stages or at high N inputs) caused TPU limitation to occur at lower intercellular CO_2 concentrations. In this way, leaf-scale source activity and TPU limitation can be adjusted by leaf N content in response to sink-source imbalance. After removal of all panicles, it was no longer required to remobilise N from the leaves to the panicles to support grain growth anymore. The resulting accumulation of N in the leaves clarified why there was no apparent impact of panicle pruning on T_p in the panicle-pruned plants when compared to the intact plants, as the feedback inhibition of whole-plant sink limitation was offset by the positive effect of increased leaf N because of decreased N remobilisation. These results revealed that T_p and leaf photosynthesis can be modulated by whole-plant source-sink relations and N budgets.

6.2 The versatile roles of nitrogen as a link across scales in leaf-colour modification

Nitrogen, an essential element for the growth and development of plants, exerts a profound influence on various physiological processes, including photosynthesis and source-sink relations (Board, 2007). As introduced in Chapter 1, the potential effects of leaf-colour modification on these physiological processes and relationships could also be associated with the intricate N dynamics across leaf, canopy, and whole-crop scales. Findings from this thesis indicate that N plays crucial roles in enhancing photosynthesis and associated source-sink relations while nitrogenous compounds function as feedforward or feedback signals between these processes and relationships across different scales. Therefore, in the context of leaf-colour

modification, understanding the multifaceted roles of N holds significant implications for improving rice productivity.

6.2.1 Enhancing photosynthesis requires optimising N partitioning at both leaf and canopy scales

Nitrogen is intricately linked to photosynthesis, determining biomass production of plants. Efficient allocation of N resources in terms of both leaf biochemistry and canopy physiology is of great importance for increasing the potential efficiency of converting light energy into biomass production in C_3 plants like rice (Gu et al., 2017a; Song et al., 2017; Yin and Struik, 2015). At leaf level, it is frequently suggested that the allocation of leaf photosynthetic N across the components of the photosynthetic apparatus is suboptimal, with an excess of N investment in chlorophyll (Evans and Clarke, 2019; Glick and Melis, 1988; Lokstein et al., 2002; Walker et al., 2018). Modifying leaf greenness was mainly targeted at two objectives at this level:

i) reducing the relative energy loss via NPQ;
ii) optimising the N investment pattern within the leaf.

In Chapter 2, the results showed that the Y-variant genotypes with lower light-absorptance ability of the leaf indeed decreased the total amount of thermal dissipation via NPQ, whereas the inherent distribution pattern of harvested energy between NPQ and photochemical quenching was not necessarily shifted, unless the reduced NPQ could be converted into more energy demand for photosynthetic metabolisms by an increased photosynthetic capacity. Of the two Y-variant genotypes, only ZF-Y (with ca. 40% reduction in chlorophyll and ca. 10% reduction in light-absorptance ability) exhibited higher photosynthetic capacity parameters (i.e., A_{max}, J_{max}, and V_{cmax}) and photosynthetic N-use efficiency compared with its C genotype, implying a potential enhancement in the efficiency of leaf photosynthetic N partitioning. The positive correlation between relative Rubisco content from proteomic data and relative Rubisco carboxylation activity from gas exchange data suggests that the higher Rubisco activity in the ZF-Y genotype came from more N investment in Rubisco-related proteins. Chapter 2 confirmed the feasibility of the second objective: properly reducing leaf chlorophyll coupled with distributing saved N into more beneficial investments in proteins that limit leaf photosynthetic rate results in improved performance. In contrast, the Y variant from the WYJ (cv. Wuyunjing 3) background represented an imbalanced N partitioning pattern, probably due to overly

reduced N investment in chlorophyll (ca. 80% reduction). Therefore, maintaining optimal N partitioning within the leaf is required to maximise whole-leaf photosynthesis.

When upscaling photosynthesis from leaf to canopy level, it is crucial to consider the spatial N partitioning and its acclimation to the light profile within the rice canopy (Gu et al., 2017a; Yin and Struik, 2015). The establishment of leaf N gradients, which align closely with the distribution of light within the canopy (with an optimal condition that K_N:K_L = 1), can contribute to an elevated A_c (Connor et al., 1995; Field, 1983; Goudriaan 1995; Hikosaka and Terashima, 1995). However, it has been commonly observed that N gradients in actual canopies always lag behind the light gradients with the K_N:K_L ratios being lower than 0.5 (Hikosaka, 2016; Ouyang et al., 2021; also in Chapter 3). Thus, studies that have proposed the concept of implementing a light-coloured canopy through reducing leaf chlorophyll content (Ort et al., 2015, 2011; Slattery and Ort, 2021; Walker et al., 2018), may actually help improve the closeness of K_N to K_L, particularly in a dense canopy. Chapter 3 confirmed this theoretical concept by assessing a decline in K_L and thus an increase in the K_N:K_L ratio in Y-variant genotypes. Nevertheless, an optimised canopy light profile alone may not necessarily result in an increase in A_c, as the benefits from a reduced K_L could be offset by, or even not compensate for, the lower leaf light-absorptance ability (due to increased reflectance, see Walker et al., 2018), resulting in a local photosynthetic capacity profile that does not necessarily follow more closely the light profile, as was the case in the Y variant from the WYJ background. Nevertheless, the substantial increase in A_c in the other Y variant from the ZF background was attributed to the adaptive adjustment of N distribution to the light profile across the canopy (i.e., increased K_N). This adjustment in the yellower-leaf canopy involved a steeper N gradient with a higher allocation of N to the upper leaf layer of the canopy, representing a greater efficiency in the utilisation of N at the whole-plant level. These results suggest that the higher A_c resulting from an increased K_N:K_L ratio is primarily due to a higher K_N, rather than a lower K_L.

6.2.2 Enhancing source-sink relations requires regulating N trade-off between source and sink organs at crop scale

At crop level, the importance of N in the growth of rice spans the entire life cycle, from the early stages of seed germination and seedling establishment to the later stages of reproductive development and maturity (Leghari et al., 2016). During the reproductive phase of rice plants, N availability and remobilisation play a crucial role in influencing grain filling and crop productivity (sink growth) by regulating the post-flowering biomass production (source

capacity) (Leghari et al., 2016; Xu et al., 2006). This is because grain yield in rice is mostly derived from the assimilates produced after flowering (Liu et al., 2023; Ning et al., 2013). In Chapter 4, both leaf-colour modified (greener or yellower) traits affected the source capacity during grain filling by regulating N budgets (including N metabolism and N remobilisation), but the underlying mechanisms may be different.

The G traits exhibited by certain genotypes impede or delay chlorophyll catabolism, preventing its degradation to amino-acids, which serves as a source of remobilised N during senescence (Patra, 2020). However, this distinctive characteristic as reflected by retaining chlorophyll is typically observed during the late grain-filling phase (Chapter 2). Compared with the C genotypes, G-variant genotypes exhibited a delay in decline of source activity of leaves only when approaching maturity. This process was reflected by the enhanced leaf longevity and delayed N remobilisation from leaves (Chapter 4), which contributed to a slightly later increase in the total source capacity. However, the benefit from this late increase did not fully compensate for the initial decrease caused by decreased maximum and mean rates of leaf-source activity, resulting in a decline in total source capacity. According to the study of Mu et al. (2018), plants prefer to start the degradation of other macromolecular proteins (e.g., Rubisco or thylakoid proteins) earlier than chlorophyll to support grain filling at the initial phase. This presumably suggests that the main factors limiting photosynthesis, such as the activity and content of Rubisco that determines the carboxylation rate, were not retained in the same manner as chlorophyll in leaves, thereby causing no observable differences in source capacity of all G-variant genotypes with their C genotypes (Chapter 4).

In contrast, the Y-variant genotypes displayed a similar extended leaf-source duration as the G traits, but their impact on the source capacity was more complicated. The uptake of N by roots is partially influenced by the amount of light intercepted by the canopy (Reich et al., 1998). Reducing total light interception of the canopy, as mentioned in Chapter 3, represents a weakness in biomass accumulation before the full canopy was established, leading to lower N accumulation during the vegetative phase (Chapter 4). This, however, also reserved more N resources for post-flowering N-uptake from soil, thereby supporting sustained photosynthetic production during the reproductive phase. In this context, increased N availability and N-uptake from the soil after flowering reduce the reliance on N reallocation from leaves to grains, thus prolonging the functional leaf-N duration for greater biomass production in the same phase (Chapter 4). Among the two Y-variant genotypes, the one from the WYJ background benefitted less from this optimised N trade-off between pre-flowering and post-flowering N-uptake, as

biomass (or N) accumulation was primarily limited by the light-interception ability when upscaling from leaf to canopy levels (Chapters 2 and 3). In summary, the application of Y-variant genotypes to regulate N trade-off at crop level requires careful attention to avoid compromising the intrinsic photosynthetic performance at both leaf and canopy levels while attempting to enhance source capacity during grain filling.

6.2.3 Sink limitation across scales is regulated by whole-plant N budgets

Via establishing relationships between parameters by introducing altered sink-source ratios under different N supply conditions, Chapter 5 revealed that both triose phosphate utilisation (indicated by a biochemical parameter T_p, reflecting the local sink size in the leaf; Sharkey, 1985) and photorespiration-associated N assimilation (indicated by parameter α_S, representing the proportion of glycolate carbon exported from the photorespiratory pathway in the form of serine; Busch et al., 2018) were closely correlated with leaf N content. Higher values of T_p and α_S were commonly observed at early growth stages of rice plants, when the leaves were rich in N content to produce more assimilates to support the demands of rice vegetative growth, as leaves at these stages serve not only as source organs but also as potential sink organs. Among genotypes, the C genotypes with more canopy chlorophyll exhibited higher growth vigour as reflected by biomass and N accumulation for accelerating canopy development (Chapter 3), representing a higher sink demand for photosynthetic production and N assimilation. This higher sink demand probably accounted for the observation that the C genotypes involved more leaf N assimilation associated with the photorespiratory pathway than their Y-variant genotypes at this phase (Chapter 5). However, such a scenario can potentially result in oversupply, where the supply of assimilates exceeds the actual demand for organ development (Luquet et al., 2006). During the vegetative growth period, the rice plants with high leaf-N and thus high leaf photosynthetic capacity showed TPU limitation occurring at a lower intercellular CO_2 concentration (C_i) (Chapter 5).

When entering the grain-filling period, there is a shift in the sink demand from latent growth to storage in large organs such as panicles. This shift prompts the remobilisation of both carbon and N assimilates from leaves to fill the grains (Chapter 4). With the increase in sink demand and the depletion of leaf N, the possibility of leaf photosynthesis to be limited by TPU gradually diminishes, as indicated by lower T_p and higher threshold C_i (at which TPU becomes limiting). The photosynthetic stimulation by photorespiration-associated N assimilation during grain filling was comparatively greater in Y-variant genotypes, particularly the one from the ZF

background. This could be associated with the following facts: firstly, the significantly higher spikelet numbers observed in the Y-variant genotypes compared to their C genotypes indicate a larger sink size, emphasizing an increased demand for biomass and N remobilisation (Chapter 3); secondly, there was an increase in post-flowering N availability in the ZF-Y variant (Chapter 4). Despite the anticipated feedback inhibition of leaf photosynthesis by whole-plant sink limitation after removal of all panicles (Arp, 1991; Aslani et al., 2020; Tanaka and Fujita, 1974), rice plants could exhibit plasticity in response to this feedback inhibition by allowing vegetative organs to temporarily function as storage organs, storing assimilates in leaves or stems. Chapter 5 showed that panicle pruning conducted under ambient [CO_2] level does not negatively affect T_p values, suggesting that the feedback inhibition of photosynthesis by whole-plant sink limitation could be offset by the positive effect of increased leaf N content because of less N remobilisation. In contrast, a significant decline in T_p observed by the study of Fabre et al. (2019, 2020) was attributed to the superimposed effect of sink limitation achieved by both panicle pruning and elevated [CO_2]. Overall, all these results suggest an intrinsic connection between TPU-limited photosynthesis and source-sink relations, and this process is modulated by whole-plant N budgets.

6.3 Implications for improving rice productivity

Leaf-colour modification has opened exciting opportunities for future research in crop improvement. In this thesis, the primary approach to producing leaf-colour modified variant genotypes has been random mutagenesis followed by phenotypic selection. Initially employed in mass culture of the green alga *Chlamydomonas reinhardtii* (Polle et al., 2003), this approach provided early insights into genes responsible for the biogenesis and assembly of light-harvesting complexes (Mitra et al., 2012; Mussgnug et al., 2005). However, it is essential to note that this process can trigger pleiotropic effects of genes (Slattery et al., 2017; also see Chapter 3). Frequently, it has been observed that leaf-colour modification can induce genetic and phenotypic variations in multiple traits (like these N-related traits as discussed above) among rice genotypes. For example, previous research reported that a rice variant with spontaneous chlorophyll deficiency showed an enhanced NPQ amplitude under high-light conditions compared with its control counterpart (Zhao et al., 2017), while distinct results were found in Chapter 2, where both non-allelic Y-variants exhibited significantly lower NPQ amplitudes compared to their C genotypes. Intriguingly, the variations in photosynthetic rate and photosynthetic N-use efficiency were opposite among these two Y-variants from WYJ and

ZF genetic backgrounds, respectively (Chapter 3). These contrasts in NPQ behaviour and photosynthetic performance of the Y-variant genotypes from different backgrounds could potentially be linked to randomness of radiation mutagenesis in unrelated genes, which resulted in different multifactorial effects.

In this context, loci for favourable traits may be scattered over the entire genome and the genes associated with these traits might not be easily identified, making it comparatively challenging to integrate all the traits into one rice variety through genetic or breeding efforts in response to a defined environment. Hence, to advance breeding and cultivation strategies, it is necessary to identify the favourable yield determining physiological characteristics affected by leaf-colour modification, and quantify the extent to which these traits can be translated into higher crop productivity in response to current and future environments. Below, based on previous experiments and analysis, I will summarise the implications of leaf-colour modification for rice breeding and cultivation.

6.3.1 Implications of leaf-colour modification for crop breeding

For several decades, leaf greenness has been regarded as a key characteristic for efficient utilisation of light and N resources, particularly following the successful attainment of higher yields in maize through intense breeding and screening for stay-green varieties (Duvick et al., 2010; Purcell et al., 2011). However, due to the abundant application of N and deliberate breeding selection, the chlorophyll content in crop leaves has reached a surplus level, potentially leading to a suboptimal efficiency of solar energy conversion caused by reciprocal shading of the plants and steep vertical light gradients within the canopy. In this case, it would be unwise to continue breeding for green-leaf crops; instead, application of light-coloured canopies could alleviate excess of light interception by the upper leaves and increase light penetration into the lower leaves of the canopy. Chapter 3 confirmed that reducing leaf and canopy chlorophyll alone can improve the canopy light profile whereas it did not contribute to an enhanced A_c, in line with recent study of Song et al. (2023). Through my study, it became clear that the substantial improvement in photosynthetic N-use efficiency in a specific Y-variant genotype from the ZF background lies in its corresponding optimal N partitioning observed at both leaf and canopy scales. For the leaf scale, the ZF-Y genotype showed an efficient reallocation of saved N from leaf chlorophyll to more rate-limiting proteins, e.g., Rubisco (Chapter 2). For the canopy scale, the ZF-Y genotype employed an optimised strategy to match vertical light and N profiles, evidenced by a steeper N gradient along the canopy and more N

content in the upper leaf layer of the canopy (Chapter 3). Until now, it is unclear whether the altered N partitioning pattern in the ZF background as a result of random mutagenesis was totally optimal or not. However, the physiological components influenced by leaf-colour modification, as observed in the ZF background, are desirable, given that the ZF-Y genotype had advantages in photosynthesis under high-light environments. This provides a valuable direction for breeding programmes or genetic engineering efforts aimed at designing a rice ideotype with higher yield potential. To achieve this goal, further studies are necessary, requiring more comprehensive genomic and proteomic information to fine-tune N partitioning strategies.

6.3.2 Implications of leaf-colour modification for crop cultivation

A crop management strategy is a carefully designed cultivation approach tailored to the specific growth and developmental characteristics of crops, aimed at maximising crop yields while efficiently utilising available resources in a defined environment. In contrast to conventional green-leaf rice cultivars, the Y-variant genotypes exhibited a weakened light-interception ability of the canopy (Chapter 3), representing an inferior competition for light, particularly in the vegetative phase. Thus, successful cases advocating the application of light-coloured canopy for increased biomass production have primarily relied on high-density monocropping cultivation strategies (Gu et al., 2017b; Kirst et al., 2017; Slattery and Ort, 2021). Chapter 4, employing a model-fitting method to describe the rice yield formation mechanism, also revealed that local crop management practices, characterised by excessive N application and insufficient planting density, were suboptimal for the Y-variant genotype from the ZF background. This indicates promising opportunities for enhancing current crop cultivation.

In addition, the sink-source traits altered by leaf-colour modification could also be exploited to develop new crop cultivation strategies in response to futural climate environment (e.g., elevated [CO_2]). In Chapter 4, most of the local rice cultivars exhibited positive post-flowering biomass source-sink differences (i.e., source capacity > sink growth). The surplus of source could become even greater if the pre-flowering reserves are considered. This reflects the common situation of limited sinks under current field cultivation practices for rice. With the increasing atmospheric CO_2 concentration as a result of climate changes, leaf source activity will be further enhanced in rice plants, potentially resulting in a more severe feedback inhibition of sink limitation (Dingkuhn et al., 2020). To self-regulate this enhanced sink limitation, plants tend to store accumulated carbon in leaves and stems, which dilutes N in photosynthetic leaves,

just like these panicle-pruned rice as observed in Chapter 5. This behaviour, known as photosynthetic acclimation to elevated [CO_2], suppresses to a certain extent the crop yield that should have been increased by the 'CO_2-fertilisation' effect (Yin, 2013). In response to this phenomenon, the induced traits in the Y-variant genotypes (observed in Chapter 3) could bring two important benefits:

i) significantly increased numbers of spikelets, indicating a larger sink demand, can alleviate the feedback inhibition from sink limitation;
ii) higher canopy-averaged leaf-N content can compensate for the potential impact of N dilution under elevated [CO_2] condition.

Overall, these leaf-colour modified variations could be considered adaptive traits to the futural climate change, where whole-plant source-sink ratios will be altered by higher CO_2 levels and plant N will be diluted by greater biomass. Further research aims to effectively adjust crop cultivation strategies to these phenotypic variations caused by leaf-colour modification for higher crop productivity, while considering the genotype-environment interactions.

6.4 Concluding remarks

With the aim of exploring the potential of modifying leaf colour to increase rice productivity, in this thesis, comprehensive studies have been conducted in rice genotypes from different genetic backgrounds, which had been modified to have either the stay-green trait or the yellow-leaf trait or both. I examined the effects of leaf-colour modification on photosynthesis and associated source-sink relationships from leaf to canopy and to crop scales. The results revealed the versatile roles of N as a regulatory mechanism across scales following leaf-colour modification, which can be concluded as:

- Leaf-colour modification can improve rice photosynthesis and biomass accumulation only if the N-associated traits (e.g., N distribution from leaf to canopy) are adjusted synergistically, and this improvement depends on genetic backgrounds.
- Leaf-colour modification affects source more than sink traits, with effects varying based on genetic backgrounds, and regulation occurring through N trade-off between pre-flowering and post-flowering phases, as well as N remobilisation between source and sink organs.

- TPU-limited leaf photosynthesis, involving photorespiration-associated N assimilation, can be modulated by whole-plant source-sink ratios and N budgets in rice, suggesting a close inter-connection between leaf-level and whole-plant sink limitations.

As discussed above, the wide phenotypic variations observed resulting from leaf-colour modification have significant implications for crop breeding and cultivation efforts. Follow-up research would be to integrate understandings as presented in this thesis regarding optimal N partitioning and cross-scale feedback mechanisms, and translate these understandings into quantitative algorithms that can be used in a crop growth model. This integration can result in a powerful tool capable of identifying the most favourable combinations of component traits for current and future climate conditions. Ultimately, this tool can provide promising directions for crop breeding and cultivation, aiming to maximise rice photosynthesis and yield.

References

Anten NPR, Schieving F, Werger MJA. 1995. Patterns of light and nitrogen distribution in relation to whole canopy carbon gain in C_3 and C_4 mono- and dicotyledonous species. *Oecologia* 101, 504–513.

Arp WJ. 1991. Effects of source-sink relations on photosynthetic acclimation to elevated CO_2. *Plant, Cell & Environment* 14, 869–875.

Aslani L, Gholami M, Mobli M, Sabzalian MR. 2020. The influence of altered sink-source balance on the plant growth and yield of greenhouse tomato. *Physiology and Molecular Biology of Plants* 26, 2109–2123.

Board JE. 2007. Physiology of Crop Production. *Crop Science* 47, 426–426.

Busch FA, Sage RF, Farquhar GD. 2018. Plants increase CO_2 uptake by assimilating nitrogen via the photorespiratory pathway. *Nature Plants* 4, 46–54.

Connor DJ, Sadras VO, Hall AJ. 1995. Canopy nitrogen distribution and the photosynthetic performance of sunflower crops during grain filling - a quantitative analysis. *Oecologia* 101, 274–281.

Dingkuhn M, Luquet D, Fabre D, Muller B, Yin X, Paul MJ. 2020. The case for improving crop carbon sink strength or plasticity for a CO_2-rich future. *Current Opinion in Plant Biology* 56, 259–272.

Duvick DN, Smith JSC, Cooper M. 2010. Long-term selection in a commercial hybrid maize breeding program. *Plant Breeding Reviews* 24, 109–152.

Evans JR, Clarke VC. 2019. The nitrogen cost of photosynthesis. *Journal of Experimental Botany* 70, 7–15.

Fabre D, Dingkuhn M, Yin X, Clément-Vidal A, Roques S, Soutiras A, Luquet D. 2020. Genotypic variation in source and sink traits affects the response of photosynthesis and growth to elevated atmospheric CO_2. *Plant, Cell & Environment* 43, 579–593.

Fabre D, Yin X, Dingkuhn M, Clément-Vidal A, Roques S, Rouan L, Soutiras A, Luquet D. 2019. Is triose phosphate utilization involved in the feedback inhibition of photosynthesis in rice under conditions of sink limitation. *Journal of Experimental Botany* 70, 5773–5785.

Field C. 1983. Allocating leaf nitrogen for the maximization of carbon gain: Leaf age as a control on the allocation program. *Oecologia* 56, 341–347.

Fu M, Cheng S, Xu F, Chen Z, Liu Z, Zhang W, Zheng J, Wang L. 2021. Advance in mechanism of plant leaf colour mutation. *Notulae Botanicae Horti Agrobotanici Cluj-Napoca* 49, 12071–12071.

Glick RE, Melis A. 1988. Minimum photosynthetic unit size in System I and System II of barley chloroplasts. *Biochimica et Biophysica Acta (BBA)-Bioenergetics* 934, 151–155.

Goudriaan J. 1995. Optimization of nitrogen distribution and of leaf area index for maximum canopy photosynthesis rate. *In: Thiyagarajan, T.M., ten Berge, H.F.M., Wopereis, M.C.S. (Eds.), Nitrogen Management Studies in Irrigated Rice. AB-DLO and TPE-WAU, SARP Research Proceedings*. pp. 85–97.

Gu J, Chen Y, Zhang H, Li Z, Zhou Q, Yu C, Kong X, Liu L, Wang Z, Yang J. 2017a. Canopy light and nitrogen distributions are related to grain yield and nitrogen use efficiency in rice.

Field Crops Research 206, 74–85.

Gu J, Zhou Z, Li Z, Chen Y, Wang Z, Zhang H. 2017b. Rice (*Oryza sativa* L.) with reduced chlorophyll content exhibit higher photosynthetic rate and efficiency, improved canopy light distribution, and greater yields than normally pigmented plants. *Field Crops Research* 200, 58–70.

Hikosaka K. 2016. Optimality of nitrogen distribution among leaves in plant canopies. *Journal of Plant Research* 129, 299–311.

Hikosaka K, Terashima I. 1995. A model of the acclimation of photosynthesis in the leaves of C_3 plants to sun and shade with respect to nitrogen use. *Plant, Cell & Environment* 18, 605–618.

Kirst H, Gabilly ST, Niyogi KK, Lemaux PG, Melis A. 2017. Photosynthetic antenna engineering to improve crop yields. *Planta* 245, 1009–1020.

Leghari SJ, Wahocho NA, Laghari GM, Hafeez Laghari A. 2016. Role of nitrogen for plant growth and development: A review. *Advances in Environmental Biology* 10, 209–219.

Liu G, Yang Y, Guo X, Liu W, Xie R, Ming B, Xue J, Wang K, Li S, Hou P. 2023. A global analysis of dry matter accumulation and allocation for maize yield breakthrough from 1.0 to 25.0 Mg ha^{-1}. *Resources, Conservation and Recycling* 188, 106656.

Lokstein H, Tian L, Polle JEW, DellaPenna D. 2002. Xanthophyll biosynthetic mutants of Arabidopsis thaliana: Altered nonphotochemical quenching of chlorophyll fluorescence is due to changes in Photosystem II antenna size and stability. *Biochimica et Biophysica Acta (BBA)-Bioenergetics* 1553, 309–319.

Long SP, Zhu XG, Naidu SL, Ort DR. 2006. Can improvement in photosynthesis increase crop yields? *Plant, Cell & Environment* 29, 315–330.

Luquet D, Dingkuhn M, Kim H, Tambour L, Clement-Vidal A. 2006. EcoMeristem, a model of morphogenesis and competition among sinks in rice. 1. Concept, validation and sensitivity analysis. *Functional Plant Biology* 33, 309–323.

Makino A, Mae T, Ohira K. 1985. Photosynthesis and ribulose-1,5-bisphosphate carboxylase/oxygenase in rice leaves from emergence through senescence. Quantitative analysis by carboxylation/oxygenation and regeneration of ribulose 1,5-bisphosphate. *Planta* 166, 414–420.

Makino A, Mae T, Ohira K. 1984. Relation between nitrogen and ribulose-1,5-bisphosphate carboxylase in rice leaves from emergence through senescence. *Plant and Cell Physiology* 25, 429–437.

Mitra M, Kirst H, Dewez D, Melis A. 2012. Modulation of the light-harvesting chlorophyll antenna size in Chlamydomonas reinhardtii by TLA1 gene over-expression and RNA interference. *Philosophical Transactions of the Royal Society B: Biological Sciences* 367, 3430–3443.

Mu X, Chen Q, Chen F, Yuan L, Mi G. 2018. Dynamic remobilisation of leaf nitrogen components in relation to photosynthetic rate during grain filling in maize. *Plant Physiology and Biochemistry* 129, 27–34.

Mussgnug JH, Wobbe L, Elles I, Claus C, Hamilton M, Fink A, Kahmann U, Kapazoglou A, Mullineaux CW, Hippler M, Nickelsen J, Nixon PJ, Kruse O. 2005. NAB1 is an RNA

binding protein involved in the light-regulated differential expression of the light-harvesting antenna of Chlamydomonas reinhardtii. *The Plant Cell* 17, 3409–3421.

Ning P, Li S, Yu P, Zhang Y, Li C. 2013. Post-silking accumulation and partitioning of dry matter, nitrogen, phosphorus and potassium in maize varieties differing in leaf longevity. *Field Crops Research* 144, 19–27.

Ort DR, Merchant SS, Alric J, Barkan A, Blankenship RE, Bock R, Croce R, Hanson MR, Hibberd JM, Long SP, Moore TA, Moroney J, Niyogi KK, Parry MAJ, Peralta-Yahya PP, Prince RC, Redding KE, Spalding MH, van Wijk KJ, Vermaas WFJ, von Caemmerer S, Weber APM, Yeates TO, Yuan JS, Zhu XG. 2015. Redesigning photosynthesis to sustainably meet global food and bioenergy demand. *Proceedings of the National Academy of Sciences* 112, 8529–8536.

Ort DR, Zhu X, Melis A. 2011. Optimizing antenna size to maximize photosynthetic efficiency. *Plant Physiology* 155, 79–85.

Ouyang W, Yin X, Yang J, Struik PC. 2021. Roles of canopy architecture and nitrogen distribution in the better performance of an aerobic than a lowland rice cultivar under water deficit. *Field Crops Research* 271, 108257

Patra M. 2020. A review : Stay-green trait and its physiological and genetic basis of yield variation in rice. *Journal of Pharmacognosy and Phytochemistry* 9, 1311–1321.

Polle JEW, Kanakagiri SD, Melis A. 2003. Tla1, a DNA insertional transformant of the green alga Chlamydomonas reinhardtii with a truncated light-harvesting chlorophyll antenna size. *Planta* 217, 49–59.

Purcell LC, Mozaffari M, Karcher DE, Andy King C, Marsh MC, Longer DE. 2011. Association of "Greenness" in corn with yield and leaf nitrogen concentration. *Agronomy Journal* 103, 529–535.

Ray DK, Mueller ND, West PC, Foley JA. 2013. Yield Trends Are Insufficient to Double Global Crop Production by 2050. *PloS One* 8, e66428.

Reich PB, Walters MB, Tjoelker MG, Vanderklein D, Buschena C. 1998. Photosynthesis and respiration rates depend on leaf and root morphology and nitrogen concentration in nine boreal tree species differing in relative growth rate. *Functional Ecology* 12, 395–405.

Sharkey TD. 2019. Is triose phosphate utilization important for understanding photosynthesis. *Journal of Experimental Botany* 70, 5521–5525.

Sharkey TD. 1985. Photosynthesis in intact leaves of C3 plants: Physics, physiology and rate limitations. *The Botanical Review* 51, 53–105.

Slattery RA, Ort DR. 2021. Perspectives on improving light distribution and light use efficiency in crop canopies. *Plant Physiology* 185, 34–48.

Slattery RA, Vanloocke A, Bernacchi CJ, Zhu XG, Ort DR. 2017. Photosynthesis, light use efficiency, and yield of reduced-chlorophyll soybean mutants in field conditions. *Frontiers in Plant Science* 8, 549.

Song Q, Liu F, Bu H, Zhu X. 2023. Quantifying Contributions of Different Factors to Canopy Photosynthesis in 2 Maize Varieties : Development of a Novel 3D Canopy Modeling Pipeline. *Plant Phenomics* 5.

Song Q, Wang Y, Qu M, Ort DR, Zhu XG. 2017. The impact of modifying photosystem

antenna size on canopy photosynthetic efficiency—Development of a new canopy photosynthesis model scaling from metabolism to canopy level processes. *Plant, Cell & Environment* 40, 2946–2957.

Tanaka A, Fujita K. 1974. Nutrio-physiological studies on the tomato plant IV. Source-sink relationship and structure of the source-sink unit. *Soil Science and Plant Nutrition* 20, 305–315.

Thomas H, Ougham H. 2014. The stay-green trait. *Journal of Experimental Botany* 65, 3889–3900.

Venkateswarlu B, Visperas RM. 1987. Source-sink relationships in crop plants. *IRRI Research Paper Series* 125.

Walker BJ, Drewry DT, Slattery RA, VanLoocke A, Cho YB, Ort DR. 2018. Chlorophyll can be reduced in crop canopies with little penalty to photosynthesis. *Plant Physiology* 176, 1215–1232.

White AC, Rogers A, Rees M, Osborne CP. 2016. How can we make plants grow faster? A source-sink perspective on growth rate. *Journal of Experimental Botany* 67, 31–45.

Xu ZZ, Yu ZW, Wang D. 2006. Nitrogen translocation in wheat plants under soil water deficit. *Plant and Soil* 280, 291–303.

Yin X. 2013. Improving ecophysiological simulation models to predict the impact of elevated atmospheric CO_2 concentration on crop productivity. *Annals of Botany* 112, 465–475.

Yin X, Busch FA, Struik PC, Sharkey TD. 2021. Evolution of a biochemical model of steady-state photosynthesis. *Plant, Cell & Environment* 44, 2811–2837.

Yin X, Schapendonk AHCM, Struik PC. 2018. Exploring the optimum nitrogen partitioning to predict the acclimation of C_3 leaf photosynthesis to varying growth conditions. *Journal of Experimental Botany* 70, 2435–2447.

Yin X, Struik PC. 2015. Constraints to the potential efficiency of converting solar radiation into phytoenergy in annual crops: From leaf biochemistry to canopy physiology and crop ecology. *Journal of Experimental Botany* 66, 6535–6549.

Zhao X, Chen T, Feng B, Zhang C, Peng S, Zhang X, Fu G, Tao L. 2017. Non-photochemical quenching plays a key role in light acclimation of rice plants differing in leaf color. *Frontiers in Plant Science* 7, 1968.

Zhu XG, Long SP, Ort DR. 2010. Improving photosynthetic efficiency for greater yield. *Annual Review of Plant Biology* 61, 235–261.

Summary

Historically, leaf greenness conferred advantages in natural ecosystems, acting as a reliable indicator of dominant competition for light and nitrogen (N) resources. Empirical evidence from research on rice cultivation in the last century also suggested that green leaves with higher chlorophyll content were typically linked to higher photosynthetic rate and higher yield potential. However, this appeared to be only part of the story. In the realm of modern rice farming, where purposeful breeding selection for persistent green leaf colour and abundant N fertilizer application are prevalent, investment in leaf chlorophyll of rice plants becomes excessive, especially in high-density monocropping fields. This is unwise as such a condition can result in suboptimal conversion efficiency from intercepted photosynthetically active radiation into biomass, because of reciprocal shading among plants and steep vertical light gradients within the canopy. To address this problem, optimising leaf chlorophyll content has been proposed in recent years as a relevant means to manipulate canopy light penetration and photosynthesis, with the ultimate goals of boosting rice productivity, safeguarding global food security and increasing resource-use efficiency.

In the General introduction (**Chapter 1**), I presented the importance of rice production and introduced the potential of using leaf-colour modifications (involving changes into "stay-green" and "yellow-leaf" traits) as a promising strategy to improve rice photosynthesis and yield. With the recognition that manipulation of leaf colour essentially represents an alteration of the leaf-N investment in chlorophyll, further research was to examine the potential effects of modifying leaf chlorophyll content on photosynthesis and associated source-sink relationships of rice genotypes from diverse genetic backgrounds. This research scaled up from cellular level to canopy and crop levels, with a focus on adjustment of carbon and nitrogen budgets and their interactions.

Although the original intention of leaf-colour modification was to increase canopy photosynthesis by an optimised vertical light environment, effects of altering leaf chlorophyll content on photosynthesis at leaf level are yet to be investigated thoroughly. In **Chapter 2**, the impact of leaf-colour modification on leaf photosynthetic physiology was investigated in four rice cultivars, in which each cultivar had modified leaf colour with leaves that were either yellower or greener than the default type. The relative proportion of absorbed light energy used for non-photochemical quenching (NPQ) vs the relative proportion used for photochemistry

was quantified to examine the relationship between NPQ and modified leaf chlorophyll content. The distribution of leaf N among various photosynthetic proteins was assessed based on proteomic and model analyses. Results showed that earlier and larger effects of yellow-leaf variants than stay-green variants were observed. The yellow-leaf variants had lower SPAD values and leaf absorptance, but higher stomatal conductance and high-light tolerance, compared to their control genotypes. Model and proteomic analyses indicated that reducing leaf greenness reduced the relative energy loss via NPQ. Improving leaf photosynthetic capacity and photosynthetic N-use efficiency, however, would require an improved N distribution pattern within the leaf. Our results confirmed the feasibility of reducing chlorophyll content of leaves coupled with distributing saved N into more beneficial investments on proteins (e.g., Cyt b_6/f and Rubisco) that limit leaf photosynthetic rate. Our results also showed that this improvement in leaf-N partitioning pattern depended on genetic background, as only the Y-variant from the "Zhefu" background exhibited advantages in photosynthesis under high-light environments.

The research aims of **Chapter 3** were to investigate whether and how enhanced light penetration can increase canopy photosynthesis and crop yield, and whether leaf-colour modification influences other growth-related traits. In this Chapter, I examined agronomic, developmental, physiological and canopy structural characteristics in rice leaf-colour variants from different genetic backgrounds. The impacts of yellow-leaf modifications were greater than those of stay-green cases: the restricted leaf area and lower tiller number in yellow-leaf variants allowed to maintain a higher N concentration per unit leaf area, which delayed senescence as also occurred in the stay-green variants. For yellow-leaf variants, light expectedly penetrated more into the lower parts of the canopy with significantly reduced light extinction coefficients, but the leaf-N profile did not necessarily acclimate more closely to the light profile. Compared with its default genotype, the increase in canopy photosynthesis and daily average crop growth rate (and thus grain yield) of the yellow-leaf variant of one genetic background (the "Zhefu" background) was attributed to its higher N partitioning efficiency from both leaf (i.e. improved leaf photosynthetic N use efficiency) and canopy level (i.e. steeper N gradient with more N content in the upper leaf layer of the canopy). Our results suggest that besides increased canopy light penetration, other phenotypic characteristics caused by leaf-colour modification can be exploited to enhance rice biomass and yield.

Leaf-colour modification has been considered as an effective means to improve canopy photosynthesis and source capacity, but whether it will have an impact on sink growth and

source-sink relationships, and if so, whether these leaf-colour modified traits can effectively adapt to current standard crop management practices, especially in relation to planting density, remain unclear. In **Chapter 4**, I used a model-fitting method to quantify the dynamics of source activity and sink demand for both biomass and N accumulation among genotypes from different genetic backgrounds grown in a greenhouse experiment and a field experiment. The source-sink (im)balance of biomass and N during grain filling in these rice genotypes was subsequently assessed. Leaf-colour modification affected biomass source-sink relationships, predominantly through the adjustment of the post-flowering source capacity, but the approach to attaining this varied across different genetic backgrounds. Among all genotypes, only the Y-variant genotype from one genetic background (the "Zhefu" background) showed a simultaneous increase in source capacity and sink growth compared to the default genotype. The genotype with higher source capacity was associated with prolonged leaf-N duration, necessitating enhanced post-flowering N uptake and thus reduced N remobilisation from leaves to panicles. Finally, the same model analysis was applied to the data collected from a planting density field experiment using genotypes of the "Zhefu" background. The results suggest that the current standard crop management practices, involving superfluous N fertiliser application and insufficient planting density, need to be tailored accordingly for the leaf-colour variants to realise their yield potential.

With the recognition that the effect of leaf-colour modification on source-sink relations were associated with N budgets (**Chapter 4**) and also based on the existing understanding in the literature on sink limitation at the leaf scale, further research was specifically designed for **Chapter 5** that aimed to study the mechanism on the dynamic feedback of sink limitation across different scales. Triose phosphate utilisation (TPU) limitation to leaf photosynthesis is a biochemical process indicating carbon sink-source imbalance within leaves, and this process may be linked to the photorespiratory pathway in that amino acids are exported from the pathway as an additional carbon outlet. This biochemical limitation process differs from the sink (panicles) limitation on source (leaves) activity agronomists commonly define at the whole-plant or crop scale. While sink limitations at sub-foliar and whole-plant scales are not necessarily independent, few studies have been conducted on their connections. Also, it is unclear whether this connection between the two scales is associated with whole-plant N budgets. In this chapter, these questions were addressed by model analyses of gas-exchange data measured at three growth stages on leaves of rice genotypes from two genetic backgrounds grown at two N levels, where three means (yellower-leaf modification, comparison of adaxial vs abaxial measurements, and panicle pruning) were applied to alter source-sink ratios. Results

showed that the rate of TPU (T_p) was associated with leaf-N, and high-N leaves (observed at early growth stages or high-N inputs) led to occurrence of TPU limitation at lower intercellular CO_2 level. Moreover, more photorespiration-associated N assimilation was happened in high-N leaves while less in the leaves from Y-variant genotypes and from panicle-pruned plants particularly under abaxial measurement. A positive correlation between T_p and local sink-source ratio confirmed the effect of sink size on leaf source activity. After removal of all panicles, T_p was little affected under this apparently sink-limited condition, presumably indicating that the feedback inhibition of panicle pruning was offset by the increased N in leaves caused by decreased N remobilisation. All in all, these results suggest an intrinsic connection between leaf-level and whole-plant sink limitations, and this connection can be modulated by whole-plant N budgets.

Chapter 6 responds to the research objectives described in **Chapter 1** and presents reflections on the insights obtained in this thesis. In this chapter, I first summarised and elucidated the main findings obtained from **Chapters 2−5**, then discussed the versatile roles of N as a link across scales in leaf-colour modification, impacting the leaf and canopy photosynthesis, and source-sink relations. Finally, based on the wide range of phenotypic variations as a result of random mutagenesis, the implications of leaf-colour modification for breeding and cultivation of rice were discussed further.

The overall conclusion of this thesis suggests that leaf-colour modification can be considered as a promising strategy to improve rice photosynthesis and yield.

Acknowledgements

I am deeply grateful and humbled when I reflect on the incredible journey that has brought me to this point in my academic pursuit. Completing my PhD would not have been possible without the unwavering support, encouragement, and guidance of numerous institutions and individuals.

First of all, I am grateful to the China Scholar Council for funding my PhD fellowship. I would like to extend my appreciation to the College of Agriculture in Yangzhou University for the financial and technological support of the field research work reported in this dissertation.

Second, I would like to express my sincere gratitude to my supervision team, which consists of:

1) Promotor: Prof. Paul C. Struik [Centre for Crop Systems Analysis (CSA), Wageningen University & Research (WUR), the Netherlands];
2) Supervisors: Dr. Xinyou Yin (CSA, WUR) and Prof. Jianchang Yang [College of Agriculture, Yangzhou University (YZU), China];
3) Advisor: Prof. Junfei Gu (YZU);
4) Technician: Peter E.L. van der Putten (CSA, WUR).

This team provided comprehensive support, enabling me to successfully accomplish this demanding task. **Paul**, thank you very much for your excellent guidance and patience during my PhD study and your positive encouragement whenever I felt nervous or frustrated. Working with you has invigorated me, as your prompt recognition of even minor accomplishments fuels my enthusiasm. Apart from the professional assistance, you've generously supported me in various life aspects, enabling me to focus wholeheartedly on completing the final thesis writing. **Xinyou**, I deeply appreciate your unwavering support throughout my PhD journey. The memory of my arrival in the Netherlands remains vivid. On that very first day, you and your wife, **Yarong**, graciously fetched me from Bennekom and guided me to the school campus of Wageningen city. Your kind efforts included introducing me to the working environment and giving me an insightful tour of the greenhouse system. In the academic training process, I gained invaluable knowledge from you, encompassing literature review, hypothesis formulation, experimental design, and the art of crafting scholarly articles. I consider myself incredibly fortunate to have had you as my daily supervisor, with your office always welcoming my ideas and addressing any concerns. These stimulating conversations with you were instrumental in expediting the completion of my graduation thesis. **Prof. Yang**, you've been my supervisor since my master's degree, and I am deeply thankful for your willingness to welcome me back to

Yangzhou University to conduct field experiment and data collection for my PhD research during the pandemic. Your substantial support throughout this process has been invaluable. Meanwhile, I extend my gratitude to your wife, **Zhiqin Wang**, for her essential technical support, which was instrumental in the successful completion of my field experiment during my stay in Yangzhou. Without her assistance and arrangement, it would not have gone as smoothly as it went.

I would like to express my heartfelt gratitude to two other important persons for my journey. I deeply thank my advisor, **Junfei Gu**, for your priceless support and help from my master study, leading me into the captivating realm of rice photosynthesis research. Your knowledge, enthusiasm, and dedication to this field have not only broadened my horizons but also instilled in me a profound passion for the subject. **Peter van der Putten**, I will always remember your kind help during my academic journey, where you taught me the intricacies of gas exchange and chlorophyll fluorescence measurement using the LI-COR 6800, facilitated communication with UNIFARM staff, and ensured the timely arrangement of required experimental equipment. I am grateful for all your technical assistance and the excellent communication we have had, whether in the Radix or Nova building.

My gratitude also goes to all the previous and current members at both YZU and WUR, for their direct or indirect support and help. For my eight-month working visit to Agricultural College of YZU, I would like to express my deep thanks to Prof. Lijun Liu, Prof. Zujian Zhang, Prof. Hao Zhang, Prof. Weiyang Zhang, Prof. Yunji Xu, and Dr. Kuanyu Zhu, for their kindness and hospitality; I have to thank many fellow researchers and friends in the YZU Crop Physiology group: Qun Zhou, Daojian Gu, Jing Chen, Zhikang Li, Liexiang Huangpu, Jiang He, Chenhua Wei, Hao Xie, Yong Shen, Jiaqian Yan, Siyu Li, Kun Liu, for providing enjoyable working environment. I wish to specifically acknowledge the contributions of three individuals: Zhangyi Xue, Wendi Zhang, and Yong Yang, all your generous support and dedicated efforts in facilitating my fieldwork were crucial for the completion of my experiments and timely data collection.

For my stay and study in WUR, I want to first thank our secretaries in the CSA group: Nicole Wolffensperger and Petra Rozema, for arranging all kinds of formalities. Nicole, I am very thankful for your assistance to format the thesis and Petra, I am very grateful for your help with the application of my health insurance in my last year of PhD study. I want to thank Dr. Steven M. Driever, Dr. Moges Retta, and Dr. Yazen Al-Salman for all the engaging conversations we

have had. I would like to thank many PhD fellows and friends: Luuk van Dijk, Ambra Tosto, Phuong Thi Nguyen, Thomas Awio, Robbert van den Dool, Paulinaansaa Asante, Lucette Adet, Zohralyn Homulle, Amandrie Louw, Viriato Cossa, Wenjing Ouyang, Zichang Zhang, Qian Li, Liping Shao, Shuangwei Li, Chen Feng, Qi Wang, Chunfeng Gu, Bei Dong, Zishen Wang, Panpan Fan, Liang Fang, Hongyu Sun, Dong Wang, Jin Wang, Zhuo Xu, Zhan Xu, Jie Lu, Qingyue Zhao, Jiahui Gu, Yanjie Chen, Yujuan He, Lu Liu, and Hao Liu, who provided an engaging and collaborative environment where ideas were freely exchanged. Scientific discussions (e.g., PhD meetings, Lunch seminars, Journal club, and CSA symposium) provided within CSA were excellent platforms where knowledge was shared. Also, Yalin Liu and Qian Liu, thank you for being my paranymphs. The camaraderie and support I found within this community have been a source of inspiration and motivation.

Last but by no means least, I am indebted to my family for their unconditional love and encouragement. Your belief in me sustained me during moments of doubt and kept me focused on pursuing my career abroad.

In closing, this journey has been one of growth, challenges, and triumphs. The culmination of this effort is a testament to the collective contributions of those mentioned above and many more whose names may not appear here but whose impact on my journey is no less significant. With a heart full of gratitude, I step forward into the next chapter of my life, carrying the lessons and experiences of this academic endeavour with me.

Zhenxiang Zhou

Wageningen, The Netherlands,

November, 2023

List of Publications

Zhou Z, Struik PC, Gu J, van der Putten PEL, Wang Z, Yang J, Yin X. Quantifying source-sink relationships in leaf-colour modified rice genotypes during grain filling phase (submitted).

Zhou Z, Zhang Z, van der Putten PEL, Fabre D, Dingkuhn M, Struik PC, Yin X. (2023) Triose phosphate utilization in leaves is modulated by whole-plant sink-source ratios and nitrogen budgets in rice. Journal of Experimental Botany, erad329.

Zhou Z, Struik PC, Gu J, van der Putten PEL, Wang Z, Yin X, Yang J. (2023) Leaf-colour modification affects canopy photosynthesis, dry-matter accumulation and yield traits in rice. Field Crops Research, 290, 108746.

Zhou Z, Struik PC, Gu J, van der Putten PEL, Wang Z, Yin X, Yang J. (2023) Enhancing leaf photosynthesis from altered chlorophyll content requires optimal partitioning of nitrogen. Crop and Environment, 2(1), 24-36.

PE&RC Training and Education Statement

With the training and education activities listed below the PhD candidate has complied with the requirements set by the C.T. de Wit Graduate School for Production Ecology and Resource Conservation (PE&RC) which comprises of a minimum total of 32 ECTS (= 22 weeks of activities)

Review/project proposal (9 ECTS)

- Physiological limitations and possible improved approaches of rice photosynthesis
- Exploring the potential of using leaf-colour traits to increase rice productivity via improving photosynthesis and source-sink balance

Post-graduate courses (3.6 ECTS)

- Introduction to R for statistical analysis; PE&RC (2019)
- Crop physiology and climate change; Wageningen University & University of Florida (2022)
- Environmental signalling in plants; Utrecht University (2022)

Laboratory training and working visits (3 ECTS)

- Laboratory training for proteomics; Yangzhou University (2020)

Deficiency, refresh, brush-up courses (1.5 ECTS)

- Basic statistics; WUR (2022)

Competence strengthening/skills courses (4.2 ECTS)

- Searching and organising literature; WUR 92019)
- Reviewing a scientific paper; WUR (2019)
- Project and time management; WUR (2019)
- Scientific writing; WUR (2021)

Scientific integrity/ethics in science activities (0.3 ECTS)

- Ethics in plant and environmental sciences; WUR (2019)

PE&RC Annual meetings, seminars and the PE&RC weekend (2.1 ECTS)

- PE&RC First year's weekend (2019)
- PE&RC Day: reflecting on the past to transform the future (2021)
- PE&RC Day: artificial intelligence and sustainability (2022)
- PE&RC Last year's weekend (2023)

Discussion groups/local seminars or scientific meetings (9 ECTS)

- SKiPR-Sharing knowledge in photosynthesis research meeting (2020-2021)
- Photosynthesis discussion group organised by CSA and HPP (2021-2022)
- CSA Lunch seminar (2021-2023)
- CSA Journal club (2021-2023)
- FLOP Photosynthesis (2023-2024)
- SKiPR-Sharing knowledge in photosynthesis research meeting (2023-2024)

International symposia, workshops and conferences (4.7 ECTS)

- 2nd Global conference on agriculture; oral presentation; Berlin, Germany (2022)
- Gordon research conference on CO_2 assimilation in plants from genome to biome; poster presentation; Lucca, Italy (2023)

BSc/MSc thesis supervision (3 ECTS)

- Leaf-colour modification affects canopy photosynthesis, dry-matter accumulation and yield traits in rice

Curriculum vitae

Zhenxiang Zhou was born on 20th November, 1991 in Jiangsu Province, China. In 2010, he started his BSc study at the Agricultural College of Yangzhou University (YZU), Jiangsu, China. After completing his four-year BSc study programme, he pursued his MSc study programme in the Crop Physiology group of YZU. He studied rice photosynthesis, and in 2017, he successfully defended his thesis entitled "Effect of leaf chlorophyll content on photosynthetic physiology and grain yield of rice". In 2018, he was granted a four-year scholarship from the China Scholarship Council, which allowed him to start his PhD journey at the Centre for Crop Systems Analysis, Plant Science Group at Wageningen University & Research (WUR). Being fascinated by rice photosynthesis during the MSc study, he continued to explore the potential of modifying leaf colour to increase rice productivity via improving photosynthesis and source-sink relationships. This PhD research work was under the supervision of Prof. Paul C. Struik (WUR), Dr. Xinyou Yin (WUR), and Prof. Jianchang Yang (YZU).

Funding

The PhD fellowship was funded by the China Scholarship Council (grant number: 201808320445). The field experiment (2020) was partly financed by the College of Agriculture, Yangzhou University.

Cover designed by Sen Li

Printed by ProefschriftMaken